TOWARDS MODELS FOR THE OXYGEN EVOLVING CENTRE OF PHOTOSYSTEM II AND ANALYSIS OF LEWIS ACIDIC METALS WITHIN NOVEL SALEN DERIVATIVES

Daniel Cooper MChem. (Hons)

A thesis submitted to Cardiff University in accordance with the requirements for the degree of Doctor of Philosophy in the Faculty of Science, School of Chemistry, Cardiff University.

August 2009

ProQuest LLC
789 East Eisenhower Parkway
P.O. Box 1346
Ann Arbor, MI 48106-1346

DECLARATION

This work has not previously been accepted in substance for any degree and is not currently submitted in candidature for any degree.

Signed..  .....(candidate) Date.15-12-09

STATEMENT 1

This thesis is the result of my own independent work/investigation, except where otherwise stated.
Other sources are acknowledged by explicit references

Signed..  .....(candidate) Date.15-12-09

STATEMENT 2

I hereby give consent for my thesis, if accepted, to be made available for photocopying and for inter-library loan, and for the title and summary to be made available to outside organisations.

Signed... 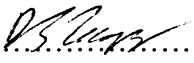 .....(candidate) Date.15-12-09

Abstract

The synthesis and characterisation of a range of ligands capable of binding four or five transition metals has been explored in an attempt to synthesise a model for the oxygen evolving centre of photosystem II. Difficulty was encountered in isolating the pure, deprotected ligands. A ligand based on 1,4,7-triazacyclononane containing three alcohol donors was isolated, investigated and compared against similar ligands.

A series of copper N-oxide Bis(N,N'–Disalicylalethylenediamine) derivatives were synthesised and fully characterised. The electron paramagnetic resonance spectra (EPR) of these complexes were measured and compared in order to determine the relative Lewis acidity of the central metal. Electron nuclear double resonance (ENDOR) spectra were recorded of the complexes; they revealed the catalytic activity of these complexes towards cyclopropanation was tested with a variety of styrene derivatives.

A zinc N-oxide Bis(N,N'–Disalicylalethylenediamine) derivative was extensively studied for enantiomeric discrimination of a small amine, methylbenzyl amine (MBA). This was monitored *via* ^{1}H NMR titrations in three different solvents, $CDCl_3$, CD_3CN and CD_3OD. The ability of MBA to displace a solvent molecule from the coordination sites was investigated and the data inserted into a kinetic model. Chloroform was found to have the weakest interaction while methanol had the strongest. The difference in affinity of *RR*-complex for *R*-MBA over *S*-MBA was also investigated and a preference for the heterochiral mixture was revealed.

Acknowledgements

Firstly I'd like to acknowledge my supervisor Dr Ian Fallis for his guidance and ideas throughout my PhD.

A huge thank you has to go to Dr Damien Murphy and Dr Emma Carter for their continued support and input towards Chapter 3. Many thanks also to Dr Niek Buurma for his help and mathematical input that went into chapter 5. The talent and patience of these people cannot be emphasised enough.

Dr Tom Tatchell deserves thanks for showing me the ropes and his continued patience throughout my initial year. He also deserves thanks, as does Dr Ben Ward, for reading the first draft of this manuscript.

Acknowledgements must also be made to the following people:

Dr Jo Day and Dr James Knight for solving all the crystal structures in this thesis from some fairly dubious looking crystals.

Dr Rob Jenkins and Robin Hicks for their continued support in all things chromatographical.

My good friends from the labs in the chemistry department who are too numerous to name here, but in particular, Matt, James, Tom, Jo, Bres, Gles and Mini.

The EPSRC for the funding of this work.

I'd also like to thank my parents, my brother and my grandparents, for the last 26 years of love and support. Dr Jo Day deserves another mention for putting up with me throughout the course of this work and for inspiring me to finish when times looked desperate.

Notes

The following abbreviations have been used in this text:

Calc.	calculated
CFSE	crystal field stabilisation energy
Cyt b	cytochrome b
DCM	dichloromethane
DFT	density functional theory
DMF	dimethylformamide
DMSO	dimethylsulfoxide
ee	enantiomeric Excess
ENDOR	electron nuclear double resonance
EPR	electron paramagnetic resonance
GC	gas chromatography
HKR	hydrolytic kinetic resolution
HPLC	high pressure liquid chromatography
IR	infra red
LHC	light harvesting centre
MBA	methylbenzylamine
*m*CPBA	*meta*-perchlorobenzoic acid
NMR	nuclear magnetic resonance
nOe	nuclear Overhauser effect
Ns	*m*-nitrobenzenesulfonate
Obs.	observed
OEC	oxygen evolving centre
Phe	phenylalanine
PSII	photosystem 2
ROMP	ring opening metathesis polymerisation
Tacn	1,4,7 – triazacyclononane
TFA	trifluoroacetamide
TMS	tetramethylsilane
Ts	*p*-toluenesulfonic acid
Tyr	tyrosine
UV	ultra violet

The following new organic compounds have been prepared within this text:

Compound	Structure	Compound	Structure
1	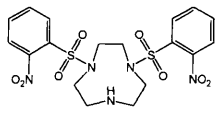	2	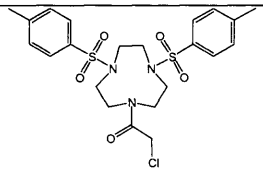
2'	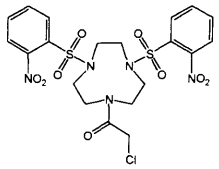	3	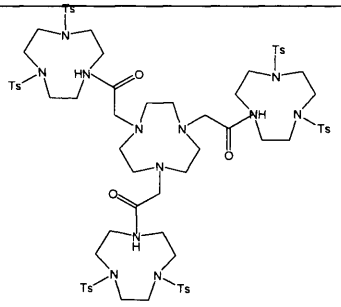
3'	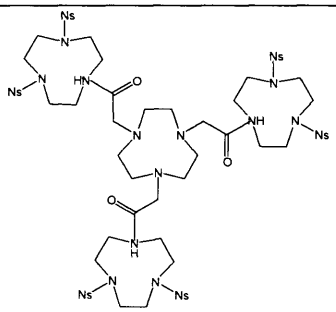	4	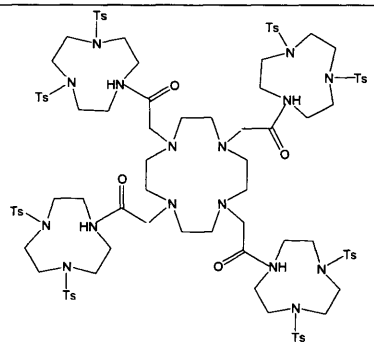
4'	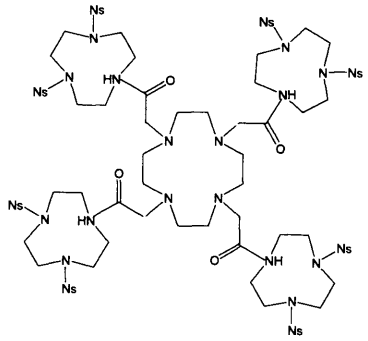	5	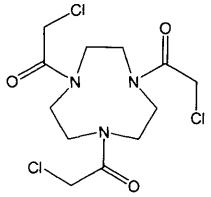
6	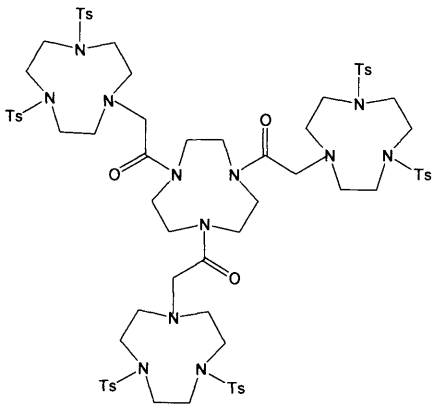	6'	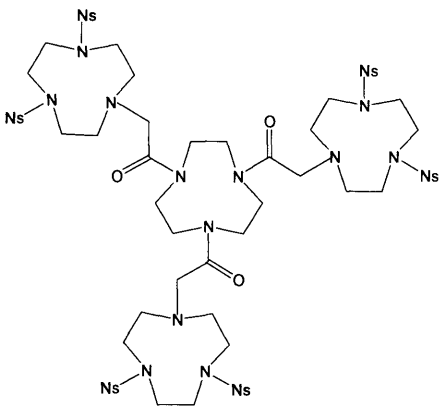

Compound	Structure	Compound	Structure
7	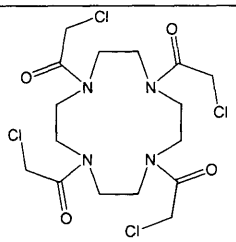	8	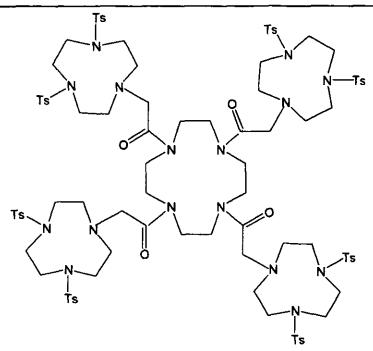
8'	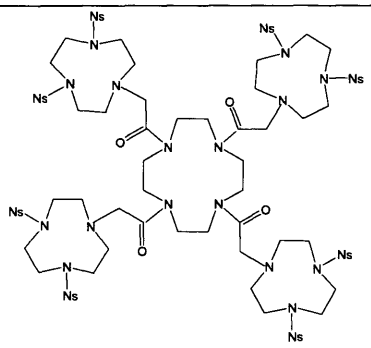	9	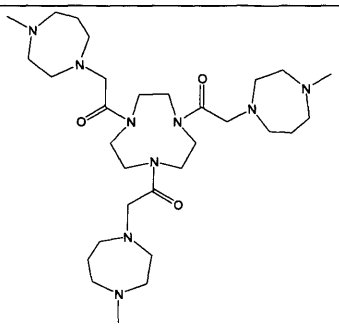
11	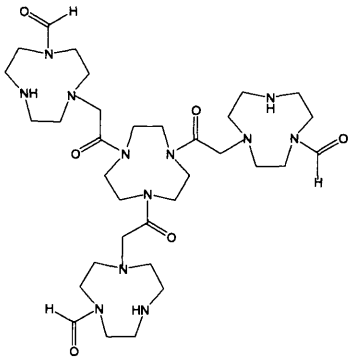	13	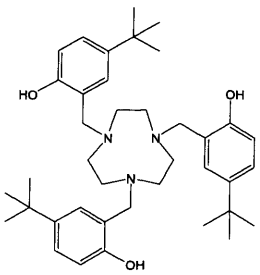
14	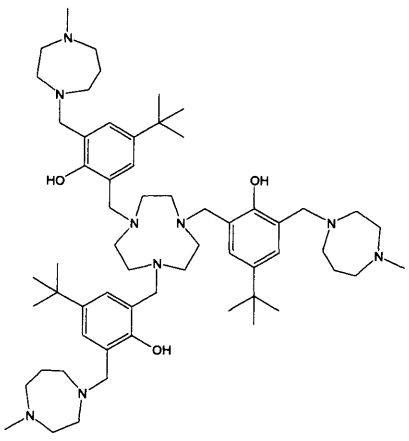	15	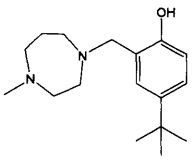

Compound	Structure	Compound	Structure
L[1]	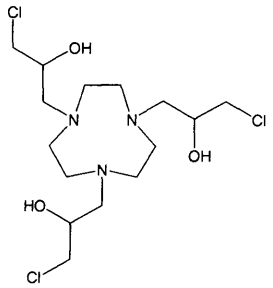	16	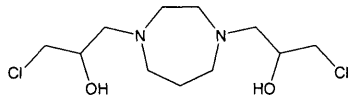
17	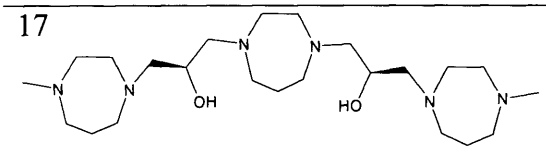	19	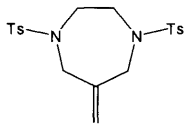
19'	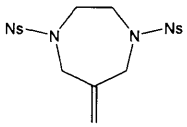	20	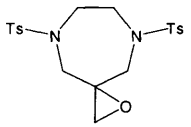
20'	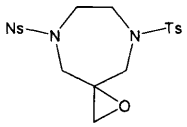	21	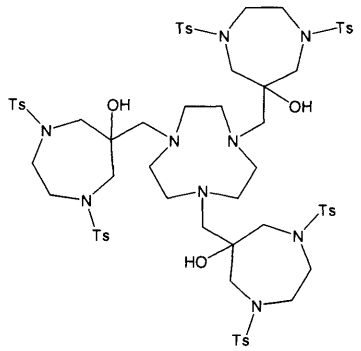
21'	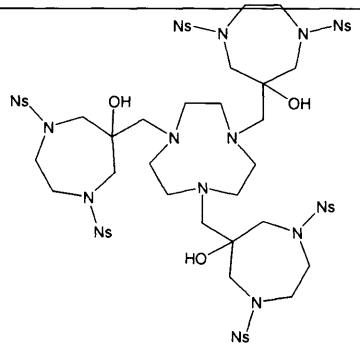	L[6]	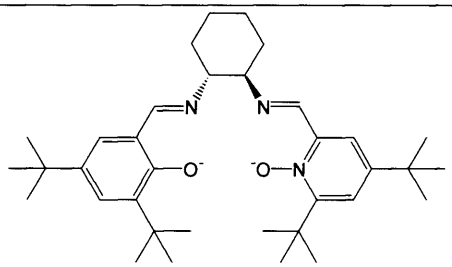
L[7]	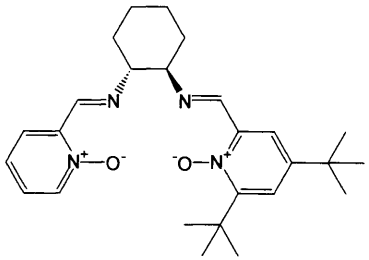	L[8]	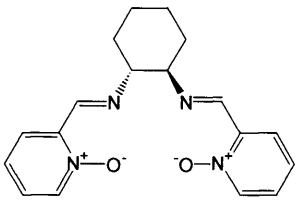

L^9	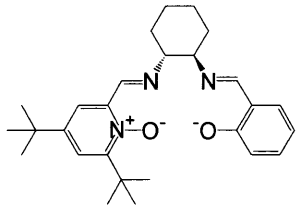	

Contents

CHAPTER 1

Introduction to the Thesis

1.1 Photosystem II

The work carried out within this thesis is aimed at probing the chemistry of high oxidation state 1st row transition metals. In addition to this general introduction, each chapter contains a small, more detailed introduction relating to the work contained within it.

The aim of the work carried out in the first chapter is primarily to synthesise a model for the tetra manganese cluster of Photosystem II (the Oxygen Evolving Centre, OEC). The approach focuses on the functionalisation of 1,4,7-triazacyclononane in order to synthesise a ligand with the capability of binding four or five first row transition metals.

Photosynthesis is the process by which almost all plants, algae and cyanobacteria convert water and carbon dioxide into carbohydrates and oxygen using photons, usually absorbed from the sun. The Hill reaction[1] (scheme 1.1) illustrates this.

$$CO_2 + nH_2O \rightarrow n(CH_2O) + nO_2$$

Scheme 1.1: The general reaction that occurs naturally in most plants and algae.[2]

The OEC is the cluster widely believed to be responsible for the water splitting process.[2] Studies have shown that this is composed of a tetra manganese cluster.[3] It has also been shown that models without calcium do not split water; therefore calcium plays an essential part of the OEC. However, its role is presently only speculated upon.

In 1937 Pirson observed that when deprived of manganese, a plant is unable to produce oxygen,[4] however, it was not until 1970 that Bessel Kok, continuing Pierre Joliot's observations published in 1969,[5] devised a five state cycle (scheme 1.2) in which four photon-induced oxidations of the manganese cluster result in the evolution of a di-oxygen molecule.[2] Kok named these five states the S states (store states) the S_4 state is the only state not to have been studied to any degree, due to its instability.

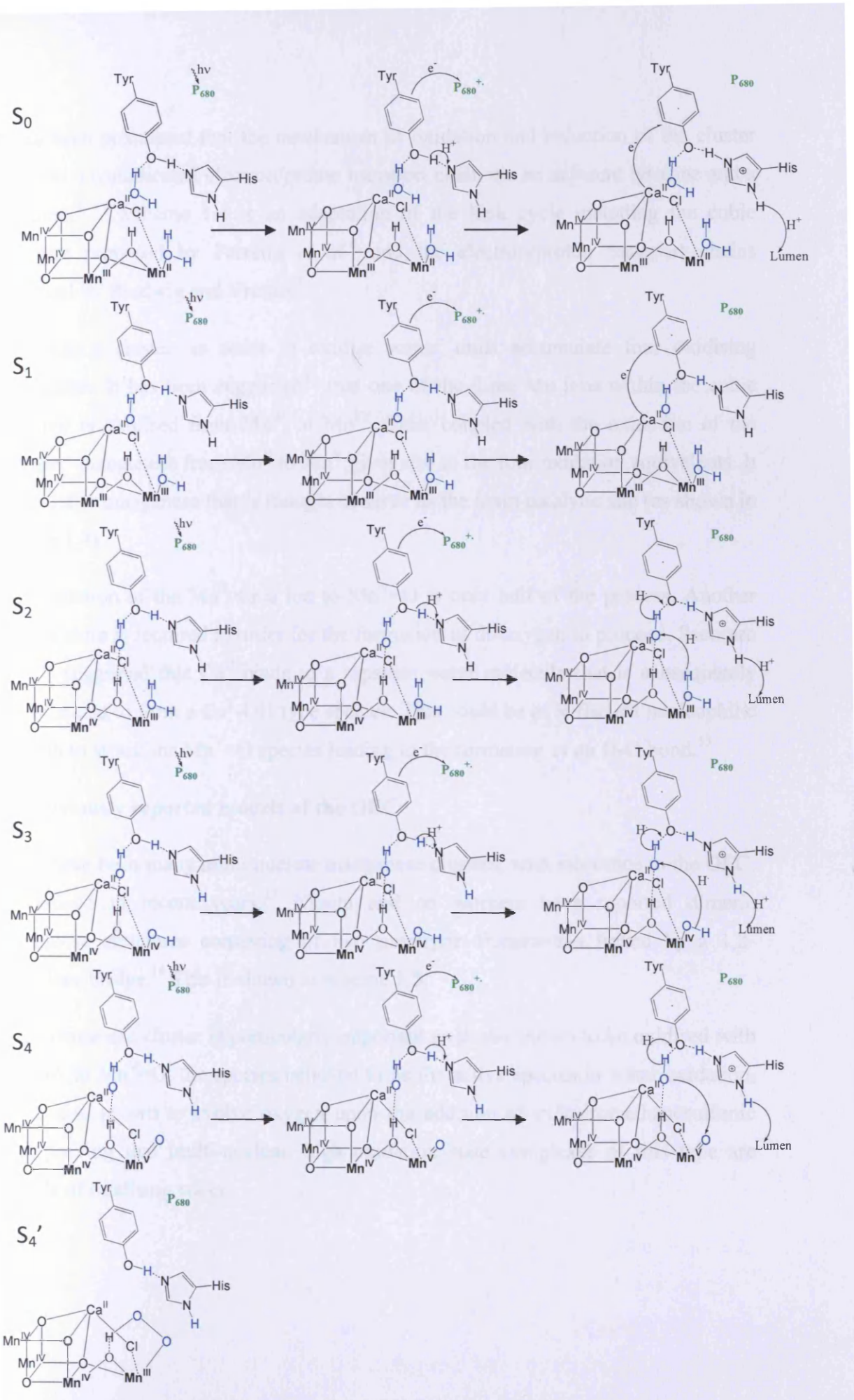

Scheme 1.4: An adapted version of the Kok cycle, depicting a possible proton transport mechanism outlined by Brudwig and Vrettos.[9]

It has been postulated that the mechanism of oxidation and reduction of the cluster involves a complicated electron/proton transport chain via an adjacent tyrosine and a histidine.[9, 10] Scheme 1.4 is an adaptation of the Kok cycle including the cubic structure proposed by Ferreira *et al.*[6] and the electron/proton transport chains proposed by Brudwig and Vrettos[9].

The Mn_4Ca cluster, in order to oxidise water, must accumulate four oxidising equivalents. It has been suggested[11] that one of the three Mn ions within the cubic structure is oxidised from Mn^{III} to Mn^{IV}. This, coupled with the oxidation of the 'dangler' manganese from Mn^{II} to Mn^{V} gives rise to the four oxidation equivalents. It is this latter manganese that is thought to serve as the main catalytic site (as shown in scheme 1.4).

The oxidation of the Mn^{II} aqua ion to Mn^{V}=O is only half of the process. Another oxygen atom is required in order for the formation of di-oxygen to proceed. Pecoraro *et al.*[12] suggested that Ca^{II} binds to a separate water molecule that is subsequently deprotonated to form a Ca^{II}-OH type species. This could be of sufficient nucleophilic strength to attack the Mn^{V}=O species leading to the formation of an O-O bond.[13]

1.2 Previously reported models of the OEC

There have been many multi nuclear manganese clusters, with relevence to the OEC, synthesised in recent years.[13] Naruta and co workers have reported dimeric manganese structures consisting of two porphyrin frameworks linked by a 1,2-phenylene bridge.[14] This is shown in scheme 1.5.

This manganese cluster is particularly important as it was shown to be oxidised with *m*CPBA to Mn^{V}=O, the species believed to be the active species in water oxidation, it was also shown to evolve oxygen upon the addition of trifluoromethanesulfonic acid, proving that multi-nuclear, high oxidation state complexes of this type are capable of oxidising water.

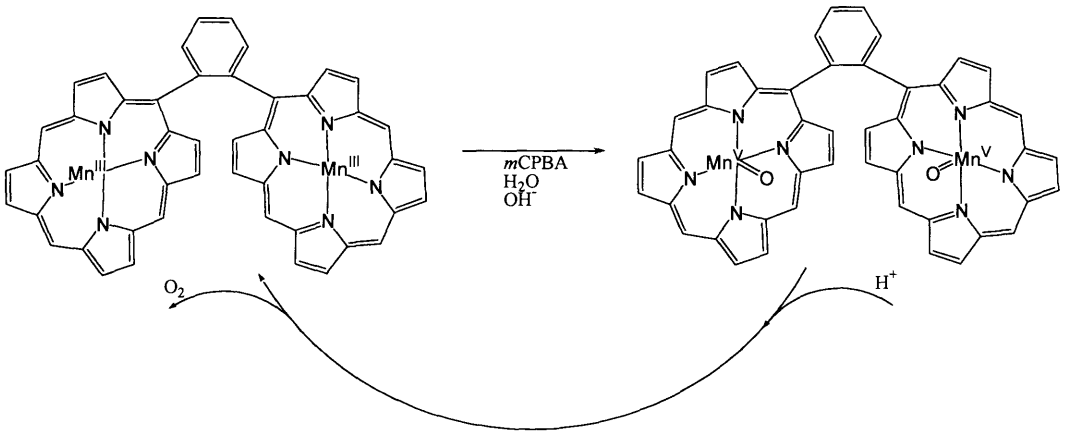

Scheme 1.5: The dimeric manganese system reported by Naruta *et al.*

More recently Chaudhuri *et al.*[15] reported the crystal structure of a trimeric manganese structure with the 2-aminophenol based ligand shown in fig. 1.2. This is a significant finding as the complex proves itself to be the first trinuclear manganese complex containing three different oxidation states (Mn^{II}, Mn^{III} and Mn^{IV}), this obviously has relevance to the OEC as the S states contain multi oxidation state manganese centres.

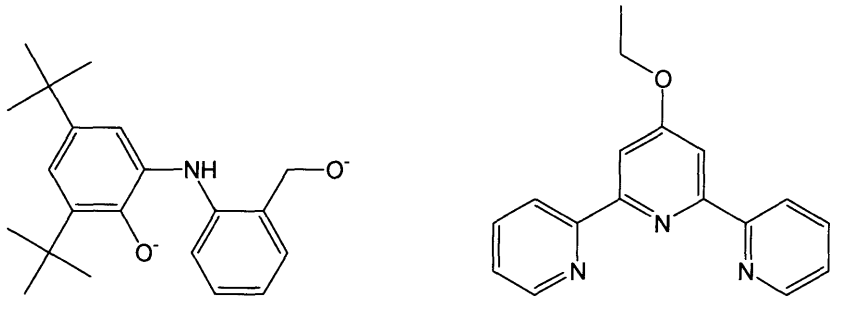

Fig. 1.2: The ligand reported by Chaudhuri and co workers (left) binds manganese in a trimeric manner (Mn_3L_4Cl), the ligand reported by Brudvig *et al* (right) binds manganese in a tetrameric manner ($Mn_4O_4L_4$).

In 2005 Brudvig *et al.*[16] published a crystal structure of a tetra manganese complex of 4'-ethoxyl-2,2':6'2''-terpyridine (fig. 1.2), although all the manganese atoms were Mn^{IV}, this proved a significant advancement due to the coordination of oxo, hydroxo and aqua species. All three of these species are thought to be present at various times during the water oxidation process.[9]

A potential model for the OEC should follow certain criteria. It should be able to coordinate four or five 1st row transition metals via relatively hard donor atoms (such as N and O). It should be flexible enough to allow for varying oxidation states, there should be the potential for oxide bridging and the metal centres should be coordinatively unsaturated to allow for solvent molecules (H_2O) to coordinate.

It is important to approach the task of synthesising a model for this cluster in a methodical way in order that adjustments to a potential model can be easily made. 1,4,7-triazacyclononane (tacn) was chosen as a basis for the ligand as it is excellent at chelating to transition metals and can be readily substituted. The fact that tacn is a triazamacrocycle is advantageous due to the fact that the OEC is surrounded by amines in the form of amino acids. The chemistry of tacn will be discussed later in this chapter.

A ligand of the type shown in fig. 1.3 was judged to address the issues stated previously; an organic framework of this type is the target molecule for this work. The circles in the schematic illustrate a coordination site (e.g. tacn). The zigzag lines depict an alkyl chain, the length of which could be adjusted. M represents a 1st row transition metal, ideally manganese.

The key features included are:

- A central coordination site surrounded by three or four coordination sites
- Coordination sites made up of N and O donors
- Hydroxide bridges between sites provided by the hydroxyl groups
- Flexibility of the ligand to accommodate varying oxidation states

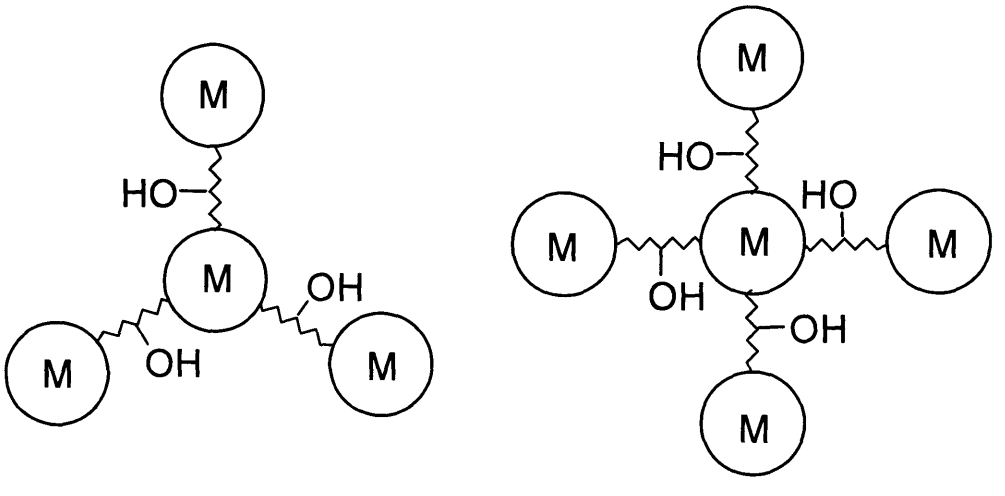

Fig. 1.3: Ligands of these types are the target molecules in this chapter.

The second chapter focuses on some of the ligands synthesised in chapter one and describes the solid state structures of complexes of these.

The final three chapters are a study of transition metals bound within a salen framework. Salens are known to be catalytically active when co-ordinating to

Mn^{V}=O, the species thought to be present in the S_4 state of the Kok cycle.[9, 10] Due to the diverse nature of manganese, copper was selected as a more predictable, experimentally accessible metal in order to probe *via* EPR and ENDOR spectroscopy. Zinc was selected for the work carried out in chapter six due to the paramagnetic nature of Zn^{II} complexes. This allows investigation by ^{1}H NMR.

1.3 Bibliography

1. Hill, R., Oxygen evolved by isolated chloroplasts. *Nature* **1937,** 139, 881-2.

2. Kok, B.; Forbush, B.; McGloin, M., Cooperation of charges in photosynthetic oxygen evolution. I. A linear four step mechanism. *Photochem. Photobiol.* **1970,** 11, (6), 457-75.

3. Rhee, K. H.; Morris, E. P.; Barber, J.; Kuhlbrandt, W., Three-dimensional structure of the plant photosystem II reaction centre at 8 A resolution. *Nature* **1998,** 396, (6708), 283-6.

4. Pirson, A., Photosynthesis and mineral nutrition. *Fortschr. landw. chem. Forsch.* **1937**, 90-9.

5. Joliot, P.; Barbieri, G.; Chabaud, R., Model of the System II photochemical centers. *Photochem. Photobiol.* **1969,** 10, (5), 309-29.

6. Ferreira, K. N.; Iverson, T. M.; Maghlaoui, K.; Barber, J.; Iwata, S., Architecture of the Photosynthetic Oxygen-Evolving Center. *Science* **2004,** 303, (5665), 1831-1838.

7. Kamiya, N.; Shen, J. R., Crystal structure of oxygen-evolving photosystem II from Thermosynechococcus vulcanus at 3.7-A resolution. *Proc Natl Acad Sci U S A* **2003,** 100, (1), 98-103.

8. Zouni, A.; Witt, H. T.; Kern, J.; Fromme, P.; Krauss, N.; Saenger, W.; Orth, P., Crystal structure of photosystem II from Synechococcus elongatus at 3.8 A resolution. *Nature* **2001,** 409, (6821), 739-43.

9. Vrettos, J. S.; Brudvig, G. W., Water oxidation chemistry of photosystem II. *Philos. Trans. R. Soc. London, Ser. B* **2002,** 357, (1426), 1395-1405.

10. Vrettos, J. S.; Brudvig, G. W., Oxygen evolution. *Compr. Coord. Chem. II* **2004,** 8, 507-547.

11. McEvoy, J. P.; Brudvig, G. W., Water-Splitting Chemistry of Photosystem II. *Chem Rev.* **2006,** 106, 4455-4483.

12. Precoraro, V. L.; Baldwin, M. J.; Caudle, M. T., A proposal for water oxidation in photosystem II. *Pure and Applied Chemistry* **1998,** 70, 925-931.

13. Mullins, C. S.; Pecoraro, V. L., Reflections on small molecule manganese models that seek to mimic photosynthetic water oxidation chemistry. *Coord. Chem. Rev.* **2008,** 252, (3+4), 416-443.

14. Shimazaki, Y.; Nagano, T.; Takesue, H.; Ye, B. H.; Tani, F.; Naruta, Y., Characterization of a dinuclear MnV=O complex and its efficient evolution of O2 in the presence of water. *Angew. Chem., Int. Ed.* **2004,** 43, (1), 98-100.

15. Mukherjee, C.; Weyhermueller, T.; Wieghardt, K.; Chaudhuri, P., A trinuclear complex containing MnIIMnIIIMnIV, radicals, quinone and chloride ligands potentially relevant to PS II. *Dalton Trans.* **2006**, (18), 2169-2171.

16. Chen, H.; Collomb, M. N.; Duboc, C.; Blondin, G.; Riviere, E.; Faller, J. W.; Crabtree, R. H.; Brudvig, G. W., New Linear High-Valent Tetranuclear Manganese-Oxo Cluster Relevant to the Oxygen-Evolving Complex of Photosystem II with Oxo, Hydroxo, and Aqua Coordinated to a Single Mn(IV). *Inorg. Chem.* **2005,** 44, (25), 9567-9573.

CHAPTER 2

Towards synthetic models for the Oxygen Evolving Centre of Photosystem II

2.1 Introduction

2.1.1 Synthetic Methodology

2.1.1.1 Protecting groups for secondary amines

In order to carry out certain synthetic transformations selectively, protecting groups need to be utilised. They work by temporarily occupying or blocking certain sites that would otherwise react with the intended reagent. When deciding on a particular protecting group to use, a number of considerations must be taken into account. The protecting group should be selectively attached and removed in good yield under conditions that will not affect the target molecule. It should also be easily separated from the product of the reaction. The protecting groups used in this work will be briefly discussed.

Toluene sulfonyl chloride (tosyl, ts) is an extremely popular reagent used for protecting secondary amines. The reason for its popularity is partly due to the relatively low cost of the starting material, tosyl chloride, but mainly due to the robust nature of the sulfonamides formed. Tosylate sulfonamides often require extreme conditions to deprotect (for example H_2SO_4, 80 °C, 24Hrs[1]), this enables a wide range of reactions to be carried out on the material before removal of the protecting group. Consequently, the use of tosylates requires the final product to be able to withstand the harsh nature of the conditions used to cleave.

In contrast, the *ortho* or *para* nitrobenzenesulfonamide (nosyl, ns) group is very easily cleaved with thiophenol under relatively mild conditions, K_2CO_3 or Cs_2CO_3 in DMF, and generally gives high yields (scheme 2.1). It is stable to strong acid but nitro groups are readily reduced, rendering nosylates unsuitable for a certain situations.[2]

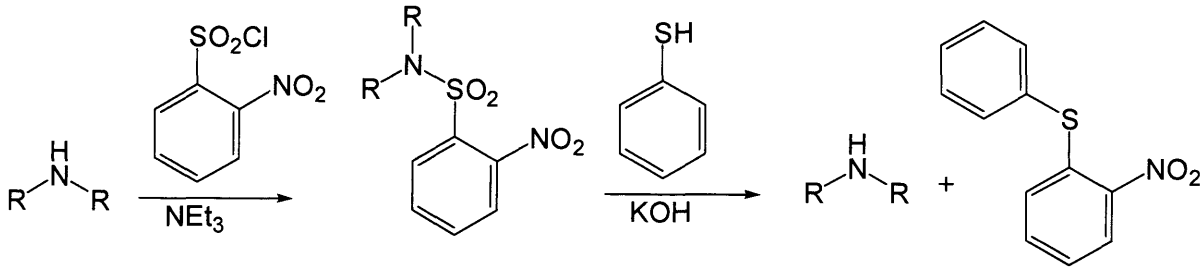

Scheme 2.1: Protection and deprotection of an amine with the ns group.[2]

2.1.1.2 Amide preparation

Amides are commonly prepared by the reaction of ammonia, a primary amine or a secondary amine with a reactive alkanoylating agent, scheme 2.2. A popular method of amide synthesis is the use of Schotten-Baumann[3] conditions, this involves the addition of excess anhydride or acyl chloride to the amine in aqueous alkaline solution. Acid anhydrides are commonly used. However, chloroacetylchloride, $ClCH_2COCl$, was used in the reactions within this chapter.

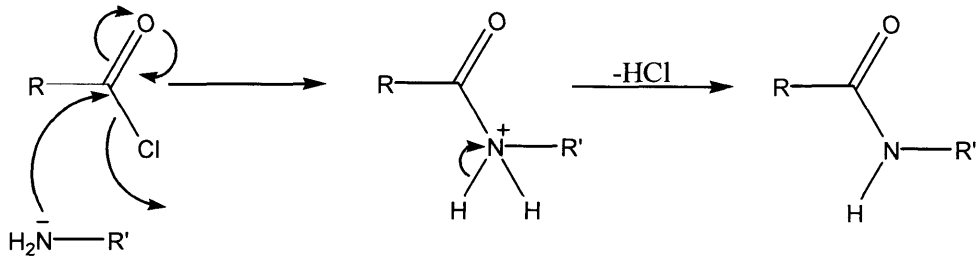

Scheme 2.2: The mechanism for the formation of an amide.

Amides can be reduced with reagents such as B_2H_6 or $LiAlH_4$, the mechanism for this is shown in scheme 2.3.

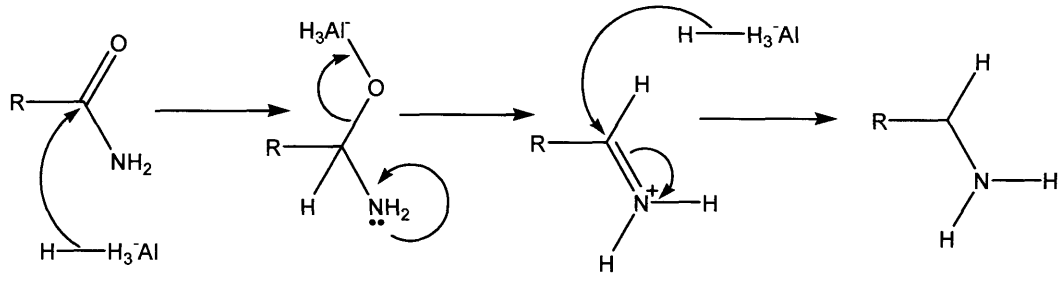

Scheme 2.3: The mechanism for the reduction of an amide.

2.1.1.3 The Mannich reaction

The Mannich reaction can be seen as the condensation of an enolizable carbonyl compound with an iminium ion, usually carried out with formaldehyde (although many aldehydes have been shown to work) is a common synthetic reaction used to introduce α-dialkylaminomethyl substituents.[4] The Mannich reaction is formally considered as the addition of an amine followed by nucleophilic substitution (scheme 2.4).

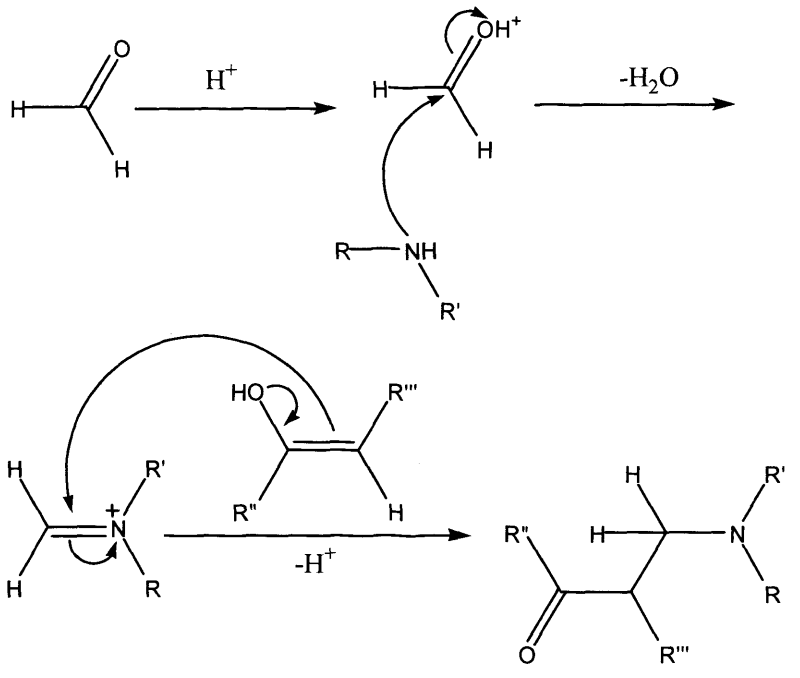

Scheme 2.4: Acid catalysed Mannich reaction.

2.1.1.4 Epoxide chemistry

Epichlorohydrin is one of the main building blocks used in this chapter. It is often used in organic synthesis as has been demonstrated recently by Roy *et al.*[5] in the addition of epichlorohydrin to a range of Morita-Baylis-Hillman adducts in the synthesis of δ-lactones; and by Lee *et al.*[6] in the preparation of pregabalin.

Epoxides, sometimes called oxiranes, were first isolated by Wurtz in 1854[7] and since then have been extensively studied due to their high reactivity. Epoxides are generally reactive species due to the highly strained nature of the three membered ring, this arises from poor overlap between the orbitals forming bonds inside the ring. The internal bond angles are 60° instead of the ideal tetrahedral angle (for carbon) of 109°28', this means that each carbon has about '49° of strain' which is a significant thermodynamic driving force for the ring opening process. However, the C-Cl bond of epichlorohydrin also possesses some electrophilic character, this gives rise to a second electrophilic centre for this class of halo-epoxide such as epichlorohydrin, the two electrophilic centres available to attack as shown in scheme 2.5. Fortunately, in the case of epichlorohydrin, attack via the 'b' route occurs to a lesser extent, such that the effects can usually be ignored.

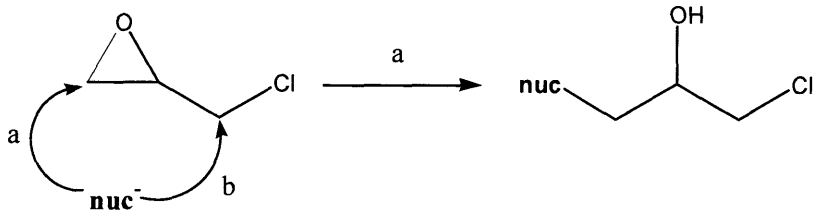

Scheme 2.5: The two sites available for nucleophilic attack on epichlorohydrin. However the predominant site is 'a', the 2-hydroxy, 3-propyl group formed is shown.

Upon attack of a secondary amine on the epoxide of epichlorohydrin, the product formed is the 2-hydroxy-3-chloropropyl group as shown. These species are sensitive to heat, as often upon heating the alkoxide ion is closed down to eliminate Cl^- forming a new epoxide which is also an electrophilic centre and can also be susceptible to nucleophilic attack.

2.1.1.5 Tacn chemistry

1,4,7-triazacyclononane (tacn) has an extremely rich chemistry for a macrocycle, partly due to the fact that it is a small, tridentate ligand that binds to most metals in an η^3 fashion. The central cavity formed by the ring is too small for most metals to fit inside in an equatorial manner, thus it tends to form a cis site capping configuration, leaving space for other ligands to attach to the metal centre. As expected, due to the macrocyclic effect, the thermodynamic stabilities of tacn complexes exceed those of the analogous open chain complexes (i.e. those of diethylenetriamine).

The first reported synthesis of tacn was in 1972 by Koyama and Yoshino[8] by cyclisation of *N,N',N''*-tris(p-toluenesulfonyl)diethylene-triamine and 1,2-dibromoethane (although it should be noted that Peacock *et al*[9] reported the synthesis of the di-tosylate of tacn in 1937). This was carried out in high dilution to avoid polymerisation to obtain low yields of *N,N',N''*-tris(p-toluenesulfonyl)-1,4,7-triazacyclononane.

The group then went on to study the complexation of tacn with cobalt to form Co^{3+} bis-tacn sandwich type complexes, and tacn(Co)tris halide complexes shown in fig. 2.1. This synthesis however was inefficient and it wasn't until 1974 when Richman and Atkins[10] reported a simple, general synthesis of 9 to 21 membered saturated macrocycles containing 3 to 7 heteroatoms (including tacn) that the exploration of this type of ligand on a large scale became plausible. The tacn used in this project was prepared using the methods described in the original synthesis by Richman *et al.*

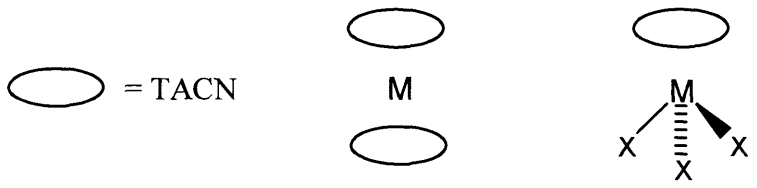

Fig. 2.1: Early studies of tacn by Koyama and Yoshino involved the complexation of tacn into 'sandwich' complexes (left) and 'piano stool' complexes (right).[8]

Since then there has been a great deal of interest in the chemistry of this macrocycle. Complexes of the type $(tacn)MX_3$ where X is a monodentate ligand such as X^-, CO or OH_2 have been well studied, partly due to their readiness to form. Also, the (tacn)M unit is kinetically inert leaving the other coordination sites readily available for substitution[11]. To date there have been over 1050 publications involving tacn. Two of the more recent ones will be discussed.

In 2007 Yan *et al.*[12] described the use of tacn in the synthesis of novel dinuclear copper(II) and zinc(II) complexes in which the metal centres are bound to each other via an oxo bridge, the ligand is shown in fig. 2.2. This was with the aim of developing an artificial nuclease. It proved that the two complexes are able to cleave DNA.

Liu and co workers,[13] in 2008, prepared an *N,N',N"*tri-functionalised tacn ligand (fig. 2.1) that is capable of forming complexes with gadolinium(III), indium(III), iron(III) and copper(II) with a view to develop new radio labelling systems. They found that the ligand is capable of binding metals with a wide range of ionic radii, this is attributable to the flexibility of the ligand.

These two studies show the relative versatility of tacn in coordination chemistry, since it was first prepared, it has become an extremely useful component in the field of macrocyclic ligand design.

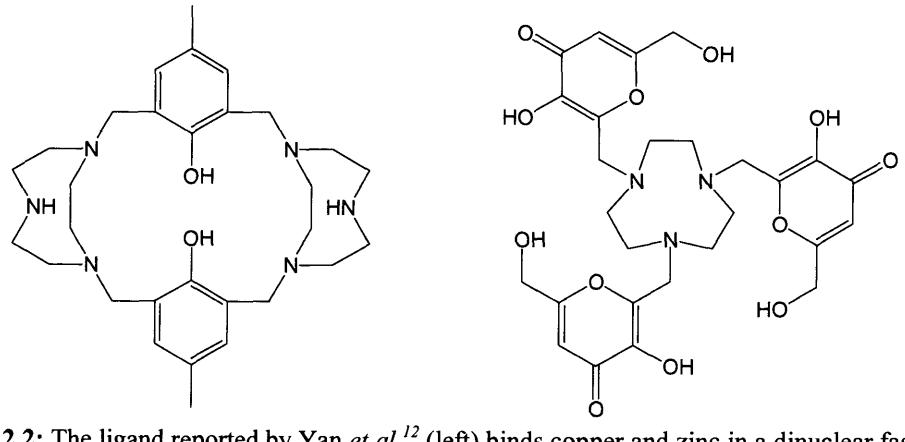

Fig. 2.2: The ligand reported by Yan *et al.*[12] (left) binds copper and zinc in a dinuclear fashion, the ligand synthesised by Liu *et al.*[13] (right) binds many 1st row transition metals of varying ionic radii.

2.2 Experimental

2.2.1 Preparation and purification of solvents and reagents

Several compounds prepared during the course of this research were only accessible *via* certain commercially unavailable precursors. Such starting materials have been prepared from readily available reagents as described in the following tables. Some of the commercially available reagents were purchased and used as supplied without further purification. However many starting materials and solvents required purification prior to use. The sources and necessary methods of purification for the various compounds used are found in table 2.1.

Table 2.1: Chemical suppliers and purification methods

Compound	**Source**	**Quoted Purity**	**Method**
Reagents			
Chloroacetyl chloride	Sigma-Aldrich	99%	Used as supplied
3-Chloro-2-(chloromethyl)prop-1-ene	Sigma-Aldrich	99%	Used as supplied
$CoCl_2$	Sigma-Aldrich	97%	Used as supplied
m-CPBA	Sigma-Aldrich	77%	Used as supplied
$CrCl_3$	Sigma-Aldrich	99%	Used as supplied
$Cu(ClO_4)_2 \cdot 6H_2O$	Sigma-Aldrich	97%	Used as supplied
$Cu(ClO_4)_6$	Sigma-Aldrich	98%	Used as supplied
R, R-1,2-Diaminocyclohexane	Sigma-Aldrich	98%	Used as supplied
R-Epichlorohydrin	Sigma-Aldrich	99%	Used as supplied

Homopiperazine	Sigma-Aldrich	98%	Used as supplied
Hydrochloric acid	Sigma-Aldrich	37%	Used as supplied
3,5-di-*tert*-butyl-2-hydroxybenzaldehyde	Sigma-Aldrich	98%	Used as supplied
R-MBA	Sigma-Aldrich	99%	Used as supplied
S-MBA	Sigma-Aldrich	99%	Used as supplied
1-Methyl homo piperazine	Sigma-Aldrich	98%	Used as supplied
2-Methyl-styrene	Sigma-Aldrich	99%	Used as supplied
4-Methyl-styrene	Sigma-Aldrich	99%	Used as supplied
$Mn(ClO_4)_2.6H_2O$	Sigma-Aldrich	95%	Used as supplied
NH_4PF_6	Sigma-Aldrich	95%	Used as supplied
$NiCl_2.6H_2O$	Sigma-Aldrich	95%	Used as supplied
2-Nitrobenzene sulfonyl chloride	Sigma-Aldrich	95%	Used as supplied
Paraformaldehyde	Sigma-Aldrich	95%	Used as supplied
p-tert-Butyl phenol	Sigma-Aldrich	98%	Used as supplied
Potassium carbonate	Sigma-Aldrich	98%	Used as supplied
Sodium hydroxde	Sigma-Aldrich	99%	Used as supplied
Sodium iodide	Sigma-Aldrich	99%	Used as supplied
Sodium thiosulfate	Sigma-Aldrich	99%	Used as supplied
Styrene	Sigma-Aldrich	99%	Used as supplied
TMS	Sigma-Aldrich	99.99%	Used as supplied

Triethylamine	Sigma-Aldrich	98%	Used as supplied
$Zn(ClO_4)6.nH2O$	Sigma-Aldrich	95%	Used as supplied
Solvents			
Acetonitrile	Fisher	99+%	Heated under reflux over CaH_2 followed by distillation
Dichloromethane	Fisher	99+%	Heated under reflux over CaH_2 followed by distillation
Diethyl Ether	Fisher	99+%	Heated under reflux over sodium followed by distillation
Ethanol	Fisher	99+%	Used as supplied
Hexanes	Fisher	99+%	Heated under reflux over potassium followed by distillation
Methanol	Fisher	99+%	Used as supplied
Toluene	Fisher	99+%	Heated under reflux over sodium followed by distillation
Deuerated Solvents			
Acetonitrile-d_3	Goss	99.8%	Used as supplied
Chloroform-d	Goss	99.8%	Used as supplied
Dichloromethane-d_2	Goss	99.8%	Used as supplied
Deuterium Oxide	Goss	99.9%	Used as supplied

DMSO-d_6	Goss	99.5%	Used as supplied

2.2.2 Synthetic experimental

Preparation of 1,4-bis-2-nitrophenylsulfonyl -1,4,7-triazacyclononane. (1')

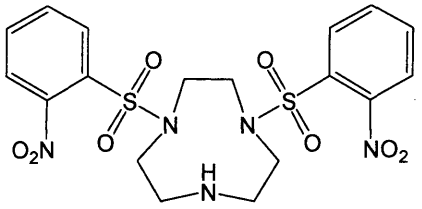

A solution of 1,4,7-triazacyclononane trihydrobromide (10.0g, 27 mmol) in water (50 ml) was added to a solution of NaOH (5 equivalents, 5.36g) in water (5 ml). 2-nitrobenzene sulfonyl chloride in ether (1.5dm^3) was added in one portion and the resulting mixture was stirred vigorously for two hours. The white precipitate was filtered and washed with large quantities of water to yield an off-white powder which was recrystallised from hot acetone yielding 8.6g, (64%). δ_H (CD_3CN): 2.95 (m, 4H, $S(O_2)NCH_2CH_2NS(O_2)$); 3.25-3.29 (m, 4H, B $S(O_2)NCH_2$); 3.68 (s, 4H, $S(O_2)NCH_2CH_2$); 7.55 (m, 2H, CCH); 7.65 (m, 4H, CCHCHCH); 7.85 (dd, 2H, $CC(NO_2)CH$, J_{HH} = 7.52, J_{HH} = 1.72). δ_C (CD_3CN): 48.8, 52.3, 53.6, 124.3, 130.3, 131.8, 131.9, 133.8, 148.6. IR (KBr disc, cm^{-1}): 2924(m), 1681(b), 1540(s), 1462(s), 1376(s), 1343(s), 1163(m).). MS(EI), MH^+ exact mass (calc.) *m/z* 500.0912 *(obs.)* 500.0905.

Preparation of N,N',N''-(1,4,7-triazonane)(bis N,N'-toluenesulfonyl) (N''-chloroethanone). (2)

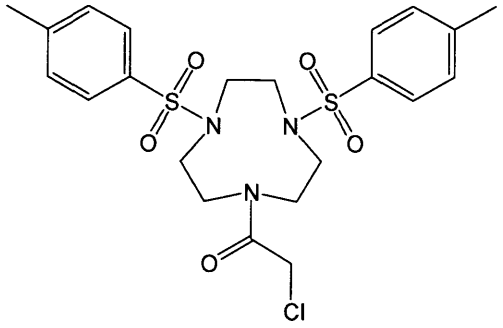

2 equivalents of chloroacetyl chloride (91 mg, 0.80 mmol) were added to a solution of 1,4-ditoluenesulfonyl-1,4,7-triazonane[14] in DCM (175 mg, 0.40 mmol) containing

a suspension of 2 equivalents of potassium carbonate (110 mg, 0.80 mmol). The mixture was stirred for 2 hours. The solution was filtered, the solvent and excess chloroacetyl chloride was removed under reduced pressure to yield a white solid film. δ_H (400.1 MHz, 25 °C, $CDCl_3$): δ 2.41 (s, 6H, CH_3), 3.38-3.84 (m, 12H, NCH_2), δ 4.16-4.28 (s, 2H, $C(O)CH_2$), δ 7.45-7.92 (m, 10H, Ar). ^{13}C NMR: (100.6 MHz, 25 °C, $CDCl_3$) δ 20.2, 49.6, 50.4, 50.2, 50.3, 51.5, 52.9, 123.3, 129.1, 129.6, 131.0, 133.3, 133.5, 147.5, 167.2. IR: (Nujol, cm^{-1}) 1659(s), 1588(s), 1545(s), 1458(b) and 1364(b). MS(EI), MH^+ exact mass (*calc.*) *m/z* 513.1159 *m/z (obs.)* 513.1161.

Preparation of N,N',N''-(1,4,7-triazonane)(bis 2-nitrophenylsulfonyl) (N''-chloroethanone). (2')

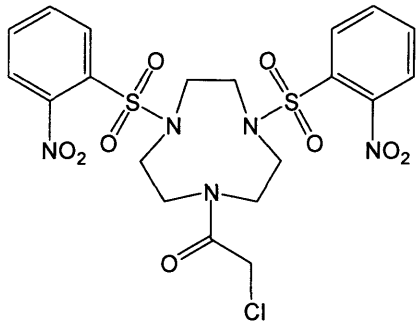

2 equivalents of chloroacetyl chloride (91 mg, 0.80 mmol) were added to a solution of 1,4-bis-2-nitrophenylsulfonyl -1,4,7-triazacyclononane, 1', in DCM (200 mg, 0.40 mmol) containing a suspension of 2 equivalents of potassium carbonate (110 mg, 0.80 mmol). The mixture was stirred for 2 hours. The solution was filtered, the solvent and excess chloroacetyl chloride was removed under reduced pressure to yield a white solid film. δ_H (400.1 MHz, 25 °C, $CDCl_3$): δ 3.42-3.78 (m, 12H, NCH_2), δ 4.15-4.25 (s, 2H, $C(O)CH_2$), δ 7.54-7.88 (m, 8H, Ar). ^{13}C NMR: (100.6 MHz, 25°C, $CDCl_3$) δ 48.5, 49.4, 50.2, 50.3, 51.5, 52.9, 123.3, 129.1, 129.6, 131.0, 133.3, 133.5, 147.5, 167.2. IR: (Nujol, cm^{-1}) 1655(s), 1588(s), 1543(s), 1454(b) and 1374(b). MS(EI), MH^+ exact mass (*calc.*) *m/z* 575.0547 *(obs.)* 575.0544.

Preparation of 1,1',1''-(1,4,7-triazonane-1,4,7-triyl)tris(2-(4,7-ditoluenesulfonyl-1,4,7-triazonan-1-yl)ethanone). (3)

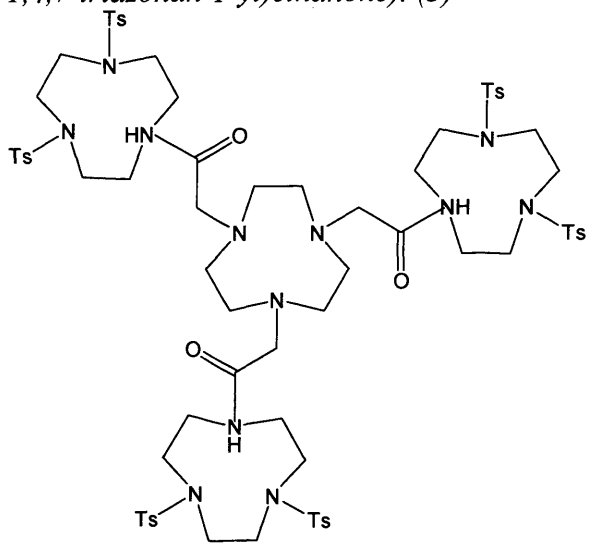

1,4,7-Triazacyclononane (129 mg, 1 mmol) in acetonitrile (20 ml) was added to 4 equivalents of compound **2** (2.05 g, 4 mmol) with a trace of sodium iodide. The mixture was stirred for 72 hours. The solution was filtered and solvent removed to leave an off white solid, this was purified under flash column conditions using a solvent system of 95% $CHCl_3$, 4% MeOH and 1% NEt_3, Rf = 0.6. The solvent was removed to yield 894 mg (57%) of an white solid. δ_H (400.1 MHz, 25°C, d^6DMSO): 2.45 (s, 18H, CH_3), 3.02 (s, 12H, NCH_2), 3.05 (s, 12H, NCH_2), 3.46 (s, 12H, NCH_2), 3.52 (m, 18H, NCH_2, $COCH_2$), 7.42 (d, 12H, Ar), 7.74 (d, 12H, Ar), δ_C (100.6 MHz, 25°C, d^6DMSO) 21.2, 47.3, 50.8, 51.2, 56.1, 57.3, 79.9, 127.5, 129.1, 135.2, 143.2, 171.1. IR (KBr disc, cm^{-1}), 2955(s), 1638(s), 1338(s) and 1162(m). MS(EI), MH^+ exact mass (*calc.*) *m/z* 1561.5521 *(obs.)* 1561.5484.

Preparation of N,N',N''-(1,4,7-triazonane-1,4,7-triyl)tris(2-(4,7-nitrophenylsulfonyl - 1,4,7-triazonan-1-yl)ethanone). (3')

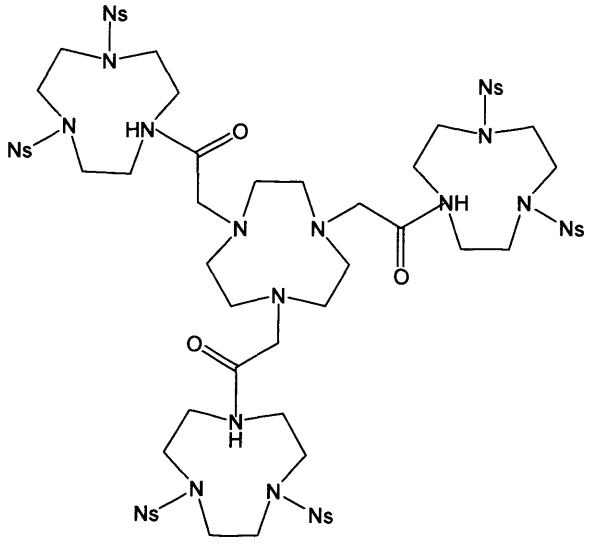

1,4,7-Triazacyclononane (129 mg, 1 mmol) in acetonitrile (20 ml) was added to 4 equivalents of compound **2'** (2.3 g, 4 mmol) with a trace of sodium iodide, this was stirred for 72 hours. The solution was filtered and solvent removed to leave an off-white solid, this was purified under flash column conditions using a solvent system of 95% $CHCl_3$, 4% MeOH and 1% NEt_3, Rf = 0.6. The solvent was removed to yield 851 mg (49%) of a white solid. δ_H (400.1 MHz, 25°C, d_6DMSO): 2.95 (s, 12H, NCH_2), 3.09 (s, 12H, NCH_2), 3.43 (s, 12H, NCH_2), 3.50 (m, 18H, NCH_2, $COCH_2$), 7.38-7.85 (m, 18H, Ar), δ_C (100.6 MHz, 25°C, d_6DMSO) 48.9, 52.3, 51.0, 56.9, 129.8, 131.8, 132.3, 133.4, 147.5, 166.3. IR (KBr disc, cm^{-1}), 2962(s), 1652(s), 1342(s) and 1142(m). MS(EI), MH^+ exact mass (*calc.*) *m/z* 1608.6381 *(obs.)* 1608.6324.

*Preparation of N,N',N'',N'''-(1,4,7,10-tetraazacyclododecane-1,4,7,10-tetrayl) tetrakis(2-(4,7-ditoluenesulfonyl-1,4,7-triazonan-1-yl)ethanone). (**4**)*

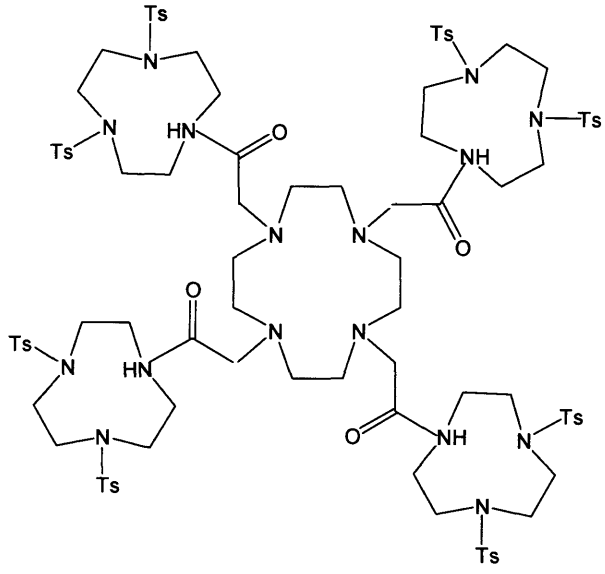

1,4,7,10-Tetraazacyclododecane (172 mg, 1 mmol) in acetonitrile (20 ml) was added to 5 equivalents of compound **2** (2.56 g, 5 mmol) with a trace of sodium iodide. The mixture was stirred for 72 hours. The solution was filtered and solvent removed to leave an off white solid, this was purified under flash column conditions using a solvent system of 95% $CHCl_3$, 4% MeOH and 1% NEt_3, Rf = 0.45. The solvent was removed to yield 956 mg (47%) of a white solid (956 mg, 47%). δ_H (400.1 MHz, 25 °C, d_6DMSO): 2.45 (s, 24H, CH_3), 3.02 (s, 16H, NCH_2), 3.05 (s, 16H, NCH_2), 3.46 (s, 16H, NCH_2), 3.52 (m, 24H, NCH_2, $COCH_2$), 7.42 (d, 16H, Ar), 7.74 (d, 16H, Ar), δ_C (100.6 MHz, 25 °C, d_6DMSO) 21.0, 47.0, 50.1, 51.5, 58.3, 59.6, 80.4, 127.2,

130.0, 136.5, 144.5, 172.1. IR (KBr disc, cm^{-1}), 2958(s), 1642(s), 1346(s) and 1178(m). MS(EI), MH^+ exact mass (*calc.*) *m/z* 2080.7256 *(obs.)* 2080.7302.

Preparation of 1,1',1'',1'''-(1,4,7,10-tetraazacyclododecane-1,4,7,10-tetrayl) tetrakis(2-(4,7-nitrophenylsulfonyl-1,4,7-triazonan-1-yl)ethanone). ***(4')***

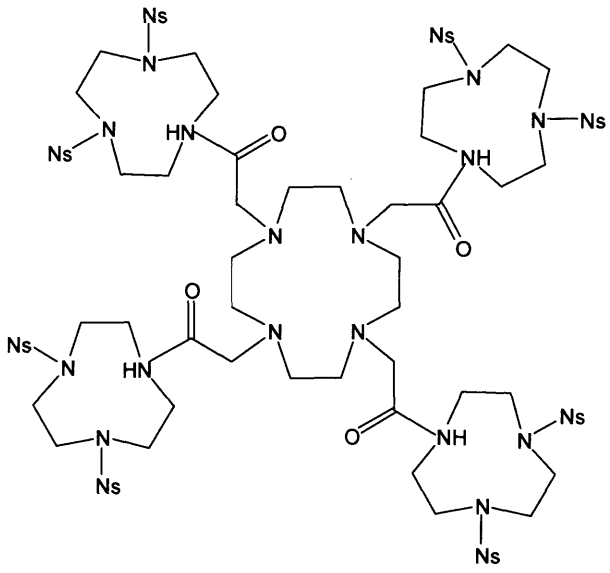

1,4,7,10-Tetraazacyclododecane (172 mg, 1 mmol) in acetonitrile (20 ml) was added to 5 equivalents of compound **2'** (2.88 g, 5 mmol) with a trace of sodium iodide. The mixture was stirred for 72 hours. The solution was filtered and solvent removed to leave an off white solid, this was purified under flash column conditions using a solvent system of 95% $CHCl_3$, 4% MeOH and 1% NEt_3, Rf = 0.45. The solvent was removed yielding 1.01 g (43%) of a white solid (1.01 g, 43%). δ_H (400.1 MHz, 25 °C, d_6DMSO) 3.00 (s, 16H, NCH_2), 3.14 (s, 16H, NCH_2), 3.56 (s, 16H, NCH_2), 3.53 (m, 24H, NCH_2, $COCH_2$), 7.41-7.90 (m, 24H, Ar), δ_C (100.6 MHz, 25 °C, d_6DMSO) 48.8, 53.3, 50.0, 52.8, 127.6, 131.2, 131.6, 132.0, 149.2, 169.3. IR (KBr disc, cm^{-1}), 2958(s), 1642(s), 1346(s) and 1178(m). MS(EI), MH^+ exact mass (*calc.*) *m/z* 2328.4811 *(obs.)* 2328.4886.

Preparation of N,N',N''-(1,4,7-triazonane-1,4,7-triyl)tris(2-chloroethanone). ***(5)***

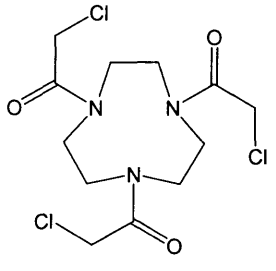

1,4,7-triazacyclononane.3HBr (2 g, 5.4 mmol) in water (20 ml) was mixed with sodium hydroxide (1.5 g, 38 mmol), the solution was cooled to 0 °C. To the solution was added chloroacetyl chloride (6.0 g, 53 mmol) in dichloromethane (30 ml). The resulting mixture was vigorously stirred for 6 hours. The dichloromethane layer was washed with water (3x20 ml), dried with magnesium sulphate and the solvent removed. The product was recrystallised from boiling ethanol to yield 0.56 g (30%) of white needles. δ_H (400.1 MHz, 25 °C, $CDCl_3$): 3.50 (s, 6H, CH_2N), 3.71 (m, 6H, CH_2N), 4.12 (s, 6H, CH_2CO). δ_C (100.6 MHz, 25 °C, $CDCl_3$): 41.2, 48.8, 51.1 and 168.4. IR (KBr disc, cm^{-1}): 2949 (b), 1659 (b), 1461 (s), 1412 (s), 1360 (s). MS(EI), MH^+ exact mass (*calc.*) *m/z* 358.0492 *(obs.)* 358.0475.

*Preparation of N,N',N''-(1,4,7-triazonane-1,4,7-triyl)tris(2-(4,7-toluenesulfonyl - 1,4,7-triazonan-1-yl)ethanone). (**6**)*

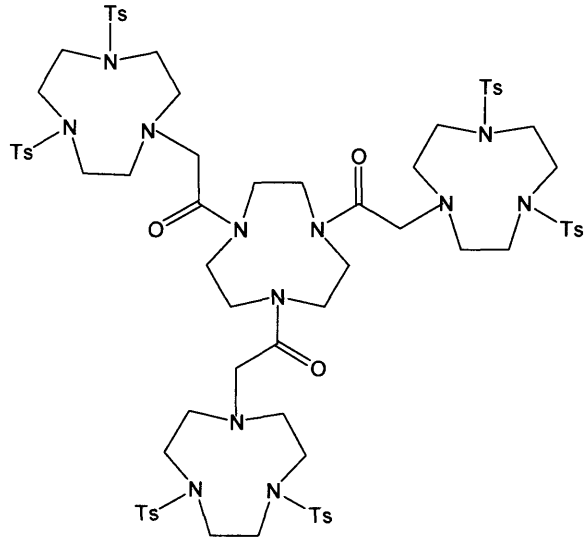

1,4,7-triazacyclononane tris acetyl chloride (203 mg, 0.57 mmol) in acetonitrile (50 ml) was stirred with 4 equivalents of 1,4-ditoluenesulfonyl-1,4,7-triazonane (997 mg, 2.28 mmol) and a trace of sodium iodide for 72 hours. The solution was filtered and solvent removed to leave a yellow solid, this was purified under flash column conditions using a solvent system of 95% $CHCl_3$, 4% MeOH and 1% NEt_3, Rf = 0.5. The solvent was removed yielding 0.55 g (62%) of a white solid. δ_H (400.1 MHz, 25 °C, d_6DMSO): 2.40 (s, 18H, CH_3), 2.95 (s, 12H, NCH_2), 3.09 (s, 12H, NCH_2), 3.43 (s, 12H, NCH_2), 3.50 (m, 18H, NCH_2, $COCH_2$), 7.42 (d, 12H, Ar), 7.70 (d, 12H, Ar), δ_C (100.6 MHz, 25 °C, d_6DMSO) 21.5, 47.6, 50.1, 51.0, 56.8, 57.0, 79.7, 127.5,

129.6, 135.1, 143.2 and 171.0. IR (KBr disc, cm^{-1}), 2950(s), 1645(s), 1335(s) and 1158(m). MS(EI), MH^+ exact mass (*calc.*) *m/z* 1561.5521 *(obs.)* 1561.5475.

Preparation of N,N',N''-(1,4,7-triazonane-1,4,7-triyl)tris(2-(4,7-nitrophenylsulfonyl - 1,4,7-triazonan-1-yl)ethanone). ***(6')***

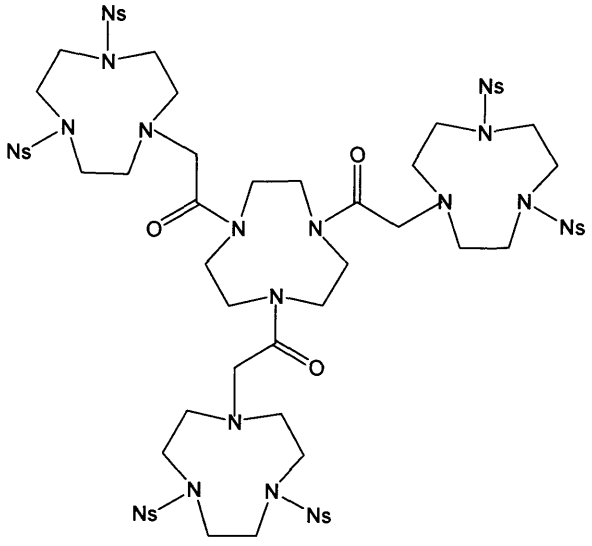

*N,N',N''*trisacetylchloride 1,4,7-triazacyclononane (253 mg, 0.90 mmol) in acetonitrile (50 ml) was stirred with 4 equivalents of 1,4-bis(2-nitrophenylsulfonyl)-1,4,7-triazonane (1.57 g, 3.60 mmol) and a trace of sodium iodide for 72 hours. The solution was filtered and solvent removed to leave a yellow solid, this was purified under flash column conditions using a solvent system of 95% $CHCl_3$, 4% MeOH and 1% NEt_3, Rf = 0.5. The solvent was removed to yield 0.62 g (43%) of a white solid. δ_H (400.1 MHz, 25 °C, d_6DMSO): 2.84 (s, 12H, NCH_2), 3.12 (s, 12H, NCH_2), 3.36 (s, 12H, NCH_2), 3.60 (m, 18H, NCH_2, $COCH_2$), 7.31-7.87 (m, 18H, Ar), δ_C (100.6 MHz, 25 °C, d_6DMSO) 49.2, 53.8, 54.2, 56.0, 130.2, 131.4, 132.0, 134.7, 148.6, 166.0. IR (KBr disc, cm^{-1}), 2962(s), 1652(s), 1342(s) and 1142(m). MS(EI), MH^+ exact mass (*calc.*) *m/z* 1608.6381 *(obs.)* 1608.6431.

Preparation of N,N',N'',N'''-(1,4,7,10-tetraazacyclododecane-1,4,7,10-tetrayl) tetrakis(2-chloroethanone). (7)

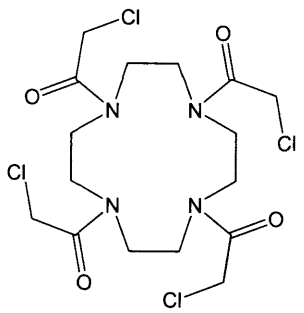

1,4,7,10-tetraazacyclododecane (1 g, 5.8 mmol) in water (20 ml) was stirred with sodium hydroxide (4.64 g, 116 mmol) and the solution was cooled to 0 °C. To the solution was added chloroacetyl chloride (13 g, 116 mmol) in dichloromethane (30 ml). The resulting mixture was vigorously stirred for 6 hours. The resulting white precipitate was filtered and washed with di-ethyl ether to yield 1.75 g (63%) of a white powder. δ_H (400.1 MHz, 25 °C, d_6DMSO): 3.65 (s, 16H, CH_2N), 4.51 (s, 8H, CH_2Cl). δ_C (100.6 MHz, 25 °C, d_6DMSO): 42.1, 46.8, 54.9, 166.7. IR (KBr disc, cm^{-1}): 3007 (m), 2949 (m), 1665 (s), 1475 (s), 1428 (b), 1321 (m). MS(EI), MH^+ exact mass *(calc.)* *m/z* 477.0630 *(obs.)* 477.0634.

Preparation of N,N',N'',N'''-(1,4,7,10-tetraazacyclododecane-1,4,7,10-tetrayl) tetrakis(2-(4,7-ditoluenesulfonyl-1,4,7-triazonan-1-yl)ethanone). ***(8)***

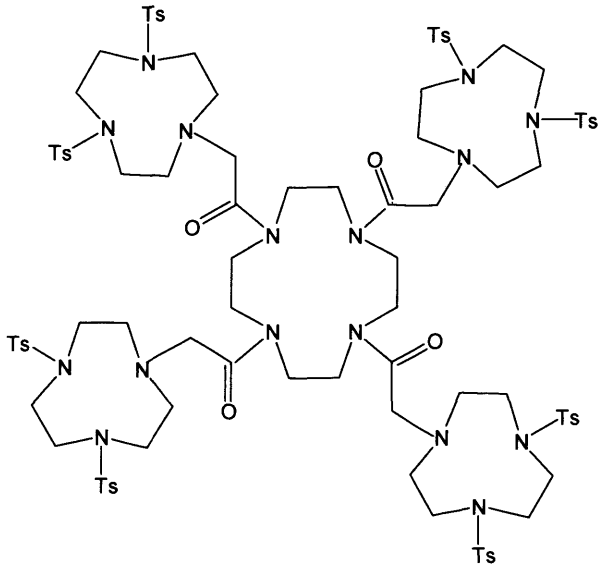

Compound **7** (239 mg, 0.5 mmol) in acetonitrile (40 ml), was added to 4 equivalents of 1,4-ditoluenesulfonyl-1,4,7-triazonane (874 mg, 2 mmol) and a trace of sodium iodide for 72 hours. The solution was filtered and solvent removed to leave a yellow solid, this was purified under flash column conditions using a solvent system of 95% $CHCl_3$, 4% MeOH and 1% NEt_3, Rf = 0.6. The solvent was removed yielding 0.45 g (43%) of a white solid. δ_H (400.1 MHz, 25 °C, d_6DMSO): 2.42 (s, 24H, CH_3), 2.85 (s, 16H, NCH_2), 3.05 (s, 16H, NCH_2), 3.50 (s, 16H, NCH_2), 3.65 (m, 24H, NCH_2, $COCH_2$), 7.42 (d, 16H, Ar), 7.74 (d, 16H, Ar), δ_C (100.6 MHz, 25 °C, d_6DMSO) 21.0, 47.0, 50.1, 51.8, 59.6, 60.2, 80.8, 127.2, 131.2, 139.6, 145.6, 174.4. IR (KBr disc, cm^{-1}), 2958(s), 1642(s), 1346(s) and 1178(m). MS(EI), MH^+ exact mass *(calc.)* *m/z* 2080.7256 *(obs.)* 2080.7214.

*Preparation of 1,1',1'',1'''-(1,4,7,10-tetraazacyclododecane-1,4,7,10-tetrayl) tetrakis(2-(4,7-nitrophenylsulfonyl-1,4,7-triazonan-1-yl)ethanone). (**8'**)*

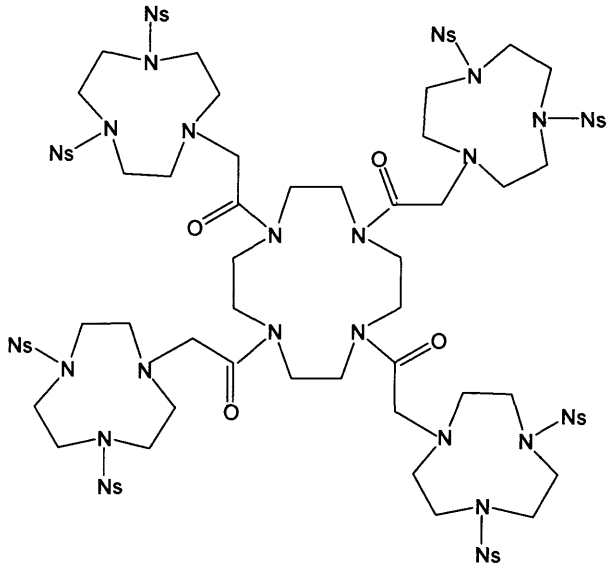

Compound **7** (239 mg, 0.5 mmol) in acetonitrile (40 ml) was added to 4 equivalents of 1,4-bis(2-nitrophenylsulfonyl)-1,4,7-triazonane (998 mg, 2 mmol) and a trace of sodium iodide. The mixture was stirred for 72 hours and filtered. The solvent was removed to leave a yellow solid, this was purified under flash column conditions using a solvent system of 95% $CHCl_3$, 4% MeOH and 1% NEt_3, Rf = 0.6. The solvent was removed yielding 0.45 g (43%) of a white solid. δ_H (400.1 MHz, 25 °C, d_6DMSO) 3.00 (s, 16H, NCH_2), 3.36 (s, 16H, NCH_2), 3.56 (s, 16H, NCH_2), 3.53 (m, 24H, NCH_2, COCH_2), 7.39-7.85 (m, 24H, Ar), δ_C (100.6 MHz, 25 °C, d_6DMSO) 49.0, 50.0, 54.7, 57.9, 126.7, 131.2, 131.9, 135.1, 152.4, 171.5. IR (KBr disc, cm^{-1}), 2958(s), 1642(s), 1346(s) and 1178(m). MS(EI), MH^+ exact mass (*calc.*) *m/z* 2328.4811 *(obs.)* 2328.4875.

*Preparation of N,N',N''-(1,4,7-triazonane-1,4,7-triyl)tris(2-(1-methyl homopiperazine)ethanone). (**9**)*

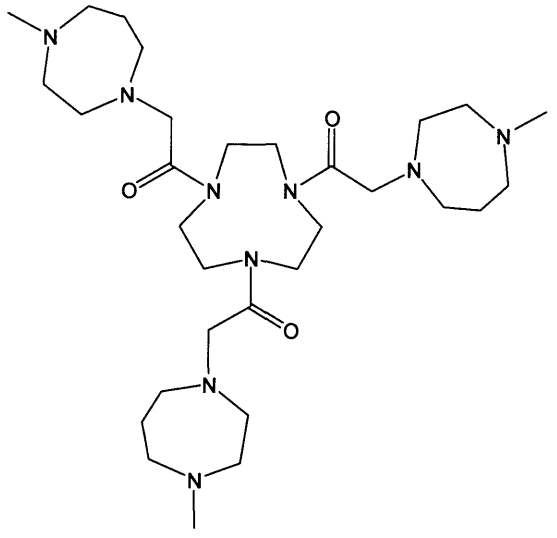

*N,N',N"*trisacetylchloride 1,4,7-triazacyclononane (220 mg, 0.6 mmol) in acetonitrile (50 ml) was stirred with 4 equivalents of 1-methyl homo piperazine (281 mg, 2.4 mmol) and a trace of sodium iodide for 8 hours. The solution was filtered and the solvent and excess 1-Me homo piperazine was removed *in vacuo* yielding 102 mg (29%) of a hygroscopic oil. δ_H (400.1 MHz, 25 °C, d_6DMSO): 2.05 (s, 9H, CH_3), 2.91 (s, 12H, NCH_2), 3.24-3.44 (m, 36H, CH_2). δ_C (100.6 MHz, 25 °C, d_6DMSO) 23.2, 42.8, 43.1, 46.5, 50.8, 52.7, 54.6, 57.7, 61.0, 172.4. IR (KBr disc, cm^{-1}), 30210(s), 1624(s), 1425(s) and 1274(m). MS(EI), MH^+ exact mass (*calc.*) *m/z* 592.4663 *(obs.)* 592.4687.

Preparation of hexa-amide 4,4',4"-(2,2',2"-(1,4,7-triazonane-1,4,7-triyl)tris(2-oxoethane-2,1-diyl))tris(1,4,7-triazonane-1-carbaldehyde). ***(11)***

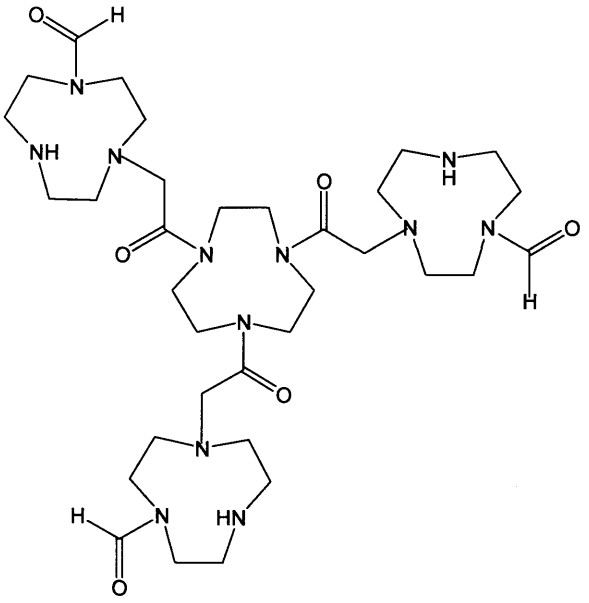

*N,N',N"*trisacetylchloride 1,4,7-triazacyclononane (2 g, 5.9 mmol) in acetonitrile (30 ml) was added to orthoamide, **10**,[15] (2.56 g, 19 mmol) in acetonitrile (20 ml). The solution was heated at reflux for 12 hours. The solution was allowed to cool and di-ethyl ether (50 ml) was added, the precipitate was filtered, this was dissolved in methanol (50 ml) and hydrochloric acid (5 ml). The mixture was then stirred for a further hour and di-ethyl ether (100 ml) was added dropwise and the white precipitate was filtered and washed with hexanes (20 ml). The product was dried *in vacuo* yielding 3.3 g (63%). δ_H (400.1 MHz, 25 °C, D_2O): 2.50-3.72 (m, 57H, NCH_2), 7.91 (s, 3H, NC*H*O). δ_C (100.6 MHz, 25 °C, d_6DMSO) 44.6, 45.1, 45.8, 47.5, 48.4, 48.8,

49.7, 50.2, 21.6, 53.3, 56.7, 57.7, 166.4, 166.8, 174.3, 174.5. IR (KBr disc, cm^{-1}): 3372 (b), 1636 (m), 1455 (m). MS(EI), MH^+ exact mass (*calc.*) *m/z* 721.4837 *(obs)* 721.4863.

Preparation of N,N,'N''tris(4-tert-butyl-2-phenol)(1,4,7-triazonan-1-ylmethyl). ***(13)***

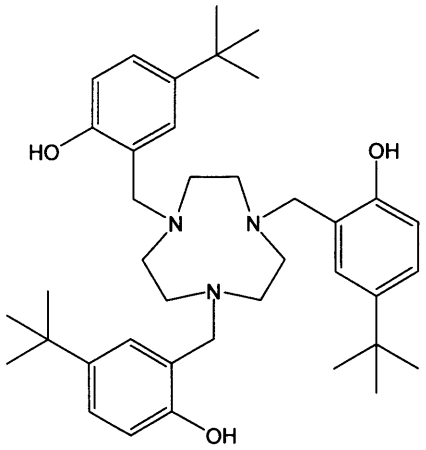

A mixture of 1,4,7-triazacyclononane (0.5 g, 3.9 mmol) and paraformaldehyde (0.36 g, 12 mmol) in methanol (100 ml) was heated under reflux for 2 hours, 20 equivalents of *p-tert*-butyl phenol (11.7 g, 78 mmol) in methanol (200 ml) and 2 drops of hydrochloric acid were added, the resultant mixture was heated a reflux for 3 hours. The white precipitate was filtered and washed with cold methanol (20 ml) yielding 1.3 g (54%). The product required no further purification. δ_H (400.1 MHz, 25 °C, $CDCl_3$): 1.18 (s, 27H, *t*Bu*H*); 2.76 (s, 12H, NCH_2); 3.68 (s, 6H, CCH_2); 6.72 (d, 3H, Ar*H*, *J*=8.23Hz); 6.86 (d, 3H, Ar*H*, *J*=2.32Hz); 7.12 (dd, 3H, Ar*H*, J_1=2.32Hz J_2=8.23Hz). δ_C (100.6 MHz, 25 °C, $CDCl_3$): 31.6, 34.0, 55.5, 63.0, 115.5, 121.2, 125.9, 142.1, 154.9.IR (KBr disc, cm^{-1}): 2961(m), 1699(m), 1617(s), 1503(m), 1463(s), 1393(m). MS(EI), MH^+ exact mass (*calc.*) *m/z* 616.4478 *(obs.)* 616.4506.

*Preparation of N,N,'N''tris(4-tert-butyl-6-1methylhomopiperazine-2-phenol)(1,4,7-triazonan-1-ylmethyl). (**14**)*

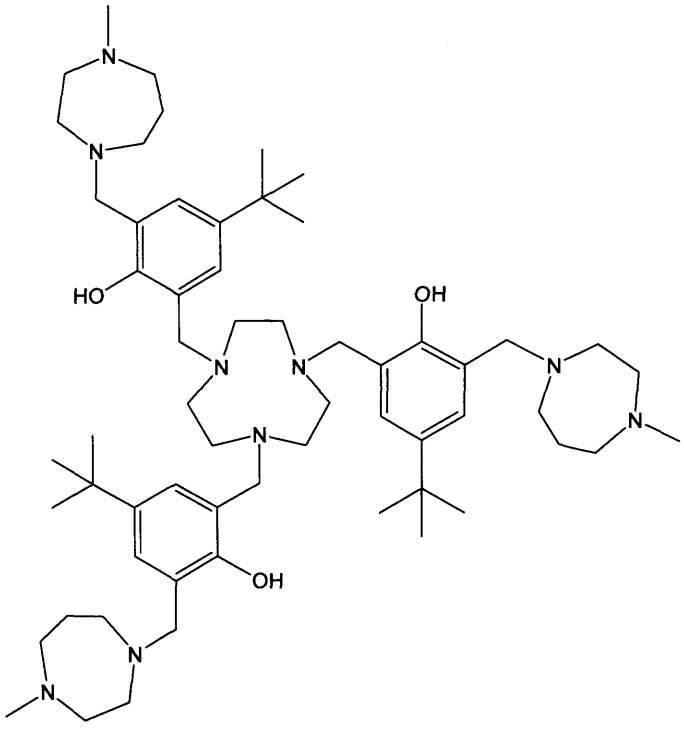

1-Me homo piperazine (334 mg, 2.9 mmol) was heated under reflux with paraformaldehyde (88 mg, 2.9 mmol) in methanol (20 ml) for 2 hours. To this solution was added compound **13** (300 mg, 0.48 mmol) suspended in methanol (10 ml) and 1 drop of hydrochloric acid. This mixture was heated under reflux for 16 hours. The solvent was removed and a small amount analysed by mass spectrometry. MS(EI), MH^+ exact mass (*calc.*) *m/z* 994.7949 (*obs.*) 994.7901. No further analysis was carried out (see section 1.3.2).

*Preparation of 4-tert-butyl-2-[(4-methyl-1,4-diazepan-1-yl)methyl]phenol. (**15**)*

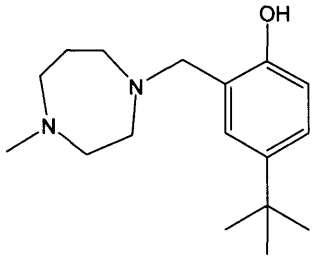

1-Me homo piperazine (114 mg, 1 mmol) was heated under reflux with paraformaldehyde (38 mg, 1.25 mmol) in methanol (20 ml) for 2 hours. To this solution was added *p-tert*-butyl phenol (150 mg, 1 mmol) in methanol (10 ml) and 1 drop of hydrochloric acid. This mixture was heated under reflux for 48 hours, this

was then purified under flash chromatography conditions using a solvent system of 80% $CHCl_3$ and 20% MeOH, Rf = 0.4. The solvent was removed and the product dried *in vacuo* yielding 243 mg (88%). δ_H (400.1 MHz, 25 °C, $CDCl_3$): 1.12 (s, 9H, *t*Bu*H*); 1.67 (s, 3H, NCH_2); 2.05 (s, 2H, CCH_2); 2.35-2.61 (m, 10H, CH_2); 6.81-6.95 (m, 3H, Ar*H*,). δ_C (100.6 MHz, 25 °C, $CDCl_3$): 18.2, 32.1, 38.4.0, 39.4, 40.0, 42.9, 44.1, 47.5, 55.5, 114.1, 118.1, 122.9, 145.1, 148.4, 154.9. IR (KBr disc, cm^{-1}): 2952(m), 1721(m), 1572(s), 1489(s), 1442(b), 1243(m). MS(EI), MH^+ exact mass (*calc.*) *m/z* 277.2280 *(obs.)* 277.2287.

Preparation of 3,3',3''-(1,4,7-triazonane-1,4,7-triyl)tris(1-chloropropan-2-ol). ($L^1.H_3$)

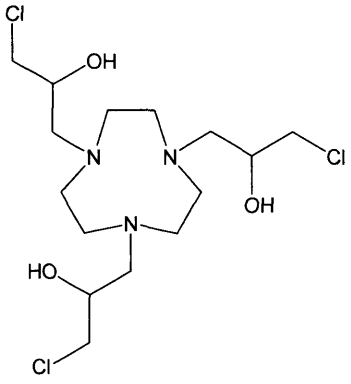

1,4,7-triazacyclononane (129 mg, 1 mmol) in ethanol (20 ml), was added to 4 equivalents of *R*-epichlorohydrin (370 mg, 4 mmol). The solution was stirred at room temperature for 3 hours. The solvent and excess epichlorohydrin was removed *in vacuo* yielding 340 mg (84%) of colourless oil. δ_H (400.1 MHz, 25 °C, $CDCl_3$): 2.88-3.10 (m, 6H, NCH_2CHOH); 3.25 (s, 12H, NCH_2); 3.26-3.48 (m, 6H, CH_2Cl); 3.98-4.09 (m, 3H, C*H*). δ_C (100.6 MHz, 25 °C, $CDCl_3$): 46.7, 49.9, 59.6, 66.4. IR (KBr disc, cm^{-1}): 3018(b), 1615(m), 1504(m), 1434(m), 1086(m). MS(EI), MH^+ exact mass (*calc.*) *m/z* 406.1431 *(obs.)* 406.1426.

*Preparation of 3,3'-(1,4-diazepane-1,4-diyl)bis(1-chloropropan-2-ol). (**16**)*

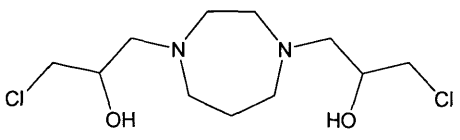

Homopiperazine (100 mg, 1 mmol) in ethanol (10 ml) and 2.3 equivalents of *R*-epichlorohydrin (213 mg, 2.3 mmol) were stirred for 3 hours. The solvent was removed *in vacuo* yielding 247 mg (87%) of a colourless oil. δ_H (400.1 MHz, 25 °C,

$CDCl_3$): 2.14 (s, 3H, NCH_3); 2.72-3.01 (m, 10H, CH_2); 3.25-3.51 (m, 5H, CH_2CHCH_2). δ_C (100.6 MHz, 25 °C, $CDCl_3$): 19.5, 31.2, 46.4, 48.5, 50.2, 57.5, 61.4, 64.5, 76.2. IR (KBr disc, cm^{-1}): 3054(b), 1575(m), 1484(b), 1424(s), 1286(s). MS(EI), MH^+ exact mass (*calc.*) *m/z* 285.1137 *(obs.)* 285.1142.

*Preparation of 3,3'-(1,4-diazepane-1,4-diyl)bis(1-propan-2-ol,3-(1-methylhomopiperazine)). (**17**)*

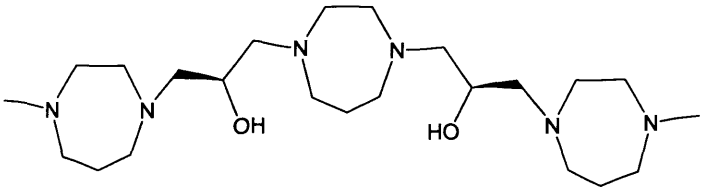

Compound **16** (284 mg, 1 mmol) in dry DCM (50 ml) and potassium carbonate (1.38 g, 10 mmol) was stirred under an inert atmosphere (N_2) for 24 hours. To this mixture was added a solution of 1-Methyl homo piperazine (228 mg, 2 mmol) in methanol (10 ml), the mixture was stirred for 72 hours. The solvent was removed *in vacuo* yielding 334 mg (76%) of a pale yellow oil. δ_H (400.1 MHz, 25 °C, $CDCl_3$): 1.42 (m, 6H, CH_3); 2.76-3.57 (m, 40H, CH_2). δ_C (100.6 MHz, 25 °C, $CDCl_3$): 18.5, 24.1, 25.5, 27.6, 29.1, 46.5, 50.3, 60.1, 64.3. IR (KBr disc, cm^{-1}): 3020(b), 1621(m), 1542(m), 1342(m), 1175(m). MS(EI), MH^+ exact mass (*calc.*) *m/z* 441.3917 *(obs.)* 441.3922.

*Preparation of 6-methylene-1,4-bis(2-toluenesulfonyl)-1,4-diazepane. (**19**)*

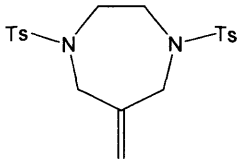

A solution of 3-chloro-2-(chloromethyl)prop-1-ene (139 mg, 1.1 mmol) in DMF (5 ml) was added dropwise to a mixture of di-ts-ethylene diamine (410 mg, 1.1 mmol) and caesium carbonate (1.09 g, 3.3 mmol) in DMF (5 ml). The resulting solution was stirred at 80 °C for 12 hours. The solution was filtered, the solvent removed and the product recrystallised from hot methanol to yield 282 mg (61%) of an off-white powder. δ_H (400.1 MHz, 25 °C, $CDCl_3$): 2.04 (s, 6H, CH_3); 3.62 (s, 4H, CH_2CH_2); 4.24 (s, 4H, NCH_2); 5.25 (s, 2H, CCH_2); 7.42 (m, 4H, ArH); 7.78 (m, 4H, ArH). δ_C (100.6 MHz, 25 °C, $CDCl_3$): 20.5, 49.9, 51.9, 114.7, 125.9, 128.9, 135.0, 141.0,

142.7. IR (KBr disc, cm^{-1}),: 2924 (b), 1598 (m), 1495 (s), 1443 (s), 1337 (m), 1158 (m). MS(EI), MH^+ exact mass (*calc.*) *m/z* 421.1256 *(obs.)* 421.1251.

Preparation of 6-methylene-1,4-bis(2-nitrophenylsulfonyl)-1,4-diazepane. ***(19')***

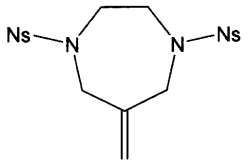

A solution of 3-chloro-2-(chloromethyl)prop-1-ene (5.00 g, 40 mmol) in DMF (500 ml) was added dropwise to a mixture of di-nos-ethylene diamine (17.2 g, 40 mmol) and caesium carbonate (39.0 g, 120 mmol) in DMF (400 ml). The resulting solution was stirred for 12 hours. The solvent was removed and the product recrystallised from hot chloroform to yield 10.8 g (56%) of an off-white powder. δ_H (400.1 MHz, 25 °C, $CDCl_3$): 3.56 (s, 4H, CH_2CH_2); 4.08 (s, 4H, NCH_2); 5.10 (s, 2H, CCH_2); 7.56-7.70 (m, 6H, Ar*H*); 7.92-7.96 (m, 2H, Ar*H*). δ_C (100.6 MHz, 25 °C, $CDCl_3$): 51.6, 53.2, 115.5, 124.4, 130.9, 131.9, 132.6, 134.0, 142.1. IR (KBr disc, cm^{-1}): 3090(m), 1543(s), 1441(s), 1326(b), 1156(b). MS(EI), MH^+ exact mass (*calc.*) *m/z* 483.0644 *(obs.)* 483.0621.

Preparation of 5,8-bis(toluenesulfonyl)-1-oxa-5,8-diazaspiro[2.6]nonane. ***(20)***

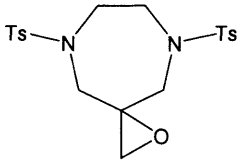

A solution of *m*-CPBA (6.6 g, 37 mmol) in chloroform (200 ml) was added dropwise to a solution of di-ts-6-methylene-1,4-diazepane, compound **19**, (4 g, 9.2 mmol) in chloroform (75 ml) the solution was heated under reflux for 8 hours. The solution was treated with 1M sodium thiosulphate and washed with 0.5M sodium hydroxide, the organic layer was dried and the solvent removed. The product was dissolved in chloroform (150 ml) and precipitated with methanol to yield 2.2 g (55%) of a white powder. δ_H (400.1 MHz, 25 °C, $CDCl_3$): 2.35 (s, 6H, CH_3), 2.74 (s, 2H, OCH_2), 3.31 (s, 4H, NCH_2), 3.40 (s, 4H, NCH_2), 7.20-7.31 (m, 4H, Ar*H*), 7.65-7.74 (m, 4H, Ar*H*). δ_C (100.6 MHz, 25 °C, $CDCl_3$): 21.5, 39.8, 51.8, 52.8, 58.3, 127.0, 130.0, 135.9, 143.9. IR (KBr disc, cm^{-1}): 2923 (b), 1598 (m), 1489 (s), 1442 (s), 1348 (m). MS(EI), MH^+ exact mass (*calc.*) *m/z* 437.1205 *(obs.)* 437.1199.

*Preparation of 5,8-bis(2-nitrophenylsulfonyl)-1-oxa-5,8-diazaspiro[2.6]nonane. (**20'**)*

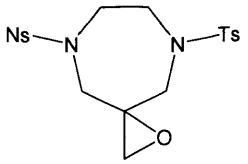

A solution of *m*-CPBA (14.3 g, 83 mmol) in chloroform (300 ml) was added dropwise to a solution of di-nos-6-methylene-1,4-diazepane, compound **19'**, (10.0 g, 21 mmol) in chloroform (100 ml) the solution was heated under reflux for 8 hours. The solution was treated with 1M sodium thiosulphate and washed with 0.5M sodium hydroxide, the organic layer was dried and the solvent removed. The product was then recrystallised from hot chloroform to yield 7.11 g (68%) of a white powder. δ_H (400.1 MHz, 25 °C, $CDCl_3$): 2.83 (s, 2H, OC*H*$_2$); 3.48-3.76 (m, 8H, NC*H*$_2$); 7.58-7.75 (m, 6H, Ar*H*); 7.94-7.99 (m, 2H, Ar*H*). δ_C (100.6 MHz, 25 °C, $CDCl_3$): 51.2, 51.7, 52.6, 123.5, 130.2, 130.9, 131.4, 133.0, 146.9. IR (KBr disc, cm^{-1}): 1543(m), 1442(s), 1341(m), 1125(s), 1073(s). MS(EI), MH^+ exact mass (*calc.*) *m/z* 499.0593 *(obs.)* 499.0603.

*Preparation of 6,6',6''-(1,4,7-triazonane-1,4,7-triyl)tris(methylene)tris(1,4-bis(2-toluenesulfonyl)-1,4-diazepan-6-ol). (**21**)*

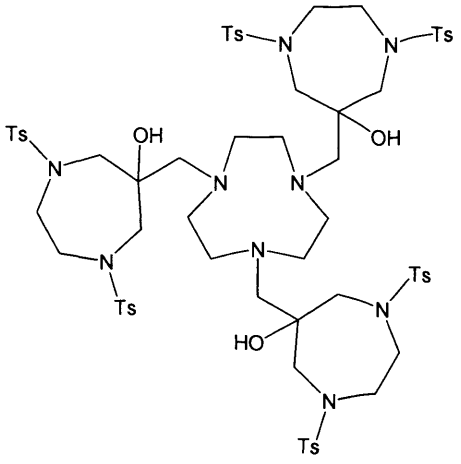

Di-ts-1-oxa-5,8-diazaspiro[2.6]nonane (3.0 g, 6.9 mmol) and 1,4,7-triazacyclononane (296 mg, 2.3 mmol) in ethanol (100 ml) was heated to reflux and stirred at this temperature for 14 days. The solvent was removed *in vacuo* to yield 0.86 g (26%) of a hygroscopic off white solid. δ_H (400.1 MHz, 25 °C, $CDCl_3$): 2.10 (s, 18H, C*H*$_3$), 2.72 (s, 6H, CC*H*$_2$N), 2.93 (s, 12H, C*H*$_2$C*H*$_2$), 3.31-3.84 (m, 24H, C*H*$_2$), 4.06 (s, 3H, O*H*), 7.18-7.35 (m, 12H, Ar*H*), 7.58-7.96 (m, 12H, Ar*H*).δ_C (100.6 MHz, 25 °C,

$CDCl_3$): 24.5, 53.4, 58.9, 62.4, 63.3, 71.3, 127.4, 133.8, 134.9, 138.7, 139.3, 164.2. IR (KBr disc, cm^{-1}),: 3487 (b), 2826 (b), 1548 (m), 1443 (s), 1345 (s), 1184 (m). MS(EI), MH^+ exact mass (*calc.*) *m/z* 1438.3724 *(obs.)* 1438.3696.

Preparation of 6,6',6''-(1,4,7-triazonane-1,4,7-triyl)tris(methylene)tris(1,4-bis(2-nitrophenylsulfonyl)-1,4-diazepan-6-ol). ***(21')***

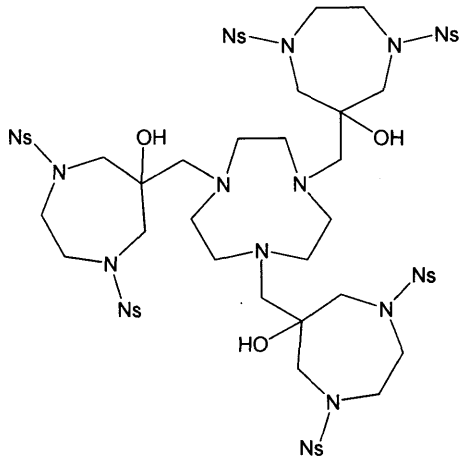

Di-nos-1-oxa-5,8-diazaspiro[2.6]nonane (3.3 g, 6.6 mmol) and 1,4,7-triazacyclononane (281 mg, 2.2 mmol) in acetonitrile (50 ml) and ethanol (10 ml). Was heated to 75 °C and stirred at this temperature for 3 days. The white precipitate was removed and the product recrystallised from boiling acetone to yield 2.1 g (66%) of a white powder. δ_H (400.1 MHz, 25 °C, $CDCl_3$): 2.65 (s, 6H, CCH_2N), 2.87 (s, 12H, CH_2CH_2), 3.42-3.70 (m, 24H, CH_2), 3.98 (s, 3H, O*H*), 7.69-7.78 (m, 18H, Ar*H*), 7.92-8.00 (m, 6H, Ar*H*). δ_C (100.6 MHz, 25 °C, $CDCl_3$): 52.5, 58.5, 60.1, 66.1, 70.2, 125.4, 131.2, 132.5, 133.4, 135.4, 139.3. IR (KBr disc, cm^{-1}),: 3517 (b), 2905 (b), 1550 (m), 1460 (m), 1372 (s), 1158 (m). MS(EI), MH^+ exact mass (*calc.*) *m/z* 1624.2890 *(obs.)* 1624.2961.

2.3 Results and Discussion

2.3.1 Synthesis of ligands *via* amide containing compounds

The first attempt at synthesising a multi nuclear ligand was aimed at connecting four tacn rings together via three ethylene bridges (fig. 2.3). It was envisaged that this could be achieved by utilising the reactivity of amides and secondary amines, once formed, the amides could potentially be reduced and the ligand metallated.

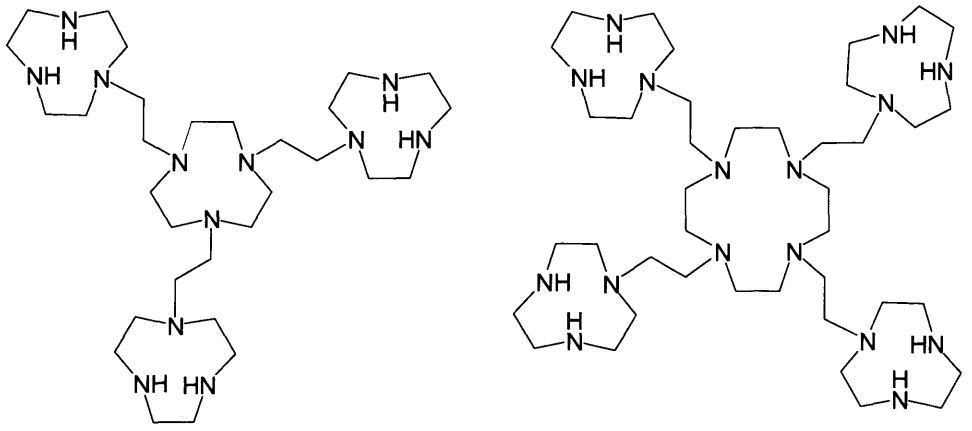

Fig. 2.3: The target molecule contains aza macrocycles connected via ethylene bridges

Compound **2** (scheme 2.6) was synthesised from bis protected tacn, 1, in relatively good yield (typically 50 – 70%); via an *in situ* Finkelstein type reaction in the presence of tacn gave compounds **3** and **3'**. The analogous reaction for cyclen yielded compounds **4** and **4'**.

Multiple attempts to reduce the amides of compounds **3**, **3'**, **4** and **4'** (by the common reagents of B_2H_6[16] and $LiAlH_4$[17]) yielded a mixed product of mono, bis, tris and tetra amides that were inseparable by chromatography. It is believed that the products are too highly basic for effective separation by silica. In light of this, chromatographic separation by reverse phase silica was attempted, but no solvent system was found that would separate the products.

A slightly different approach was simultaneously adopted, compounds **5** and **7** (scheme 2.7) were prepared in a similar manner to compound **2**, in good yield, the peripheral chlorides were successfully displaced by bis-protected tacn (compounds **6**, **6'**, **8** and **8'**). However, reduction of the three amides was once again only partially successful and chromatographic attempts to separate them failed.

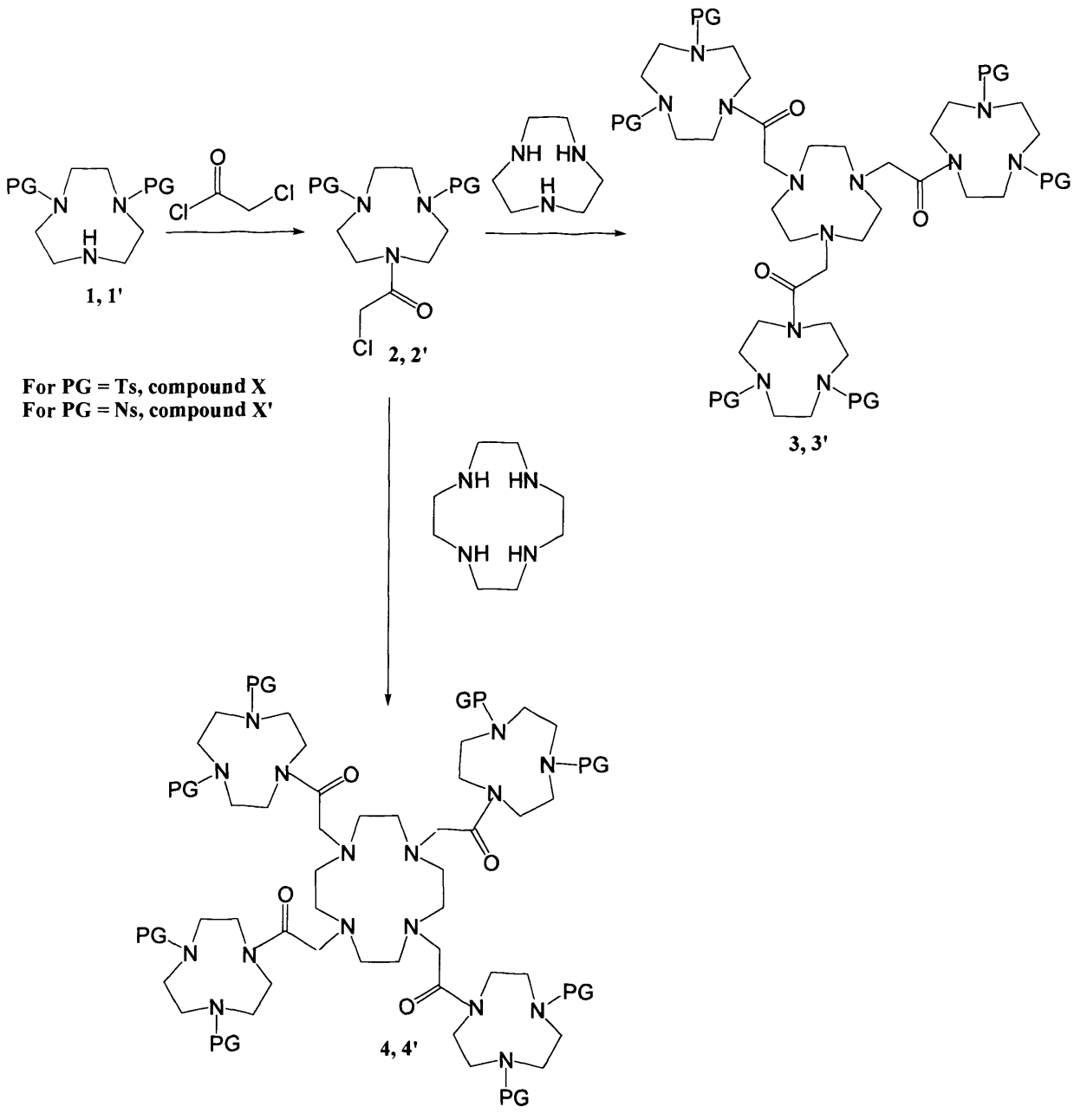

Scheme 2.6: Aza macrocyclic amide compounds.

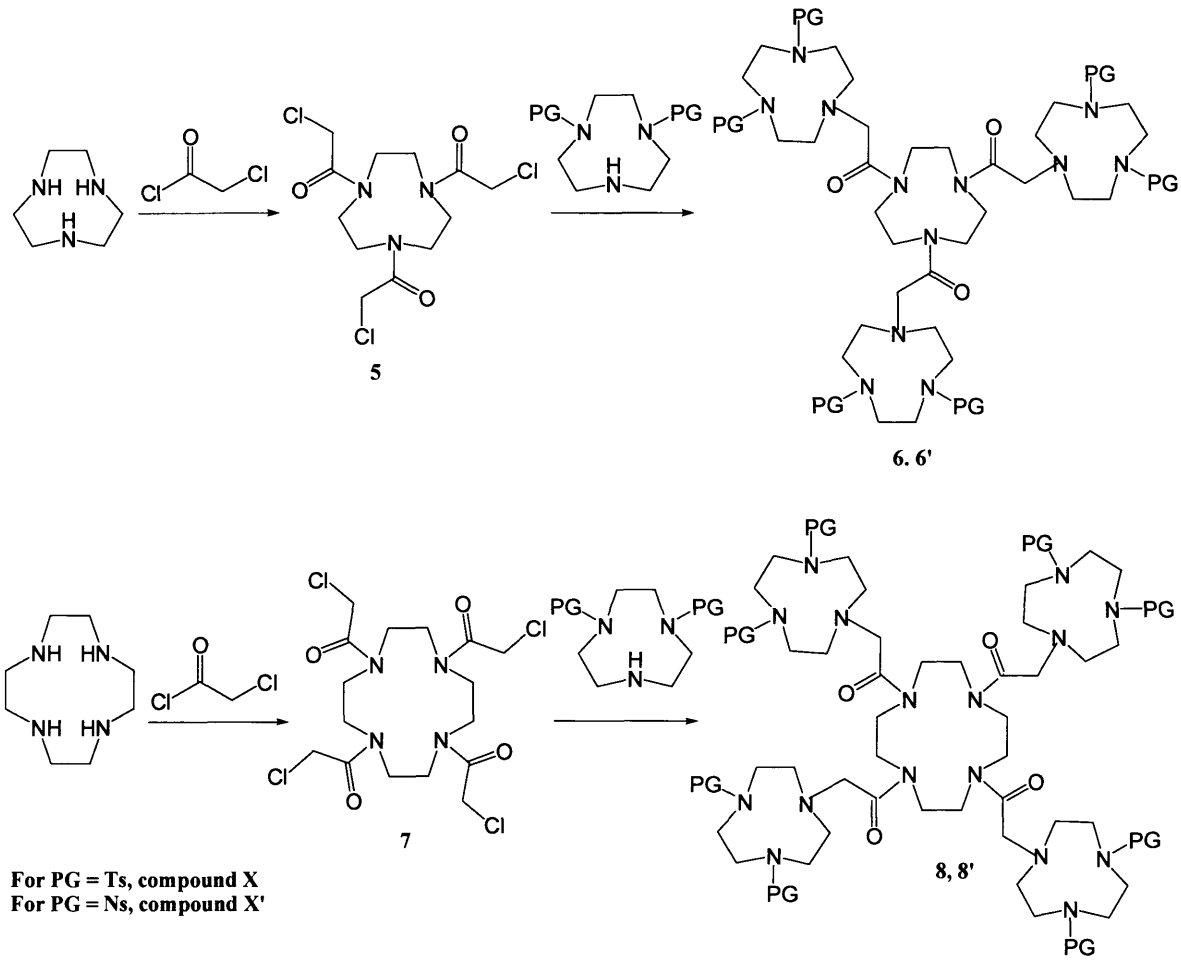

Scheme 2.7: Aza macrocyclic amide compounds.

It was considered possible that the six tosyl moieties were affecting the reduction in some way, possibly by steric or elecronic effects. To rule this out, compound **9** was synthesised in a similar manner to compound **6** using 1-Me-homopiperazine instead of bis protected tacn. Attempts to reduce this compound were also unsuccessful, this result probably eliminates the possibility that the protecting groups adversely affect reduction of the amides.

Another approach to form a similar compound utilised orthoamide **10**, which is a related compound to tacn, and is well documented in the literature[18]. The presence of the three tertiary amines make it susceptible to ring opening and nucleophilic attack on an electrophilic species (such as an acetyl chloride) as shown in scheme 2.8.

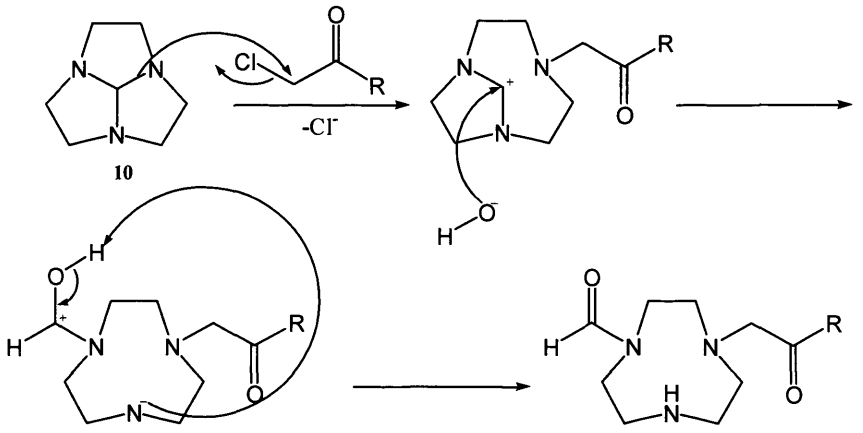

Scheme 2.8: The mechanism of nucleophilic attack of orthoamide **10**.

An attempt was made to utilise this reaction to remove the need for a protecting group; compound **11** was isolated in good yield by the reaction of orthoamide **10** with tris amide **5** (scheme 2.9). This molecule now only requires reduction to obtain the desired product. However, as with previous attempts on reduction, BH_3 and $LiAlH_4$ proved ineffective in the complete reduction of the amides.

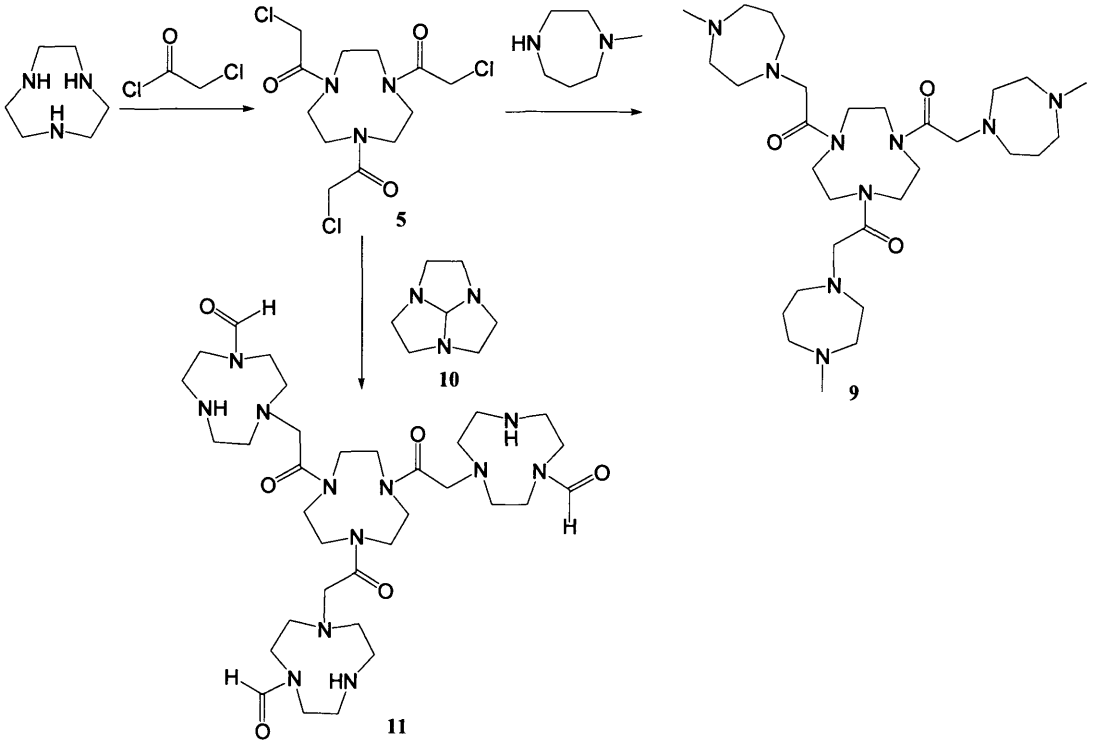

Scheme 2.9: The synthesis of hexa-amide, **11** via the addition of orthoamide, **10** to tris-amide, **5**.

2.3.2 Synthesis of ligands *via* the Mannich reaction

In 1997 Wieghardt *et al.*[19] synthesised compound **12** (scheme 2.10) by a simple Mannich style reaction, this was carried out in slight excess of 2,4-di-*tert*-butylphenol

in order that the reaction would go to completion. This is possible because there is only 1 remaining activated site on the phenol for the reaction to occur.

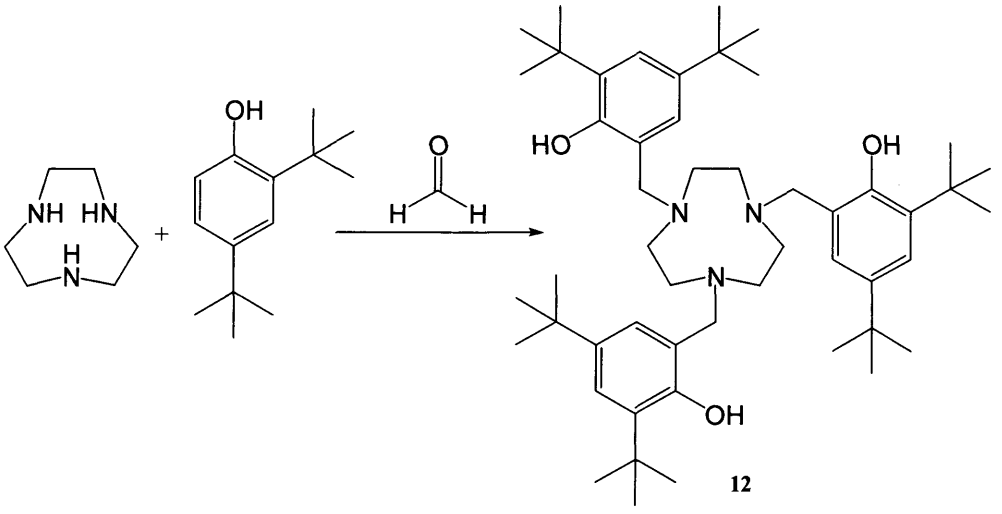

Scheme 2.10: Mannich style chemistry carried out by Wieghardt *et al.*

A variation of this reaction was attempted (scheme 2.11) with mono *tert*-butyl phenol, this creates the potential for a further Mannich reaction, that would form a ligand using the phenol moiety as a linker between the four macrocyclic sites (fig. 2.4).

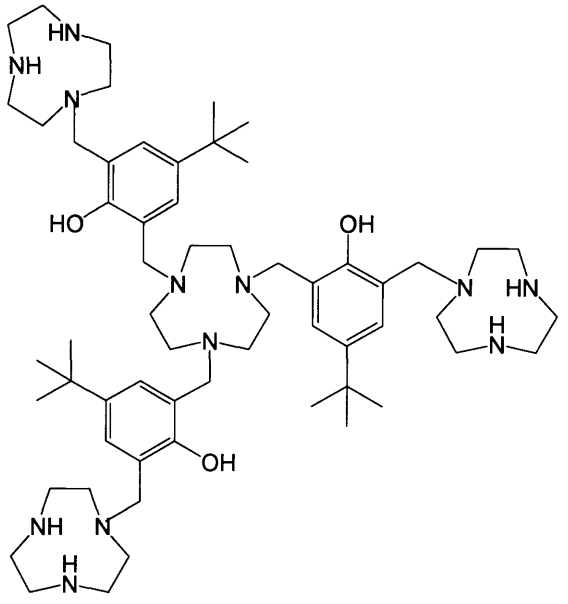

Fig. 2.4: The target ligand would be an aza macrocycle linked to three others via *tert*-butyl phenol bridges.

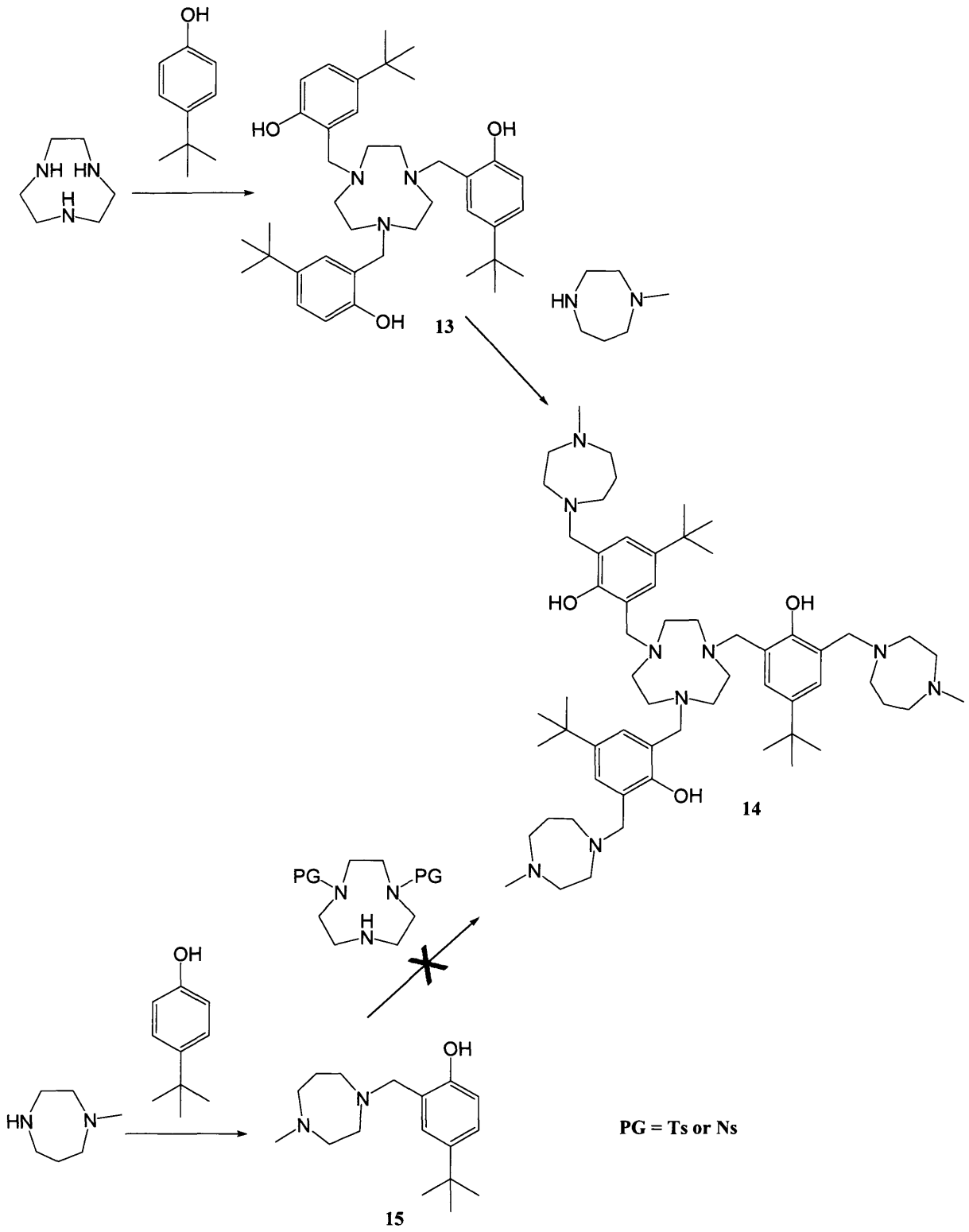

Scheme 2.11: Mannich style reactions attempted.

Compound **13** was isolated in good yield (~50%) considering the potential for side reactions to occur. This compound proved highly insoluble, the loss of three *tert*-buyl groups makes the compound only soluble in DMSO, which is too highly boiling and reactive to consider using as a solvent, all reactions carried out on this molecule were done so as a finely ground suspension.

A small scale test reaction was carried out to determine whether the remaining phenolic *ortho* positions are available for Mannich addition. The secondary amine used was 1-Me homo piperazine, although attempts at purifying the compound were unsuccessful, the product was detected by high resolution ESI-MS which was considered proof that all three sites are available to attack. When attempted on bis-protected tacn, the reaction would not go to completion, a range of reaction conditions were attempted, but, even by the relatively sensitive ESI-MS technique, none of the target material was detected.

One plausible reason for the inability of a bis protected tacn to react in this way is steric hindrance, it is possible, that, due to the huge amount of bulk surrounding the central tacn (*tert*-butyl phenol) and the large volume of the protecting groups, there is simply not enough space for a second or third mannich addition to occur. However, a much smaller secondary amine, such as 1-Methyl homo piperazine, has more chance of fitting around the central tacn three times, as demonstrated by the observation of compound **14**. This observation is consistent with the relative ease of isolation of the bis protected forms of tacn itself.[14] The third NH group is no longer a good nucleophile, this makes it difficult to utilise bis protected tacn in a mannich style addition.

An alternative route was attempted, this involved the Mannich addition of 1-Me homo piperazine to 4-*tert*-butyl phenol to give compound **15** and the subsequent addition of this to tacn, once again, this proved unsuccessful as no traces of the desired product were found in the mass spectrum.

2.3.3 Synthesis of ligands *via* epoxide containing compounds

There has been much study into the coordination chemistry of tri-substituted tacn compounds containing pendant alcohol moieties,[20-24] these will be discussed in detail in chapter three.

With this in mind, some test reactions were carried out on the addition of epichlorohydrin on homo piperazine, with a view to synthesise the compound shown in fig. 2.5. Compound **16** was isolated in good yield. However this was found to decompose if exposed to air for more than 2 days (scheme 2.12). The two peripheral

chlorides were then successfully displaced with 1-Me homo piperazine to form compound **17**.

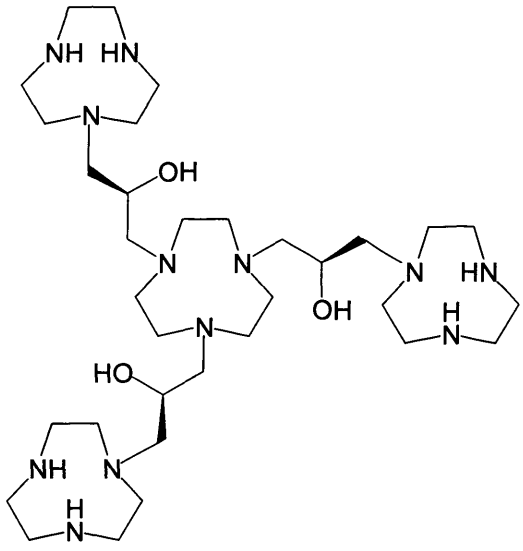

Fig. 2.5: This ligand would connect four azo macrocycles with propan-2-ol bridges.

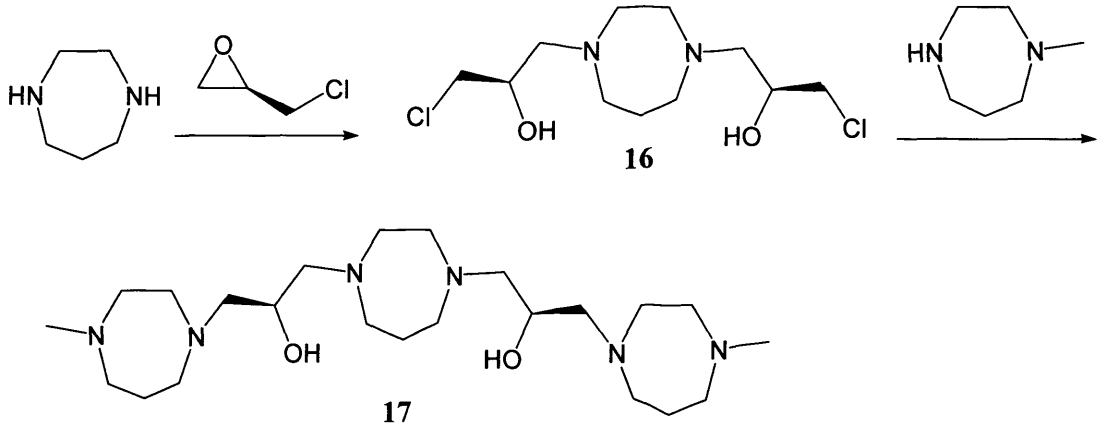

Scheme 2.12: Test reactions carried out on secondary amines and epichlorohydrin.

This chemistry was then applied to tacn, with the aim of forming a compound of four tacn rings connected via propan-2-ol bridges. Compound $\mathbf{L}^1.H_3$ was successfully isolated (scheme 2.13). However attempts at substituting the peripheral chlorides with a secondary amine, such as bis protected tacn, resulted in little to no reaction, and eventual decomposition of the compound into an intractable mixture of compounds.

A possible reason for the inability of $\mathbf{L}^1.H_3$ to react with a secondary amine could be that as the reaction proceeds, HCl is eliminated, this could then form the ammonium chloride salt of the bis protected tacn, rendering it non nucleophilic and halting the reaction.

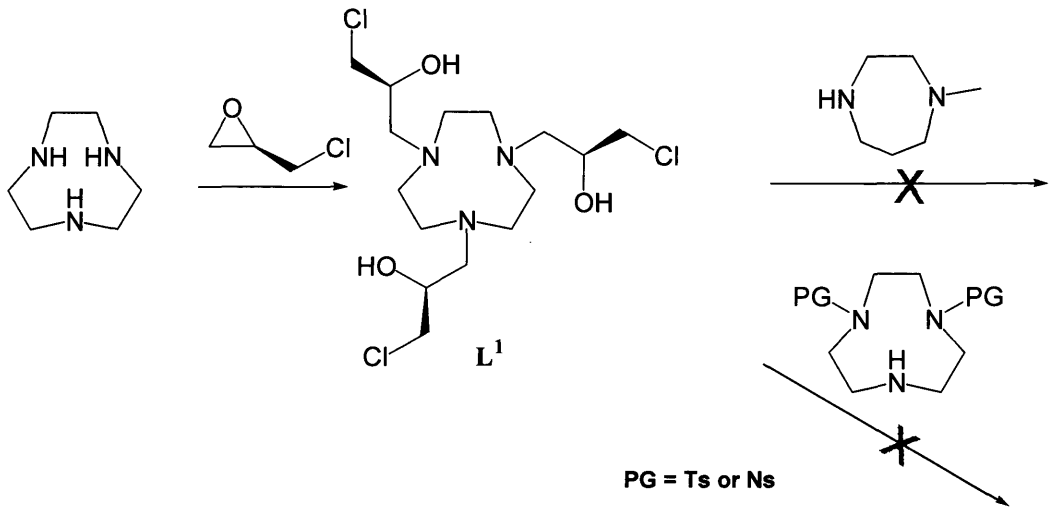

Scheme 2.13: The synthesis and reactions attempted of $\mathbf{L}^1.H_3$.

It was considered that, as $\mathbf{L}^1.H_3$ is a new ligand, transition metal complexes could be made of this, these will be discussed in chapter three.

The final attempt was designed to utilise epoxide chemistry, but involves just one central tacn ring, with three peripheral homo-piperazine moieties, these would probably each be capable of binding a small, 1st row transition metal due to the presence of two secondary amines and an alcohol group (fig. 2.6).

Bis protected (both Ts and Nos) homo piperazine derivative, compounds **19** and **19'**, were isolated in good yield (~60%), scheme 2.14. It was conceived that the terminal alkene could be oxidised with a simple oxidising agent, such as *m*CPBA, to form the epoxide (compounds **20** and **20'**), these were also isolated in good yields (~70%).

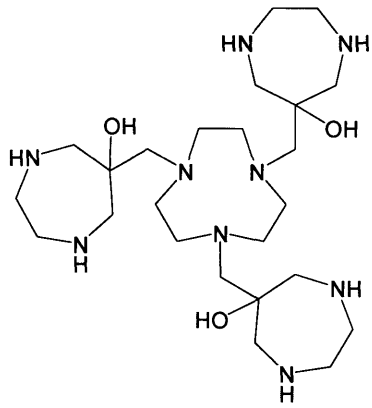

Fig. 2.6: A different approach would create a ligand with just one tacn connected to three homo-piperazine moieties.

The epoxides were reacted for with $^1/_3$ equivalents of tacn; compounds **21** and **21'** were purified by recrystallisation from hot acetone. It is interesting to note that the tosylate, compound **20**, took 14 days under reflux to completely add to tacn, while the corresponding nosylate (compound 20') took just 3 days under the same conditions.

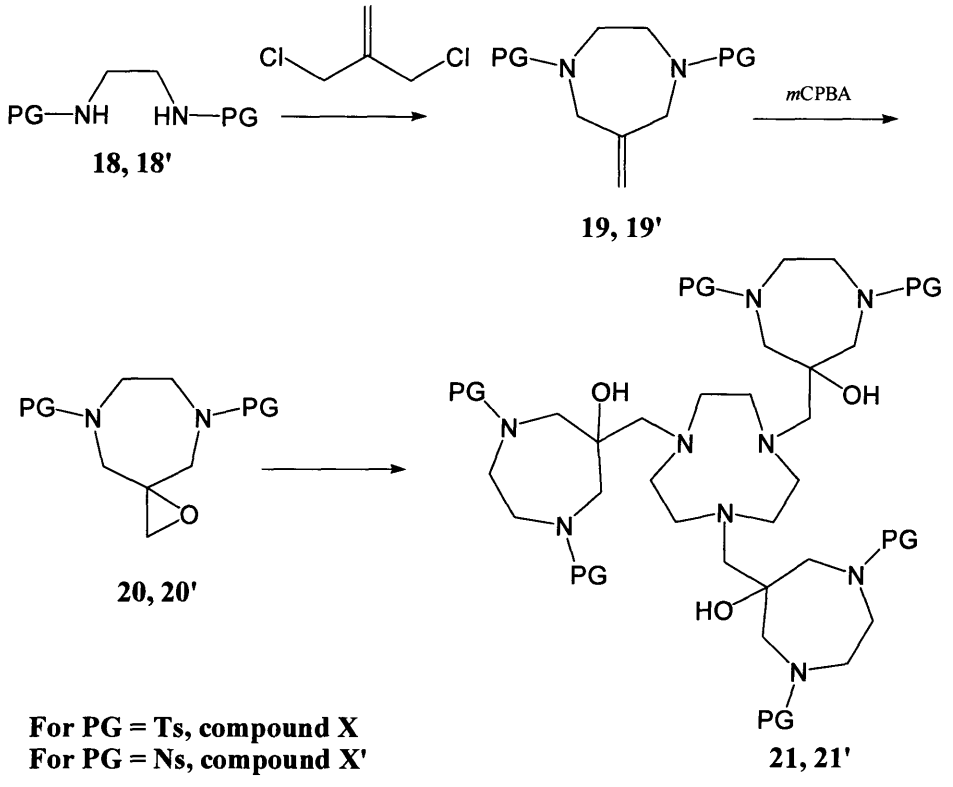

Scheme 2.14: The homo piperazine derivatives synthesised.

The deprotection of both **21** and **21'** (by H_2SO_4 and thiocresol/Cs_2CO_3 respectively) failed, the tosylate (compound **21**) seemed to decompose under the rather harsh reaction conditions. The nosylate (compound **21'**) was partially deprotected by Cs_2CO_3 as determined by high resolution mass spectrometry, peaks were identified that correspond to the start material, mono, bis, tris, tetra, penta and fully deprotected compounds. However, the work up of this reaction proved unsuccessful partly due to the large amount of side products within the reaction mixture and partly due to the extremely high polarity of the target material.

Attempts were made to metallate macrocyclic compounds **21** and **21'** with manganese, iron, copper, and zinc, but no reaction was observed. It was postulated that the protecting groups are too sterically hindering to enable coordination to either the amines or the alcohol moieties.

2.4 Conclusions

Many new organic compounds have been synthesised. However, problems with deprotection and/or reduction of amides halted the investigation into metallation studies. This leaves a lot of scope for future work, it may be possible to overcome the problems found by using a smaller protecting group such as trifluoroacetamide (TFA), or a more labile protecting group such as benzyloxycarbonyl (Z).

A new coordinating tris pendant alcohol tacn ligand has been isolated ($\mathbf{L^1}.H_3$), this is discussed in chapter three. With respect to the attempts on displacing the peripheral chlorides on $\mathbf{L^1}.H_3$, a stronger base may be required to prevent the formation of ammonium salts.

2.5 Bibliography

1. Greene, T. W.; Wuts, P. G. M., *Greene's Protective Groups in Organic Synthesis*. 4th Edition ed.; 2006.

2. Kurosawa, K.; Kan, T.; Fukuyama, T., Preparation of Secondary Amines From Primary Amines via 2-Nitobenzenesulfonamides. *Org. Synth.* **2002,** 79, 186-191.

3. Marvel, C. S., dl-Phenylalanine. *Org. Synth.* **1941,** 21, 99-102.

4. Mannich, C.; Schumann, P., 3,5-Alkylated 4-oxopiperidines. *Ber. Dtsch. Chem. Ges. B* **1936,** 69B, 2299-305.

5. Mandal, S. K.; Paira, M.; Roy, S. C., Titanocene(III) Chloride Mediated Radical-Induced Addition to Baylis-Hillman Adducts: Synthesis of (E)- and (Z)-Trisubstituted Alkenes and alpha -Methylene/Arylidene delta -Lactones. *J. Org. Chem.* **2008,** 73, (10), 3823-3827.

6. Ok, T.; Jeon, A.; Lee, J.; Lim, J. H.; Hong, C. S.; Lee, H. S., Enantiomerically Pure Synthesis of beta -Substituted gamma -Butyrolactones: A Key Intermediate to Concise Synthesis of Pregabalin. *J. Org. Chem.* **2007,** 72, (19), 7390-7393.

7. Wurtz, M. A., New observations on butyl alcohol. *C. R. Hebd. Seances Acad. Sci.* **1854,** 39, 335-338.

8. Koyama, H.; Yoshino, T., Syntheses of some medium-sized cyclic triamines and their cobalt(III) complexes. *Bull. Chem. Soc. Jap.* **1972,** 45, (2), 481-4.

9. Peacock, D. H.; Gwan, Y. S., Polyamines. III. Preparation of unsymmetrical amines of the type NHRC2H4NHC2H4NH2 and NH2C2H4NHC3H6NH2 and the action of ammonia on di-p-toluenesulfonylbis(beta -chloroethyl)ethylenedinmine. *J. Chem. Soc.* **1937**, 1468-71.

10. Richman, J. E.; Atkins, T. J., Nitrogen analogs of crown ethers. *J. Amer. Chem. Soc.* **1974,** 96, (7), 2268-70.

11. Chaudhuri, P.; Wieghardt, K., The Chemistry of 1,4,7-Triazacyclononane and Related Tridentate Macrocyclic Compounds. *Prog. Inorg. Chem* **1987,** 35, 329-436.

12. Qian, J.; Gu, W.; Liu, H.; Gao, F.; Feng, L.; Yan, S.; Liao, D.; Cheng, P., The first dinuclear copper(II) and zinc(II) complexes containing novel Bis-TACN: syntheses, structures, and DNA cleavage activities. *Dalton Trans* **2007**, (10), 1060-6.

13. Yang, C. T.; Sreerama, S. G.; Hsieh, W. Y.; Liu, S., Synthesis and characterization of a novel macrocyclic chelator with 3-hydroxy-4-pyrone chelating arms and its complexes with medicinally important metals. *Inorg. Chem.* **2008,** 47, (7), 2719-2727.

14. Weisman, G. R.; Vachon, D. J.; Johnson, V. B.; Gronbeck, D. A., Selective N-protection of medium-ring triamines. *J. Chem. Soc., Chem. Commun.* **1987**, (12), 886-7.

15. Atkins, T. J., Tricyclic Trisaminomethanes. *J Am Chem Soc* **1980,** 102, 6364-6365.

16. Banfi, L.; Narisano, E.; Riva, R.; Stiasni, N.; Hiersemann, M., *Encyclopedia of Reagents for Organic Synthesis*. Wiley: 2004.

17. Barnier, J. P.; Champion, J.; Conia, J. M., Preparation of Cyclopropanecarboxaldehyde. *Org. Synth.* **1981,** 60.

18. Erhardt, J. M.; Grover, E. R.; Wuest, J. D., Transfer of hydrogen from orthoamides. Synthesis, structure, and reactions of hexahydro-6bH-2a,4a,6a-triazacyclopenta[cd]pentalene and perhydro-3a,6a,9a-triazaphenalene. *J. Am. Chem. Soc.* **1980,** 102, (20), 6365-9.

19. Adam, B.; Bill, E.; Bothe, E.; Goerdt, B.; Haselhorst, G.; Hildenbrand, K.; Sokolowski, A.; Steenken, S.; Weyhermueller, T.; Wieghardt, K., Phenoxyl radical complexes of gallium, scandium, iron and manganese. *Chem.--Eur. J.* **1997,** 3, (2), 308-319.

20. Fallis, I. A.; Farrugia, L. J.; Macdonald, N. M.; Peacock, R. D., Synthesis and crystal structure of zinc-vanadium complex [ZnII(LH3)(L)VIV][PF6]3 [LH3 = N,N',N''-tris(2S)-2-hydroxypropyl-1,4,7-triazacyclononane]: a chiral mixed-metal pendant-arm macrocyclic dimer containing nonvanadyl vanadium(IV). *Inorg. Chem.* **1993,** 32, (6), 779-80.

21. Fallis, I. A.; Farrugia, L. J.; Macdonald, N. M.; Peacock, R. D., Synthesis and coordination chemistry of the sterically demanding pendant-arm macrocycle N,N',N''-tris[(2R)-2-hydroxy-3-methylbutyl]-1,4,7-triazacyclononane. *J. Chem. Soc., Dalton Trans.* **1993**, (18), 2759-63.

22. Blake, A. J.; Fallis, I. A.; Gould, R. O.; Parsons, S.; Ross, S. A.; Schroder, M., Selective derivatization of aza macrocycles. *J. Chem. Soc., Dalton Trans.* **1996**, (23), 4379-4387.

23. Blake, A. J.; Fallis, I. A.; Heppeler, A.; Parsons, S.; Ross, S. A.; Schroeder, M., Synthesis, structure and characterization of amido derivatives of [9]aneN3 (1,4,7-triazacyclononane). *J. Chem. Soc., Dalton Trans.* **1996**, (1), 31-43.

24. Blake, A. J.; Fallis, I. A.; Parsons, S.; Ross, S. A.; Schroder, M., Asymmetric functionalization of aza macrocycles. Syntheses, crystal structures and electrochemistry of [Ni(Bz[9]aneN3)2][PF6]2 and [Pd(Bz[9]aneN3)2][PF6]2.2MeCN

(Bz[9]aneN3 = 1-benzyl-1,4,7-triazacyclononane). *J. Chem. Soc., Dalton Trans.* **1996**, (4), 525-32.

CHAPTER 3

Analysis and comparison of complexes of $\mathbf{L}^1.H_3$ and $\mathbf{L}^2.H_3$

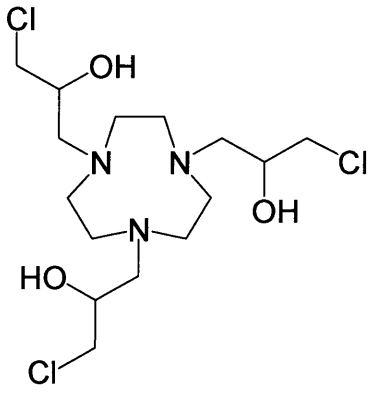

$\mathbf{L}^1.H_3$

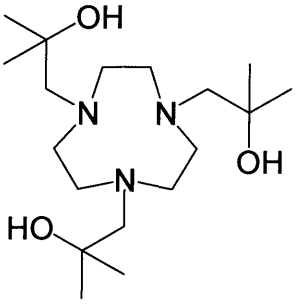

$\mathbf{L}^2.H_3$

3.1 Introduction

3.1.1 The Chelate Effect

It is well documented that multidentate ligands give rise to increased stability constants in comparison to their monodentate analogues. This is known as the chelate effect. The complexes in scheme 3.1 illustrate this. The tetradentate ligand forms complexes with much greater thermodynamic stability than the others. This can be shown by considering the increased entropic value when four ammonia molecules are not bound compared to two en molecules. For multidentate systems, the entropic factor gives rise to a larger free energy.

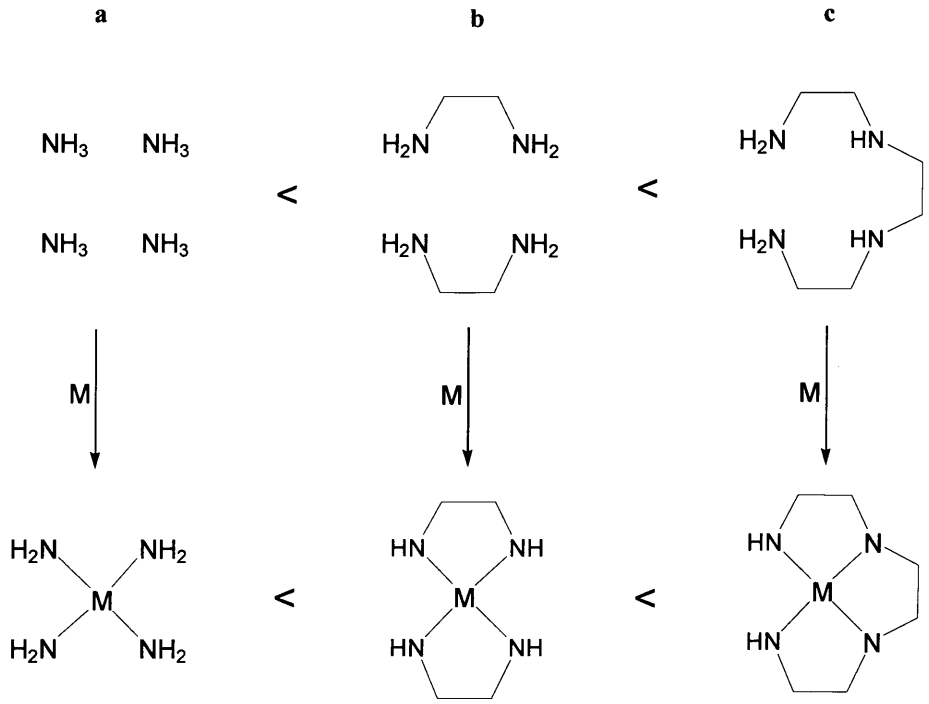

Scheme 3.1: Higher dentate ligands give rise to more stable complexes than the monodentate analogues.

Table 3.1 illustrates the differences in entropic values for system a and b.[1] It is clear that the enthalpic terms for both reactions are almost identical, indicating that both sets of ligands (both being secondary amines) give rise to M-N bonds of similar strength. The entropic values though are greatly different, this gives rise to the observation of differing free energy values.

Table 3.1: The two reactions illustrate the entropic origins of the chelate effect.

1. $Cd^{II}_{(aq)} + 4CH_3NH_{2(aq)} \rightleftharpoons [Cd(NH_2CH_3)_4]^{2+}_{(aq)}$

2. $Cd^{II}_{(aq)} + 2H_2NCH_2CH_{2(aq)} \rightleftharpoons [Cd(en)_2]^{2+}_{(aq)}$

Ligand	$\Delta H°$ / kJmol^{-1}	$\Delta S°$ / Jmol^{-1} deg^{-1}	$\Delta G°$ / kJmol^{-1}
$4CH_3NH_2$	-57.3	-67.3	-37.2
2en	-56.5	14.1	-60.7

A further (kinetic) aspect of the chelate effect is that once part of a multidentate ligand has bound to a metal, the rest of the ligand is close to the metal centre, therefore increasing the chance that the remainder of the ligand will bind soon after.

3.1.2 The Macrocyclic Effect

The macrocyclic effect can be argued as an extension to the chelate effect, the stabilisation observed by a macrocycle is much larger than that of an open-chain analogue (scheme 3.2). The term 'macrocyclic effect' was first used in 1969 by Cabbiness and Margerum[2] while comparing the stability of Cu^{II} complexes with a tetraamine macrocycle with its open chain counterpart. It was shown that the macrocyclic complex has a stability constant 10,000 times greater.[3] Further work showed the macrocycles form complexes much slower than the open chain analogues, dissociation was also shown to be more difficult. It has since been shown that the macrocyclic effect originates from a combination of factors including the extra chelate ring formed in complexation of a macrocycle to a metal. Enthalpic and entropic contributions have been shown to vary for different metals, ligands and solvents, this makes the macrocyclic effect difficult to quantify.[1]

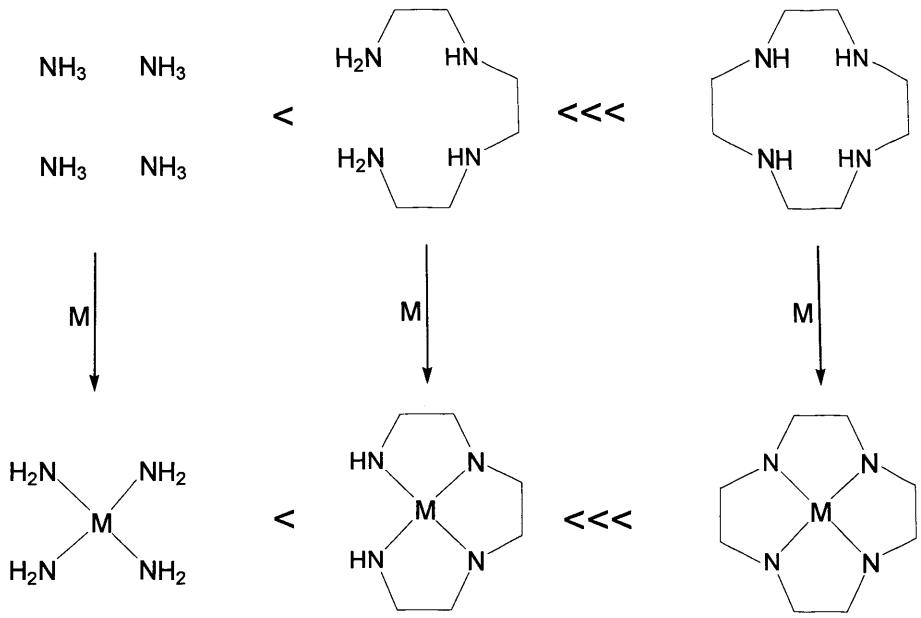

Scheme 3.2: The stabilisation of a macrocyclic ligand is much greater than that of the open chain counterparts.

3.1.3 N,N',N"tris-2-hydroxy-1,4,7-triazacyclononane compounds

The chemistry of *N,N',N"*tris-2-hydroxy tacn compounds (fig. 3.1) first came to light in 1983, Hancock *et al.*[4] reported the synthesis of tris hydroxyethyl tacn. Soon after, Peacock *et al.*[5] reported the reaction of tacn with propylene oxide to form compound **22**. They subsequently described the coordination chemistry of this ligand.[6] It was shown that coordination of the ligand to Co^{III} gives the dinuclear complex $[Co^{III}LH_3Co^{III}][PF_6]_3$, fig. 3.1, where one half has three amine donors and three alcohol donors while the other half has three amines and three alkoxide donors.

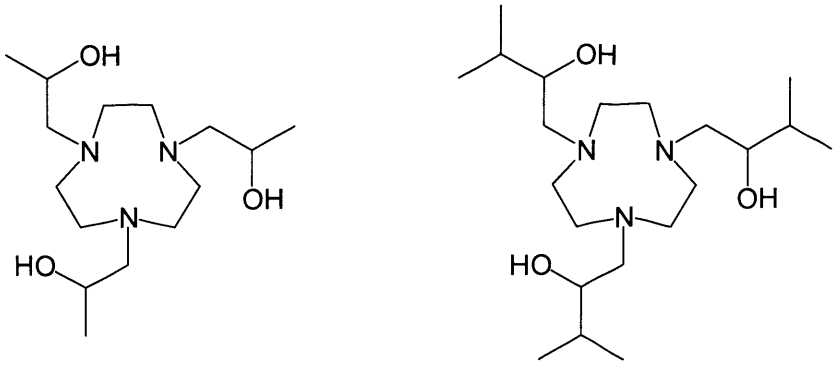

22 **23**

Fig. 3.1: The first *N,N',N"*tris-2-hydroxy tacn compound (**22**) forms a dinuclear structure with cobalt as reported by Peacock *et al.* Compound **23** preferentially forms monomeric structures.

It was found that the N_3 and O_3 donor sets are twisted away from ideal octahedral geometries by angles of 10.2° and 11.2° respectively, it was also noted that the N_3

(tacn) donor set is trigonally elongated while the O_3 (2-hydroxy propyl) donor set is trigonally compressed. Peacock showed that the structure of the complex is pH dependant, the UV spectra of the complex at pH 1 being shifted by about 30 nm less than that of the complex at pH 14. They proposed that this is brought about by the protonation of one pendant hydroxyl group. This results in the hydroxyl group becoming more labile, thus leaving space for a solvent molecule to coordinate.

The same group published the Cr^{III} structure,[7] which is very similar to the Co^{III} structure, the main difference noted is the nature of the hydrogen bridge, that of the Cr complex is symmetric, while the Co analogue contains an asymmetric hydrogen bridge. Also the twist angle away from an ideal octahedral geometry is larger for the Cr structure (15°) than the Co structure (10°-11°). In 1991 the group published a mixed valent Mn^{II} Mn^{IV} dinuclear complex containing the same ligand,[8] they postulated that the reason Mn^{IV} is observed and not only Mn^{II} may be due to the steric restrictions of the ligand upon the metal, constricting it in such a way that the tetragonal Jahn-Teller distortions required by a d^4 metal are more unfavourable than the formation of a d^3 metal centre, such as Mn^{IV}.

Peacock also reported the synthesis and crystal structure of a heteronuclear complex containing the ligand, $[Zn^{II}LH_3LV^{IV}][PF_6]_3$.[9] The Zn^{II} took a trigonal prismatic geometry while the V^{IV} adopted a *pseudo*-octahedral state. It was noted that the Zn-O and Zn-N bond lengths are all similar, whereas the V-N bonds are about 0.3 Å longer than the V-O bonds. This was attributed to donation from filled p orbitals on the oxygen to the t_{2g} orbitals on the metal which gives rise to shorter V-O bonds. With zinc, the t_{2g} orbitals are full so no such bonding is possible, hence the observation that all bonds are roughly equal in length. When compared to the manganese structure, the half-filled t_{2g} set allows partial π^* donation and differences of 0.1Å (Mn^{II}) and 0.2 Å (Mn^{III}) are observed.[8]

It was shown in 1993, that the presence of the more bulky isopropyl group (**23**, fig. 3.1) prevents formation of the dinuclear structure;[10] monomers of ligand **23** were isolated with V^{IV}, Cr^{III}, Mn^{IV} and Ni^{II}. Monomeric structures of ligand **22** have been isolated; in 1991 Farrugia *et al.*[11] reported the Ni^{II} structure and the Cu^{II}, Co^{III}, and Zn^{II} monomeric structures were published in 2007 by Wang and co workers.[12]

Ditopic tacn based ligands capable of binding two transition metals have been reported, such as compound **24** (scheme 3.3), the synthesis and coordination chemistry of which has been described by Schröder *et al.*[13] They reported the synthesis, characterisation and single crystal X-ray structures of the dinuclear Co^{II}, Ni^{II}, Zn^{II} and Cu^{II} species'.

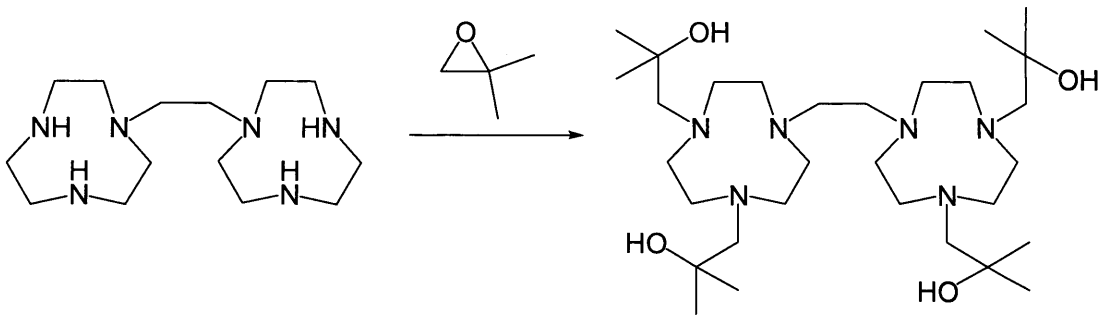

24

Scheme 3.3: The synthesis of binucleating tacn based ligand, 24, as reported by Schröder *et al.*

In 1998 Huskens and Sherry[14] described the synthesis and coordination chemistry (with mg^{II} and Ca^{II}) of compound $\mathbf{L^2}.H_3$, fig. 3.2. In the article, they describe the differences in relative affinities for ligands of this type by calcium and magnesium. They showed that there is little selectivity between Mg^{II} and Ca^{II} for $\mathbf{L^2}.H_3$. This is the only publication on ligand $\mathbf{L^2}.H_3$.

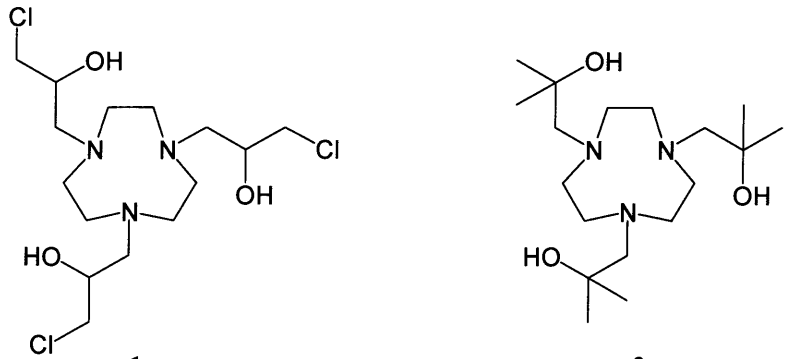

$\mathbf{L^1}.H_3$ $\mathbf{L^2}.H_3$

Fig. 3.2: The ligands used in this chapter. $\mathbf{L^1}.H_3$ is previously unreported, $\mathbf{L^2}.H_3$ reported by Huskens and Sherry.[15]

Ligands $\mathbf{L^1}.H_3$ and $\mathbf{L^2}.H_3$ are sufficiently similar to a possible central site of compounds **21** and **21'** (see section 1.3.3) that a study of complexes of them could be informative. The nature of a possible metallated central site of compound **21** could be explored. It was with this in mind that the synthesis and characterisation of

complexes of $\mathbf{L^1}.H_3$ and $\mathbf{L^2}.H_3$ were undertaken, such that an understanding of a species formed of a deprotected and metallated version of **21** could be made.

3.2 Experimental Procedures

Preparation of RRR $[Co^{II}L^1H_3L^1Co^{III}][PF_6]_2$

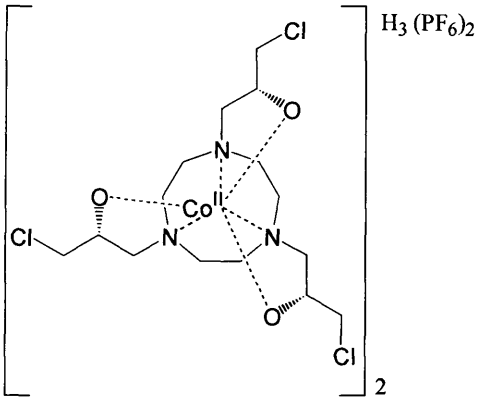

A solution of *R*-epichlorohydrin (287 mg, 2.3 mmol) in ethanol (2 ml) was added dropwise to a solution of 1,4,7-triazacyclononane (100 mg, 0.78 mmol) in ethanol (5 ml), over a period of 2 minutes at 0 °C. The mixture was stirred at 0 °C for 30 minutes and allowed to reach room temperature where stirring continued for a further 3 hours. The solvent and excess epichlorohydrin was then removed under vacuum to leave the free ligand $\mathbf{L^1}$. The ligand was dissolved in water (5 ml) and a solution of $CoCl_2$ (96 mg, 0.78 mmol) in ethanol (5 ml) was added. This was stirred in air for 1 hour. The solvent was removed under reduced pressure and the residue dissolved in water (10 ml). Ammonium hexafluorophosphate (1.27 g, 7.8 mmol) in water (10 ml) was added dropwise to the complex. The purple precipitate was collected by vacuum filtration. Further purification was achiveved by slow diffusion of diethyl ether into an acetonitrile solution yielding 502 mg (64%). IR (KBr disc, cm^{-1}), 2955(s), 1638(s), 1338(s), 1162(m) and 840(s). UV/Vis (acetonitrile): λ_{max} = 398nm, ε = 123 $cm^{-1}mol^{-1}dm^3$; 553nm, ε = 148 $cm^{-1}mol^{-1}dm^3$. MS(EI), MH^+ exact mass (*calc.*) *m/z 715.8588 (obs.) 715.8618.*

Preparation of RRR $[Ni^{II}L1H3][PF_6]_2$

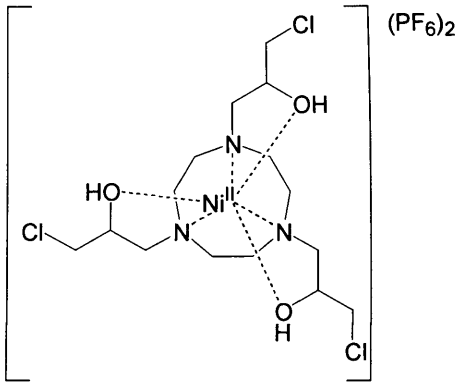

A solution of epichlorohydrin (287 mg, 2.3 mmol) in ethanol (2 ml) was added dropwise to a solution of 1,4,7-triazacyclononane (100 mg, 0.78 mmol) in ethanol (5 ml), over a period of 2 minutes at 0 °C. The mixture was stirred at 0 °C for 30 minutes, the mixture was allowed to reach room temperature where stirring continued for a further 3 hours. The solvent and excess epichlorohydrin was removed under vacuum to leave the free ligand $\mathbf{L^1}.H_3$. This was dissolved in ethanol (10 ml) and a solution of 0.95 equivalents of $NiCl_2.6H_2O$ (175 mg, 0.736 mmol) in ethanol was added and the mixture stirred for 5 minutes. Diethylether (20 ml) was added to the pale blue solution and the pale blue precipitate was filtered. This was dissolved in a minimum amount of water and 2 equivalents of NH_4PF_6 were added and the solution stirred for an additional 5 minutes. The solvent was removed to yield 377 mg (64%) of a purple solid. IR: (KBr disc, cm^{-1}) 3650(b), 3136(s), 1662(s), 1465(m), 1099(s) and 832(s). UV/Vis (acetonitrile): λ_{max} = 358, ε = 74; 562, ε = 44; 942, ε = 106. MS(EI), MH^+ exact mass (*calc.*) *m/z 464.0784 (obs.) 464.0821.*

Preparation of RRR $[Cr^{II}L^1H_3L^1Cr^{III}][PF_6]_2$

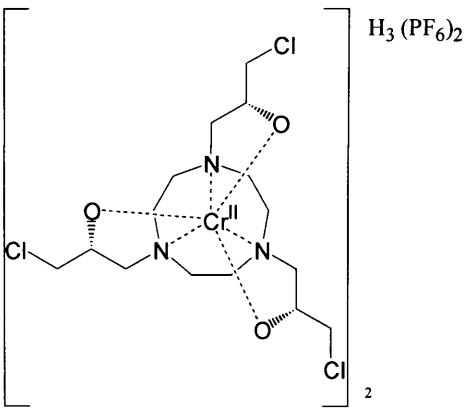

The following procedure was carried out using dried solvents and standard schlenk line techniques. A solution of epichlorohydrin (386 mg, 4.2 mmol) in ethanol (2 ml) was added dropwise to a solution of 1,4,7-triazacyclononane (180 mg, 1.4 mmol) in ethanol (5 ml), over a period of 2 minutes at 0 °C. The mixture was stirred at 0 °C for 30 minutes, the mixture was allowed to reach room temperature where stirring continued for a further 3 hours. The solvent and excess epichlorohydrin was then removed under vacuum to leave the free ligand $\mathbf{L^1}.H_3$. To the schlenk was added a solution of chromium trichloride (220 mg, 1.4 mmol) and a trace of zinc in thf (20 ml), the solution was heated to 90 °C for 12 hours. The solution was allowed to cool and filtered, the solvent was removed to leave a dark blue residue. This was dissolved in water and 2 drops of hydrochloric acid were added followed by ammonium hexafluorophosphate (2.24 g, 14 mmol). The solid was filtered and recrystallised by slow diffusion of di-ethyl ether into an acetonitrile solution yielding 1.02 g (73%). IR: (KBr disc, cm^{-1}) 3645(b), 3164(s), 1702(s), 1482(m), 1112(s) and 862(s). UV/Vis (acetonitrile): λ_{max} = 402, ε = 395; 522, ε = 404. MS(EI), MH^+ exact mass (*calc.*) *m/z 708.8691 (obs.) 708.8946.*

Preparation of RRR $[Ni^{II}L^2H_3][ClO_4]_2$

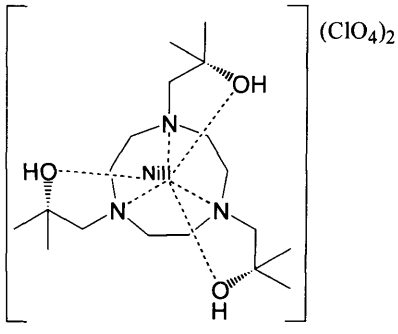

The ligand $\mathbf{L^2}.H_3$ was prepared as described by Sherry *et al.*[14] $\mathbf{L^2}.H_3$ (121 mg, 0.36 mmol) in ethanol (5 ml) was added to an ethanolic solution of $Ni(ClO_4)_2.6H_2O$ (129 mg, 0.36 mmol), the solution was stirred for 30 minutes. The green precipitate was isolated by vacuum filtration and recrystallised by slow diffusion of di-ethyl ether into an acetonitrile solution yielding 152 mg (50%). IR: (KBr disc, cm^{-1}) 3652(b), 3141(s), 1582(s), 1472(m), 1091(s) and 861(s). UV/Vis (acetonitrile): λ_{max} = 372, ε = 13; 589, ε = 12; 871, ε = 20. MS(EI), MH^+ exact mass (*calc.*) *m/z 655.0278 (obs.) 655.0221.*

Preparation of RRR $[Mn^{II}H_3L^2][ClO_4]_2$

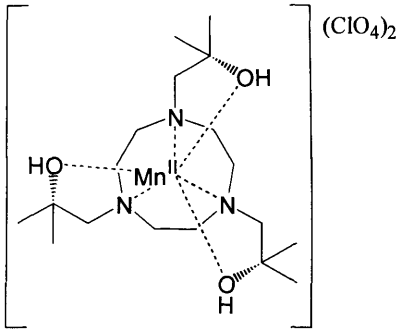

The ligand $\mathbf{L^2}.H_3$ was prepared as described by Sherry *et al.*[14] $\mathbf{L^2}.H_3$ (121 mg, 0.36 mmol) in ethanol (5 ml), to this solution was added an ethanolic solution of $Mn(ClO_4)_2.6H_2O$ (128 mg, 0.36 mmol), the solution was stirred in air for 3 days, the solvent was removed and the residue recrystallised by slow diffusion of di-ethyl ether into an acetonitrile solution yielding 71 mg (23%). IR: (KBr disc, cm^{-1}) 3641(b), 3128(s), 1668(s), 1474(m), 1108(s) and 853(s). MS(EI), MH^+ exact mass (*calc.*) *m/z 652.0305 (obs.) 652.0265.*

Preparation of RRR $[CuL^2H_3][ClO_4]_2$

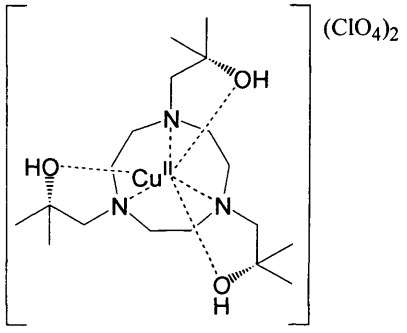

The ligand $\mathbf{L^2}.H_3$ was prepared as described by Sherry *et al.*[14] $\mathbf{L^2}.H_3$ (121 mg, 0.36 mmol) in ethanol (5 ml), to this solution was added an ethanolic solution of $Cu(ClO_4)_2 \cdot 6H_2O$ (131 mg, 0.36 mmol), this solution was stirred for 1 hour, the blue precipitate was isolated by vacuum filtration and recrystallised by slow diffusion of di-ethyl ether into an acetonitrile solution yielding 60 mg (19%). IR: (KBr disc, cm^{-1}) 3578(b), 3131(s), 1676(s), 1452(m), 1087(s) and 858(s). UV/Vis (acetonitrile): λ_{max} = 723, ε = 56. MS(EI), MH^+ exact mass (*calc.*) *m/z 660.0320 (obs.) 660.0342.*

3.3 Results and Discussion

3.3.1 $\mathbf{L^1}.H_3$ Complexes

3.3.1.1 $[NiL^1](PF_6)_2$ and $[Ni^{II}L^1H_3L^1Ni^{II}](PF_6)$

The reaction of ligand $\mathbf{L^1}.H_3$ with $NiCl_2(H_2O)_6$ in ethanol, followed by metathesis with $NaPF_6$ gave a monomeric complex $[Ni\mathbf{L^1}][PF_6]_2$. Single crystals of $[Ni\mathbf{L^1}][PF_6]_2$ suitable for an X-ray diffraction study were grown from the slow diffusion of diethyl ether into acetonitrile. The molecular structure is shown in fig. 3.4 and selected bond lengths and angles are provided in Table 3.2. The structure shows an octahedral coordination geometry about Ni, this is typical of complexes with bulky pendant arms such as those reported by Peacock *et al.*[10] In 1990 Farrugia *et al.*[11] defined the twist angle, φ, of the metal centre as 180°-TA where TA = the mean of the three torsion angles O-O(CT)-N(CT)-N which are closest to 180° and O(CT) and N(CT) are centroids of the O_3 and N_3 donor sets (fig. 3.3). Hence, a purely octahedral system would have φ = 0° and any deviation from this ideal system is a measure of trigonal distortion. In this way, φ was found to be 16.6°, implying $[Ni\mathbf{L^1}][PF_6]_2$ is 'more' octahedral in geometry than the nickel complex of compound **22**, in which φ was reported to be 19.0°.

This could suggest that the pendant chloride moieties of $[Ni\mathbf{L^1}][PF_6]_2$ impose steric constraints upon the ligand framework such that the metal is forced to adopt a more ideal geometry in the complex of $[Ni\mathbf{L^1}][PF_6]_2$ compared to compound **22**.

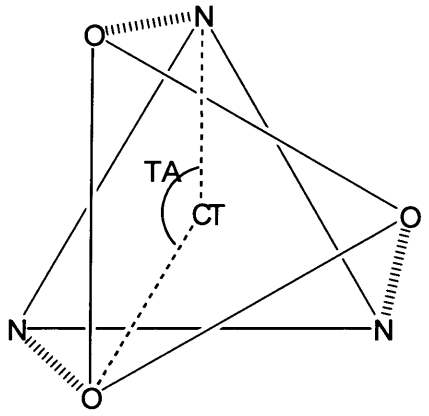

Fig. 3.3: Derivation of TA as described by Farrugia and Peacock.

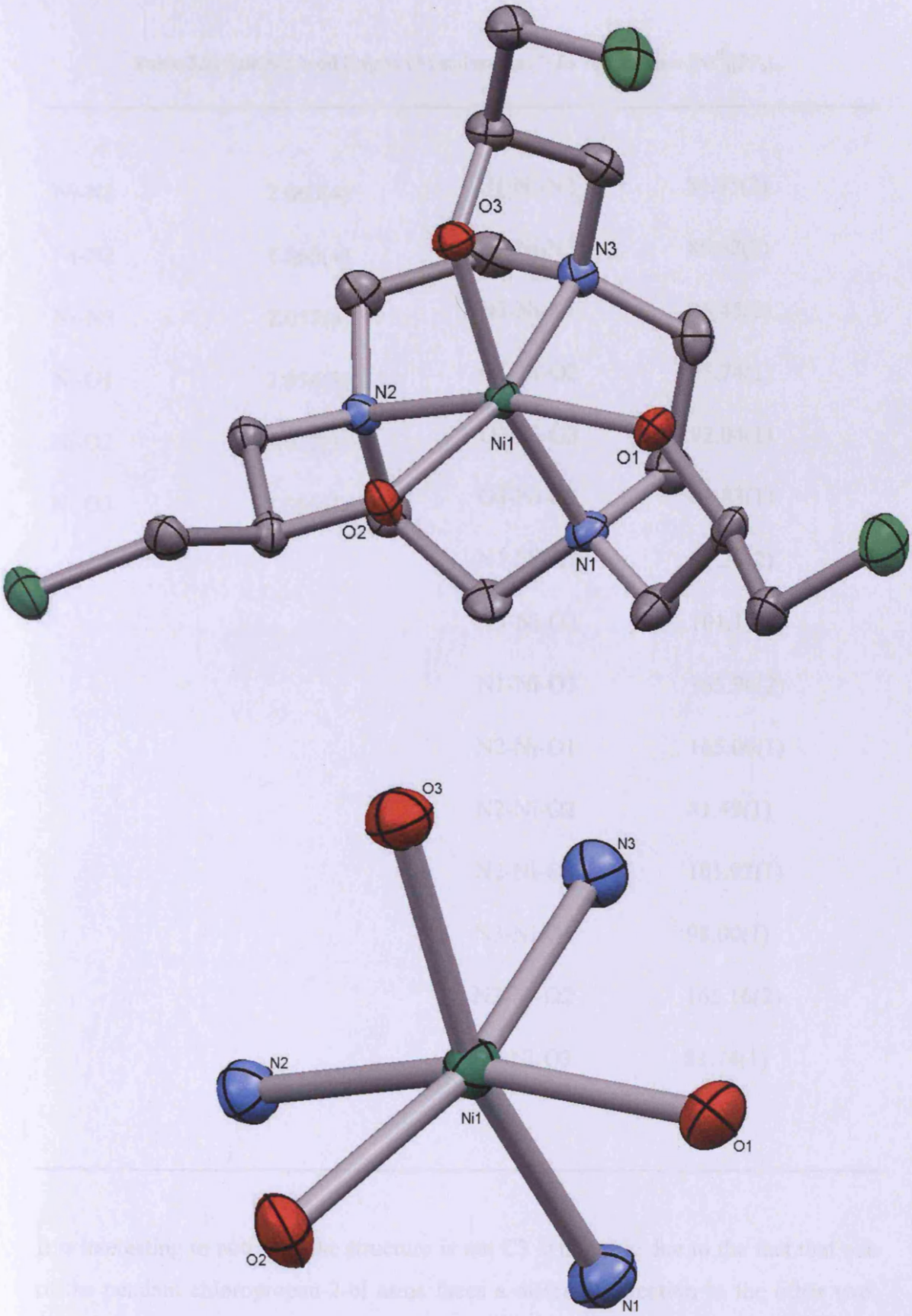

Fig 3.4: Top: Molecular structure of $[Ni^{II}\mathbf{L}^1][PF_6]_2$ counterions and hydrogens omitted for clarity, thermal ellipsoids set at the 50% probability level. Bottom: $[Ni^{II}\mathbf{L}^1][PF_6]_2$, metal centre and the coordinating atoms only, showing the geometry of the metal centre.

Table 3.2: Selected bond lengths (Å) and angles (°) for the complex $[Ni^{II}][PF_6]_2$.

Ni-N1	2.060(4)	N1-Ni-N2	84.85(2)
Ni-N2	2.060(4)	N2-Ni-N3	86.62(2)
Ni-N3	2.057(4)	N3-Ni-N1	86.45(2)
Ni-O1	2.056(3)	O1-Ni-O2	95.74(1)
Ni-O2	2.077(3)	O2-Ni-O3	92.04(1)
Ni-O3	2.085(3)	O3-Ni-O1	92.83(1)
		N1-Ni-O1	81.28(2)
		N1-Ni-O2	101.19(2)
		N1-Ni-O3	165.96(2)
		N2-Ni-O1	165.06(1)
		N2-Ni-O2	81.49(1)
		N2-Ni-O3	101.92(1)
		N3-Ni-O1	98.00(1)
		N3-Ni-O2	165.16(2)
		N3-Ni-O3	81.74(1)

It is interesting to note that the structure is not C3 symmetric due to the fact that one of the pendant chloropropan-2-ol arms faces a different direction to the other two. This asymmetry is represented in the bond lengths, Ni-O1 (2.056 Å) is significantly shorter than Ni-O2 and Ni-O3 (2.077 and 2.085 Å respectively).

An attempt was made to displace the peripheral chlorides in $[Ni\mathbf{L}^1][PF_6]_2$ with a secondary amine, upon reaction of $Ni\mathbf{L}^1.H_3$ with N-methyl homopiperazine in ethanol the reaction mixture changed colour from purple to blue. Crystals obtained, unexpectedly showed the $[Ni^{II}\mathbf{L}^1H_3\mathbf{L}^1Ni^{II}][PF_6]$ complex had been formed (fig. 3.5, table 3.3) by deprotonation of half of the alcohol moieties. The crystal data shows two slightly different Ni environments for the two halves of the complex, one for the neutral O donors and one for the anionic O donors. The Ni1 half of the complex has shorter Ni-N bonds than the Ni2 half (2.075 and 2.088 Å respectively). This would imply a greater degree of π-bonding in the Ni1 half indicating that this is the deprotonated half of the complex. This description should be treated with caution as the bond lengths are close enough to each other to indicate a dinuclear species where both half units share the three protons between six partial alkoxide species.

Further investigation by mass spectrometry and chromatography did indeed prove the pendant chlorides are no longer available for substitution. This is probably because the coordination of the alcohol essentially removes the 'chlorohydrin' nature of the pendant donor (scheme 3.4).

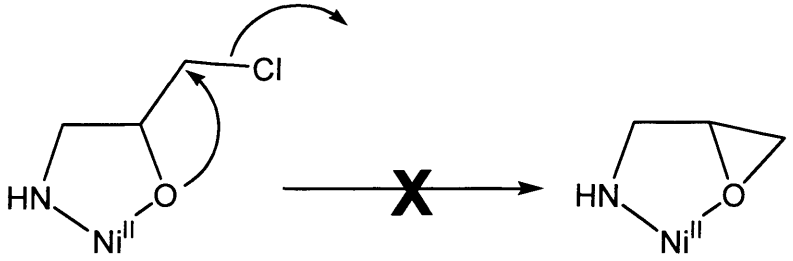

Scheme 3.4: Donation of the oxygen lone pairs to the nickel(II) ion probably prevents nucleophilic attack on the electrophilic carbon centre.

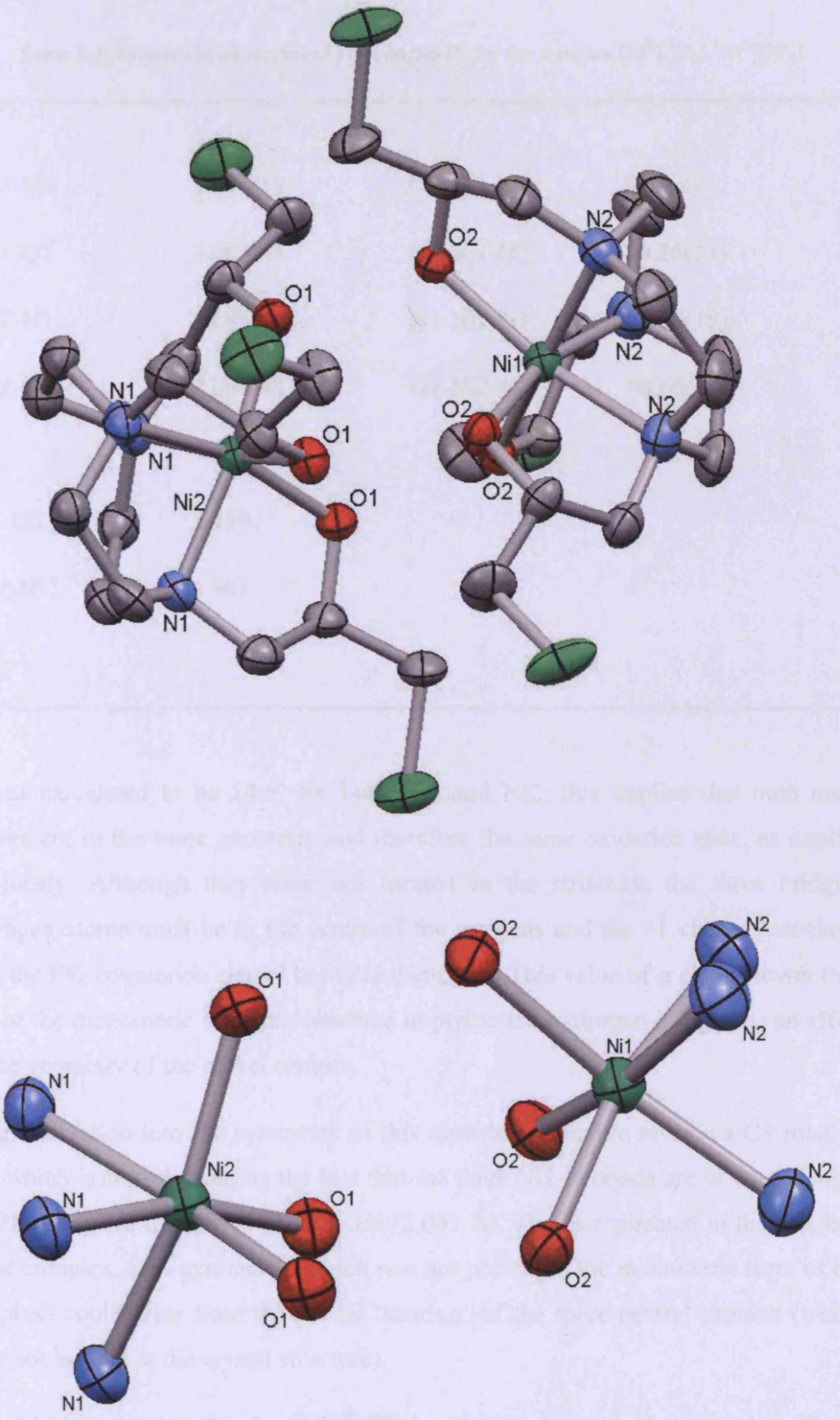

Fig. 3.5: Top: Molecular structure of $[Ni^{II}\mathbf{L}^{1}H_{3}\mathbf{L}^{1}Ni^{II}][PF_{6}]$ counterions and hydrogens omitted for clarity, thermal ellipsoids set at the 50% probability level. Bottom: $[Ni^{II}\mathbf{L}^{1}H_{3}\mathbf{L}^{1}Ni^{II}][PF_{6}]$, metal centre and the coordinating atoms only, showing the geometry of the metal centre.

(1.912 – 2.340, mean 2.114 Å for 100 examples).[16, 17] The Ni-O bond lengths in complex $[NiL^1][PF_6]_2$ (2.073 Å) and the dinucleic form, $[NiL^1H_3L^1Ni]$ (2.062 Å) were also found to be of average length on comparison with structurally related complexes $(RO)_3NiX_3$ in the Cambridge Structural Database (1.901 – 2.262, mean 2.073 Å)[18, 19].

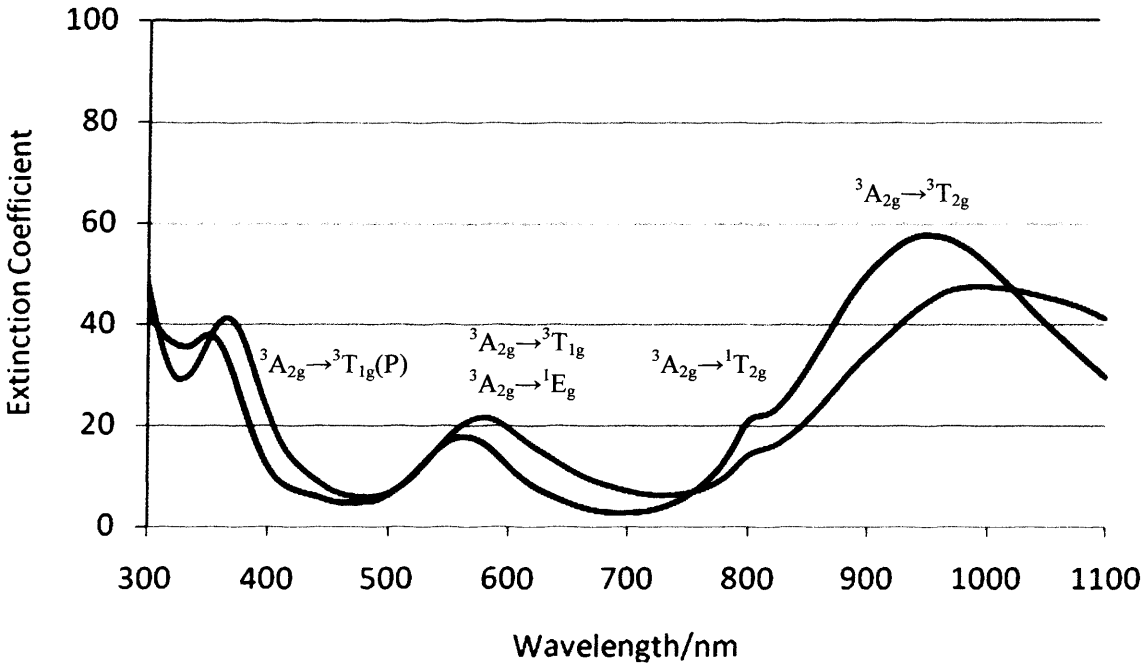

Fig 3.6: The UV spectra of $[NiL^1][PF_6]_2$ in acidic (black) and basic conditions (blue). Transitions are assigned from the Tunabe Sugano diagram shown in fig 3.7.

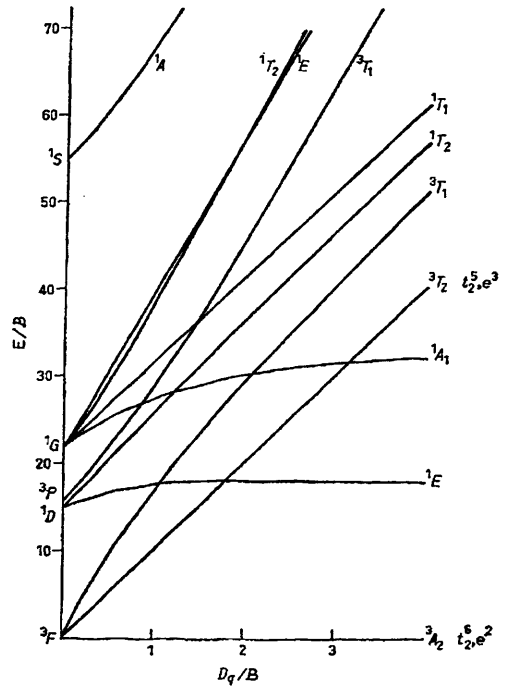

Fig. 3.7: Tanabe Sugano energy level diagram for d^8 ions in an octahedral field.[20]

The Tanabe Sugano energy level diagram for a d^8 ion in an octahedral field (fig. 3.7)[20] shows three spin allowed transitions: $^3A_{2g}\rightarrow{}^3T_{2g}$, $^3A_{2g}\rightarrow{}^3T_{1g}$ and $^3A_{2g}\rightarrow{}^3T_{1g}(P)$, they normally occur between 750-14,000 nm, 500-900 nm and 350-530 nm respectively. In addition, it is common to observe two spin forbidden transitions in octahedral d^8 complexes, the first is $^3A_{2g}\rightarrow{}^1E_g$ and occurs very close to, or obscured by the second spin allowed transition, it is probable that this is the origin of the relatively broad nature of the $^3A_{2g}\rightarrow{}^3T_{1g}$ peak. The second spin forbidden transition occurs between the second and third spin allowed absorptions, this is attributable to the $^3A_{2g}\rightarrow{}^1T_{2g}$ transition and is believed to be the shoulder visible at 816 nm.

The complex in basic conditions gives rise to a similar electronic spectrum to that of the complex in acidic conditions, the main difference being a shift of about 20nm for each of the peaks. The acidic form of the complex contains three alcohol donors, while the basic form contains alkoxide donors. The UV's confirm this by suggesting a slightly smaller Δ_0 for the acidic form. From the spectrochemical series, alcohol is a weaker field donor than alkoxide and therefore should give rise to a smaller Δ_0, hence a smaller wavelength in the electronic spectrum.

The UVs and crystal structures obtained on this complex prompted interest into the chemistry of the pendant alcohols. The pKa's of the coordinated alcohol groups were undeterminable by titrometric analysis due to the reactivity of the peripheral chlorides on the ligand. A smooth titration curve was unobtainable, therefore a suitable substitute was sought after. This was found in $[Ni^{II}\mathbf{L}^2H_3][ClO_4]_2$ (discussed later in this chapter), as it possesses no reactive chloride atoms, the titration afforded a smooth curve (fig. 3.8) and the pKa of the coordinated alcohol groups was determined to be 7.51. The programs used in the derivation of this value were Glee[21] and Hyperquad.[22]

This value is of a similar order of magnitude to other examples present in the literature.[23-28] For example, a pKa value of 7.7 was found for the coordinated water in the system in fig. 3.9 by Xia *et al.*[28]

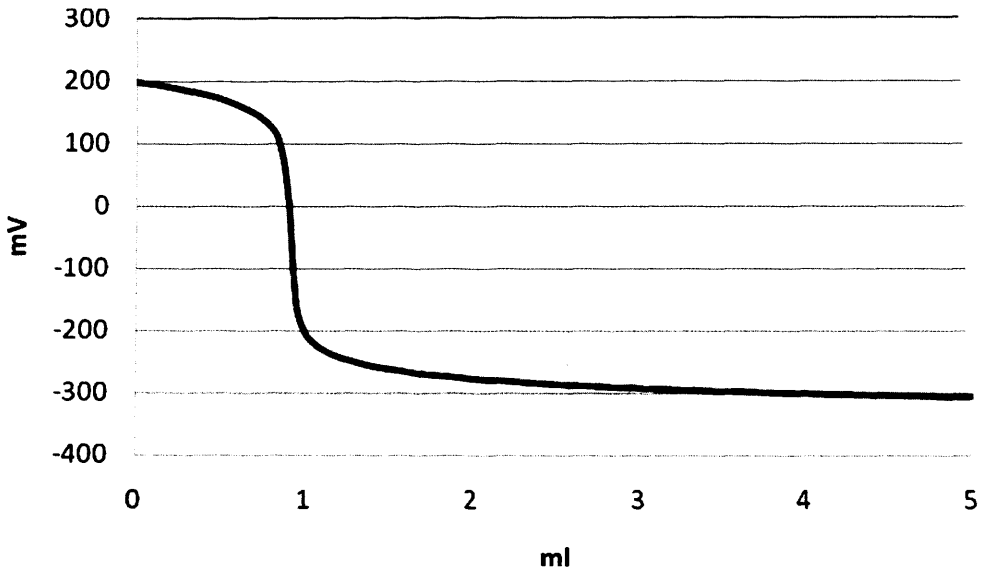

Fig. 3.8: Titration curve obtained for $[Ni^{II}\mathbf{L}^{2}H_3][ClO_4]_2$.

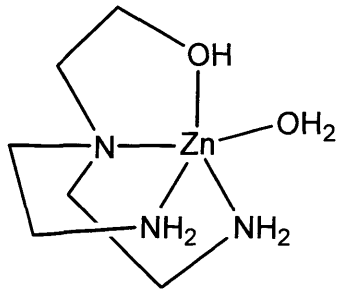

Fig. 3.9: The system studied by Xia *et al.*

There is an interest in the pKa values of certain bound water molecules in natural systems, for instance, it is known that the pKa of zinc bound water in carbonic anhydrase is between 7 and 8,[29] this is also concurrent with the value obtained for $[Ni^{II}\mathbf{L}^{2}H_3][ClO_4]_2$.

3.3.1.2 $[Co^{II}\boldsymbol{L}^{1}H_3\boldsymbol{L}^{1}Co^{III}](PF_6)_2$

Again, this complex forms a dinuclear complex (fig. 3.10) with 2 non-coordinating counterions. However, contrary to expectations, this is a mixed valence complex of the form $[Co^{II}LH_3LCo^{III}][PF_6]_2$. One metal centre is of *pseudo* octahedral geometry while the other is trigonally distorted, from table 3.4 it is clear that the octahedral metal centre has shorter bond lengths than the trigonally distorted cobalt.

Co^{III} is d^6, usually adopting a low spin conformation, due to a high crystal field stabilisation parameter (CFSE), consequently a degenerate t_{2g} set of orbitals induces a high affinity for the octahedral geometry. Also, the shorter bonds indicate a greater

degree of π^* bonding and therefore a more electron deficient atom. This is enough evidence to confidently state that the octahedral cobalt is Co^{III} and the trigonally distorted cobalt is Co^{II}.

This is interesting as the crystal structure reported by Peacock *et al.*[6] (on the propylene oxide ligand) contains two very similar half units, each containing a Co^{III} species. They reported twist angles from ideal octahedral geometry, φ, of 10.2° and 11.2°, φ, in the Co^{III} half of $[Co^{II}\mathbf{L^1}H_3\mathbf{L^1}Co^{III}][PF_6]_2$ was found to be 7.8°, implying almost complete octahedral geometry. Once again, the metal centre is closer to ideal octahedral geometry than the analogous complex of ligand 22.

The twist angle, φ, for Co2 was found to be 55.4°, this implies the two donor sets are nearly eclipsing each other, forming a trigonal prismatic geometry.

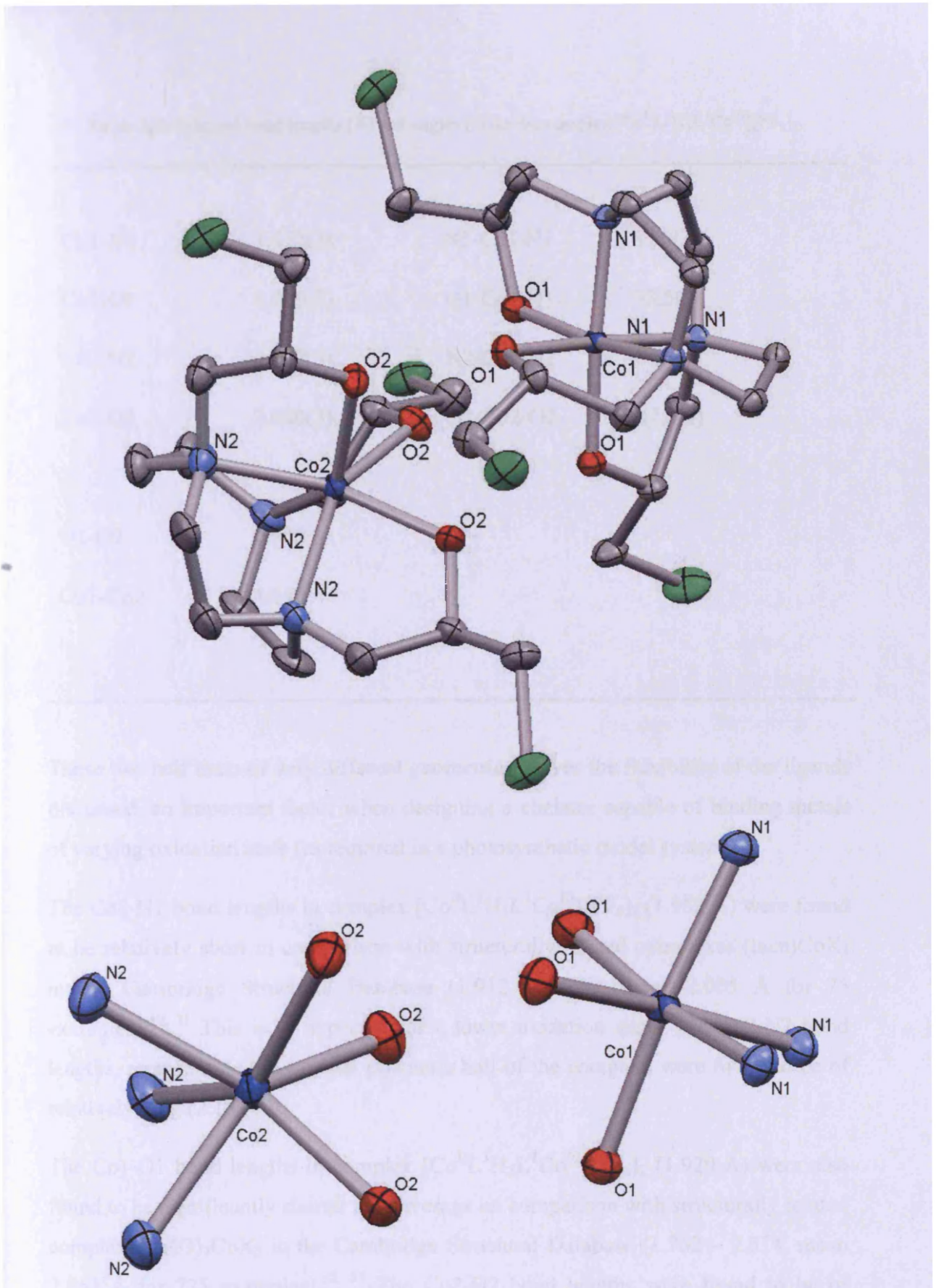

Fig. 3.10: Top: Molecular structure of $[Co^{II}\mathbf{L}^{1}H_3\mathbf{L}^{1}Co^{III}][PF_6]_2$counterions and hydrogens omitted for clarity, thermal ellipsoids set at the 50% probability level. Bottom: $[Co^{II}\mathbf{L}^{1}H_3\mathbf{L}^{1}Co^{III}][PF_6]_2$, metal centre and the coordinating atoms only, showing the geometry of the metal centre.

Table 3.4: Selected bond lengths (Å) and angles (°) for the complex $[Co^{II}\mathbf{L}^{1}H_3\mathbf{L}^{1}Co^{III}][PF_6]_2$.

Co1-N1	1.952(3)	N1-Co1-N1	87.6(3)
Co1-O1	1.920(2)	O1-Co1-O1	93.5(4)
Co2-N2	2.157(3)	N2-Co2-N2	81.1(4)
Co2-O2	2.090(3)	O2-Co2-O2	87.4(4)
O1-O2	2.500		
Co1-Co2	4.640		

These two half units of very different geometries proves the flexibility of the ligands discussed, an important factor when designing a chelator capable of binding metals of varying oxidation state (as required in a photosynthetic model system).

The Co1-N1 bond lengths in complex $[Co^{II}\mathbf{L}^{1}H_3\mathbf{L}^{1}Co^{III}][PF_6]_2$ (1.952 Å) were found to be relatively short in comparison with structurally related complexes $(tacn)CoX_3$ in the Cambridge Structural Database (1.912 – 2.239, mean 2.005 Å for 75 examples).[30, 31] This is as expected for a lower oxidation state. The Co2-N2 bond lengths, representing the trigonal prismatic half of the complex, were found to be of relatively long (2.157 Å).

The Co1-O1 bond lengths in complex $[Co^{II}\mathbf{L}^{1}H_3\mathbf{L}^{1}Co^{III}][PF_6]_2$ (1.920 Å) were also found to be significantly shorter than average on comparison with structurally related complexes $(RO)_3CoX_3$ in the Cambridge Structural Database (1.762 – 2.514, mean 2.063 Å for 725 examples).[32, 33] The Co2-O2 bond lengths were found to be of average length (2.090 Å).

The UV spectrum of the complex (fig. 3.11) shows two peaks, one at 398 nm and another at 553 nm. This is very similar to that reported by Peacock *et al.*[6] on the

dinuclear structure of compound **22**. It is possible that both d^6 and d^7 ions are present as the low spin states because the two peaks observed in the UV spectra are relatively broad. However, it is probable that the UV spectrum recorded is that of a low spin d^6 ion (Co^{III}) only.

A low spin d^6 ion in an octahedral environment would be expected to show 2 transitions in the ranges of 300-450 nm and 550-700 nm, these are assignable to the $^1A_1 \rightarrow {}^1T_{2g}$ and $^1A_1 \rightarrow {}^1T_{1g}$ transitions respectively and are shown in fig. 3.12. Six-coordinate Co^{III} complexes are almost always low spin (with the exception of some fluoride complexes),[34] it is therefore most probable that the Co is present as a low spin d^6 ion.

A high spin d^7 ion in an octahedral field is expected to give rise to three excitations: $^4T_{1g} \rightarrow {}^4T_{2g}$ (1,100-1,300 nm), $^4T_{1g} \rightarrow {}^4A_{2g}$ (500-700 nm) and $^4T_{1g} \rightarrow {}^4T_{1g}(P)$ (450-550 nm). As only two excitations are observed, this possibility can reasonably be discounted. A low spin d^7 ion should show two peaks in the ranges of 500-600 nm ($^2A_{1g} \rightarrow {}^2T_{1g}$) and 600-800 nm ($^2A_{1g} \rightarrow {}^2E_g$ and $^2A_{1g} \rightarrow {}^2T_{2g}$), the peaks observed are not within these ranges, it is therefore appropriate to assign the spectra as that of a low spin d^6 ion.

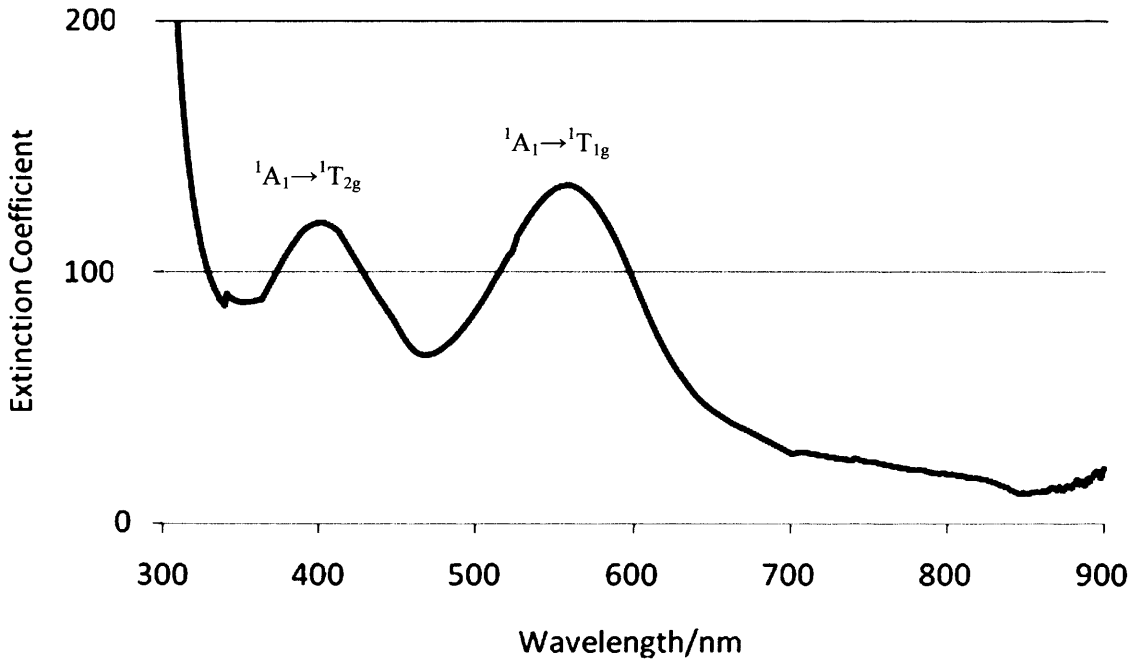

Fig. 3.11: UV spectrum of $[Co^{II}L^1H_3L^1Co^{III}][PF_6]_2$ with transitions assigned. The spectrum was measured up to 1,200nm but the region >800nm has been omitted for clarity as this shows no extra information.

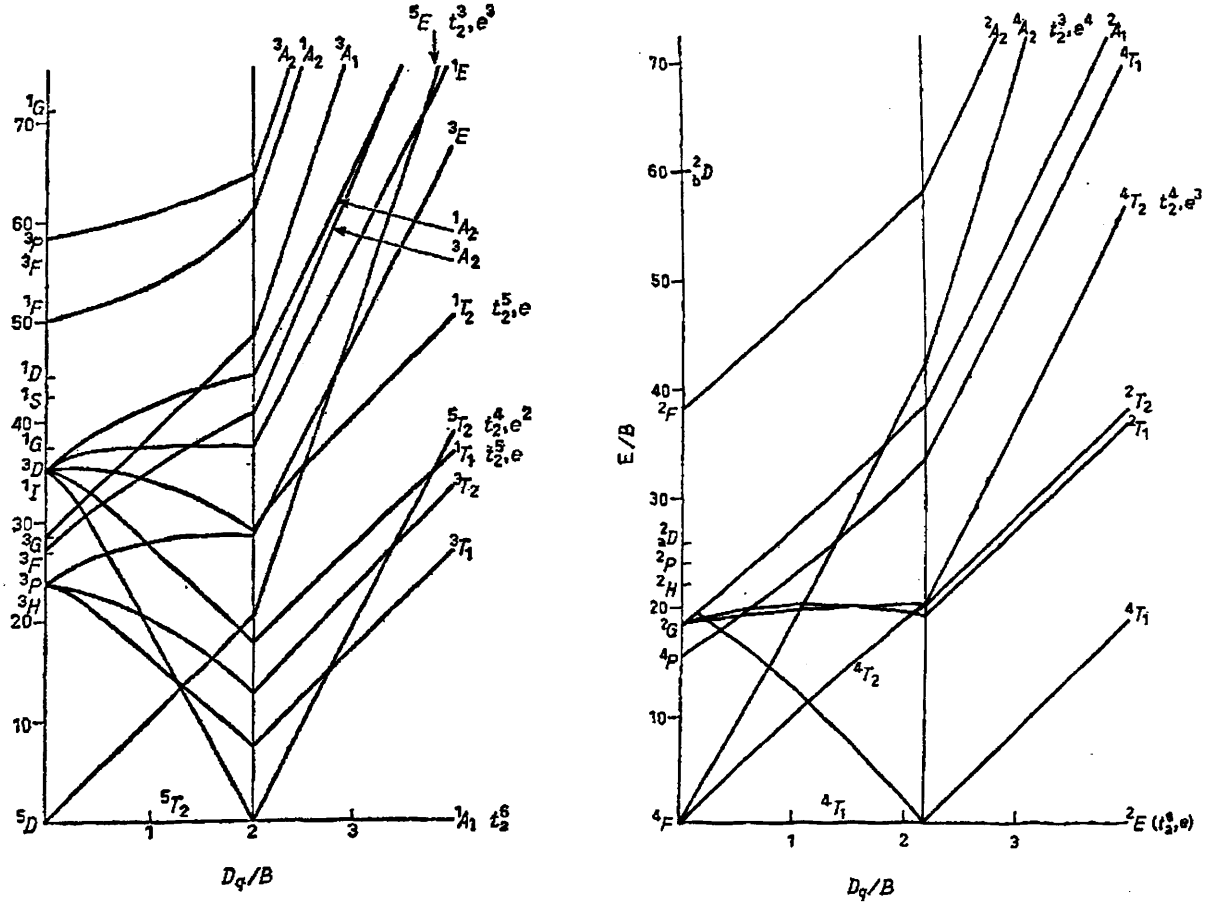

Fig. 3.12: Tanabe Sugano energy level diagrams for d^6 (left) and d^7 (right) ions in an octahedral field.[20]

3.3.1.3 $[Cr^{III}L^1H_3L^1Cr^{III}][PF_6]_3$

The crystal structure obtained from the reaction of chromium trichloride with $\mathbf{L}^1.H_3$ (fig. 3.13) once again, yielded a dinuclear complex. However, the complex observed is of the type $[Cr^{III}LH_3LCr^{III}][PF_6]_3$, and contains a *pseudo* octahedral half and a trigonally distorted half is observed, the *pseudo* octahedral half unit having shorter bonds than the other half unit (table 3.5). This is apparent when considering φ values, pseudo octahedral metal centre, Cr1, has a value of 16.7° while the Cr2 φ value is 35.3°, which places it between octahedral and trigonal prismatic geometry.

Models by Farrugia *et al.*[7] suggest that the most stable geometry for a dinuclear complex of this type is one in which one half adopts a pseudo octahedral geometry and the other adopts a trigonal prismatic geometry, as found in both Co and Cr complexes reported here. The main difference between the two structures being the

fact that the Co structure is a mixed valent complex while the Cr structure is not. This is probably due to oxidation of the d^7 Co^{II} species.

It is clear from the angles that the *pseudo* octahedral half of the structure is 'less octahedral' than the corresponding cobalt structure (the bond angles are further away from 90° than those of the Co analogue). The cobalt structure has significantly shorter M-N and M-O bonds than the chromium structure. A simple electron count of the two alkoxide M^{III} octahedral halves concurs with this observation. The Cr^{III} half gives a total of 15 electrons compared to the corresponding Co^{III} half which has a total of 18 electrons. By this reasoning the Co^{III} is a more thermodynamically stable species than Cr^{III}.

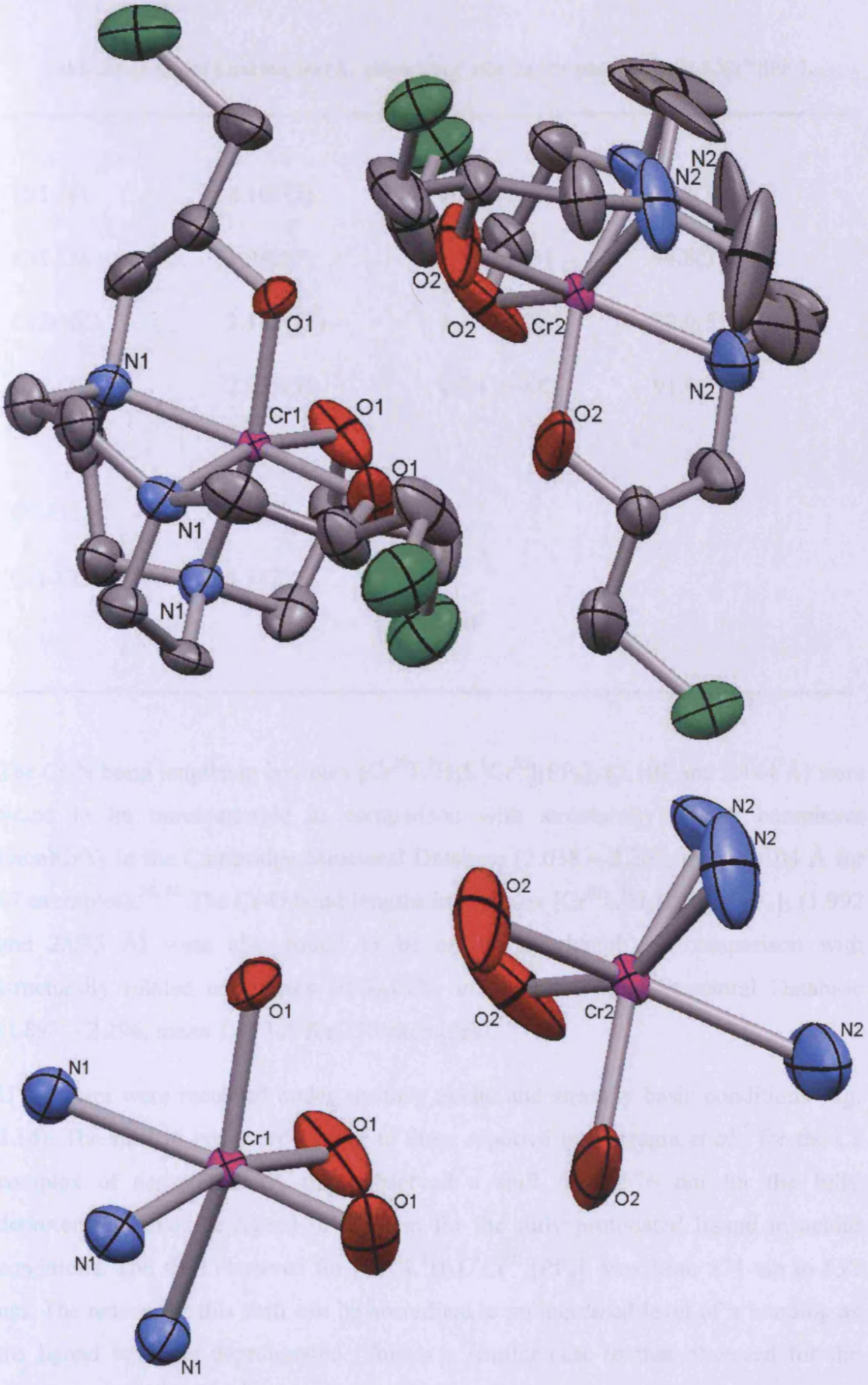

Fig. 3.13: Top: Molecular structure of $[Cr^{III}\mathbf{L}^{1}H_{3}\mathbf{L}^{1}Cr^{III}][PF_{6}]_{3}$ counterions and hydrogens omitted for clarity, thermal ellipsoids set at the 50% probability level. Bottom: $[Cr^{III}\mathbf{L}^{1}H_{3}\mathbf{L}^{1}Cr^{III}][PF_{6}]_{3}$, metal centre and the coordinating atoms only, showing the geometry of the metal centre.

Table 3.5: Selected bond lengths (Å) and angles (°) for the complex $[Cr^{III}\mathbf{L}^{1}H_3\mathbf{L}^{1}Cr^{III}][PF_6]_3$.

Cr1-N1	2.101(7)	N1-Cr1-N1	83.2(3)
Cr1-O1	1.992(7)	O1-Cr1-O1	94.8(3)
Cr2-N2	2.144(11)	N2-Cr2-N2	82.0(5)
Cr2-O2	2.035(9)	O2-Cr2-O2	91.9(3)
O1-O2	2.518		
Cr1-Cr2	4.582		

The Cr-N bond lengths in complex $[Cr^{III}\mathbf{L}^{1}H_3\mathbf{L}^{1}Cr^{III}][PF_6]_3$ (2.101 and 2.144 Å) were found to be unremarkable in comparison with structurally related complexes $(tacn)CrX_3$ in the Cambridge Structural Database (2.038 – 2.207, mean 2.104 Å for 67 examples).[35, 36] The Cr-O bond lengths in complex $[Cr^{III}\mathbf{L}^{1}H_3\mathbf{L}^{1}Cr^{III}][PF_6]_3$ (1.992 and 2.035 Å) were also found to be of average length on comparison with structurally related complexes $(RO)_3CrX_3$ in the Cambridge Structural Database (1.897 – 2.296, mean 1.973 Å for 259 examples).[37, 38]

UV spectra were recorded under strongly acidic and strongly basic conditions (fig. 3.14). The shift in peaks are similar to those reported by Farrugia *et al.*[7] for the Cr complex of compound **22**, they observed a shift from 576 nm for the fully deprotonated alkoxide ligand to 516 nm for the fully protonated ligand in acidic conditions. The shift observed for $[Cr^{III}\mathbf{L}^{1}H_3\mathbf{L}^{1}Cr^{III}][PF_6]_3$ was from 574 nm to 532 nm. The reason for this shift can be accredited to an increased level of π bonding as the ligand becomes deprotonated. This is a similar case to that observed for the complex $[Ni^{II}\mathbf{L}^{1}H_3\mathbf{L}^{1}Ni^{II}](PF_6)$ when subjected to acidic and basic conditions. However, the effect is now even more pronounced. The shift in wavelengths can again be attributed to the difference in Δ_0 between the acidic form of the complex

(alcohol donors) and the basic form (alkoxide donors). From the spectrochemical series, alcohol is a weaker field donor than alkoxide and therefore should give rise to a smaller Δ_0, hence a smaller wavelength in the electronic spectrum.

The transitions have been assigned as $^4A_{2g} \rightarrow {}^4T_{1g}$, $^4A_{2g} \rightarrow {}^4T_{1g}(F)$, these can be seen on the Tunabe Sugano diagram in fig. 3.15.

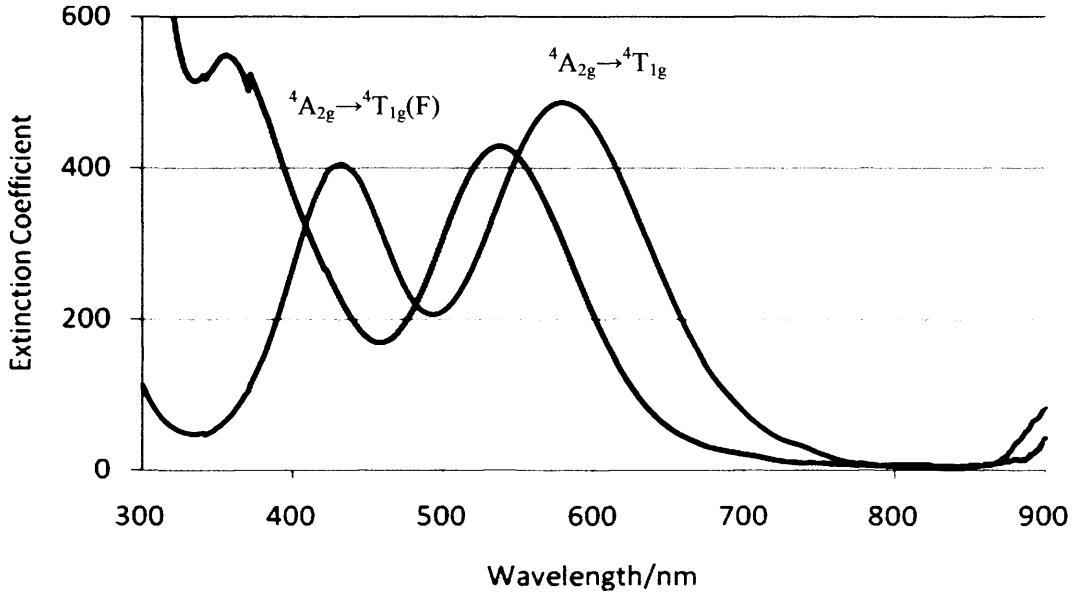

Fig. 3.14: UV spectra for the complex $[Cr^{III}L^1H_3L^1Cr^{III}][PF_6]_3$ under acidic (black) and basic (blue) conditions.

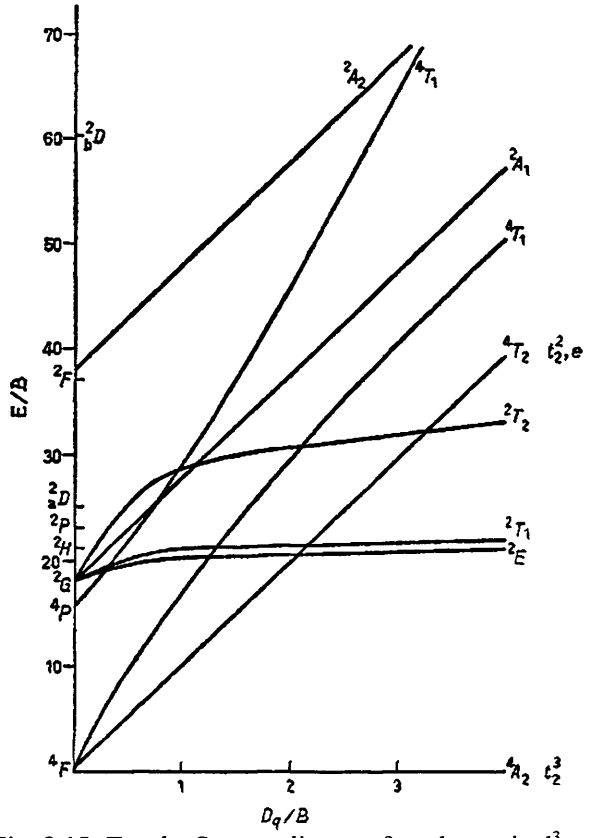

Fig. 3.15: Tunabe Sugano diagram for a low spin d^3 metal.

3.3.2 $\mathbf{L^2}$ Complexes

3.3.2.1 $[Ni^{II}\mathbf{L^2}H_3][ClO_4]_2$

The nickel complex of Sherry's ligand, $\mathbf{L^2}.H_3$, forms a monomer of the type $[Ni^{II}LH_3][ClO_4]_2$, the counterions are non-coordinating. A trigonally distorted geometry of the metal centre is observed, fig. 3.16, and, as demonstrated by table 3.6, the nickel bonds are all of similar lengths (all within 0.03Å). Dinucleation is not believed to occur due to the relative bulk of the two methyl groups present on each pendant arm of the macrocycle. This was proved by UV (fig. 3.17), the UV spectra of the complex was measured under acidic and basic conditions, the spectra are identical, implying that there is no change to the metal centre under varying conditions of acidity. It is therefore appropriate to assume that no dinucleation occurs in this complex. The metal centre exhibits a twist angle, φ, of 13.9°, this is the smallest of any of the nickel complexes discussed and demonstrates the effect extra bulk of the pendant arms can have on the geometry of the metal centre.

The Ni-N bond lengths in complex Ni$\mathbf{L^2}$ (2.048 Å) were found to be significantly shorter than average in comparison with structurally related complexes (tacn)NiX_3 in the Cambridge Structural Database (1.912 – 2.340, mean 2.114 Å for 100 examples).[16, 17] The Ni-O bond lengths in complex Ni$\mathbf{L^2}$ (2.066 Å) were found to be of average length on comparison with structurally related complexes $(RO)_3NiX_3$ in the Cambridge Structural Database (1.901 – 2.262, mean 2.073 Å for 599 examples).[18, 19]

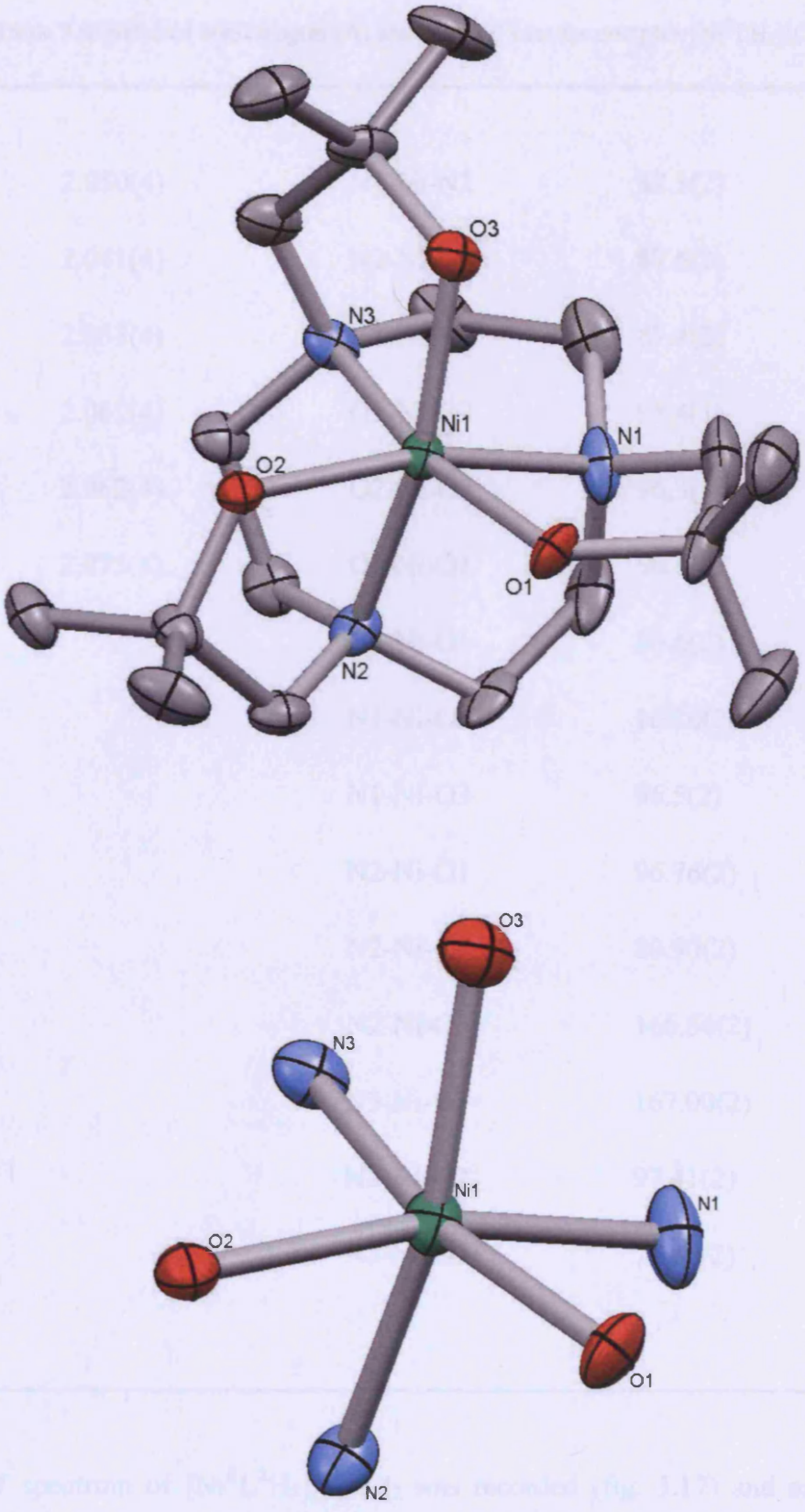

Fig. 3.16: Top: Molecular structure of $[Ni^{II}L^2H_3][ClO_4]_2$ counterions and hydrogens omitted for clarity, thermal ellipsoids set at the 50% probability level. Bottom: $[Ni^{II}L^2H_3][ClO_4]_2$, metal centre and the coordinating atoms only, showing the geometry of the metal centre.

Table 3.6: Selected bond lengths (Å) and angles (°) for the complex $[Ni^{II}LH_3][ClO_4]_2$.

Ni-N1	2.050(4)	N1-Ni-N2	87.3(2)
Ni-N2	2.041(4)	N2-Ni-N3	87.5(2)
Ni-N3	2.053(4)	N3-Ni-N1	87.4(2)
Ni-O1	2.061(4)	O1-Ni-O2	95.4(1)
Ni-O2	2.062(4)	O2-Ni-O3	96.3(1)
Ni-O3	2.075(4)	O3-Ni-O1	96.6(1)
		N1-Ni-O1	80.6(2)
		N1-Ni-O2	167.0(2)
		N1-Ni-O3	96.5(2)
		N2-Ni-O1	96.76(2)
		N2-Ni-O2	80.90(2)
		N2-Ni-O3	166.56(2)
		N3-Ni-O1	167.00(2)
		N2-Ni-O2	97.41(2)
		N3-Ni-O3	79.80(2)

The UV spectrum of $[Ni^{II}\mathbf{L}^2H_3][ClO_4]_2$ was recorded (fig. 3.17) and assigned the same as $Ni\mathbf{L}^1$, the two spectra are very similar. The UV spectra were recorded under acidic and basic conditions, it is clear that the two spectra are the same. This implies that, unlike $[Ni^{II}\mathbf{L}^1H_3][ClO_4]_2$, $[Ni^{II}\mathbf{L}^2H_3][ClO_4]_2$ cannot dinucleate under varying pH

conditions. This is due to the presence of the extra bulk on the pendant arms of the ligand that is not present for complexes of $\mathbf{L^1}$.

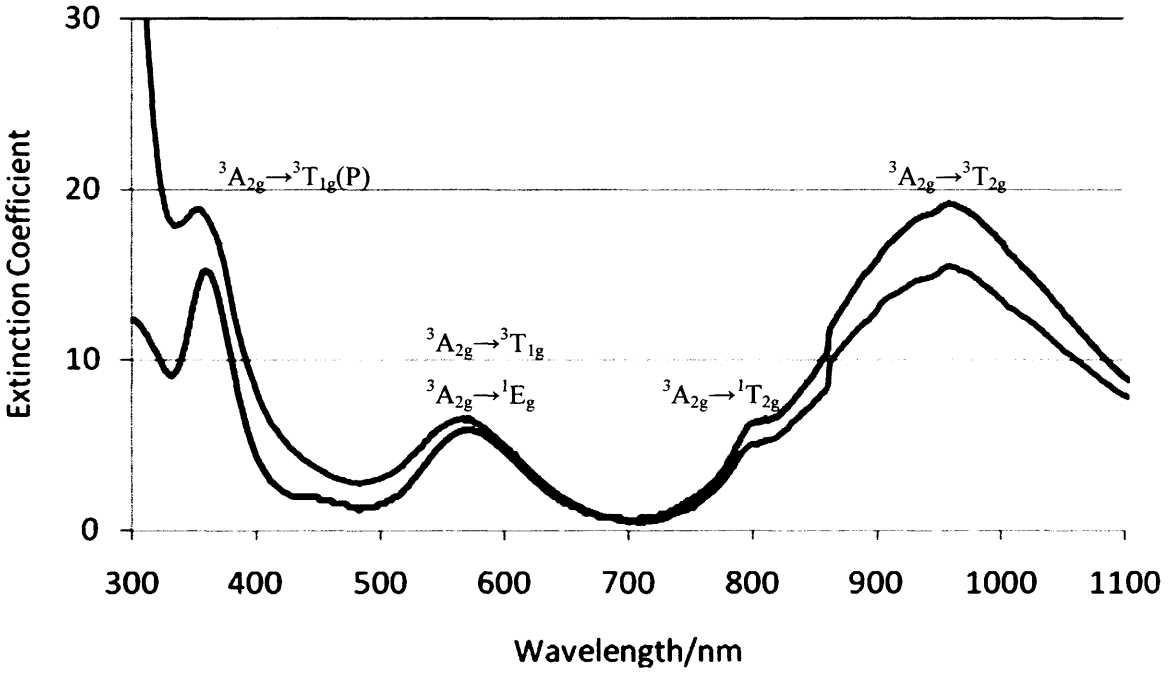

Fig. 3.17: UV spectrum of $[Ni^{II}\mathbf{L}^2H_3][ClO_4]_2$ under acidic (black) and basic (blue) conditions.

3.3.2.2 $[Mn^{II}\mathbf{L}^2H_3][PF_6]_2$

The manganese complex of $\mathbf{L}^2.H_3$ gave a similar structure as the nickel analogue (fig. 3.18), but the bonds are generally longer. The metal-O bonds are observed to be shorter than the metal-N bonds (by about 0.1 Å, table 3.7). The structure is very similar to the Mn^{II} half of the structure reported by Peacock *et al*[8] in the $Mn^{II}Mn^{IV}$ dinuclear complex of compound **22**. However, the structure was reported to be purely trigonal prismatic, the structure shown has a twist angle, φ, of 46.0° away from octahedral geometry, implying *pseudo* trigonal prismatic geometry.

The Mn-N bond lengths in complex $[Mn^{II}\mathbf{L}^2H_3][PF_6]_2$ (2.280 Å) were found to be significantly longer than average in comparison with structurally related complexes $(tacn)MnX_3$ in the Cambridge Structural Database (2.039 – 2.388, mean 2.175 Å for 93 examples).[39, 40] The Mn-O bond lengths in complex $[Mn^{II}\mathbf{L}^2H_3][PF_6]_2$ (2.162 Å) were found to be of average length on comparison with structurally related complexes $(RO)_3MnX_3$ in the Cambridge Structural Database (1.797 – 2.807, mean 2.146 Å for 854 examples).[41, 42]

As the compound is a colourless Mn^{II} complex, the UV is so weak that it is not an informative means of characterising this complex.

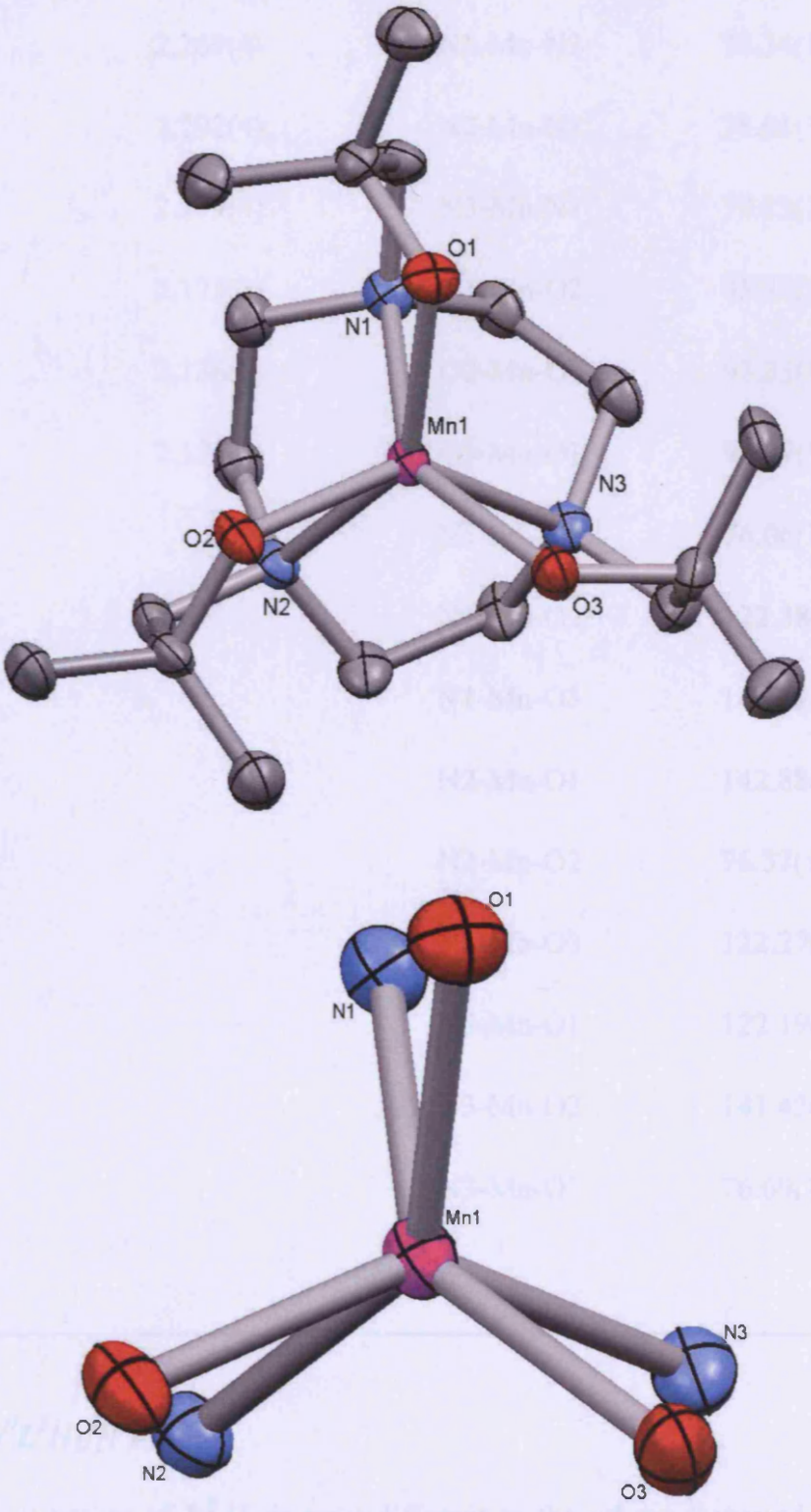

Fig. 3.18: Top: Molecular structure of $[Mn^{II}L^2H_3][PF_6]_2$, counterions and hydrogens omitted for clarity, thermal ellipsoids set at the 50% probability level. Bottom: $[Mn^{II}L^2H_3][PF_6]_2$, metal centre and the coordinating atoms only, showing the geometry of the metal centre.

Table 3.7: Selected bond lengths (Å) and angles (°) for the complex $[Mn^{II}LH_3][PF_6]_2$.

Mn-N1	2.269(4)	N1-Mn-N2	78.34(1)
Mn-N2	2.292(4)	N2-Mn-N3	78.01(1)
Mn-N3	2.279(4)	N3-Mn-N1	79.23(1)
Mn-O1	2.173(3)	O1-Mn-O2	95.31(1)
Mn-O2	2.136(3)	O2-Mn-O3	93.33(1)
Mn-O3	2.177(3)	O3-Mn-O1	93.97(1)
		N1-Mn-O1	76.06(1)
		N1-Mn-O2	122.38(1)
		N1-Mn-O3	143.32(1)
		N2-Mn-O1	142.88(1)
		N2-Mn-O2	76.37(1)
		N2-Mn-O3	122.27(1)
		N3-Mn-O1	122.19(1)
		N3-Mn-O2	141.43(1)
		N3-Mn-O3	76.69(1)

3.3.2.3 $[Cu^{II}L^2H_2][PF_6]$

The copper structure of $L^2.H_3$ is very different to the others discussed so far (fig. 3.19), it forms a 5-coordinate pseudo-square based pyramidal structure, with two amine donors, one alcohol donor and one alkoxy donor making up the base of the pyramid, and the final amine forms the apex of the pyramid. The other alcohol

remains uncoordinated. This strongly suggests Jahn-Teller distortion within this d^9 copper centre. Surprisingly it is the only example of an *N,N',N"*tris-2-hydroxy tacn complex adopting a geometry involving just five ligands. Every other crystal structure published contains a hexadentate metal.

The structure has far from ideal square based pyramidal geometry, this can be attributed to the extremely high amount of strain that would be required to force such a geometry onto the restrictive macrocyclic ligand.

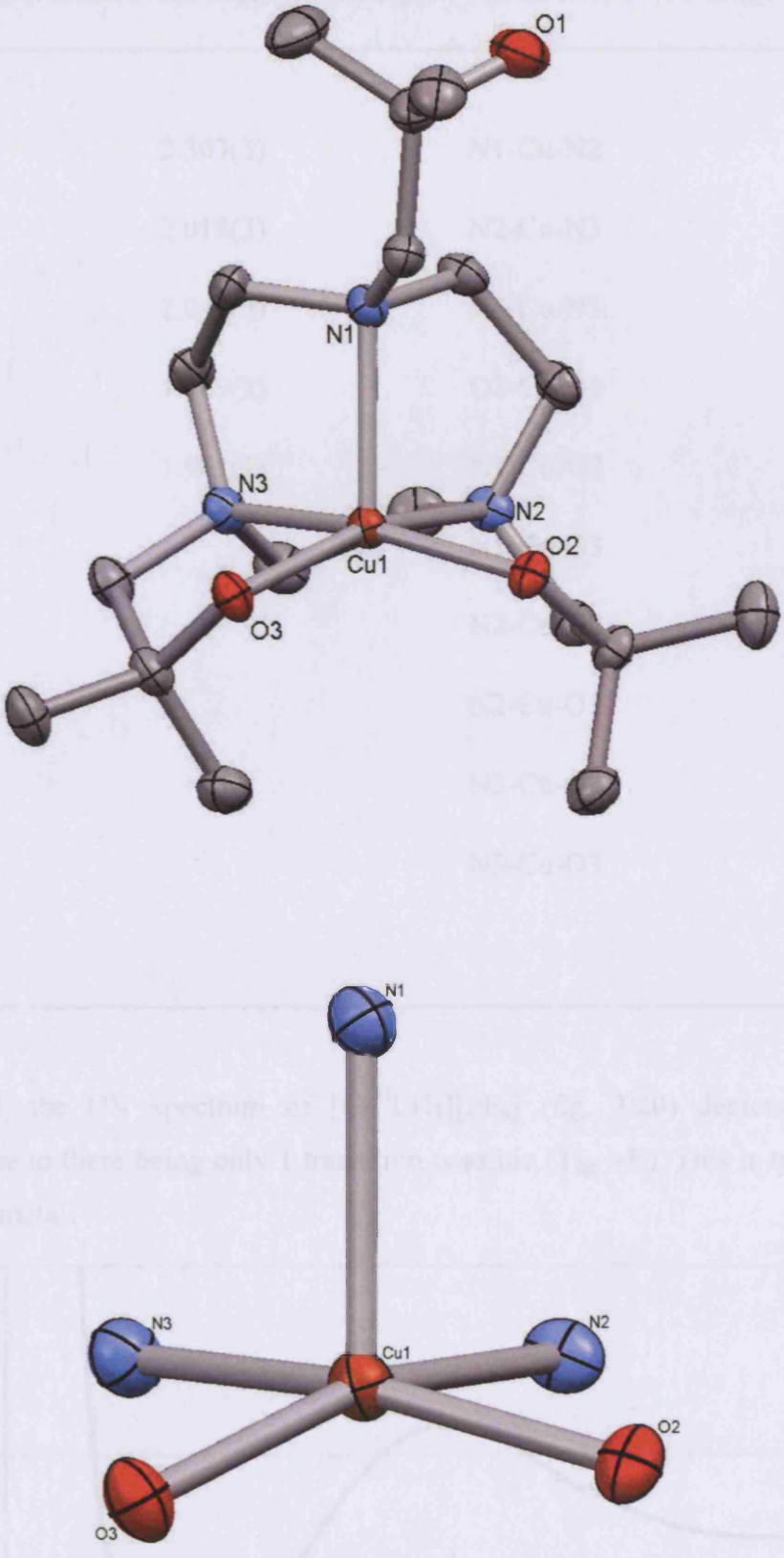

Fig. 3.19: Top: Molecular structure of $[Cu^{II}L^2H_2][PF_6]$, counterions and hydrogens omitted for clarity, thermal ellipsoids set at the 50% probability level. Bottom: $[Cu^{II}L^2H_2][PF_6]$, metal centre and the coordinating atoms only, showing the geometry of the metal centre.

Table 3.8: Selected bond lengths (Å) and angles (°) for the complex $[Cu^{II}LH_2][PF_6]$.

Cu-N1	2.303(3)	N1-Cu-N2	83.35(1)
Cu-N2	2.018(3)	N2-Cu-N3	85.07(1)
Cu-N3	2.041(3)	N3-Cu-N1	83.95(1)
Cu-O2	1.969(2)	O2-Cu-O3	104.29(1)
Cu-O3	1.941(2)	N1-Cu-O2	105.30(1)
		N1-Cu-O3	112.89(1)
		N2-Cu-O2	81.25(1)
		N2-Cu-O3	159.97(1)
		N3-Cu-O2	162.39(1)
		N3-Cu-O3	85.14(1)

As expected, the UV spectrum of $[Cu^{II}LH_2][PF_6]$ (fig. 3.20) depicts just one transition, due to there being only 1 transition possible ($T_{2g} \rightarrow E$). This is typical of a d^9 transition metal.

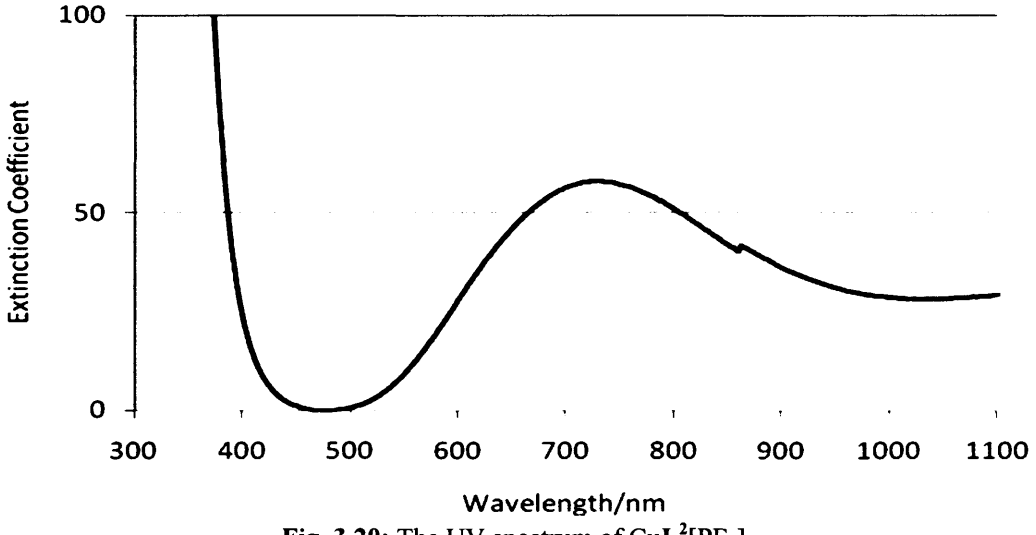

Fig. 3.20: The UV spectrum of $CuL^2[PF_6]_2$.

3.4 Conclusions and Suggestions for Further Research

The work carried out on $\mathbf{L^1}.H_3$ proves that the chloride group is not sterically large enough to prevent dinucleation, it does in fact seem favourable, depending on the pH conditions.

A theory suggested by Peacock *et al.* was that a group with sufficient bulk on the pendant arms will prevent formation of the dinuclear complex, and this was found to be the case with Sherry's ligand, $\mathbf{L^2}.H_3$.

A more detailed study into the factors affecting dinucleation of these complexes could include further potentiometric measurements with an aim of determining the pKa values of the coordinated alcohols for differing metals and ligands. Also a study into the pH at which dinucleation occurs in differing solvents would be worthwhile and interesting.

3.5 Bibliography

1. Cotton, F. A.; Wilkinson, G., *Advanced Inorganic Chemistry, Fifth Ed.* Wiley: 1988.

2. Cabbiness, D. K.; Margerum, D. W., Macrocyclic effect on the stability of copper(II) tetramine complexes. *J Am Chem Soc* **1969**, 6540-6541.

3. Cabbiness, D. K.; Margerum, D. W., Effect of macrocyclic structures on the rate of formation and dissociation of copper(II) complexes. *J Am Chem Soc* **1970**, 2151-2153.

4. Sayer, B. A.; Michael, J. P.; Hancock, R. D., Synthesis and metal binding properties of the novel ligand N,N'N''-tris(2-hydroxyethyl)-1,4,7-triazacyclononane. *Inorg Chimica Acta* **1983,** 77, L63-L64.

5. Robb, J.; Peacock, R. D., Preparation of the chiral hexadentate ligand N,N',N''-tris[(S)-2-hydroxypropyl]-1,4,7-triazacyclononane and preparation and circular dichroism spectra of its Co(III) complexes. *Inorg. Chim. Acta* **1986,** 121, (1), L15-L17.

6. Belal, A. A.; Farrugia, L. J.; Peacock, R. D.; Robb, J., Synthesis and spectroscopic studies of cobalt(III) complexes of the chiral pendant-arm macrocycle N,N',N''-tris[(2S)-2-hydroxypropyl]-1,4,7-triazacyclononane (H3L); crystal structure of the hydrogen-bridged dimer [CoLH3LCo][PF6]3. *J. Chem. Soc., Dalton Trans.* **1989**, (5), 931-5.

7. Farrugia, L. J.; Macdonald, N. M.; Peacock, R. D.; Robb, J., Synthesis, X-ray crystal structure and spectroscopy of the hydrogen-bridged dimer [CrIII(L.H3L)CrIII][PF6]3 (H3L = N,N',N''-Tris[(2S)-2-hydroxypropyl]-1,4,7-triazacyclononane). *Polyhedron* **1995,** 14, (4), 541-5.

8. Belal, A. A.; Fallis, I. A.; Farrugia, L. J.; M., M. N.; Peacock, R. D., Synthesis and crystal structure of [MnII(H3L)(L)MnIV][PF6]3 [H3L = N,N',N''-tris-(2S)-2-hydroxypropyl-1,4,7-triazacyclononane]: a mixed-valence pendant-arm macrocycle dimer in which the ligand adopts different angular geometries at the two metal centers. *J. Chem. Soc., Chem. Commun.* **1991**, (6), 402-3.

9. Fallis, I. A.; Farrugia, L. J.; Macdonald, N. M.; Peacock, R. D., Synthesis and crystal structure of zinc-vanadium complex [ZnII(LH3)(L)VIV][PF6]3 [LH3 = N,N',N''-tris(2S)-2-hydroxypropyl-1,4,7-triazacyclononane]: a chiral mixed-metal pendant-arm macrocyclic dimer containing nonvanadyl vanadium(IV). *Inorg. Chem.* **1993,** 32, (6), 779-80.

10. Fallis, I. A.; Farrugia, L. J.; Macdonald, N. M.; Peacock, R. D., Synthesis and coordination chemistry of the sterically demanding pendant-arm macrocycle N,N',N''-tris[(2R)-2-hydroxy-3-methylbutyl]-1,4,7-triazacyclononane. *J. Chem. Soc., Dalton Trans.* **1993**, (18), 2759-63.

11. Farrugia, L. J.; Peacock, R. D., Structure of 1,4,7-tris[(2S)-2-hydroxypropyl]-1,4,7-triazacyclononanenickel(II) dibromide monohydrate. *Acta Crystallographica, Section C: Crystal Structure Communications* **1991,** C47, (6), 1312-13.

12. Feng, X. M.; Zhang, Z.; Li, Y. Z.; Bian, N. S.; Wang, Z. L., Complexes of N,N',N''-tris(2-hydroxypropyl)-1,4,7-triazacyclononane (L): Structures of [CuL](ClO4)(NO3), [CoL](ClO4)2, [ZnL](ClO4)2 and the catalytic activity of [MnL](ClO4)2 towards olefin epoxidation with hydrogen peroxide. *Transition Metal Chemistry (Dordrecht, Netherlands)* **2007,** 32, (1), 95-101.

13. Blake, A. J.; Donlevy, T. M.; England, P. A.; Fallis, I. A.; Parsons, S.; Ross, S. A.; Schroeder, M., Synthesis of a new binucleating ligand LH4: synthesis and x-ray structures of anti-[Co2(LH4)(OH2)2](NO3)4.5H2O, anti-[Ni2(LH4)(NCMe)2](PF6)4.4H2O, anti-[Zn2(LH4)(NO3)2](NO3)2 and syn-[Cu2(LH2)](BPh4)2. *J. Chem. Soc., Chem. Commun.* **1994**, (17), 1981-2.

14. Huskens, J.; Sherry, A. D., Co-ordination chemistry and molecular mechanics study of the magnesium(II) and calcium(II) complexes of trisubstituted 1,4,7-triazacyclononane derivatives. *J. Chem. Soc., Dalton Trans.* **1998**, (1), 177-184.

15. Huskens, J.; Sherry, A. D., Discrimination between magnesium(II) and calcium(II) by 1,4,7-tris(2-hydroxyalkyl)-1,4,7-triazacyclononane ligands. *Chem. Commun.* **1997**, (9), 845-846.

16. Van der Merwe, M. J.; Boeyens, J. C. A.; Hancock, R. D., Optimum Ligand Hole Sizes for Stabilising Nickel (III) *Inorg Chem* **1983,** 22, 3489-3490.

17. Buchlera, S.; Meyer, F.; Kaifera, E.; Pritzkow, H., Tunable TACN/pyrazolate hybrid ligands as dinucleating scaffolds for metallobiosite modeling—dinickel(II) complexes relevant to the urease active site. *Inorg Chimica Acta* **2002,** 337, 371-386

18. Zhong, H.; Zeng, X.; Liu, Y.; Luo, Q., (8-Quinolinol-kappa2N,O)bis(8-quinolinolato-kappa2N,O)nickel(II) glyoxal hemisolvate monohydrate. *Acta Crystallogr., Sect. E: Cryst. Struct. Commun.* **2007**, m187-m189.

19. Gomes, L.; Pinho, D.; Freire, C.; de Castro, B., (1,4-Dioxane-O){3,3',5,5'-tetrachloro-2,2'-[4-methyl-4-azaheptane-1,7-diylbis(nitrilomethylidyne-N)]diphenolato-O,O'}nickel(II), [Ni(3,5-Cl4salMetrien)]. *Acta Crystallogr., Sect. C: Cryst. Struct. Commun.* **1999**, 1425-1427.

20. Lever, A. B. P., *Inorganic Electronic Spectroscopy*. 2nd Edition ed.; Elesvier: 1984.

21. Gans, P.; O'Sullivan, B., Glee, a new computer program for glass electrode calibration. *Talanta* **2000,** 51, 33-37.

22. Gans, P.; Sabatini, A.; Vacca, A., Investigation of equilibria in solution. Determination of equilibrium constants with the HYPERQUAD suite of programs. *Talanta* **1996**, (43), 1739-1753.

23. Andersson, P.; Kvassman, J.; Lindstroem, A.; Olden, B.; Pettersson, G., Effect of NADH on the pKa of zinc-bound water in liver alcohol dehydrogenase. *Eur. J. Biochem.* **1981,** 113, (3), 425-33.

24. Bertini, I.; Luchinat, C.; Rosi, M.; Sgamellotti, A.; Tarantelli, F., pKa of zinc-bound water and nucleophilicity of hydroxo-containing species. Ab initio calculations on models for zinc enzymes. *Inorg. Chem.* **1990,** 29, (8), 1460-3.

25. Caudle, M. T.; Caldwell, C. D.; Crumbliss, A. L., Dihydroxamic acid complexes of iron(III): ligand pKa and coordinated water hydrolysis constants. *Inorg. Chim. Acta* **1995,** 240, (1-2), 519-25.

26. Katz, A. K.; Glusker, J. P.; Markham, G. D.; Bock, C. W., Deprotonation of Water in the Presence of Carboxylate and Magnesium Ions. *J. Phys. Chem. B* **1998,** 102, (33), 6342-6350.

27. Cross Jason, B.; Duca Jose, S.; Kaminski James, J.; Madison Vincent, S., The active site of a zinc-dependent metalloproteinase influences the computed pK(a) of ligands coordinated to the catalytic zinc ion. *J Am Chem Soc* **2002,** 124, (37), 11004-7.

28. Xia, J.; Shi, Y.; Zhang, Y.; Miao, Q.; Tang, W., Deprotonation of zinc(II)-water and zinc(II)-alcohol and nucleophilicity of the resultant zinc(II) hydroxide and zinc(II) alkoxide in double-functionalized complexes: theoretical studies on models for hydrolytic zinc enzymes. *Inorg Chem* **2003,** 42, (1), 70-7.

29. Coleman, J. E., *Progress in Bioorganic Chemistry*. Wiley-Interscience: 1971.

30. Schweisinger, R.; Piontek, K.; Little, W.; Schweikert, O.; Prinzbach, H., Cis-trihetero-tris-homobenzenes astridentate ligandsX-ray crystal structure analysis of the complexes. *Tet Lett.* **1982**, 2427-2430.

31. Scarpellini, M.; Wu, A. J.; Kampf, J. W.; Pecoraro, V. L., Corroborative Models of the Cobalt (II) Inhibited Fe/Mn Superoxide Dismutases. *Inorg Chem* **2005**, 5001-5010.

32. Potaskalov, V. A.; Reiter, L. G.; Potaskalova, N. I.; Podberezskaya, N. V.; Pervukhina, N. V.; Virovets, A. V., Crystal structure and properties of mer-tris(2-aminoethanolato)cobalt. *Zhurnal Neorganicheskoi Khimii* **2005**, 431-434.

33. Masaoka, S.; Furukawa, S.; Chang, H.; Mizutani, T.; Kitagawa, S., A New Class of Hexamer. *Angew Chem Int Ed Engl* **2001**, 3817-3819.

34. M. D. Meyers; Cotton, F. A., The Preparation, Structures and Infrared Absorption of Salts of Cobalt(III) Hexafluoride Ion *J. Am. Chem. Soc.* **1960,** 82, (19), 5027-5030.

35. Weyhermueller, T.; Wieghardt, K.; Chaudhuri, P., Nitrogen verses Oxygen co-ordination of carboxamide-functonalised triazacyclononane ligands in transition metal complexes. *Dalton* **1998**, 3805-3813.

36. Berben, L. A.; Long, J. R., Synthesis and Metal Ion Binding Properties of Chromium (III) tri acetylide complexes. *J Am Chem Soc* **2002**, 11588-11589.

37. Gibson, V. C.; Newton, C.; Redshaw, C.; Solan, G. A.; White, A. J. P.; Williams, D. J., Low Valent Chromium Complexes Bearing N,O-Chelating pyridyl-enolate ligands. *Dalton* **2003**, 4612-4617.

38. Edelmann, F.; Behrens, U., Merhkenege Carbonyl-Chrom Komplexe. Synthese und Strukturauflklarung *j. organometallic chem. (Netherlands)* **1977**, 65-72.

39. Holtzmann, R.; Wieghardt, K.; Florke, U.; Haupt, H. J.; Weatherburn, D. C.; Bonvoisin, J.; Blondin, G.; Girerd, J. J., Spin Exchange Coupling in Heterodinuclear Complexes *J Am Chem Soc* **1992**, 1681-1686.

40. Tei, L.; Blake, A.; Wilson, C.; Schroder, M., Synthesis of Asymmetric Derivatives of 1,4,7-triazacyclononane and Trigonal Prismatic Mn(II) Complexes. *Dalton* **2002**, 1247-1249.

41. Quee-Smith, V. C.; DelPizzo, L.; Jureller, S. H.; Kerschner, J. L., Synthesis, Structure and Characterisation of a Novel Mangenses(IV) Monomer. *Inorg Chem* **1995**, 6461-6465.

42. Appelt, R.; Vahrenkamp, H., Cyanide Bridged di and tri nuclear complexes with central Cr(III) Mn(III) and Co(III) Salen Units. *Inorg Chimica Acta* **2003**, 387-398.

CHAPTER 4

Analysis and comparison of copper salen derivatives, the role of charge and steric bulk on the metal centre

4.1 Introduction

4.1.1 Privileged Chiral Catalysts

4.1.1.1 Schiff Base Ligands

Jacobsen first coined the term 'privileged chiral catalysts'[1] in relation to certain classes of compounds that enantiosectively catalyse a wide range of chemical transformations. This is notable partly due to the tendency of natural enzymes to catalyse reactions in an extremely chirally specific manner.

Chelating Schiff base ligands such as salen ('sal' – unsubstituted salicylaldehyde, 'en' – ethylene diamine) are relatively easy to synthesise via a simple condensation of an aldehyde and a 1,2-bis(primary amine) as shown in scheme 4.1. Salen was first prepared by Pfeiffer[2] in 1933. However, it was not until the early 1990s that chiral ligands were investigated and their potential for catalysis realised. Jacobsen's research into chiral Schiff bases of manganese proved so important to the field of asymmetric catalysis that this manganese catalyst is now commonly known as Jacobsen's catalyst (scheme. 3.1).[3]

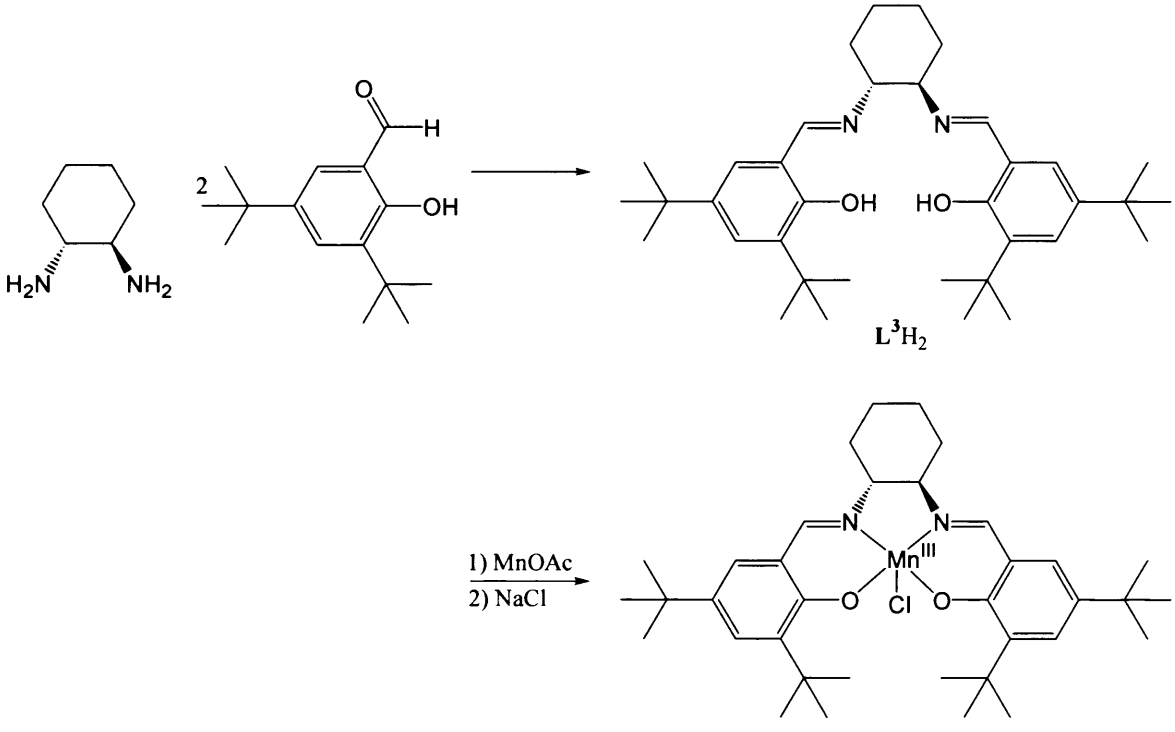

Scheme 4.1: The general synthesis of salen type complexes is relatively simple, as shown by the preparation for the epoxidation catalyst first described by Jacobsen *et al.*[3]

Ligand $\mathbf{L^3}.H_3$ has been shown to bind all the 1st row transition metals in a stable manner except scandium,[3-11] and is used to catalyse a wide range of chemical transformations, from the epoxidation of olefins[3] to the cycloaddition of dienes to aldehydes.[12]

Jacobsen's catalyst is of particular relevance to this thesis as the active oxidants of this style of catalyst all contain the Mn^V=O species.[13] The same moiety is believed to be key in the oxidation of water (see section 1.1.1).

Since the 1990s the field has expanded rapidly, partly due to the relative ease of synthesis of new Schiff base ligands, but mostly due to the versatility the complexes show towards a wide array of catalytic transformations. At the time of writing there are over 39,000 publications containing the term 'Schiff base'. Although there is a huge amount of research into new salen ligands and complexes, fairly little is known about the mode of binding of a catalyst to a substrate and what makes these complexes different from other, less versatile catalysts.

Some of the uses and recent developments of 1st row transition metal complexes of $\mathbf{L^3}$ will now briefly be discussed.

4.1.1.2 Stereoselective Reactions of Epoxides

Epoxides are an important class of compound mainly due to their high reactivity arising from the strained nature of the three membered ring as discussed in section *1.2.4*. Due to the relatively small number of enantiomerically pure epoxides available in nature, enantioenriched epoxides must be accessed via synthetic routes. Jacobsen showed in 1995 and 1997 that the complexes [Cr$\mathbf{L^3}$](Cl) and [Co$\mathbf{L^3}$](OAc) catalyse the hydrolytic kinetic resolution (HKR) of terminal epoxides (scheme 4.2).[14-16] Benefits of this procedure include the relatively small amounts of catalyst required (of the order of 1 mol%). Good yields are observed, commonly 40-50 % with enantiomeric excesses of >99 %. The diol side products are obtained in high *ee* and are frequently used as chiral building blocks in their own right.

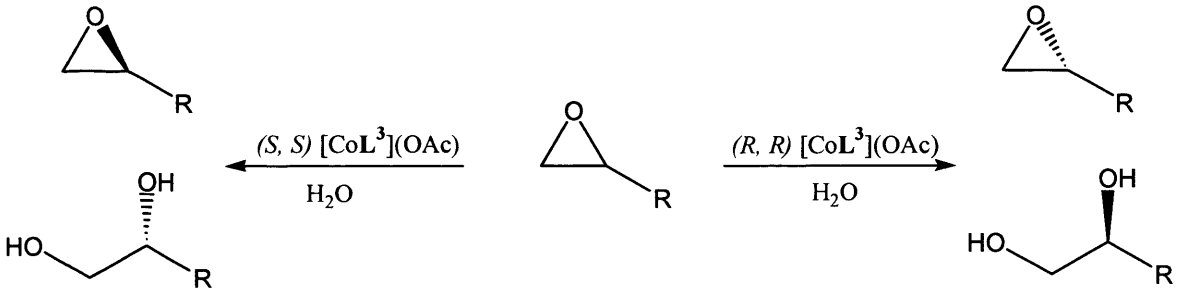

Scheme 4.2: An general scheme for the HKR of a terminal epoxide by [CoL^3](OAc).

Little work has been carried out on the mechanism of HKR on epoxides. However, it is known to proceed via second order dependence on the catalyst.[16] Jacobsen *et al.*[17] carried out a preliminary mechanistic investigation and suggested the mechanism shown in scheme 4.3. This implies [CoL^3](OAc) is acting as both precatalyst and cocatalyst. Kinetic analysis showed that enantioselectivity of the catalyst for a substrate arises not from selective binding to the catalyst, but from selective binding of an epoxide complex to the catalyst. This kinetic model was tested with calorimetric data.

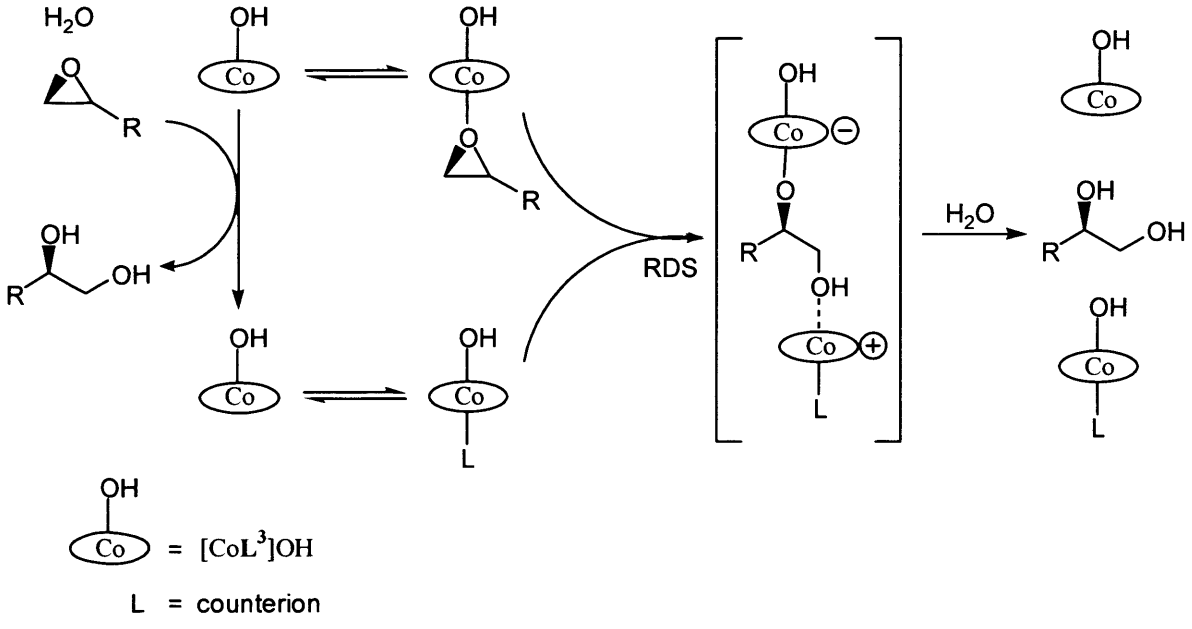

Scheme3.3: The mechanism proposed by Jacobsen *et al.* of HKR on terminal epoxides.

In the same year, Fallis *et al.*[18] reported enantio discrimination of [VOL^3] for propylene oxide. Experiments were carried out by EPR and ENDOR (see later) which clearly show subtle differences in binding orientation of the epoxide to the complex. Vanadium was chosen as a suitable paramagnetic model for cobalt. Cobalt(III) is diamagnetic it is unsuitable for analysis via EPR and ENDOR. These

data were verified by DFT calculations which confirm that the homochiral complex (i.e. RR catalyst + R substrate) of a catalyst and substrate has a higher formation constant than the heterochiral adduct (i.e. RR catalyst + S substrate). This would lead to a more rapid binding of the latter complex with free catalyst, potentially supporting Jacobsen's proposal of a dimeric catalyst species being formed (scheme 4.3).

A continuation on this study was reported in 2008 by Murphy *et al.*[19] EPR and ENDOR techniques were again used to study the interactions between [VO**L**^{3}] and *cis/trans* terminal epoxides. It was shown that at least three electrostatic hydrogen – oxygen interactions aid the weak metal-oxygen interaction. Crucially, the methine proton, H_a, (scheme 4.4) is thought to be instrumental in the orientation adopted by the epoxide relative to the catalyst. This study was carried out on *cis* and *trans* isomers of 2,3-epoxybutane. Although not chiral, it was shown that the *cis* isomer formed a more favourable interaction with the catalyst than the *trans* isomer, suggesting that subtle hydrogen bonds may play a part in enantioselective transformations of metal-salen catalysis. An electrostatic interaction was also observed between the electron rich oxygen and the electron deficient metal centre. It is perhaps not coincidental that [Mn**L**^{3}](Cl) is a good enantioselective catalyst for *cis* but not *trans* alkenes.[13]

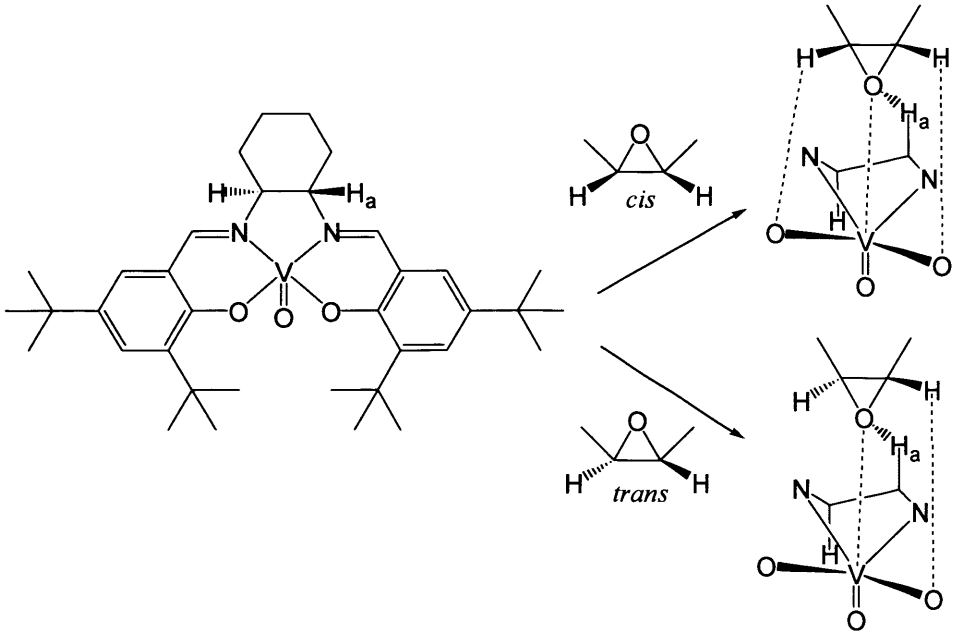

Scheme 4.4: Results published by Fallis *et al.*[18] revealed subtle electrostatic interactions between the epoxide substrate and vanadyl complex.

4.1.1.3 Polymerisation

Salen type complexes have also been used as polymerisation catalysts, Chrisholm *et al.*[20] investigated the stereoselectivity of [Al**L**^{3}]OCH_2CH_3 for lactides. The generally accepted reaction pathway for the catalytic ring-opening polymerisation (ROMP) of lactides is shown in scheme 4.5.[21] However, the mechanism that occurs in the presence of a chiral environment remains unclear. Chrisholm studied the ring opening of one equivalent of lactide with [Al**L**^{3}]OCH_2CH_3 in a range of solvents, and conflicting results were reported. Stereoselectivity was found to be unpredictable in terms of the ligand structure of the catalyst, the solvent used and the chirality of the end group.

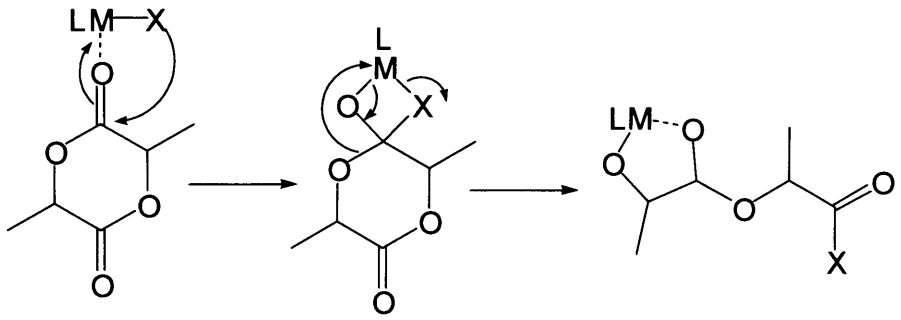

Scheme 4.5: The proposed reaction mechanism for the ROMP of lactides by a lewis acidic catalyst. [21]

The same group reported a study into the binding of propylene oxide to salen metal(III) catalysts.[21] It was noted that salen complexes of Al(III), Cr(III) and Co(III) exhibit large differences in catalytic activity towards polymerisation, even though all three have similar ionic radii. The order of reactivity of M^{III}**L**^{3} towards polymerisation of propylene oxide and CO_2 is Cr(III) > Al(III) > Co(III). It was found that the degree of Lewis acidity for complexes of the type [M^{III}**L**^{3}] increases in the order: Co(III) < Cr(III) ~ Al(III). It is probable that the d electron configuration (d^6, d^0, and d^3) of the metals is responsible for the differences, with the least electronically stable d^3 chromium complexes being the most reactive.

In 2002 Feijen *et al.*[22] showed that [Al**L**^{3}]O*i*Pr gives excellent stereocontrol in the polymerisation of lactides. They also reported good molecular weight control even in the absence of solvent, the first reaction of this type to be performed with no solvent.

Kinetic studies of the system later revealed 1st order reaction kinetics with (*R, R*)-[Al**L**^{3}]O*i*Pr initiated L-LA having a much faster rate than the (*R, R*)-[Al**L**^{3}]O*i*Pr with

D-LA.[23] This indicates that (*R, R*)-[Al**L**^{3}]O*i*Pr has a large preference for L-LA over D-LA. Polymerisation of *rac*-LA with a single enantiomer of [Al**L**^{3}]O*i*Pr was found to yield crystalline polymers of high melting point and crystallinity.

4.1.1.4 Diels Alder Cycloadditions

The Diels-Alder reaction is one of the most widely used cycloadditions in organic synthesis.[24] It provides access to many different cyclic products, for example, dihydropyranones (scheme 4.6). Increasingly, there has been demand for enantioselective methods to carry out this reaction. Jacobsen *et al.* [14, 25-27] reported the use of Cr**L**^{3}(Cl) and Co**L**^{3}(Cl) to carry out this reaction in high yields (up to 98%) and good ee (up to 93% ee). These complexes were shown to catalyse a variety of dienes and dienophiles to the desired product. It was shown that the reaction is more enantioselective in non-polar, solvents. The counterion (i.e. Cl^-) was also shown to have an effect, the less coordinating counterions giving rise to slower, less enantioselective reactions.

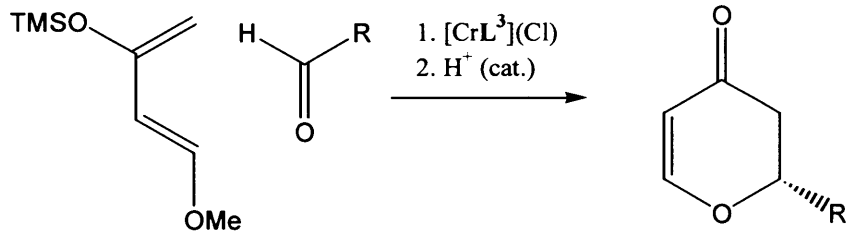

Scheme 4.6: A general scheme for the catalytic Diels-Alder cyclo-additions reported by Jacobsen *et al.*[27]

4.1.1.5 Conjugate Addition

The conjugate addition of a nucleophile to an olefin is a well established and commonly used reaction, particularly in the generation of new carbon-carbon bonds. Enantioselectivity of this reaction is commonly achieved with the use of organometallic complexes such as (binap)Rh, reported by Hayashi *et al.*[28] This proved a versatile catalyst, enabling the enantioselective conjugate addition of organometallic reagents to a wide variety of olefins, including α,β-unsaturated ketones, esters, amides and nitro compounds.[28] There are many more catalysts used for conjugate additions, these are beyond the scope of this thesis.

Jacobsen *et al.* reported the use of [Al**L**^{3}] as a catalyst for the enantioselective 1,4-addition of α,β-unsaturated imides[29] and α,β-unsaturated ketones[30] to a range of

weakly acidic compounds such as cyanide, thiols and oximes (scheme 4.7). Large amounts of catalyst were used (1-10%) but enantiomeric excesses were reported to be good for most nucleophiles reported (>90% ee). It has been suggested that single point binding of the substrate to the catalyst through the carbonyl next to the olefin is responsible for the high selectivity observed.

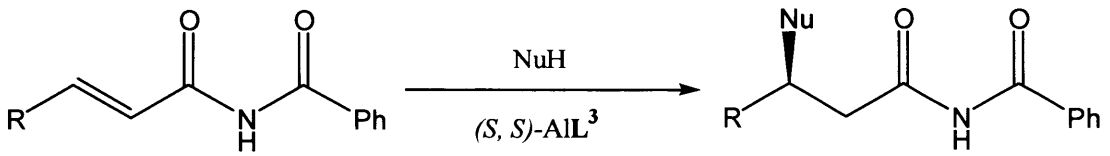

Scheme 4.7: Enantioselective conjugate addition.

4.1.2 Ligands similar to salen^{2-}

In 1999 Dyker *et al.*[31] reported the synthesis of ligand $\mathbf{L^4}$ (Fig. 4.1) as an isoelectronic analogue of $\mathbf{L^3}$. A brief catalytic study showed some chiral catalytic activity of the copper complex. To date, no other reference to this complex or its parent ligand is present in the literature. However, in 1989 Yin *et al.*[32] synthesised ligand $\mathbf{L^5}$, pyridyl N-oxide ligands of this type are still rare considering the vast amount of work carried out on phenolate Schiff base ligands such as $\mathbf{L^3}$. This is probably due to the more involved organic synthesis required to obtain the pyridyl N-oxide aldehydes required to make this class of ligand.

It was decided to investigate bis N-oxide ligands similar to $\mathbf{L^4}$ in more detail and to compare them to analogues to observe the differences that small changes in ligand has on the metal centre.

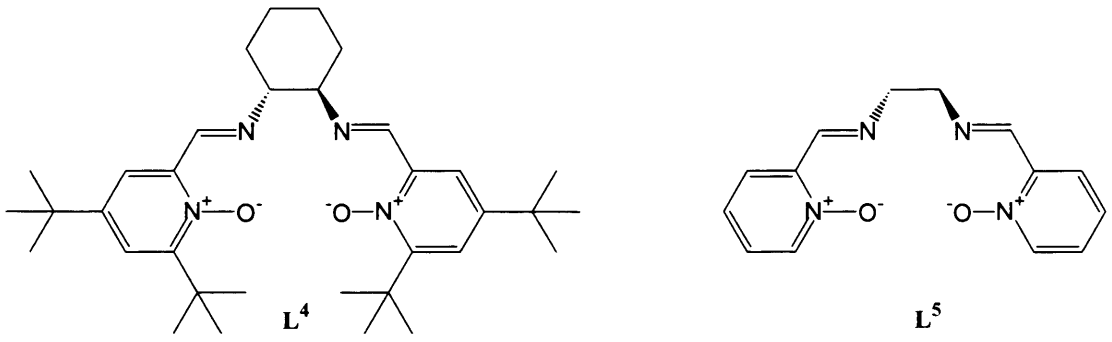

Fig. 4.1: $\mathbf{L^4}$(left) synthesised by Dyker *et al.*[31] and $\mathbf{L^5}$ first reported by Yin *et al.*[32]

4.1.3 Complexes Studied

Before high oxidation state chemistry is studied on complexes of these ligands, it is necessary to establish their basic coordination chemistry.

Three new ligands were synthesised in this research hereafter labelled $\mathbf{L^6}$, $\mathbf{L^7}$ and $\mathbf{L^8}$ (fig. 4.2) and the Cu^{2+} complexes were characterised. The synthesis of these complexes allows the investigation into two series of slightly differing ligand structure. Series A is a sequential removal of an N-oxide to the salen framework, starting from (the well studied) [Cu$\mathbf{L^3}$] with no N-oxides. Adding one gives the newly synthesised and characterised [Cu$\mathbf{L^6}$](ClO_4) and a second leads to Dyker's [Cu$\mathbf{L^4}$](ClO_4)$_2$ with two N-oxides. In addition to the N-oxides are counterions which must be considered; [Cu$\mathbf{L^3}$] is a neutral complex requiring no counterion, but [Cu$\mathbf{L^6}$](ClO_4) and [Cu$\mathbf{L^4}$](ClO_4)$_2$ require one and two counterions respectively. This could have an effect on the catalytic activity as a coordinating counterion is likely to compete with a substrate for complexation, possibly retarding any reaction that may occur.

The significance of systematically changing the charge is not known, but an insight into the differences in the chemistry of these three complexes is the aim of this research. It is thought that the presence of a pyridine N-oxide may increase the charge at the metal centre therefore shortening the metal-ligand bond lengths and increasing the strength of any interactions that may occur during a catalytic process.

The second series, B, of complexes involves perhaps a more subtle change in ligand design; i.e. the removal of the peripheral tertiary butyl groups. Starting from [Cu$\mathbf{L^4}$](ClO_4)$_2$ the removal of both *tert*-butyl groups from 1 pyridyl ring leaves [Cu$\mathbf{L^7}$](ClO_4)$_2$ and removal of both sets of *tert*-butyl groups gives [Cu$\mathbf{L^8}$](ClO_4)$_2$.

The loss of steric bulk is unlikely to affect the nature of the copper centre directly. It is expected that the geometries at the three metal centres will be different due to the removal of the restrictive *tert*-butyl groups. This could also have an effect on the potential catalytic activity of this series of complexes. It is conceivable that the *tert*-butyl groups could have an effect on the approach of a substrate to be catalysed, thereby giving rise to different stereochemical results.

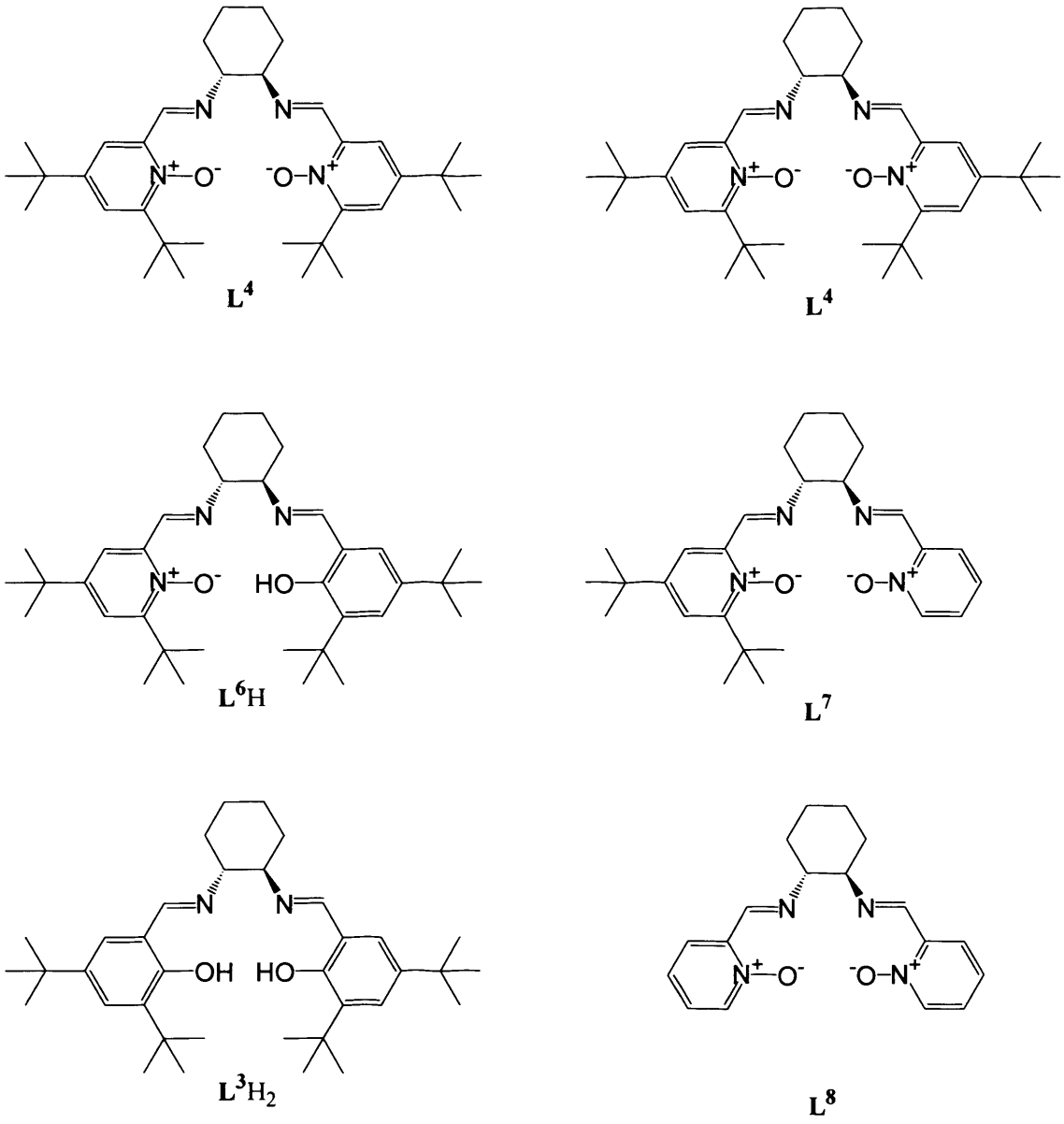

Fig. 4.2: The ligands studied in this chapter. $L^3.H_2$ and L^4 have benn previously reported.[1, 31]

4.2 Experimental

4.2.1 EPR Spectroscopy

Electron Paramagnetic Resonance (EPR) is a technique that is commonly used to probe paramagnetic transition metal ions by the absorption of microwave radiation in a magnetic field. Since this chapter deals with EPR and a related technique, ENDOR (Electron Nuclear DOuble Resonance), it is necessary to briefly describe how these techniques work and how they were used within this research.

The basic principle of EPR is that if an atom with an unpaired electron is placed within a magnetic field, B, the magnetic moment of the electron spin, μ_s, aligns either parallel or perpendicular to this applied field. Both of these states have a distinct energy associated to them, thus an energy splitting diagram can be constructed as shown in fig. 4.3, known as the Zeeman energy level diagram. This effect is known as electron Zeeman splitting.

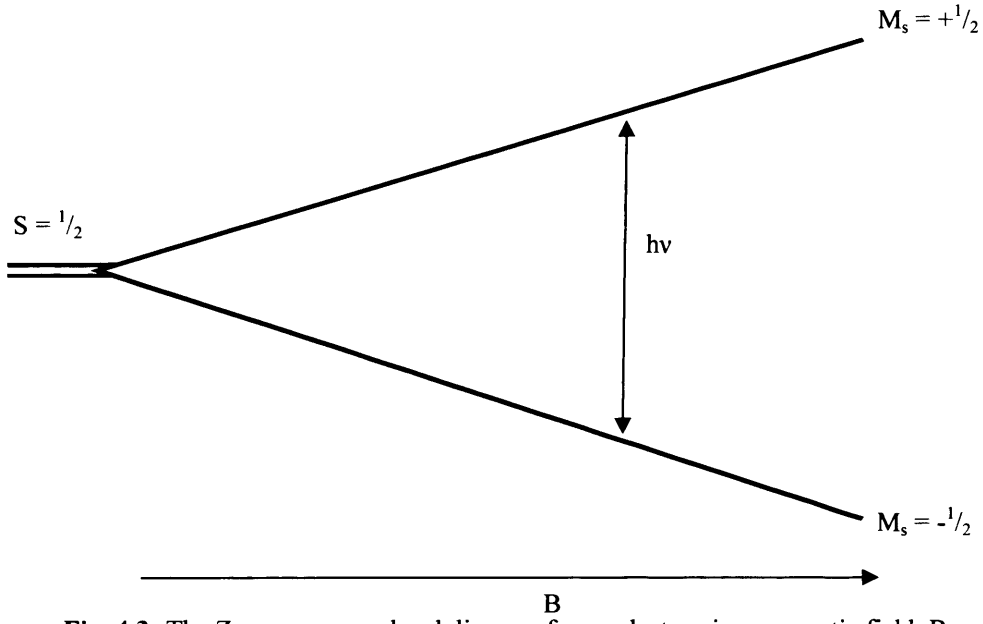

Fig. 4.3: The Zeeman energy level diagram for an electron in a magnetic field, B.

An unpaired electron is now able to move between these two energy levels by absorbing or emitting energy equal to hν. In doing so, the spin of the electron changes. This energy hν is directly proportional to the applied field as described by equation 4.1. Where g is the g factor of an unpaired electron (see later) and μ_B is the Bohr Magneton.

$$E = h\nu = g\mu_B B \qquad 4.1$$

The aim of an EPR experiment is to split the degeneracy of the electron spin states by applying a magnetic field. A transition between these states is then induced via the application of electromagnetic radiation of the correct frequency. For common X-band measurements this radiation corresponds to the microwave region ($\nu \approx 9$ GHz).

In real systems another effect has to be taken into account: any nucleus with a spin quantum number, I, greater than zero has its own magnetic moment associated with it. The simplest example of this would be a single unpaired electron (S = ½) interacting with a proton (I = ½). The magnetic field of the proton induces a second

splitting of the energy levels, called the nuclear Zeeman splitting. The interaction between the magnetic moment of the proton and that of the unpaired electron induces another shift in energy levels, known as hyperfine splitting. Both of these effects are illustrated in fig. 4.4.

The Zeeman splitting diagram is described by equation 4.2 (an extension of equation 4.1).

$$E = g\mu_B B - g_N\mu_N B + aSI \qquad 4.2$$

This chapter focuses on copper, as both Cu^{63} and Cu^{65} have spin quantum numbers of 3/2.

$$\text{no. of lines} = 2nI + 1 \qquad 4.3$$

According to equation 4.3 where n = the number of nuclei, it would be expected that under "ideal conditions" four lines of equal intensity should be observed (as seen in fig. 4.5). In reality the spectra are often distorted considerably from this idealised line shape, with significant variation in the linewidths. This variation arises from the incomplete averaging of the g and A values: i.e. they are not completely averaged out when the complex tumbles in solution. Analysis of such fluid rotation spectra can therefore be used to determine the rotational correlation time (τ_R) of the complex.[33]

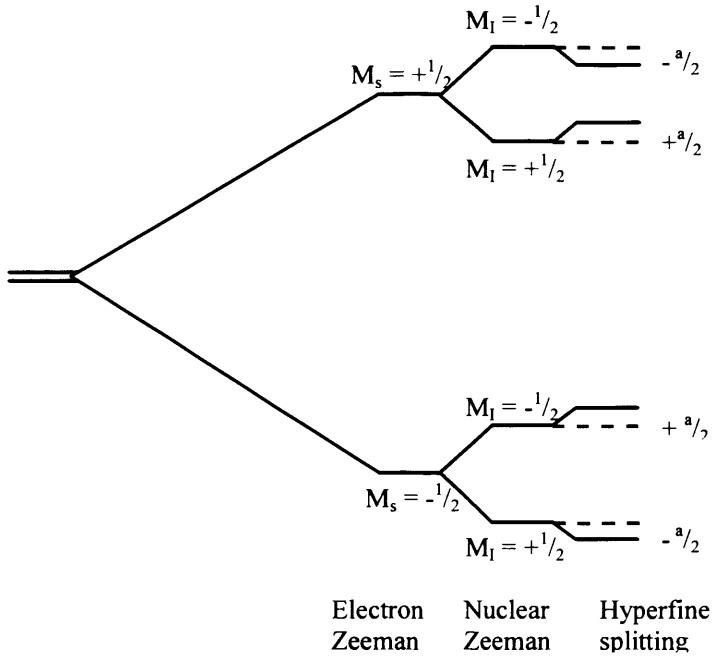

Fig. 4.4: Zeeman splitting diagram for 1 electron coupling with 1 proton.

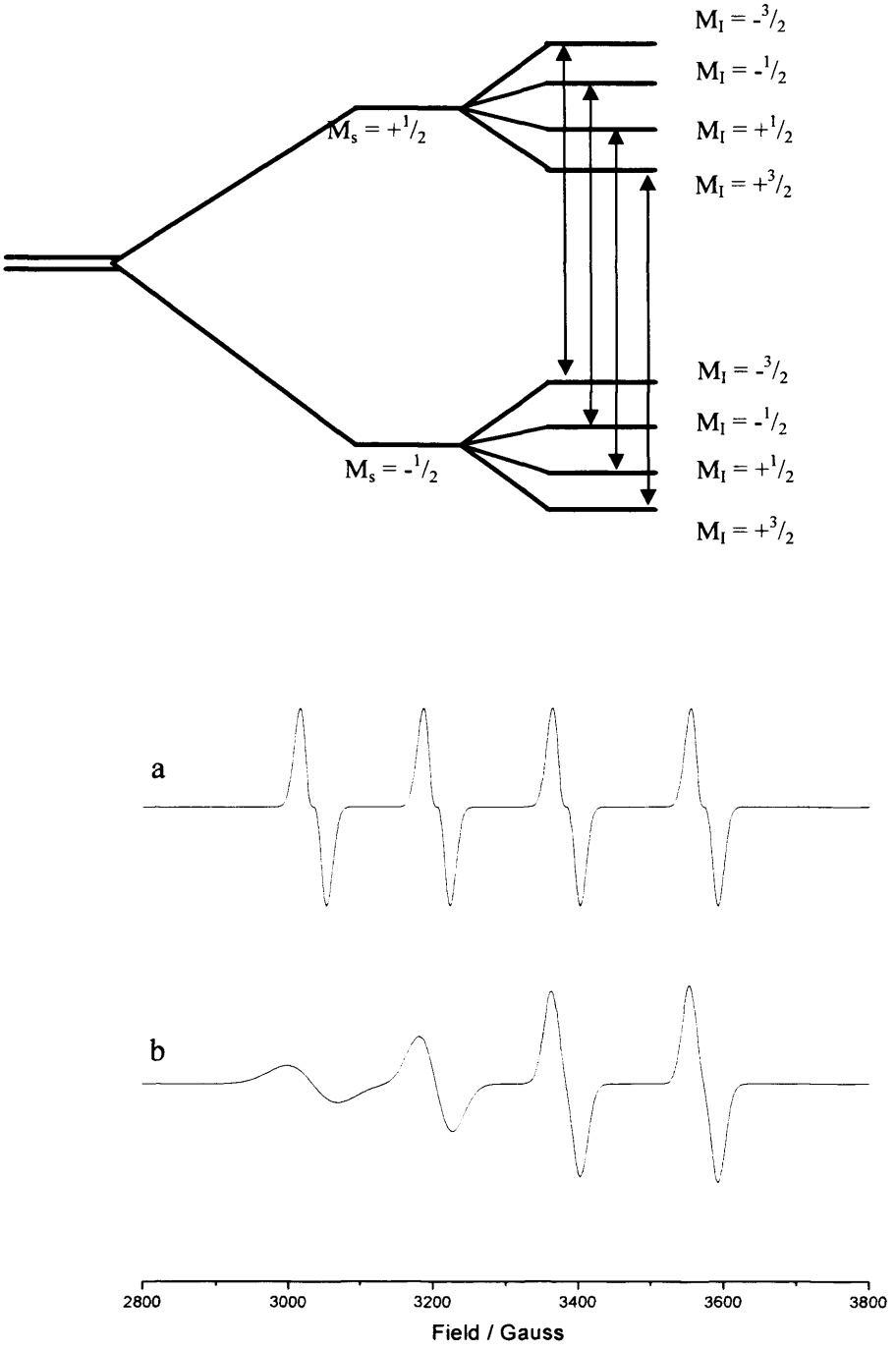

Fig. 4.5: Energy splitting diagram of copper (I = 3/2). Idealised isotropic EPR spectrum (a), realistic isotropic EPR spectrum (b).

In many cases, EPR spectra are recorded at low temperatures (liquid N_2 or liquid He temperatures). This is particularly the case for transition metal ions with fast relaxation times. When frozen, the paramagnets are randomly aligned with respect to the applied magnetic field, and this produces the so-called powder (polycrystalline) EPR spectrum. Provided the spectrum is well resolved, key turning points can be identified and related to one of the principle axes of the complex (fig. 4.6).

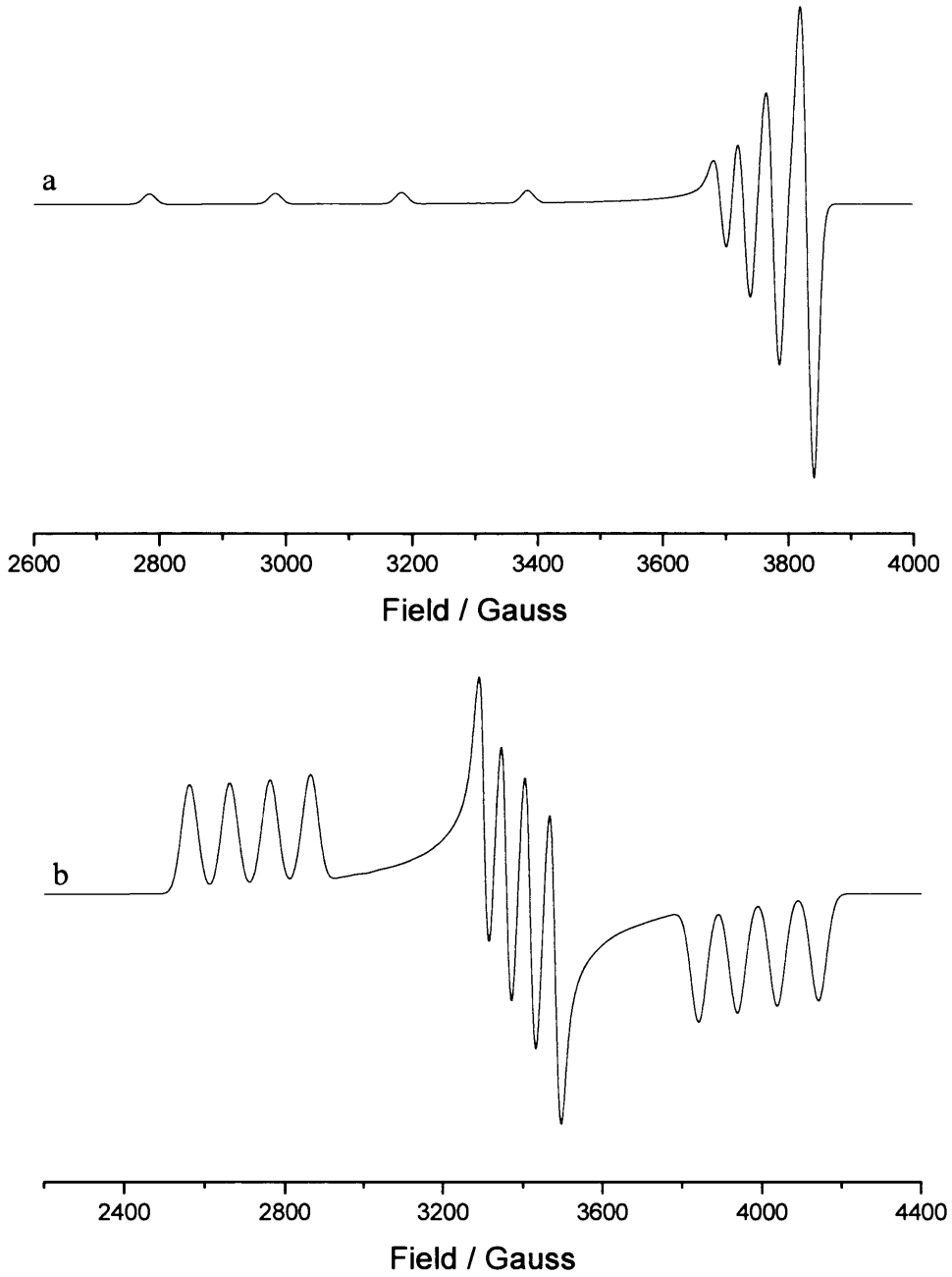

Fig. 4.6: Theoretical examples of EPR spectra of copper in an axial (a) and a rhombic (b) environment.

Of course, in most cases, n is much greater than 1. This gives rise to complicated spectra with many overlapping lines that would be impossible to interpret without a simulation program.

The spectrum shown in fig. 4.5 is characteristic of an isotropic system, i.e. $g_x = g_y = g_z$. For systems of this nature only 1 set of lines is observed. Most of the complexes studied in this chapter are approximated to be axial, i.e. $g_x = g_y \neq g_z$ and 2 sets of lines are observed, one for the case where $B_{\parallel}g_{\parallel}$ and one where $B_{\perp}g_{\perp}$ (i.e. the applied field lies in the xy plane). Axial copper spectra are of the type shown in fig. 4.6 (a).

Rhombic spectra give rise to three sets of lines since $g_x \neq g_y \neq g_z$, an example of a copper rhombic spectrum is shown in fig. 4.6 (b).

The magnetic frequencies used within this chapter are X-band (9 GHz) and Q-band (35 GHz). The advantage of X-band is that the hyperfine coupling is usually observed very clearly. However, the parallel and perpendicular regions of the spectra are much closer to each other usually resulting in a convoluted spectra. When run at higher frequencies EPR spectra tend to be better resolved, although a loss in resolution of the hyperfine splitting is now observed. Used in conjunction with each other, all necessary information can be extracted from the two spectra. Fig. 4.7 illustrates the difference between an axial copper spectrum taken at X-band and the same sample taken at Q-band.

As the copper complexes studied are coordinatively unsaturated, care has to be taken to use exactly the same solvent system throughout so that for work in this thesis direct comparisons between the spectra can be drawn. The 2 solvent systems chosen were a mixture of 10% methanol, 20% dichloromethane and 70% toluene (for series A) and 30% DMSO and 70 % DCM (for series B).

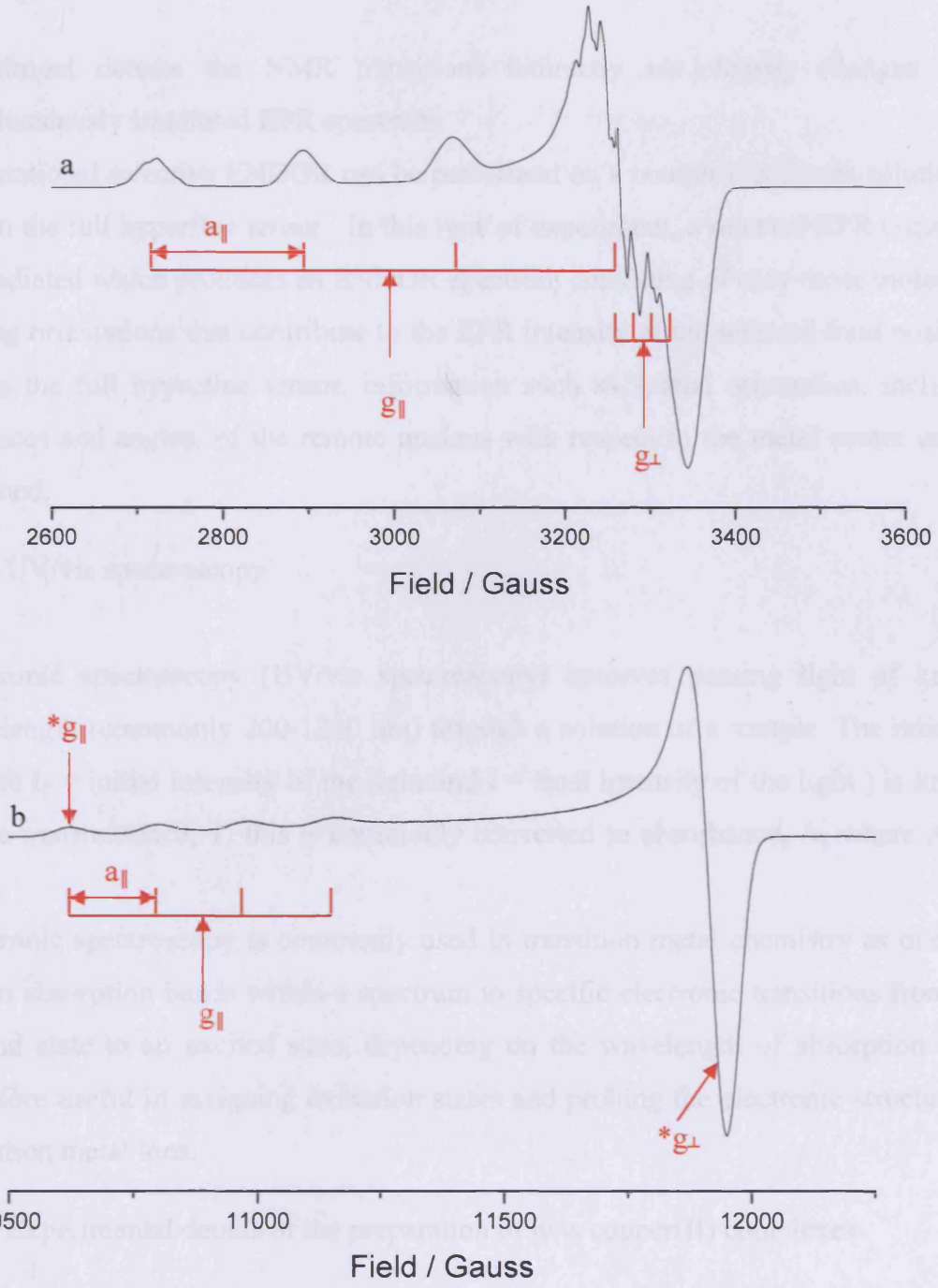

Fig. 4.7: Examples of (a) X-band and (b) Q-band axial (Cu) spectra of the same sample under otherwise identical conditions. Spectra were recorded at 50K. The field positions marked * $g_{\parallel}$ and * $g_{\perp}$ correspond to the unique orientations of $\theta = 0°$ and 90° respectively.[34]

4.2.2 ENDOR Spectroscopy

One of the limitations of EPR is the poor resolution observed when required to extract hyperfine coupling constants from remote ligand nuclei. The nuclear spin of, for example, the ligand protons on a salen complex will give rise to proton hyperfine splitting which is often unresolvable in EPR spectra. Electron Nuclear Double Resonance (ENDOR) spectroscopy provides an order of magnitude greater sensitivity over EPR, thus providing much higher resolution. An ENDOR

experiment detects the NMR transitions indirectly *via* intensity changes to a simultaneously irradiated EPR spectrum.

Orientational selective ENDOR can be performed on a complex in frozen solution to obtain the full hyperfine tensor. In this type of experiment, a selected EPR transition is irradiated which produces an ENDOR spectrum consisting of only those molecules having orientations that contribute to the EPR intensity at the selected field position. From the full hyperfine tensor, information such as spatial orientation, including distances and angles, of the remote nucleus with respect to the metal centre can be obtained.

4.2.3 UV/vis spectroscopy

Electronic spectroscopy (UV/vis spectroscopy) involves passing light of known wavelength (commonly 200-1200 nm) through a solution of a sample. The ratio I/I_0 (where I_0 = initial intensity of the light and I = final intensity of the light) is known as the transmittance, T, this is commonly converted to absorbance, A, where A = -logT.

Electronic spectroscopy is commonly used in transition metal chemistry as one can assign absorption bands within a spectrum to specific electronic transitions from the ground state to an excited state, depending on the wavelength of absorption. It is therefore useful in assigning oxidation states and probing the electronic structure of transition metal ions.

4.2.4 Experimental details of the preparation of new copper(II) complexes

*[Cu**L**^{6}](ClO$_4$)*

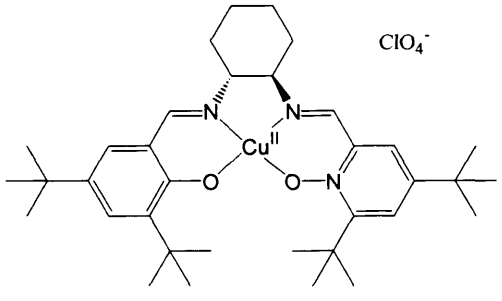

3,5-Di-*tert*-butyl-2-hydroxybenzaldehyde (101 mg, 0.43 mmol) and 3,5-di-*tert*-butylpyridine-2N-oxide aldehyde (101 mg, 0.43 mmol) were added to a solution of *R, R*-1,2-diaminocyclohexane (50 mg, 0.43 mmol) in ethanol (20 ml). The mixture

stirred for 2 hours and a solution of $Cu(ClO_4)_6$ (151 mg, 0.41 mmol) in ethanol (10 ml) was added. After stirring for a further 30 minutes the solvent was removed and the product isolated by column chromatography (SiO_2, 50:50 $CHCl_3$:Me_2CO, Rf = 0.45). Further purification by slow diffusion of ether into an ethanolic solution yielded 52 mg (15%) of a purple crystalline solid. IR: (KBr disc, cm^{-1}) 3510(b), 3012(s), 1405(s), 1078(s). UV/Vis (acetonitrile): λ_{max} = 375, ε = 1466; 570, ε = 174. MS(EI), MH^+ exact mass (*calc.*) *m/z 610.3534 (obs.) 610.3565.*

$[CuL^8](ClO_4)_2$

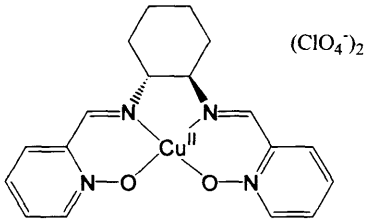

Pyridine-2N-oxide aldehyde (202 mg, 0.86 mmol) was added to *R, R*-1,2-diaminocyclohexane (50 mg, 0.43 mmol) in ethanol (20 ml). The mixture was stirred for 2 hours and a solution of $Cu(ClO_4)_6$ (151 mg, 0.41 mmol) in ethanol (10 ml) was added. After stirring for a further 30 minutes the solvent was removed and the product purified by slow diffusion of ether into an ethanolic solution yielding 212 mg (84%) of a purple crystalline solid. IR: (KBr disc, cm^{-1}) 3526(b), 2952(m), 1396(s), 1178(s). MS(EI), MH^+ exact mass (*calc.*) *m/z 387.0982 (obs.) 387.0952.*

$[CuL^7](ClO_4)_2$

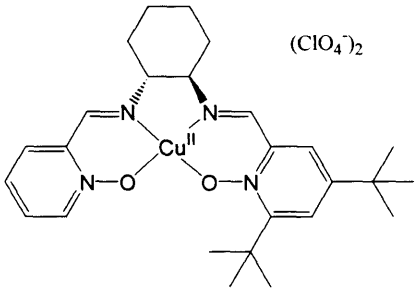

Pyridine-2N-oxide aldehyde (101 mg, 0.43 mmol) and 3,5-di-*tert*-butylpyridine-2N-oxide aldehyde (101 mg, 0.43 mmol) were added to *R, R*-1,2-diaminocyclohexane (50 mg, 0.43 mmol) in ethanol (20 ml). The mixture was stirred for 2 hours and a solution of $Cu(ClO_4)_6$ (151 mg, 0.41 mmol) in ethanol (10 ml) was added. This was stirred for a further 30 minutes. The solvent was removed and the complex purified

by column chromatography (SiO_2, 80:20 $CHCl_3$:MeOH, Rf = 0.7). Further purification by slow diffusion of ether into an ethanolic solution yielded 54mg (18%) of a purple crystalline solid. Yield 18%, 54 mg. IR: (KBr disc, cm^{-1}) 3602(b), 3024(m), 1426(s), 1016(s). MS(EI), MH^+ exact mass (*calc.*) *m/z 500.2312 (obs.) 500.2287.*

4.3 Results and Discussion

4.3.1 Effects of the counterion

In coordination chemistry it is important to assess the extent to which the counterion interacts with the metal centre. If an appreciable degree of coordination occurs, a meaningful comparison between $\mathbf{L^3}$, $\mathbf{L^6}$ and $\mathbf{L^4}$ would be difficult due to the presence of varying amounts of coordination between the three complexes. Perchlorates were chosen in anticipation that they would not coordinate strongly to the copper centre.

In order to test this, a separate sample of $[Cu\mathbf{L^4}](NO_3)_2$ was prepared and the X- and Q-band EPR spectra were taken of the two samples under identical conditions (fig. 4.8). The nitrate counterion was chosen on account of its large ability to coordinate, thus if there is a tendency for coordination to this complex, a difference would become apparent.

It is clear that there is very little difference between the EPR spectra of the perchlorate and nitrate salts. This strongly implies that the copper ion is in an extremely similar electronic environment in both compounds leading to the conclusion that the counterions are weakly or not coordinated.

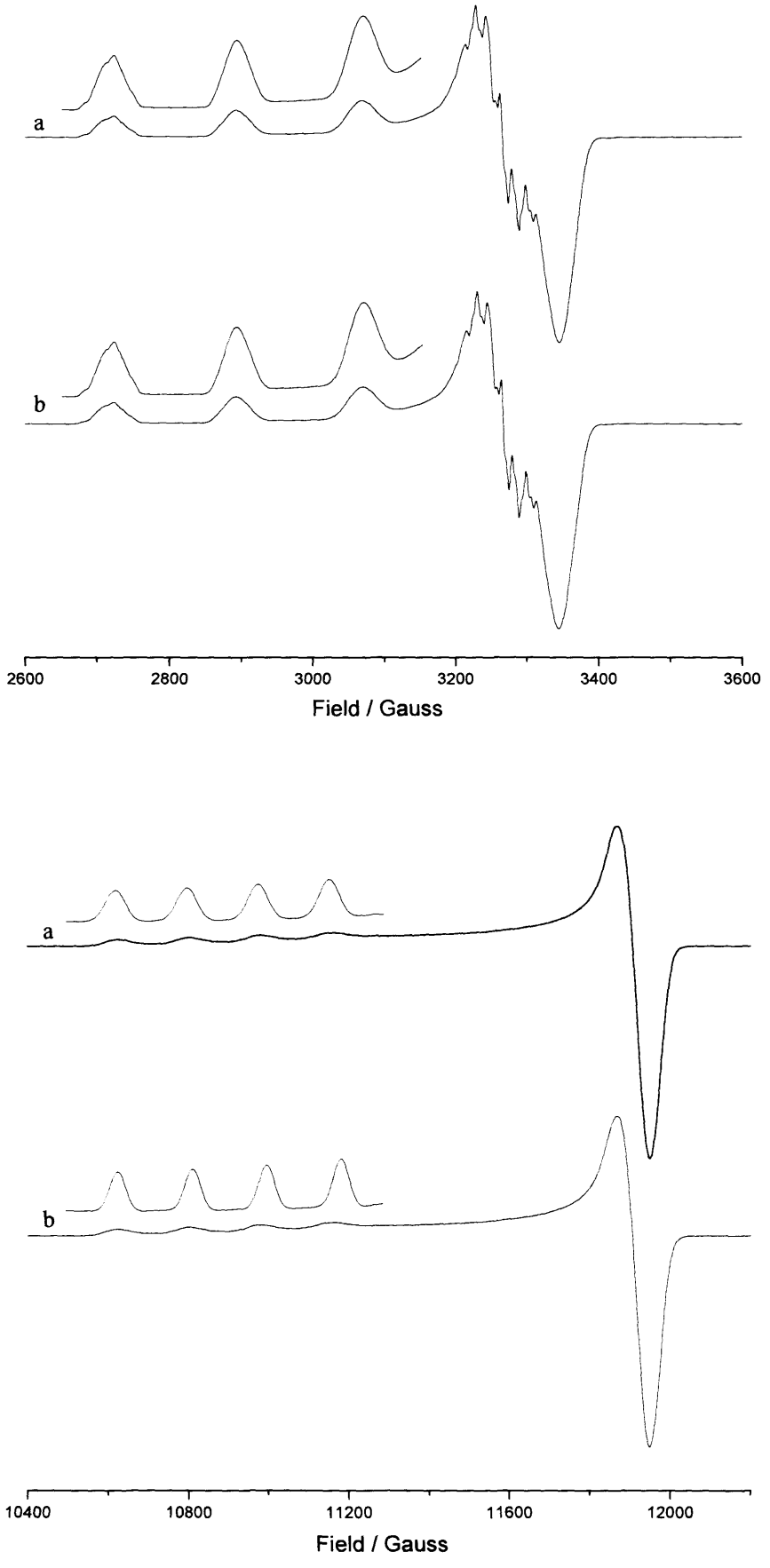

Fig. 4.8: X (top, 130 K) and Q (bottom, 10 K) band CW EPR spectra of a) $[CuL^4](ClO_4)_2$ and b) $[CuL^4](NO_3)_2$ in toluene : dichloromethane : methanol (70:20:10).

Confirmation was obtained via the use of UV spectroscopy (fig. 4.9) which gave the same result. An absorption in the range 500 - 650 nm is characteristic of a tetragonally distorted CuX_6 species, where X = N or O.[35, 36] It is therefore reasonable to assume that the complex adopts a Jahn-Teller distorted conformation with acetonitrile molecules coordinated on the z axis. It was deemed acceptable to treat the counterion as a non-coordinating species.

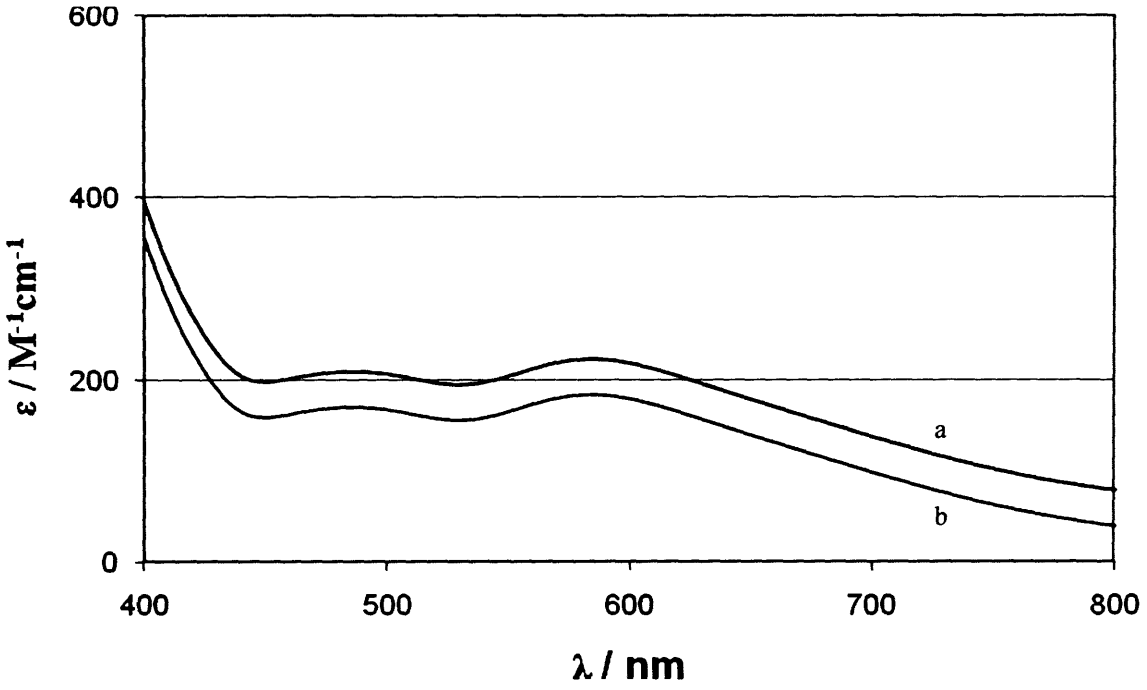

Fig. 4.9: UV spectra of (a) $[CuL^4](NO_3)_2$ and (b) $[CuL^4](ClO_4)_2$ recorded in acetonitrile at room temperature, $[CuL^4](NO_3)_2$ is offset by 40 $M^{-1}cm^{-1}$ for illustrative purposes.

4.3.2 Electronic manipulation of donor atoms to the metal centre

The X-band and Q-band EPR spectra of $[CuL^4](ClO_4)_2$ and $[CuL^6](ClO_4)_2$ were recorded and compared with those of $[CuL^3](ClO_4)_2$[37] (see fig. 4.10).

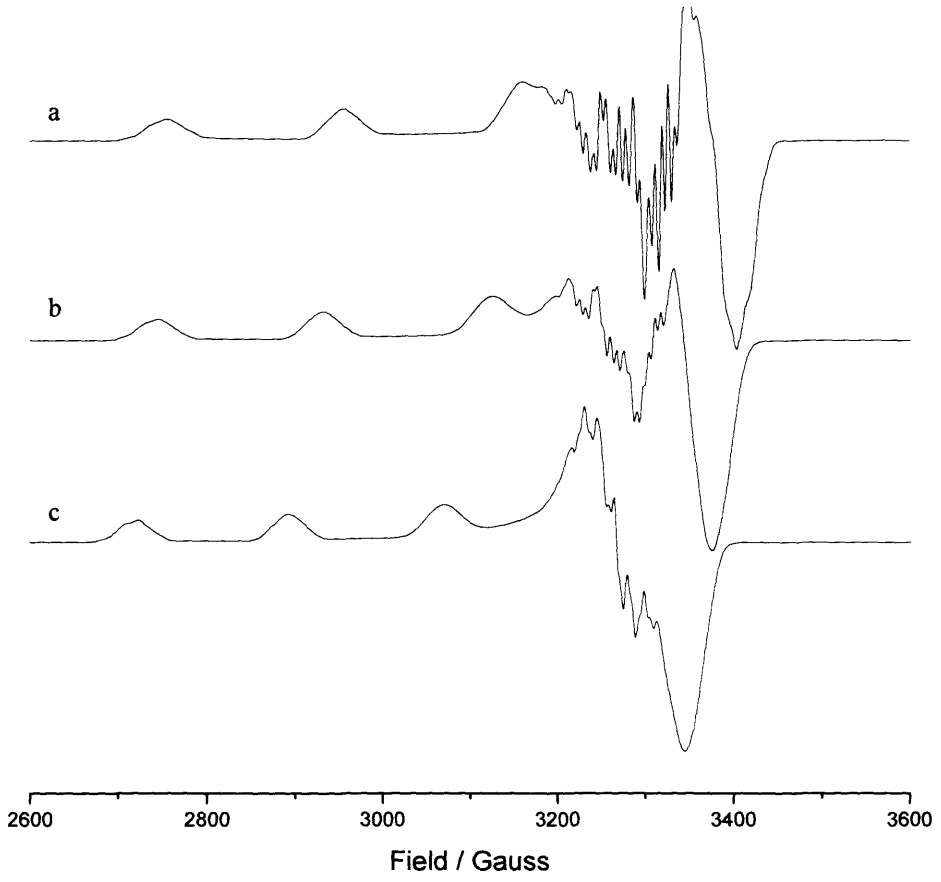

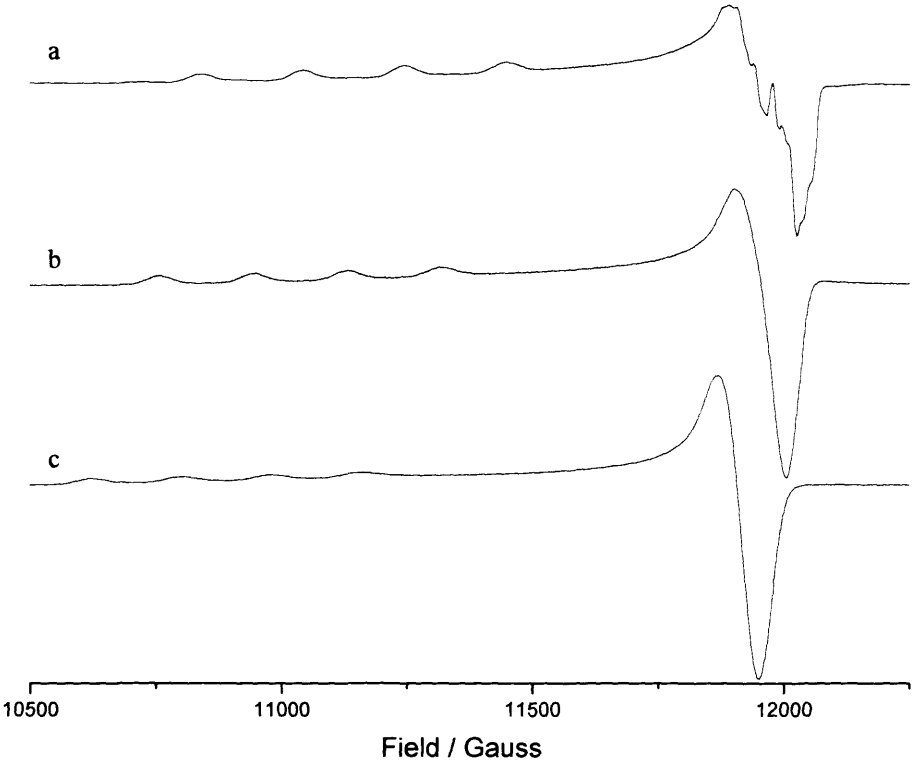

Fig. 4.10: X (top, 130 K) and Q-band (bottom, 10 K) CW EPR spectra of $[CuL^3](ClO_4)_2$ (a), $[CuL^6](ClO_4)_2$ (b) and $[CuL^4](ClO_4)_2$ (c) in methanol : dichloromethane : toluene (10:20:70).

Table 4.1: g and A^{Cu} spin Hamiltonian parameters for racemic $[CuL^3](ClO_4)_2$, $[CuL^6](ClO_4)_2$ and $[CuL^4](ClO_4)_2$ dissolved in toluene.

Complex	$g_\perp$	$g_\parallel$	$A_\perp$ / Gauss	$A_\parallel$ / Gauss
$[CuL^3](ClO_4)_2$	~2.04	2.19	31	201
$[CuL^6](ClO_4)_2$	~2.04	2.21	27	188
$[CuL^4](ClO_4)_2$	~2.05	2.25	28	174

Preliminary simulations[40] of this experimental set were obtained, and the resulting spin Hamiltonian parameters are listed in table 4.1.

It is clear from these data that the xy-axis remains largely unchanged in the three complexes, as $g_\perp$ remains fairly constant. However there is a trend of increasing $g_\parallel$ in the order $CuL^3 < CuL^6 < CuL^4$ while the $A_\parallel$ values decrease in the order $CuL^3 > CuL^6 > CuL^4$.

When interpreting EPR data, two factors affect the spin Hamiltonian parameters; the first being the relative symmetry of the paramagnetic centre, since different symmetries give rise to different d-orbital splitting. The second is the electronic environment surrounding the copper ion, since differing electronic surroundings induce differing spin density distributions.

In this series of complexes, it is assumed that both factors change markedly from one complex to another. The symmetry changes largely (see ENDOR description later) when the intermediate complex, CuL^6 is compared to the other two complexes. However, the systematic replacement of aryloxide to N-oxide donors gives rise to a large electronic change also. It is extremely difficult, and far beyond the scope of this thesis, to try to extract one component from the other, therefore, a qualitative interpretation is most appropriate.

It is known that, for a Cu(II) complex, a decrease in $g_\parallel$ and an increase in $A_\parallel$ is observed when the symmetry is decreased.[38] This is observed in Series A; CuL^3

being square planar, has the lowest symmetry, therefore the smallest $g_{\|}$ and the largest $A_{\|}$. Cu$\mathbf{L}^4$ is *pseudo*-octahedral, and possesses the highest symmetry, leading to the largest $g_{\|}$ and the smallest $A_{\|}$.

Shown in fig. 4.11 is the Peisach-Blumberg diagram, which describes the differences observed in $g_{\|}$ and $A_{\|}$ values with varying donors to the copper centre. The upper left sections of each region correspond to the more negatively charged ML_4 complexes, while the lower right sections correspond to positively charged complexes. It can be concluded from this diagram, that donors of higher negative charge will give rise to smaller $g_{\|}$ values and larger $A_{\|}$ values.

It is reasonable to suggest that $\mathbf{L}^3$ donates a larger degree of charge to the metal centre than $\mathbf{L}^4$, with $\mathbf{L}^6$ remaining the intermediate case. The alkoxides of $\mathbf{L}^3$ carry 1 negative charge each, while the N-oxides of $\mathbf{L}^4$ are formally neutral. The trends observed therefore, are justifiable by this reasoning.

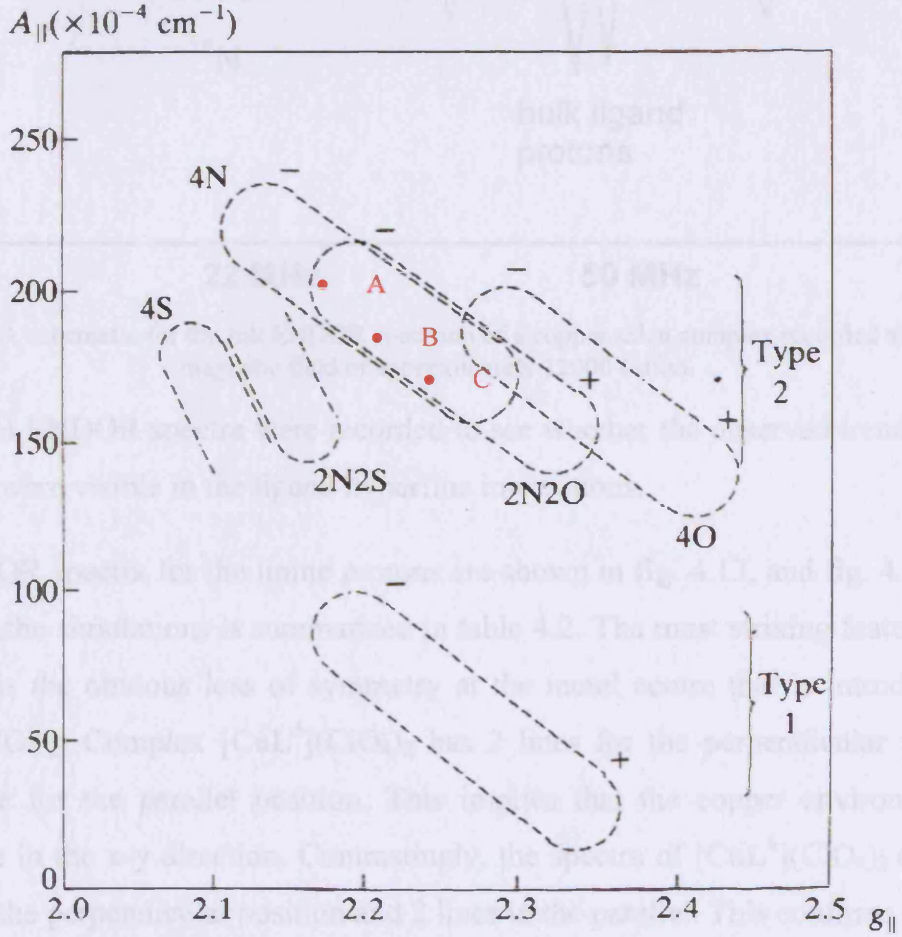

Fig. 4.11: The Peisach-Blumberg diagram. Type 1 refers to copper proteins, while type 2 refers to CuL_4 type complexes.[38] A = [Cu$\mathbf{L}^3$]$(ClO_4)_2$, B = [Cu$\mathbf{L}^6$]$(ClO_4)_2$ and C = [Cu$\mathbf{L}^4$]$(ClO_4)_2$.

To investigate this trend more closely, ENDOR measurements were carried out on the two complexes Cu$\mathbf{L}^4$ and Cu$\mathbf{L}^6$ (Cu$\mathbf{L}^3$ having been investigated extensively elsewhere).[39] In order to extract the full hyperfine interaction terms (i.e. A_1, A_2 and A_3) different regions of the ENDOR spectra were examined more closely. A schematic for the full ENDOR spectrum of a copper salen complex is shown in fig. 4.12. The ^{14}N signal observed for the amines occurs at 22MHz, while the protons are centred at 50MHz. The protons closest to the copper nucleus (the imine protons) give rise to the greatest separation. Hence the information gained from this part of the spectrum can be the easiest to interpret.

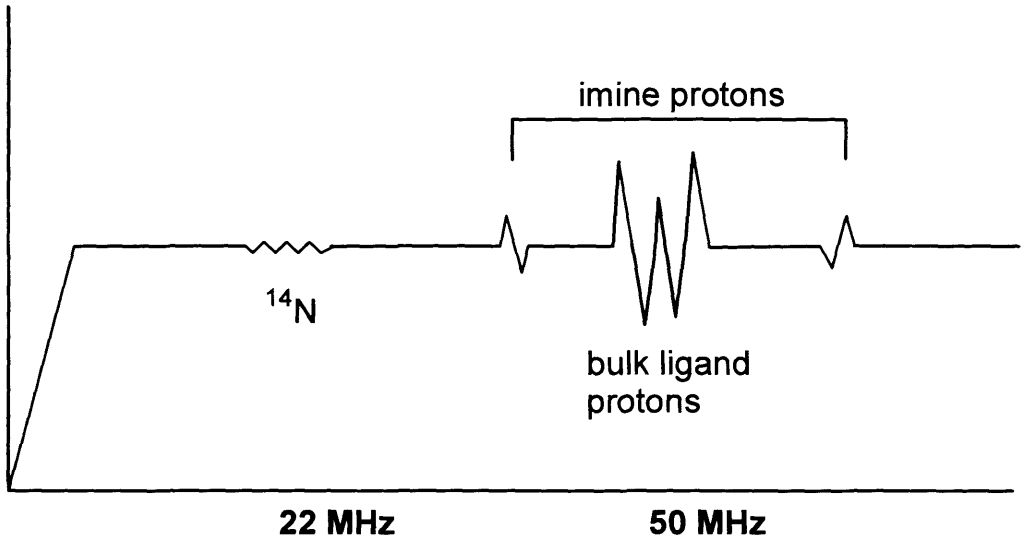

Fig. 4.12: A schematic for the full ENDOR spectrum of a copper salen complex recorded at a static magnetic field of approximately 12000 Gauss.

^{14}N and ^{1}H ENDOR spectra were recorded to see whether the observed trends in the EPR data were visible in the ligand hyperfine interactions.

The ENDOR spectra for the imine protons are shown in fig. 4.13, and fig. 4.14. The data from the simulations is summarised in table 4.2. The most striking feature from this data is the obvious loss of symmetry at the metal centre that is introduced in [Cu$\mathbf{L}^6$]$(ClO_4)_2$. Complex [Cu$\mathbf{L}^4$]$(ClO_4)_2$ has 2 lines for the perpendicular position and 1 line for the parallel position. This implies that the copper environment is symmetric in the x-y direction. Contrastingly, the spectra of [Cu$\mathbf{L}^6$]$(ClO_4)_2$ contains 4 lines in the perpendicular position and 2 lines in the parallel. This confirms the idea that the two ligands force the metal to adopt different geometries. The symmetrical ligand, $\mathbf{L}^4$, imposes an octahedral geometry, while the asymmetric ligand, $\mathbf{L}^6$, forces

the metal to adopt a trigonally distorted geometry, thus splitting the observed ENDOR lines in two.

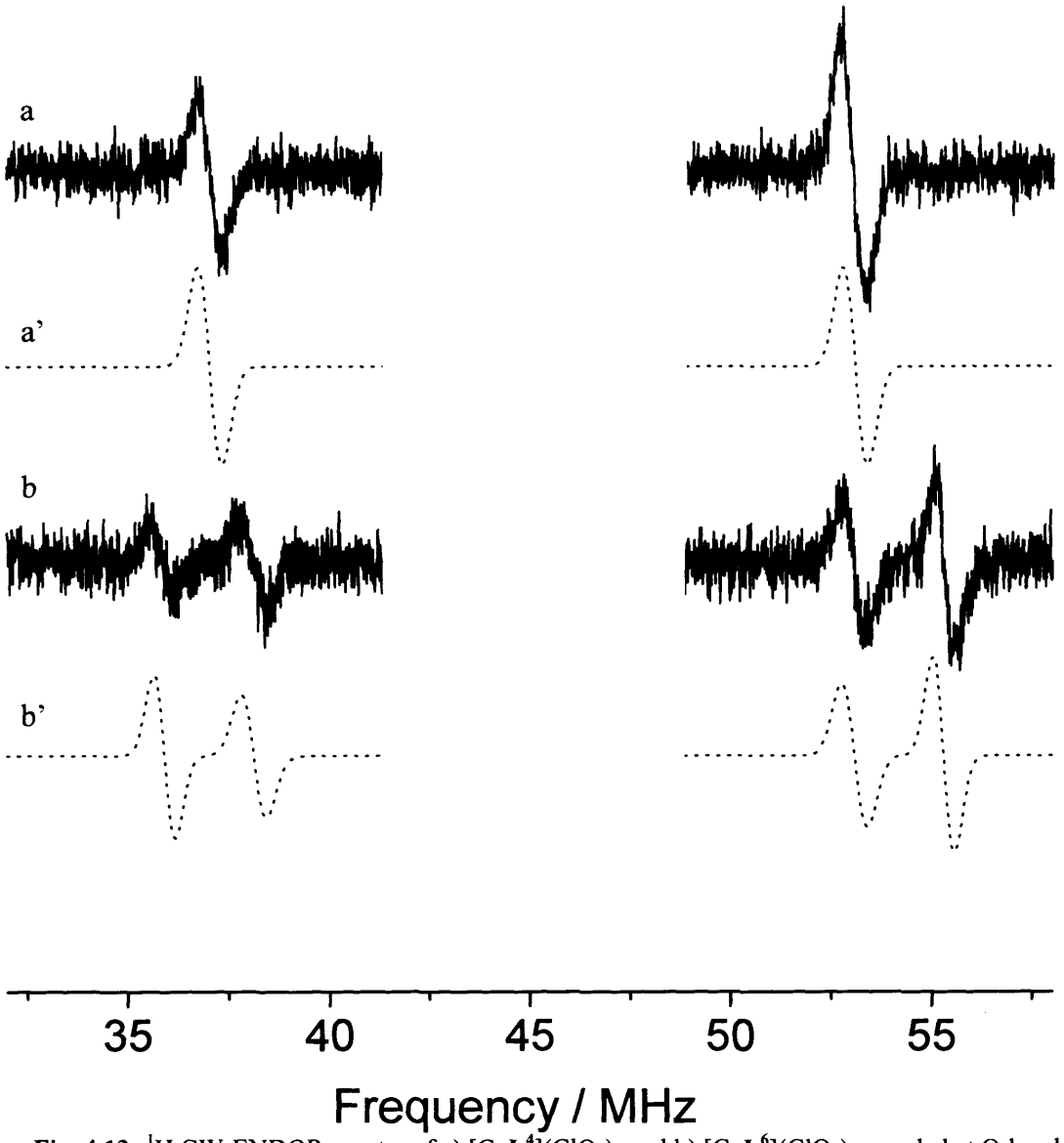

Fig. 4.13: ^{1}H CW-ENDOR spectra of a) $[CuL^{4}](ClO_4)_2$ and b) $[CuL^{6}](ClO_4)$ recorded at Q-band frequencies and 10K in 10% methanol, 20% dichloromethane and 70% toluene. The spectra were measured at the field position corresponding to $g = g$. The respective simulations are shown as a', b'.

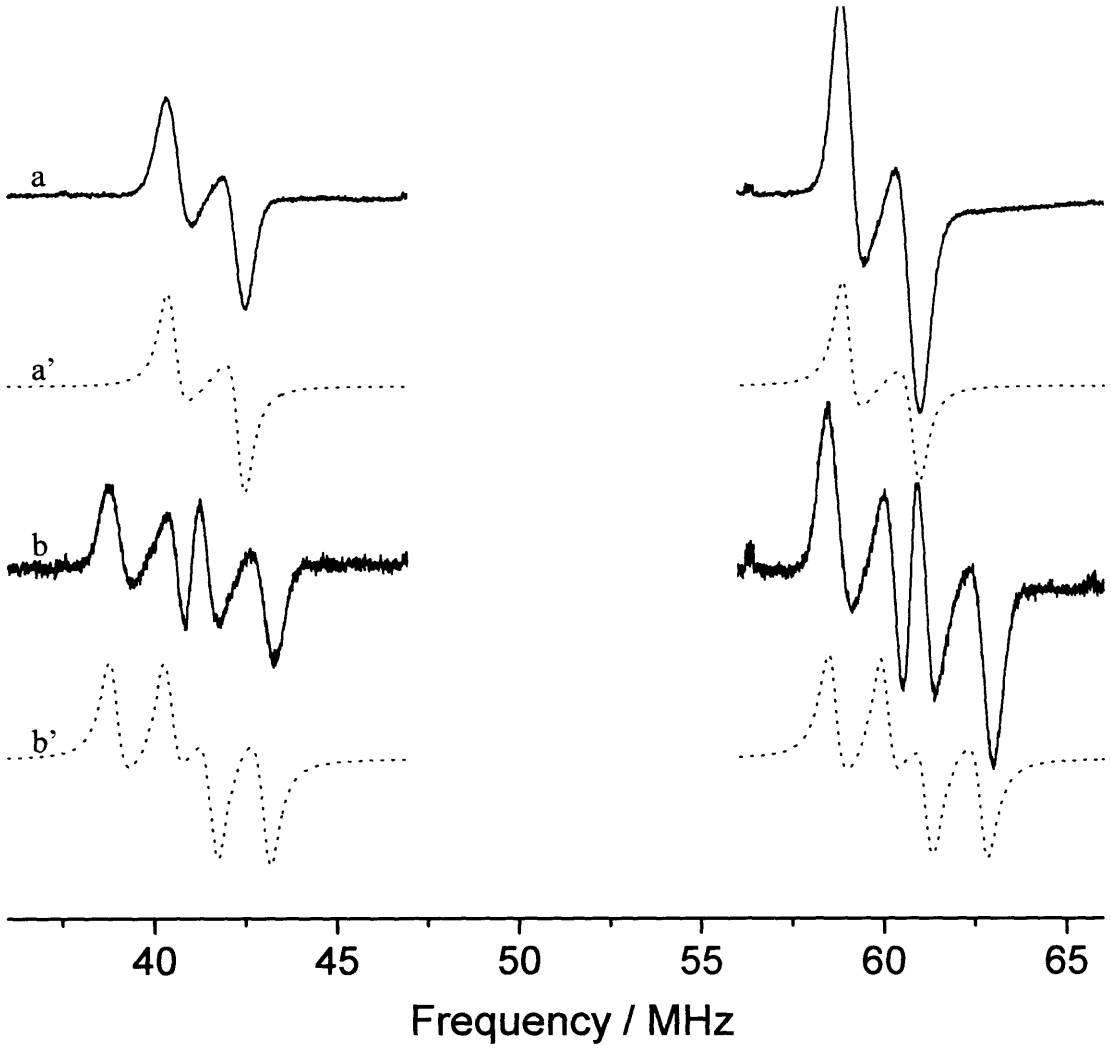

Fig. 4.14: ^{1}H CW-ENDOR spectra of a) [Cu**L**^{4}](ClO$_4$)$_2$ and b) [Cu**L**^{6}](ClO$_4$) recorded at Q-band frequencies and 10K in 10% methanol, 20% dichloromethane and 70% toluene. The spectra were measured at the field position corresponding to $g = g_\perp$. The respective simulations are shown as a', b'.

The value, R, is defined as the distance between the paramagnetic centre (copper centre) and the imine protons of the ligand. It is derived from the experimental value, A(dip) which is a dipole-dipole interaction. The first thing to note is the presence of two sets of values for **L**^{6}, one for each imine proton, while the imine protons of **L**^{4} are equivalent. However, the most striking feature of this data, is the fact that both **L**^{6} imine protons are closer (by 0.23 and 0.39 Å) to the nucleus than their **L**^{4} counterparts. This could be interpreted in two ways. First, the extra negative charge contained in the ligand **L**^{6} gives rise to a stronger Cu-L interaction (due to the extra Lewis acidity of the metal), shortening the metal ligand distances. The ligand donor atoms (of **L**^{6}) interact more strongly with the metal, this implies the metal is less Lewis acidic. This gives rise to weaker interactions of the axial ligands (counterions/solvent molecules) which implies less steric bulk around the metal. This leads to shorter metal-ligand distances. Although the asymmetry of **L**^{6} could also

give rise to the ligand binding in a less symmetric manner, and 'folding' around the metal in such a way that forces the imine protons closer to it.

Table 4.2: Simulated A (MHz) values for the ENDOR spectra shown in fig. 4.13 and fig. 4.14.

Sample	A_1	A_2	A_3	θ / °	A_{iso}	A(dip)	R / Å
CuL^4	16.6	16.0	20.5	90	17.70	2.80	3.87
CuL^6	18.35	19.25	23.85	90	20.48	3.37	3.64
	15.50	14.70	20.85	90	17.02	3.83	3.48

A_{iso} is a through bond interaction and gives information on the unpaired electron spin density at the interacting nucleus in question. The two values for L^6 are very different (20.48 and 17.02 MHz) and assigning one of these to an individual imine proton would be tentative without more characterisation. However, it is reasonable to postulate that the largest A_{iso} arises from the imine proton that is spatially closest to the copper centre, probably that closest to the alkoxide (fig. 4.15, H^a). This is because A values tend to increase with negative charge, and an alkoxide is more negative than an N-oxide.

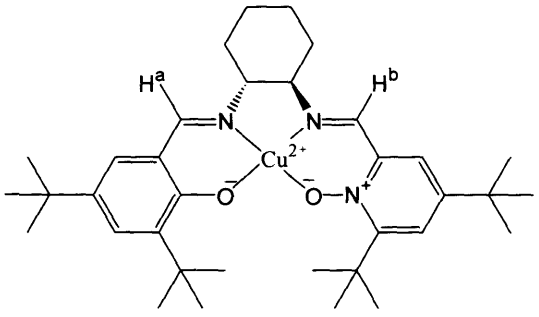

Fig. 4.15: The asymmetry of CuL^6 at the metal centre is apparent when examining the imine signals of the ENDOR spectrum.

The ^{1}H ENDOR spectra showing the remaining bulk ligand protons are shown in fig. 4.16 and the ^{14}N ENDOR spectra are shown in fig. 4.17. Although it is much less clear, there is a difference in both sets of spectra, in that those corresponding to $\mathbf{L^4}$, once again have less transitions than $\mathbf{L^6}$, indicating a reduction in symmetry.

The ^{1}H ENDOR spectra showing the remaining ligand proton peaks (i.e. the protons weakly coupled to the copper centre) are shown in fig. 4.16, recorded at the $g = g_{\perp}$ and $g = g_{\parallel}$ positions. The spectra are largely similar to each other, originating form the envelope of all remote protons. Since two components of the ^{1}H hyperfine tensor for each proton contribute to the spectrum, analysis is not straightforward.

By comparison the ^{14}N spectra (shown in fig. 4.17 recorded at the $g = g_{\perp}$ and $g = g_{\parallel}$ positions) are far more informative. The spectrum of $\mathbf{L^4}$ (3.17a) is very similar to that obtained for $\mathbf{CuL^3}$,[37] suggesting equivalent ^{14}N centres. The hyperfine and quadrupole parameters ($^{14}N_A$ and $^{14}N_Q$) are typical of Cu(salen) complexes. However the spectrum of $\mathbf{L^6}$ is significantly different. The peaks are now split, indicating an inequivalency of the two directly coordinating ^{14}N nuclei. Furthermore, the $^{14}N_A$ values of one ^{14}N nucleus has increased relative to the other (manifested by the displacement of the peaks to higher frequency). This can either be explained on the grounds of a shorter Cu-N distance (i.e. larger A(dip) value) or greater spin density on ^{14}N, or both. In any case, the ^{14}N spectra confirm the earlier ^{1}H results and confirm the asymmetric environment of copper in the ligand plane.

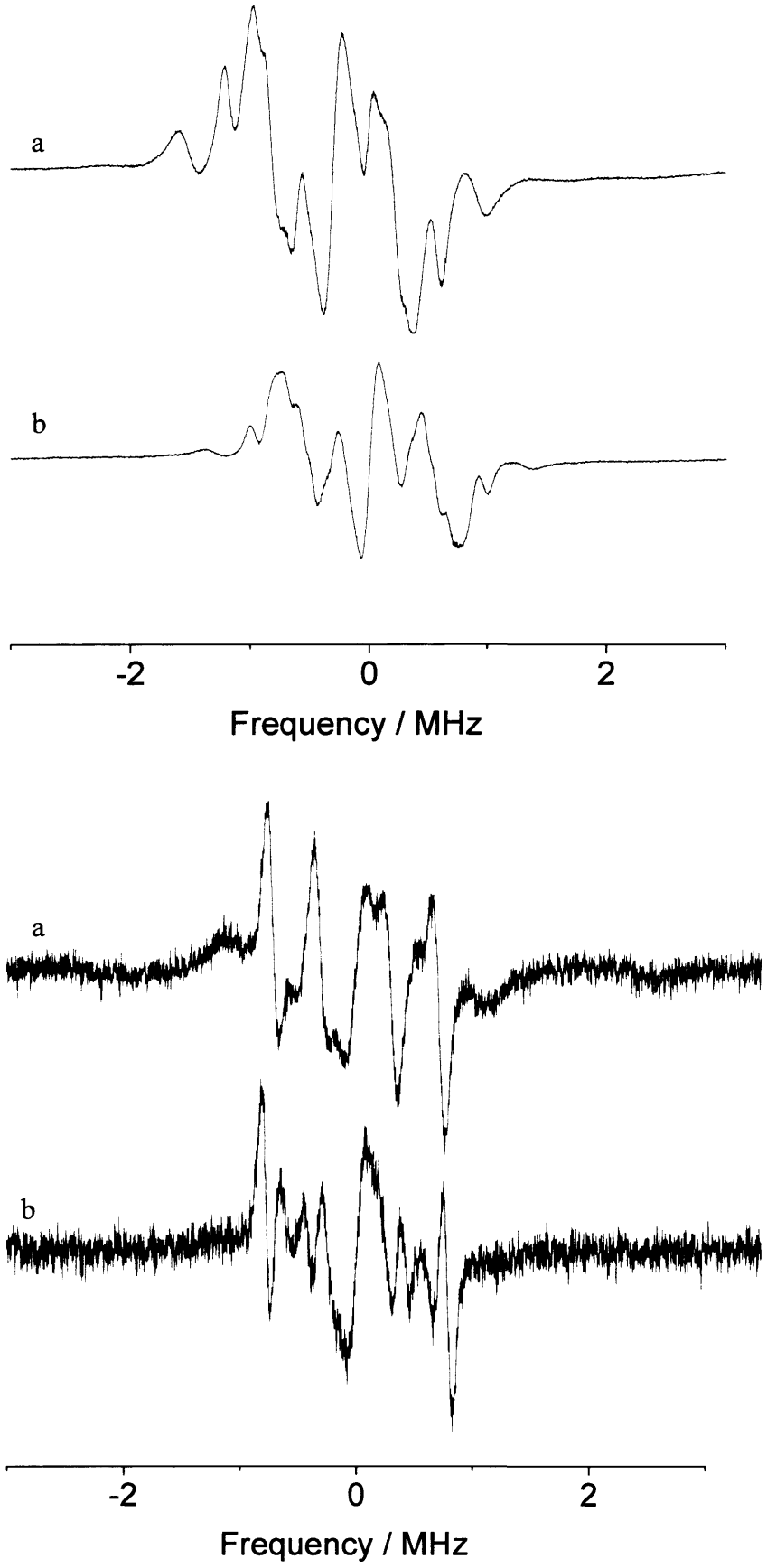

Fig. 4.16: ^{1}H CW-ENDOR spectra of (a) [Cu**L**^{4}](ClO$_4$)$_2$ and (b) [Cu**L**^{6}](ClO$_4$) recorded at Q-band frequencies and 10K in 10% methanol, 20% dichloromethane and 70% toluene. The spectra were measured at the field position corresponding to $g = g_\perp$ (top) and $g = g$ (bottom).

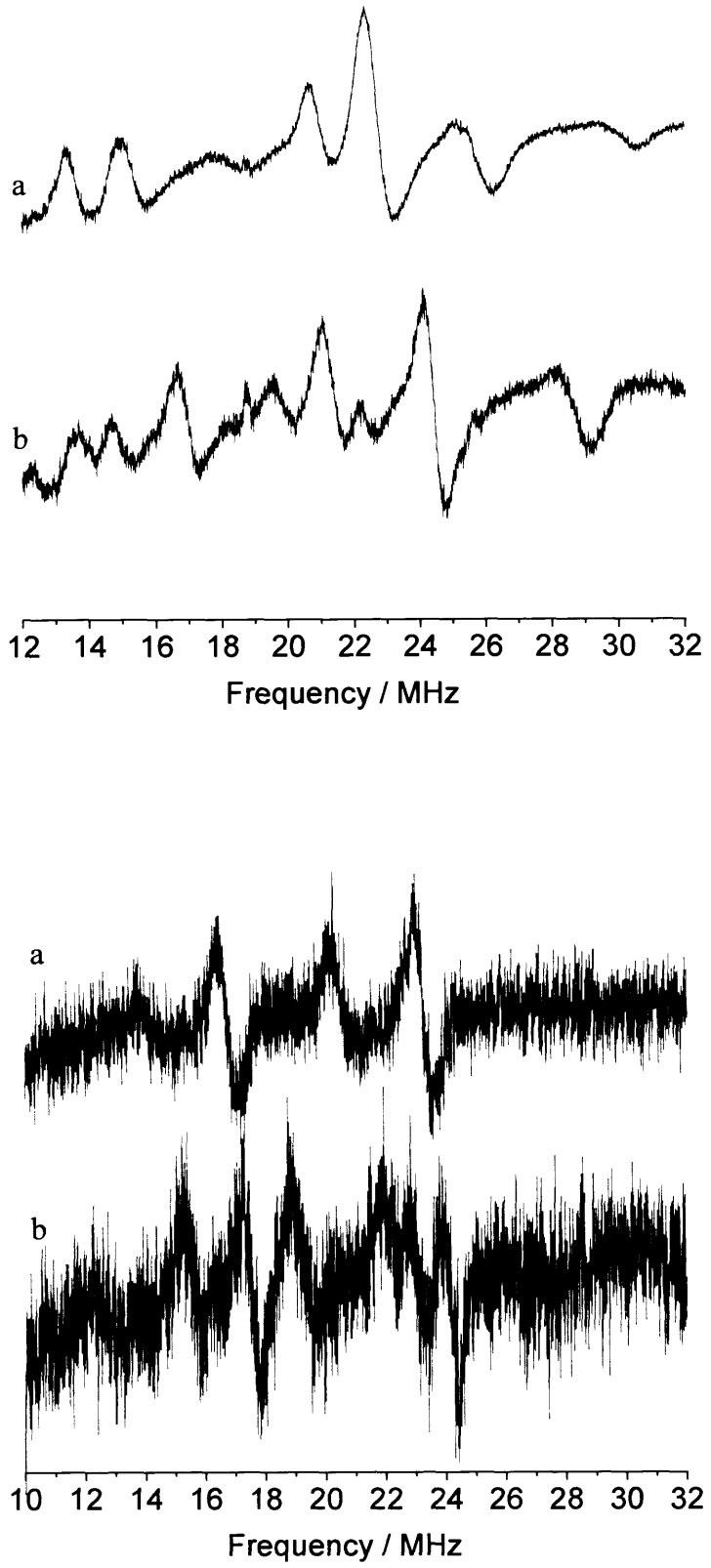

Fig. 4.17: ^{14}N CW-ENDOR spectra of (a) $[CuL^4](ClO_4)_2$ and (b) $[CuL^6](ClO_4)$ recorded at Q-band frequencies and 10K in10% methanol, 20% dichloromethane and 70% toluene. The spectra were measured at the field position corresponding to $g = g_\perp$ (top) and $g = g$ (bottom).

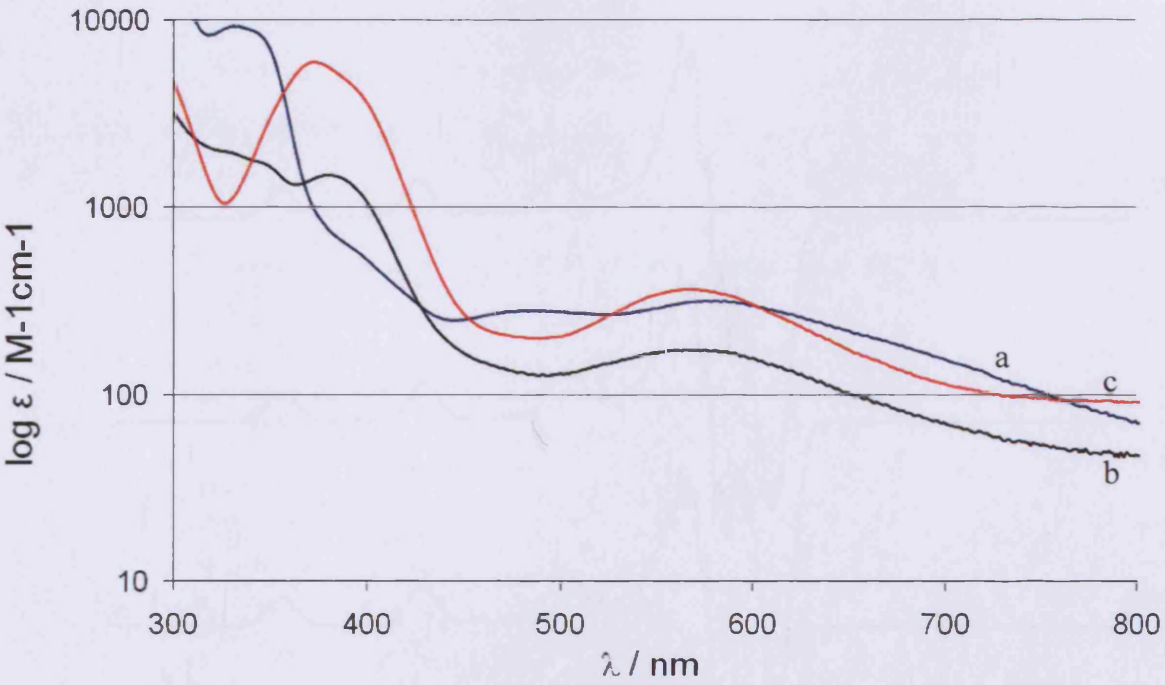

Fig. 4.18: UV spectra of (a) $[CuL^4](ClO_4)_2$, (b) $[CuL^6](ClO_4)$ and (c) CuL^3 recorded in acetonitrile at room temperature.

To confirm the validity of the conclusions made so far, UV spectra were taken of the three copper complexes, these are shown in fig. 4.18.

All three UV spectra are characteristic of a tetragonally distorted CuL_6 species (where L = N or O)[36]. The peaks at ~620 appear to shift to slightly higher wavelengths as a greater charge is placed at the metal centre ($CuL^3 < CuL^6 < CuL^4$). This implies a greater tendency for the higher charged ligand, L^4 to adopt an octahedral conformation over L^3.

Interestingly, the asymmetrical complex, CuL^6 gives rise to a smaller extinction coefficient than the two symmetrical complexes, CuL^3 and CuL^4. This can be explained by the presence of poorer orbital overlap between the metal d orbitals and the ligand p orbitals. This would imply a smaller degree of orbital mixing, giving rise to a smaller peak intensity.

4.3.3 Steric manipulation of the isosalen core

X-band EPR spectra were taken of $[CuL^4](ClO_4)_2$, $[CuL^7](ClO_4)_2$ and $[CuL^8](ClO_4)_2$ in order to investigate the effect the peripheral *tert*-butyl groups have upon the metal centre. They are shown in fig. 4.19.

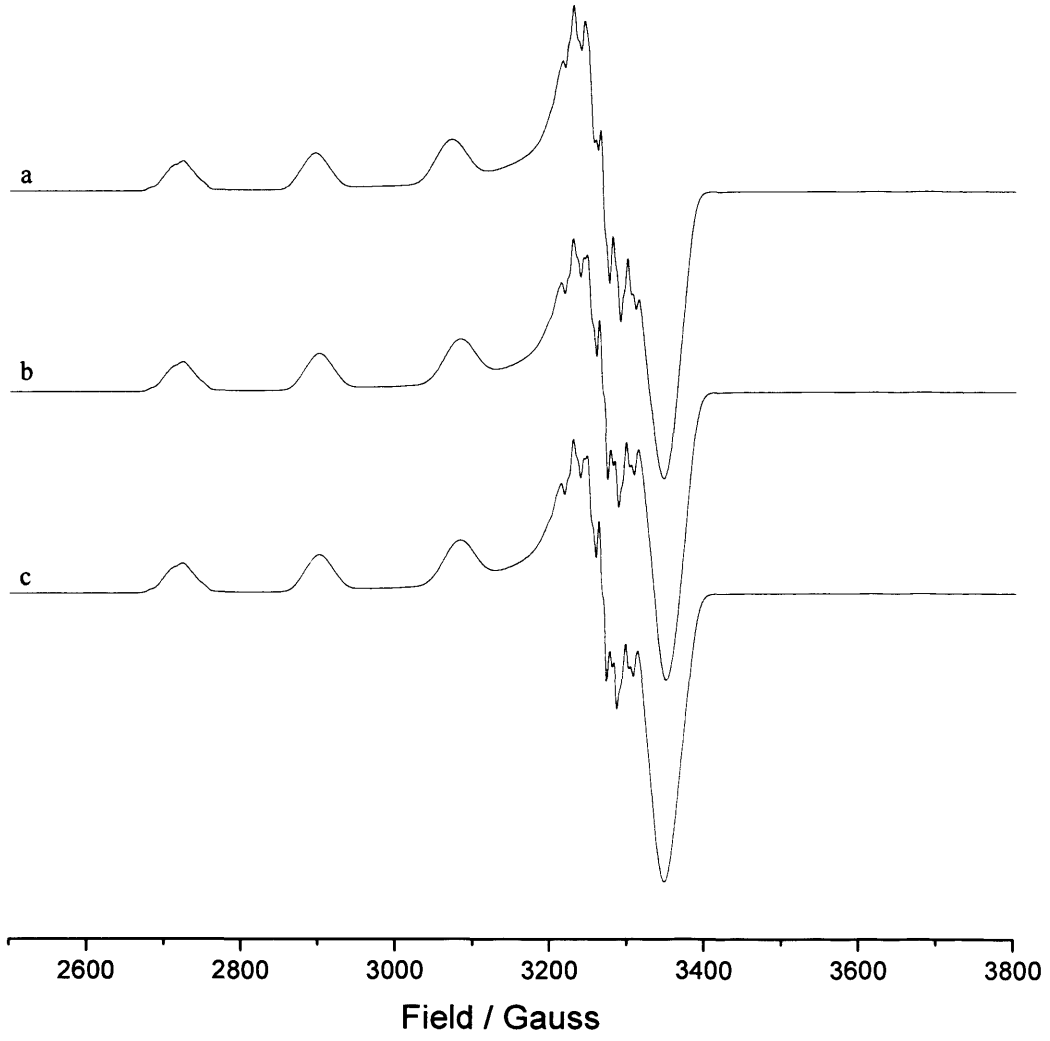

Fig. 4.19: CW X-band EPR spectra (50 K) of (a) CuL^4, (b) CuL^7 and (c) CuL^8 in DCM : DMSO (70:30).

The simulated EPR data describing these spectra are listed in table 4.3. It is clear that $g_\perp$ and $A_\perp$ remain largely unaffected by the changing ligand. This indicates a common xy-axis environment.

However there is an apparent trend of decreasing $g_\parallel$ values in the order $CuL^4 > CuL^7 > CuL^8$. Conversely, there is a trend of increasing $A_\perp$ values following the same order. This is a very similar observation as that seen in series A although the effect is much smaller. This can be attributed to the fact that it is mostly the symmetry of the copper centre that is being altered. The removal of the *tert*-butyl groups has very little effect on the electronic surroundings. However, it does have an effect on the symmetry of the complexes.

As CuL^8 has the smallest $g_\parallel$ and largest $A_\parallel$ values, lower symmetry is implied, and therefore more tetragonal distortion. The removal of the *tert*-butyl groups from the

ligand allows the ligand to adopt a more electronically favourable geometry around the metal centre, which happens to contain less symmetry than the more strained CuL^4.

Table 4.3: Simulated data for the EPR spectra simulated in fig. 4.19.

Complex	$g_\perp$	$g_\parallel$	$A_\perp$ / G	$A_\parallel$ / G
$[CuL^4](ClO_4)_2$	~2.05	2.25	28	174
$[CuL^7](ClO_4)_2$	~2.05	2.24	28	177
$[CuL^8](ClO_4)_2$	~2.05	2.24	28	183

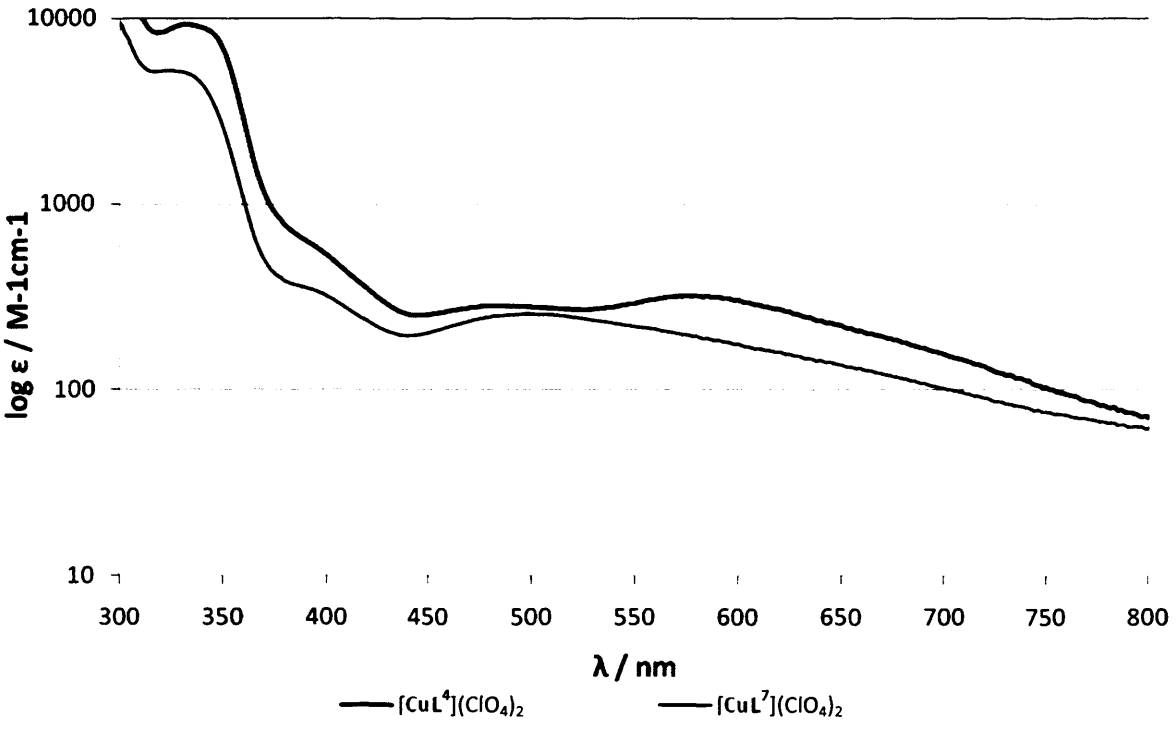

Fig. 4.20: UV spectra of CuL^4 and CuL^7 in acetonitrile at room temperature.

UV spectra were taken of CuL^4 and CuL^7. However, one could not be recorded of CuL^8 due to the insolubility of the complex. The two spectra are shown in fig. 4.20.

The complex with the highest symmetry, Cu$\mathbf{L}^4$, exhibits a slightly higher extinction coefficient than Cu$\mathbf{L}^7$. This is probably because this is tetrahedrally distorted and has no inversion centre, *i*.

4.4 Conclusions and suggestions for further research

New ligands ($\mathbf{L}^6$, $\mathbf{L}^7$ and $\mathbf{L}^8$) have been synthesised and their copper complexes fully characterised by electronic spectroscopic methods. It was found that even changing peripheral (*tert*-butyl) moieties on a copper salen complex can substantially affect the metal.

The ability to detect small changes in geometry at the metal centre when the ligand framework is adapted is a powerful tool when designing the next generation of catalysts. The degree of symmetry at the metal centre could have important implications when investigating the interaction of these complexes with chiral substrates. The work carried out herein has opened up many avenues of research; the following chapters investigate the catalytic activity of the new complexes described, and the enantioselectivity of Zn$\mathbf{L}^4$ for simple chiral substrates.

In addition to this, there is the opportunity to adapt the N-oxide salens further, exchanging the *tert*-butyl groups for other groups, such as a more electron withdrawing halide moiety. This could have an even larger effect on the metal centre, possibly making the copper even more electron deficient.

4.5 Bibliography

1. Yoon Tehshik, P.; Jacobsen Eric, N., Privileged chiral catalysts. *Science* **2003,** 299, (5613), 1691-3.

2. Pfeiffer, P.; Breith, E.; Lubbe, E.; Tsumaki, T., Tricyclic ortho-condensed partial valence rings. *Annalen der Chemie* **1933,** 503, 84-130.

3. Jacobsen, E. N.; Zhang, W.; Muci, A. R.; Ecker, J. R.; Deng, L., Highly enantioselective epoxidation catalysts derived from 1,2-diaminocyclohexane. *J. Am. Chem. Soc.* **1991,** 113, (18), 7063-4.

4. Yamate, O.; Tada, A. Charge-control agent in positively charging electrostatographic toner. 2002-98502

2003295521, 20020401., 2003.

5. Schuster, C.; Holderich, W. F., Modification of faujasites to generate novel hosts for "ship-in-a-bottle" complexes. *Catal. Today* **2000,** 60, (3-4), 193-207.

6. Tiecco, M.; Testaferri, L.; Marini, F.; Sternativo, S.; Del Verme, F.; Santi, C.; Bagnoli, L.; Temperini, A., Synthesis of enantiomerically enriched beta -hydroxy selenides by catalytic asymmetric ring opening of meso-epoxides with (phenylseleno)silanes. *Tetrahedron* **2008,** 64, (15), 3337-3342.

7. Zhou, Z.; Wang, Q.; Liu, B.; Zhao, G.; Zhou, Q.; Tang, C., (Salen)Ti(IV)-catalyzed asymmetric ring-opening of monosubstituted epoxides with dithiophosphorus acid. *Lett. Org. Chem.* **2005,** 2, (8), 752-754.

8. Dzygiel, P.; Reeve, T. B.; Piarulli, U.; Krupicka, M.; Tvaroska, I.; Gennari, C., Resolution of racemic N-benzyl alpha -amino acids by liquid-liquid extraction: a practical method using a lipophilic chiral cobalt(III) salen complex and mechanistic studies. *Eur. J. Org. Chem.* **2008**, (7), 1253-1264.

9. Storr, T.; Wasinger, E. C.; Pratt, R. C.; Stack, T. D. P., The geometric and electronic structure of a one-electron-oxidized nickel(II) bis(salicylidene)diamine complex. *Angew. Chem., Int. Ed.* **2007,** 46, (27), 5198-5201.

10. Pratt, R. C.; Stack, T. D. P., Mechanistic Insights from Reactions between Copper(II)-Phenoxyl Complexes and Substrates with Activated C-H Bonds. *Inorg. Chem.* **2005,** 44, (7), 2367-2375.

11. Wu, M.; Jing, H.; Chang, T., Synthesis of beta -amino carbonyl compounds via a Mannich reaction catalyzed by SalenZn complex. *Catal. Commun.* **2007,** 8, (12), 2217-2221.

12. Midland, M. M.; Koops, R. W., Asymmetric hetero Diels-Alder reaction of alpha -alkoxy aldehydes with activated dienes. The scope of Lewis acid chelation-controlled cycloadditions. *J. Org. Chem.* **1990,** 55, (17), 5058-65.

13. Yoon, T. P.; Jacobsen, E. N., Privileged chiral catalysts. *Science* **2003,** 299, (5613), 1691-3.

14. Tokunaga, M.; Larrow J., F.; F., K.; N., J. E., Asymmetric Catalysis with Water: Efficient Kinetic Resolution of Terminal Epoxides by Means of Catalytic Hydrolysis. *Science* **1997,** 277, 936.

15. Furrow Michael, E.; Schaus Scott, E.; Jacobsen Eric, N., Practical Access to Highly Enantioenriched C-3 Building Blocks via Hydrolytic Kinetic Resolution. *J. Org. Chem.* **1998,** 63.

16. Schaus Scott, E.; Brandes Bridget, D.; Larrow Jay, F.; Tokunaga, M.; Hansen Karl, B.; Gould Alexandra, E.; Furrow Michael, E.; Jacobsen Eric, N., Highly selective hydrolytic kinetic resolution of terminal epoxides catalyzed by chiral (salen)Co(III) complexes. Practical synthesis of enantioenriched terminal epoxides and 1,2-diols. *J Am Chem Soc* **2002,** 124, (7), 1307-15.

17. Nielsen, L. P. C.; Stevenson, C. P.; Blackmond, D. G.; Jacobsen, E. N., Mechanistic Investigation Leads to a Synthetic Improvement in the Hydrolytic Kinetic Resolution of Terminal Epoxides. *J. Am. Chem. Soc.* **2004,** 126, (5), 1360-1362.

18. Fallis, I. A.; Murphy, D. M.; Willock, D. J.; Tucker, R. J.; Farley, R. D.; Jenkins, R.; Strevens, R. R., Direct Observation of Enantiomer Discrimination of Epoxides by Chiral Salen Complexes Using ENDOR. *J. Am. Chem. Soc.* **2004,** 126, (48), 15660-15661.

19. Murphy Damien, M.; Fallis Ian, A.; Willock David, J.; Landon, J.; Carter, E.; Vinck, E., Discrimination of geometrical epoxide isomers by ENDOR spectroscopy and DFT calculations: the role of hydrogen bonds. *Angew Chem Int Ed Engl* **2008,** 47, (8), 1414-6.

20. Chrisholm, M. H.; Patmore, N. J.; Zhou, Z., Concerning the relative importance of enantiomorphic site *vs.* chain end control in the stereoselective polymerisation of lactides. *Chem Commun* **2004**.

21. Chen, H.; Collomb, M. N.; Duboc, C.; Blondin, G.; Riviere, E.; Faller, J. W.; Crabtree, R. H.; Brudvig, G. W., New Linear High-Valent Tetranuclear Manganese-Oxo Cluster Relevant to the Oxygen-Evolving Complex of Photosystem II with Oxo, Hydroxo, and Aqua Coordinated to a Single Mn(IV). *Inorg. Chem.* **2005,** 44, (25), 9567-9573.

22. Zhong, Z.; Dijkstra, P. J.; Feijen, J., [(salen)Al]-Mediated. controlled and stereoselective ring-opening polymerisation of lactide in solution and without solvent: synthesis of highly isotactic polylactide stereocopolymers from racemic D,L-lactide. *Chem Commun* **2002,** 41, 4510-4514.

23. Zhong, Z.; Dijkstra, P. J.; Feijen, J., Controlled and stereoselective polymerisation of lactide: kinetics, selectivity and microstructures. *J Am Chem Soc* **2003,** 125, 11291-11298.

24. Danishefsky, S. J.; Ninno, M. P. D., Totally Synthetic Routes to the Higher Monosaccharides. *Angew Chem Int Ed Engl* **1987,** 26, (1).

25. Martinez, L. E.; Leighton, J. L.; Carsten, D. H.; N., J. E., Highly Enantioselective Ring Opening of Epoxides Catalyzed by (salen)Cr(III) Complexes. *J Am Chem Soc* **1995,** 117, 5897.

26. Larrow Jay, F.; Schaus Scott, E.; Jacobsen Eric, N., Kinetic Resolution of Terminal Epoxides via Highly Regioselective and Enantioselective Ring Opening with TMSN3. An Efficient, Catalytic Route to 1,2-Amino Alcohols. *J Am Chem Soc* **1996,** 118.

27. Schaus, S. E.; Brnalt, J.; Jacobsen, E. N., Asymmetric Hetero-Diels-Alder Reactions Catalyzed by Chiral (Salen)Chromium(III) Complexes. *J. Org. Chem.* **1998,** 63, (2), 403-405.

28. Fagnou, K.; Lautens, M., Rhodium-Catalyzed Carbon-Carbon Bond Forming Reactions of Organometallic Compounds. *Chem Rev.* **2003,** 103.

29. Meyers, J.; N., J. E., Asymmetric Synthesis of -Amino Acid Derivatives via Catalytic Conjugate Addition of Hydrazoic Acid to Unsaturated Imides. *J Am Chem Soc* **1999,** 121.

30. Taylor, M. S.; Zalatan, D. N.; Lerchner, A. N.; Jacobsen Eric, N., Highly enantioselective conjugate additions to a, b-unsaturated ketones catalysed by a (salen)Al complex. *J Am Chem Soc* **2005,** 127.

31. Dyker, G.; Holzer, B.; Henkel, G., A chiral bis-N-oxide isoelectronic with Jacobsen's salen ligand. *Tetrahedron: Asymmetry* **1999,** 10, (17), 3297-3307.

32. Zang, Y.; Lu, Q.; Yin, Z.; Zeng, C.; Dai, A.; Zhou, Z., Studies on coordination compounds with picolinaldehyde N-oxide derivatives as ligands. (I). Syntheses and crystal structures of cupric complexes with bis-Schiff bases from

picolinaldehyde N-oxide and diamines. *Gaodeng Xuexiao Huaxue Xuebao* **1989,** 10, (1), 1-5.

33. Rieger, P. H., *Electron Spin Resonance: Analysis and Interpretation.* RSC: 2007.

34. Murphy Damien, M.; Farley Robert, D., Principles and applications of ENDOR spectroscopy for structure determination in solution and disordered matrices. *Chem Soc Rev.* **2006,** 35, 249-269.

35. Hathaway, B. J., The correlation of the electronic properties and stereochemistry of mononuclear {CuN4–6} chromophores. *Dalton Trans* **1972**, 1196-1199.

36. Lever, A. B. P., *Inorganic Electronic Spectroscopy.* 2nd Edition ed.; Elesvier: 1984.

37. Fallis Ian, A.; Murphy Damien, M.; Carter, E.; Farley Robert, D.; Caretti, I.; Van Doorslaer, S.; Goebel, M.; Willock, D. J.; Landon, J., *In prep.*

38. Pilbrow, J. R., *Transition Ion Electron Paramagnetic Resonance.* Clarendon Press: 1990.

39. Fallis, I. A.; Murphy, D. M.; Carter, E.; D., F. R.; Caretti, I.; Van Doorslaer, S.; Goebel, M.; Willock, D. J.; Landon, J., *In prep.*

40. Mabbs, F. E.; Collison, D.; *Mol. Phys. Reports* **1999**, 39-59.

CHAPTER 5

Asymmetric cyclopropanation catalysis by copper salen derivatives

5.1 Introduction

5.1.1 Catalytic Cyclopropanation

5.1.1.1 Discovery and Uses

Cyclopropanes are an important class of compounds in synthetic chemistry; they frequently appear in precursors of, or subunits of, biologically active natural and synthetic products.[1, 2] They are susceptible to ring-opening due to severe ring strain, this has the advantage that they can be converted into a wide range of useful products.[3] The development of effective methods for the formation of cyclopropane rings with control of diastereo- and enantioselectivity has been greatly studied in recent years.[4]

The first examples of metal catalysed cyclopropanation reactions of diazo compounds were published in 1966 by Nozaki *et al.*[5] using copper salicylaldimine (fig. 5.1) although enantiomeric excesses were shown to be extremely low (6%). However, this was the first reported example of homogeneous catalysis with a soluble chiral metal complex.

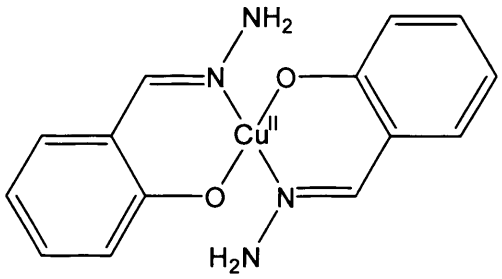

Fig. 5.1: Copper salicylaldimine, as reported by Nozaki *et al.* was the first catalyst capable of performing cyclopropanation reactions.

Aratani *et al.*[6] improved this reaction to give commercially viable yields and achieved the enantioselective synthesis of 2,2-dimethyl-3-(2-methylpropenyl)cyclopropane-carboxylic acid[6, 7] (scheme 5.1) and alkyl 3-(2,2-dichlorovinyl)-2,2-dimethyl-cyclopropanecarboxylic acid.[6, 8] These represent the acid moiety of the widely used class of insecticides, the pyrethoids; these are highly potent and possess low toxicity to mammals.[9] The Aratani asymmetric process was also utilised in the large scale production of (*S*)-2,2-dimethyl-cyclopropanecarboxylic acid, which is part of the antibiotic Imipenem, developed in 1985.[1]

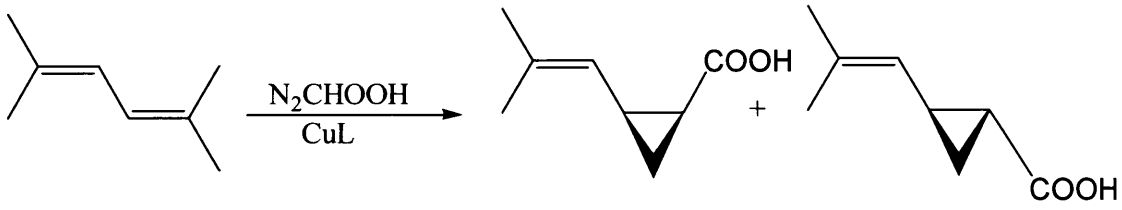

Scheme 5.1: The synthesis of 2,2-dimethyl-3-(2-methylpropenyl)cyclopropane-carboxylic acid as reported by Aratani.[6, 7]

Apart from copper, other metals which have been shown to exhibit catalytic activity towards cyclopropanation are rhodium, ruthenium and osmium.[10, 11] Copper is attractive mainly due to its relatively low cost. One of the most versatile copper cyclopropanation catalysts is the bis(*tert*-butyl)oxazoline (shown in fig. 5.2) developed by Evans *et al.*[12] It has been shown to give high yields and enantiomeric excesses of >99%, it was also shown that the *cis/trans* ratio increases with increased steric bulk on the ester group of the diazo compound.

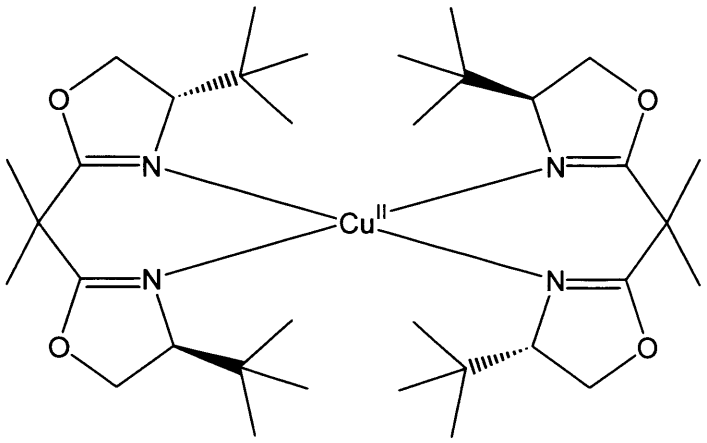

Fig. 5.2: Copper catalyst developed by Evans.[12]

5.1.1.2 Mechanistic Studies

It is well established that the *cis/trans* selectivity of all copper cyclopropanation catalysts is relatively poor with respect to the cyclopropanation of monosubstituted olefins, this is more dependant on the structure of the diazo ester rather than the complex itself.[3] 1,2-disubstitution (of the olefin) does have an effect on the *cis/trans* ratio.[3] The mechanism of this reaction is uncertain although two points are generally accepted: the catalytically active species contains Cu(I),[13] regardless of the oxidation state of the precatalyst (the di-azo compound is thought to reduce Cu(II) to Cu(I)) and that there is an electrophilic copper-carbene intermediate (fig. 5.3). The carbene

species has been observed spectroscopically in ruthenium and osmium systems,[11, 14, 15] but only twice in copper systems.[16]

The reaction has been studied extensively, both experimentally and theoretically;[17, 18] it is thought that copper catalysed cyclopropanation proceeds *via* two stages, the first being carbene complex formation, and the second being carbene transfer (scheme 5.2). It has been shown that the rate determining step is the formation of the copper carbene intermediate.[13]

Two mechanisms for the carbene transfer reaction have been proposed, the concerted pathway (direct insertion) has been observed in the Simmons-Smith cyclopropanation,[19] involving Zn(II) complexes (isoelectronic to Cu(I)). The second mechanism proposed is the stepwise pathway, in which a metallacyclobutane intermediate is formed, this has been observed in Ni(0) carbene complexes (also isoelctronic to Cu(I)), this intermediate then goes on to reductively eliminate, forming the desired cyclopropane product.[20]

A theoretical was study carried out in 2001 by Garcia *et al.*[17] on the cyclopropanation of copper complexes of *N, N'*-dimethylmalonaldiimine. The study showed that the copper atom of the carbene complex has a distorted trigonal coordination, the calculations suggested that direct carbene insertion is favoured over the stepwise mechanism. They also proved that the *cis/trans* ratio is governed by steric interactions between the carbene ester group and the substituents on the olefin double bond, a theory that has, as mentioned earlier, been experimentally observed.[3]

More recently, in 2008, Özen and Tüzün[21] reported a theoretical study on the same system, but expanded on Garcia's hypothesis by postulating that the direct insertion mechanism would indeed be favoured for catalytic reactions involving diazo compounds without a carbonyl group present, while the four-centred reductive elimination stepwise pathway would be favoured if the diazo compound contains a carbonyl moiety.

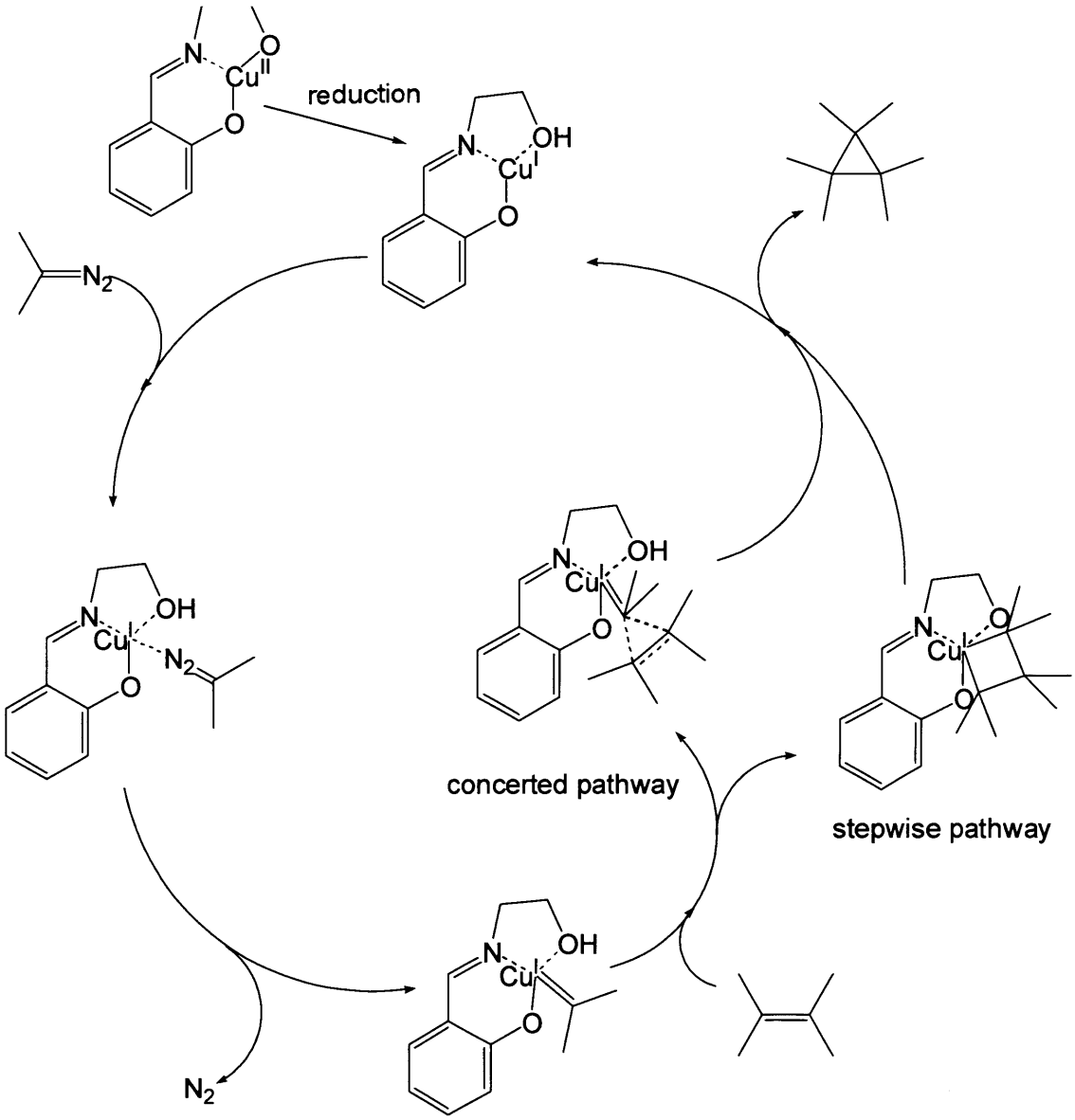

Scheme 5.2: The proposed catalytic cycle of asymmetric cyclopropanation.

There are many examples in the literature of schiff base catalysts used for cyclopropanation reactions. Iron complexes of $\mathbf{L^3}$ for example have been used in cyclopropanation reactions as reported by Edulji *et al.*[22] Good yields (up to 90%) and modest *cis/trans* ratios were reported in a variety of solvents. Of note is the fact that this Fe catalyst does not require anaerobic conditions to catalyse the cyclopropanation reaction, this is rare for an iron catalyst of this type.[22]

Ruthenium has been shown to be catalytically active with respect to cyclopropanation when present as complex $\mathbf{RuL^{10}}$ (scheme 5.3).[23] This complex was reported to enantioselectively catalyse the intramolecular cyclopropanation of *cis*-alkenyl diazoacetates (scheme 5.3).

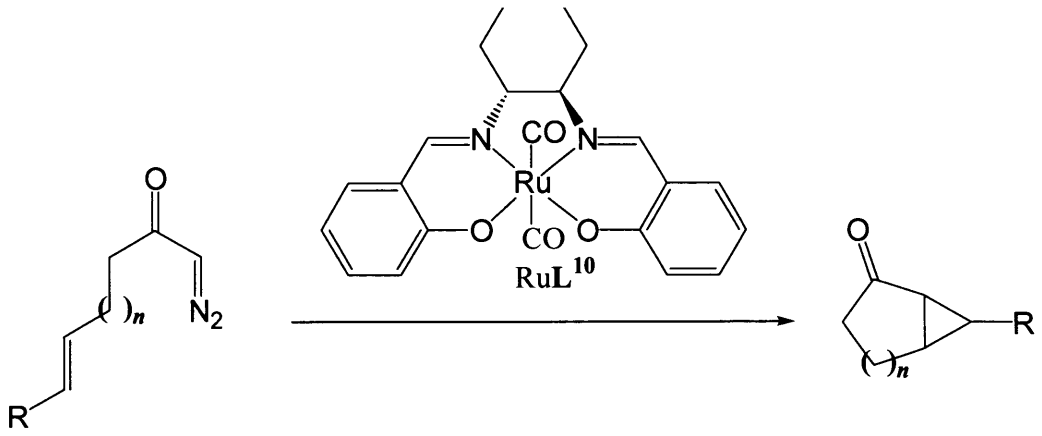

Scheme 5.3: The Ru cyclopropanation catalyst as reported by Li *et al.*[23]

Iridium has also been used with a Schiff base ligand for this important class of organic enantioselective transformation. Katsuki *et al.*[24] showed that the complex Ir**L**[11] (fig. 5.3) achieves good enantioselectivity with regard to the cyclopropanation of styrene, achieving enantiomeric excesses of > 90%. This ligand was also shown to achieve exceptional enantioselectivites when coordinated to ruthenium.[25, 26]

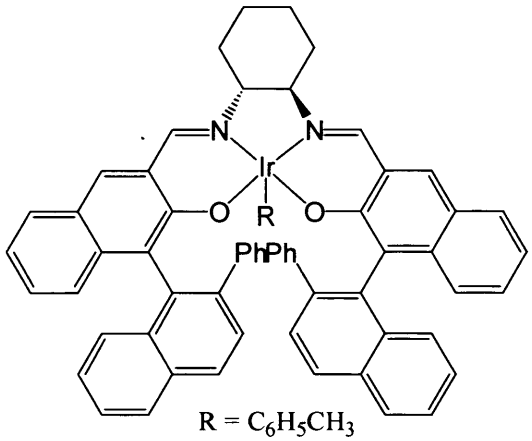

Fig. 5.3: Ir containing cyclopropanation catalyst Ir**L**[11] as described by Katsuki *et al.*[24]

Of the many schiff base cyclopropanation catalysts reported, only a few contain copper. Notably in 2000 Li *et al.*[27] reported enantiomeric excesses of more than 98% on the cyclopropanation of styrene with diazoacetate with the copper Schiff base catalyst shown in fig. 5.4. It was found that altering R^1 and R^2 dramatically alters the *ee* of the products. The addition of the sterically bulky and electron donating *tert*-butyl groups reduces the *ee* markedly. However, the addition of electron withdrawing substituents, such as chloride or nitro groups, was found to greatly increase the yields and enantiomeric excesses of the products.

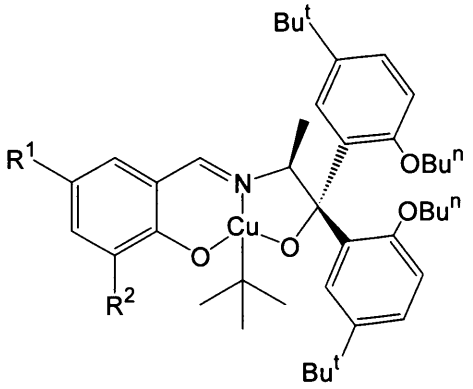

Fig. 5.4: The copper cyclopropanation catalyst reported by Li *et al.*[27]

In 2004 Itagaki *et al.*[28] published a study on the cyclopropanation of diene with Li's catalyst and reported that decreasing the temperature has a detrimental effect on the yield but markedly increases the enantiomeric excesses of the products. The effect of adding a Lewis acid to the reaction was also probed; equimolar amounts of $Al(OEt)_3$ were added, it was found that even at 20 °C a 95% yield was observed with 76% *ee*. It was postulated that the Lewis acid coordinates to the oxygen atom of the nitro group, hence lowering the electron density of the carbon in the carbene complex, therefore enhancing the reactivity. This is yet to be confirmed.

Dyker *et al.*[29] reported the use of the copper complex of $\mathbf{L^4}$ (see section 3.1.2) for the enantioselective cyclopropanation of styrene and observed a poor *cis/trans* ratio (45/55) with equally poor enantiomeric excesses of 21% and 15% respectively. A small catalytic study was carried out following the procedure laid out by Dyker *et al.*[29] to test the compounds synthesised (the copper complexes of $\mathbf{L^4}$, $\mathbf{L^6}$, $\mathbf{L^7}$ and $\mathbf{L^9}$, fig. 5.4) for catalytic activity.

5.2 Experimental

5.2.1 Synthetic experimental

Preparation of R, R $[CuL^9](ClO_4)$

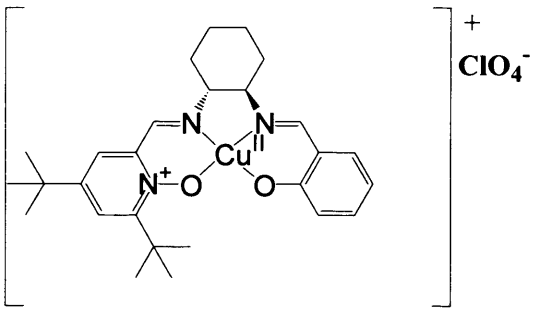

2-Hydroxybenzaldehyde (52 mg, 0.43 mmol) and 3,5-di-*tert*-butylpyridine-2N-oxide aldehyde (101 mg, 0.43 mmol) were added to *R, R*-1,2-Diaminocyclohexane (50 mg, 0.43 mmol) in ethanol (20 ml). The mixture was stirred for 2 hours and $Cu(ClO_4)_6$ (151 mg, 0.41 mmol) in ethanol (10 ml) was added. This was stirred for a further 30 minutes. The solvent was removed and the product was isolated by column chromatography (SiO_2, 50:50 $CHCl_3$:Me_2CO, Rf = 0.6). Further purification by slow diffusion of ether into an ethanolic solution yielded 68 mg (21%) of a purple crystalline solid. IR: (KBr disc, cm^{-1}) 3541(b), 3012(m), 1568(s), 1474(m), 1201(s). UV/Vis (acetonitrile): λ_{max} = 372nm, ε = 1427 $cm^{-1}mol^{-1}dm^3$; 566nm, ε = 174 $cm^{-1}mol^{-1}dm^3$. MS(EI), MH^+ exact mass (*calc.*) *m/z 752.9566 (obs.) 752.9598.*

5.2.2 Cyclopropanation procedure

A general procedure for the cyclopropanation of styrene with the copper(II) salen complexes discussed is outlined below. For continuity, all catalytic reactions were rigorously adhered to this procedure in order that direct comparisons could be made between the results obtained.

A solution of $[Cu\mathbf{L}^4](ClO_4)_2$ (100 mg, 0.12 mmol) in dry dichloromethane (10 ml) was prepared, to this was added an excess of sodium borohydride (20 mg) under a nitrogen atmosphere, the resulting suspension was stirred for 5 minutes. The solution was filtered and styrene (370 mg, 3.6 mmol) was added. After 5 minutes ethyl diazo acetate (502 mg, 4.4 mmol) was added dropwise, the resulting mixture was stirred at room temperature for 2 hours. This was then purified flash chromatographically (hexane/ether, 20/1), this was deemed of sufficient purity for GC analysis and the sample was injected directly into the column.

5.2.3 Gas Chromatographic Procedure

Enantiomeric excesses and *cis/trans* ratios were determined by the use of chiral gas chromatography. The instrument used was a Perkin Elmer 8700 series gas chromatograph equipped with a split/splitless injection system and flame ionisation detector (FID). Separation of the various mixtures was achieved using a β- DexTM fused silica capillary column, (30 M x 0.25 mm . 0.25 μm) using a 1μL injection volume, an isothermal temperature programme (120 °C), and a helium carrier gas

flow rate of 1 ml min^{-1}. The injector and detector temperatures were both set at 250 °C. A typical GC trace is shown in fig. 5.5.

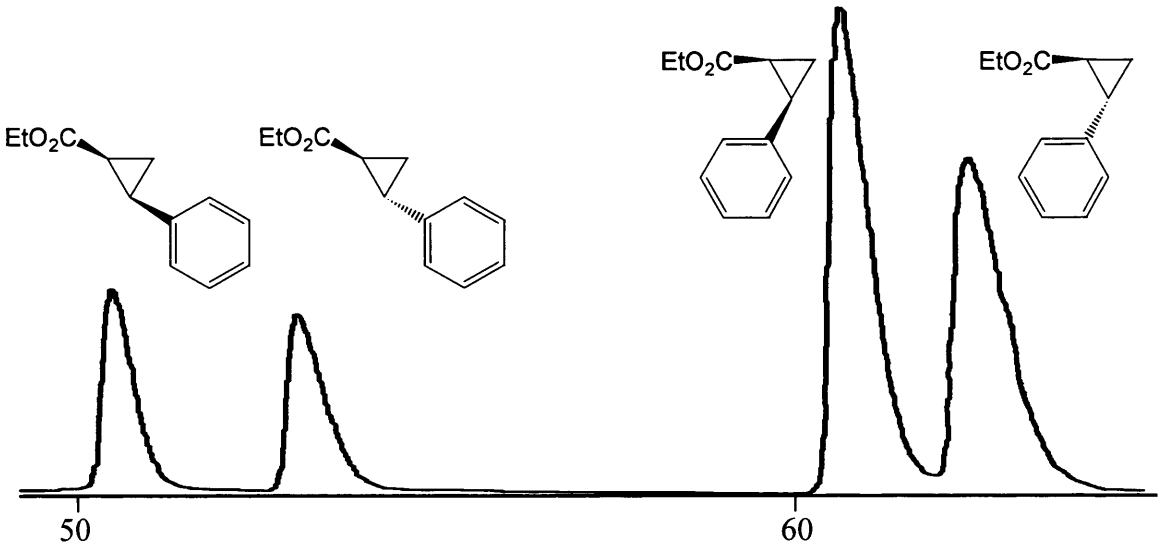

Fig. 5.5: A GC spectrum representative of that obtained for the catalytic studies carried out.

5.3 Results and Discussion

The four enantiomerically pure complexes (fig. 5.6) described in detail in Chapter four were tested for catalytic activity with regards to cyclopropanation as described above. The olefin originally chosen was styrene, because it is readily available, there has been much work carried out on this olefin and it is the olefin originally reported by Dyker *et al.*[29] therefore, by using the method described in that article, direct comparisons could be made. The diazo ester used was ethyl diazo acetate, again due to the fact that it's readily available and this is the reagent used by Dyker *et al.*

Table 5.1: Results of catalytic activity towards the cyclopropanation of styrene.

Catalyst	***Yield***	***cis/trans***	***ee (cis)***	***ee (trans)***
CuL^4	89%	60/40	14%	10%
CuL^6	91%	63/37	9%	2%
CuL^7	82%	75/25	8%	1%
CuL^9	85%	68/32	19%	40%

In comparison to Evan's catalyst (which achieves *ee* values of >95% for many styrene derivatives, fig. 5.2) the enantiomeric excesses found for these complexes are mediocre at best. However, a catalyst that can achieve high *ee* values universally to a range of olefins is yet to be reported.[30] There is merit, therefore in testing these catalysts for activity on other olefins and other diazoesters.

It is interesting to note the large difference in *ee*(*trans*) between CuL^6 and CuL^9, the only difference between them being the presence of the *tert*-butyl groups on one half of the catalyst. This strongly implies that the extra asymmetry induced by removing two *tert*-butyl groups on the alkoxide side of the complex preferentially aids the formation of one enantiomer greatly over the other. Further study into this may reveal insights into the mechanisms of this transformation.

Comparison of the results of CuL^9 and CuL^7 also may prove useful, it is clear that CuL^9 produced a much greater *ee*(*trans*) than CuL^7, the only difference between these two complexes being the presence of 1 extra N-oxide in the ligand framework, there is a larger degree of symmetry at the metal centre for CuL^7 than CuL^9, this could be a reason for the apparent lack of enantiomeric discrimination for CuL^7. It is clear from these results, that CuL^9 is the complex that is most worth pursuing in terms of catalytic activity.

Having discovered that Cu**L**^{9} is the most efficient at cyclopropanation under these conditions, it was decided that Cu**L**^{9} would be tested with some different olefins, in order to probe the extent to which this catalyst could be utilised. 2-methyl styrene and 4-methyl styrene were chosen, as they differ by the original olefin by just one methyl group (fig. 5.7). The results are shown in table 5.2.

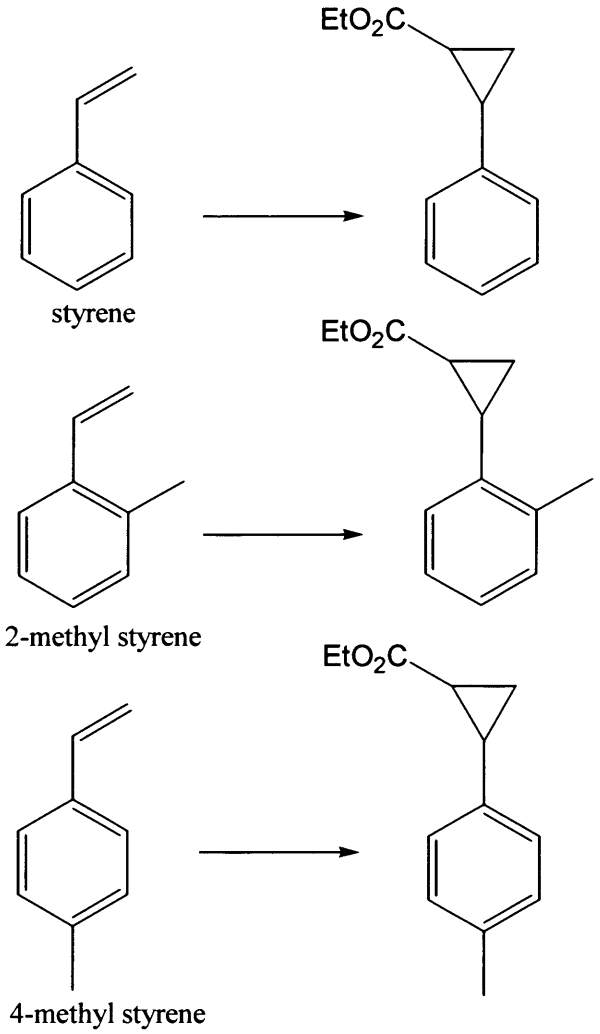

Fig. 5.7: The olefins used in this study and the cyclopropane products formed in the catalytic transformations.

The *cis/trans* ratios are very similar for all three olefins tested, as are the enantiomeric excesses. This implies the presence of a small amount of steric bulk, such as a methyl group, on the phenyl ring makes little difference to the stereogenic reactivity of the system. A possible reason for the poor performances of these catalysts may be due to the hard nature of the Cu(I) intermediates. Soft donors such as P or S may be required in the ligand to stabilise the intermediates.

Table 5.2: Results for catalytic cyclopropanation study on CuL[9].

Styrene	*Yield*	*cis/trans*	*ee (cis)*	*ee (trans)*
Styrene	88%	68/32	19%	40%
2-methyl styrene	85%	57/43	21%	34%
4-methyl styrene	82%	59/41	22%	32%

Demonceau *et al.*[31] reported the first reasonably selective ruthenium cyclopropanation catalyst shown in fig. 5.8. This took the form of a ruthenacarborane complex, which, when tested for catalytic activity on a range of substituted styrenes gave *cis/trans* ratios of 0.73 – 1.02. These values are of a similar order to those found for CuL[9].

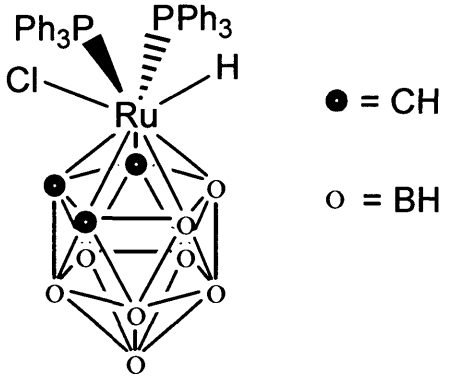

Fig. 5.8: The ruthenacarborane first reported by Demonceau *et al.* is the first reported ruthenium catalyst to achieve good *ee* in a range of cyclopropanation reactions.[26, 31]

Since then, as discussed previously (section 4.1.1) Katsuki *et al.* have reported exceptional *trans* selectivity (up to 93/7) with high enantioselectivity (up to 97%).[24] When compared to recent examples of cyclopropanation catalysts,[26, 30] CuL[9] shows mediocre stereo and enantioselectivity towards styrenes. However other olefins should be tested for activity with this particular catalyst.

5.4 Conclusions and Suggestions for Further Research

This small chapter of research has opened up many avenues for future work. There are many possibilities for optimisation of the cyclopropanation reaction using the catalysts described. The olefin may be varied, the choice of diazoester could be investigated, and the reaction conditions could be altered. More interestingly, metals other than copper (such as Fe, Ir, Ru or Rh) could be investigated for their catalytic activity.

The catalysts could be investigated for use into catalytic reactions other than cyclopropanation. Chiral copper catalysts are used in such reactions as diels alder transformations,[32] oxidations[33] and arylation reactions.[34] A study of the potential activity of the copper complexes developed into these reactions would certainly be worthwhile.

5.5 Bibliography

1. Doyle, M. P.; McKervey, M. A.; Ye, T., *Modern Catalytic Methods for Organic Synthesis with Diazo Compounds: From Cyclopropanes to Ylides*. 1998; p 652 pp.

2. Wong, H. N. C.; Hon, M. Y.; Tse, C. W.; Yip, Y. C.; Tanko, J.; Hudlicky, T., Use of cyclopropanes and their derivatives in organic synthesis. *Chem. Rev.* **1989,** 89, (1), 165-98.

3. Jacobsen, E. N.; Pfaltz, A.; Yamamoto, H., *Comprehensive Asymmetric Catalysis*. Springer: 2004.

4. Salaun, J., Optically active cyclopropanes. *Chem. Rev.* **1989,** 89, (5), 1247-70.

5. Nozaki, H.; Moriuti, S.; Takaya, H.; Noyori, R., Asymmetric induction in carbenoid reactions by means of a dissymmetric copper chelate. *Tetrahedron Lett.* **1966**, (43), 5239-44.

6. Aratani, T., Catalytic asymmetric synthesis of cyclopropanecarboxylic acids: an application of chiral copper carbenoid reaction. *Pure Appl. Chem.* **1985,** 57, (12), 1839-44.

7. Aratani, T.; Yoneyoshi, Y.; Nagase, T., Asymmetric synthesis of chrysanthemic acid. Application of copper carbenoid reaction. *Tetrahedron Lett.* **1975**, (21), 1707-10.

8. Aratani, T.; Yoneyoshi, Y.; Nagase, T., Asymmetric synthesis of permethric acid. Stereochemistry of chiral copper carbenoid reaction. *Tetrahedron Lett.* **1982,** 23, (6), 685-8.

9. Matsui, M.; Yamamoto, I., *Naturally occuring insectisides*. Marcel Dekker: 1971.

10. Doyle, M. P.; Forbes, D. C., Recent Advances in Asymmetric Catalytic Metal Carbene Transformations. *Chem. Rev.* **1998,** 98, (2), 911-935.

11. Jacobsen, E. N.; Pfaltz, A.; Yamamoto, H., *Comprehensive Asymmetric Catalysis*. Springer: 1999.

12. Evans, D. A.; Woerpel, K. A.; Hinman, M. M.; Faul, M. M., Bis(oxazolines) as chiral ligands in metal-catalyzed asymmetric reactions. Catalytic, asymmetric cyclopropanation of olefins. *J. Am. Chem. Soc.* **1991,** 113, (2), 726-8.

13. Salomon, R. G.; Kochi, J. K., Copper(I) catalysis in cyclopropanations with diazo compounds. Role of olefin coordination. *J. Amer. Chem. Soc.* **1973,** 95, (10), 3300-10.

14. Smith, D. A.; Reynolds, D. N.; Woo, L. K., Cyclopropanation catalyzed by osmium porphyrin complexes. *J. Am. Chem. Soc.* **1993,** 115, (6), 2511-13.

15. Park, S.-B.; Sakata, N.; Nishiyama, H., Aryloxycarbonylcarbene complexes of bis(oxazolinyl)pyridineruthenium as active intermediates in asymmetric catalytic cyclopropanations. *Chem.--Eur. J.* **1996,** 2, (3), 303-6.

16. Straub, B. F.; Hofmann, P., Copper(I) carbenes: the synthesis of active intermediates in copper-catalyzed cyclopropanation. *Angew. Chem., Int. Ed.* **2001,** 40, (7), 1288-1290.

17. Fraile, J. M.; Garcia, J. I.; Martinez-Merino, V.; Mayoral, J. A.; Salvatella, L., Theoretical (DFT) insights into the mechanism of copper-catalyzed cyclopropanation reactions. Implications for enantioselective catalysis. *J Am Chem Soc* **2001,** 123, (31), 7616-25.

18. Buhl, M.; Terstegen, F.; Loffler, F.; Meynhardt, B.; Kierse, S.; Muller, M.; Nather, C.; Luning, U., On the mechanism and stereoselectivity of the copper(I)-catalyzed cyclopropanation of olefins - a combined experimental and density functional study. *Eur. J. Org. Chem.* **2001**, (11), 2151-2160.

19. Bernardi, F.; Bottoni, A.; Miscione, G. P., A DFT study of the Simmons-Smith cyclopropanation reaction. *J. Am. Chem. Soc.* **1997,** 119, (50), 12300-12305.

20. Jennings, P. W.; Johnson, L. L., Metallacyclobutane Complexes of the Group Eight Transition Metals: Synthesis, Characterizations, and Chemistry. *Chem. Rev.* **1994,** 94, (8), 2241-90.

21. Ozen, C.; Tuzun, N. S., A DFT Study on the Mechanism of Cyclopropanation via Cu(acac)2-Catalyzed Diazo Ester Decomposition. *Organometallics* **2008,** 27, (18), 4600-4610.

22. Edulji, S. K.; Nguyen, S. T., Catalytic Olefin Cyclopropanation Using micro - Oxo-bis[(salen)iron(III)] Complexes. *Organometallics* **2003,** 22, (17), 3374-3381.

23. Li, G.-Y.; Zhang, J.; Chan, P. W. H.; Xu, Z.-J.; Zhu, N.; Che, C.-M., Enantioselective Intramolecular Cyclopropanation of cis-Alkenes by Chiral Ruthenium(II) Schiff Base Catalysts and Crystal Structures of (Schiff base)ruthenium Complexes Containing Carbene, PPh3, and CO Ligands. *Organometallics* **2006,** 25, (7), 1676-1688.

24. Kanchiku, S.; Suematsu, H.; Matsumoto, K.; Uchida, T.; Katsuki, T., Construction of an aryliridium-salen complex for highly cis- and enantioselective cyclopropanations. *Angew. Chem., Int. Ed.* **2007,** 46, (21), 3889-3891.

25. Katsuki, T.; Irie, R.; Uchida, T., cis- and Enantio-selective Cyclopropanation with Chiral (ON+)Ru–Salen Complex as a Catalyst *tetrahedron* **2000,** 56, 3501-3509.

26. Maas, G., Ruthenium-catalyzed carbenoid cyclopropanation reactions with diazo compounds. *Chem. Soc. Rev.* **2004,** 33, (3), 183-190.

27. Li, Z.; Liu, G.; Zheng, Z.; Chen, H., Assymetric cyclopropanation of styrene catalyzed by Cu(chiral schiff base) complexes. *Tetrahedron* **2000,** 56.

28. Itagaki, M.; Hagiya, K.; Kamitamari, M.; Masumoto, K.; Suenobu, K.; Yamamoto, Y., Highly efficient chiral copper Schiff base catalyst for assymetric cyclopropanation of 2,5 dimethyl 2,4 hexadiene. *Tetrahedron* **2004,** 60.

29. Dyker, G.; Holzer, B.; Henkel, G., A chiral bis-N-oxide isoelectronic with Jacobsen's salen ligand. *Tetrahedron: Asymmetry* **1999,** 10, (17), 3297-3307.

30. Doyle, M. P.; Protopopova, M. N., New aspects of catalytic asymmetric cyclopropanation. *Tetrahedron* **1998,** 54, (28), 7919-7946.

31. Demonceau, A.; Saive, E.; de Froidmont, Y.; Noels, A. F.; Hubert, A. J.; Chizhevsky, I. T.; A., L. I.; Bregadze, V. I., Olefin cyclopropanation reactions catalysed by novel ruthenacarborane clusters. *Tet Lett.* **1992,** 33, 2009-2012.

32. Barroso, S.; Blay, G.; Al-Midfa, L.; Munoz, M. C.; Pedro, J. R., Copper(II)-Bis(oxazoline) Catalyzed Asymmetric Diels-Alder Reaction with alpha '-Arylsulfonyl Enones as Dienophiles. *J. Org. Chem.* **2008,** 73, (16), 6389-6392.

33. Rong, M.; Liu, C.; Han, J.; Sheng, W.; Zhang, Y.; Wang, H., Catalytic Oxidation of Alcohols by a Novel Copper Schiff Base Ligand Derived from Acetylacetonate and L-Leucine in Ionic Liquids. *Catal. Lett.* **2008,** 125, (1-2), 52-56.

34. Lam, M. S.; Lee, H. W.; Chan, A. S. C.; Kwong, F. Y., Copper(I)-picolinic acid catalyzed N-arylation of hydrazides. *Tetrahedron Lett.* **2008,** 49, (43), 6192-6194.

CHAPTER 6

Probing the role of interaction strengths in enantiomer discrimination by chiral metal complexes

6.1 Introduction

6.1.1 Cu Salen Coordination Studies

As mentioned previously, Fallis *et al.*[1, 2] have reported the use of EPR and ENDOR to determine the spatial arrangement of various adducts of vanadyl salen complexes such as [VO**L**^{3}]. The study of the coordination of small coordinating molecules, such as primary amines and terminal epoxides, is important with respect to mechanistic studies on such catalytic complexes and the development of new catalysts. Factors such as binding strength, regio- and enantio-discrimination and the stability of the catalyst resting state all can be explored to gain a better understanding of a system.[3]

Fallis *et al.*[4] have also studied the affinity of α-methylbenzyl amine (MBA) for [Cu**L**^{3}] by paramagnetic techniques such as ENDOR. It was found that the homochiral (i.e. *RR* complex + *R*-MBA) adduct is less thermodynamically favourable than the heterochiral adduct (i.e. *RR* complex + *S*-MBA). In a system containing enantiomerically pure [Cu**L**^{3}] and *rac*-MBA, the selectivity was found to be 70%. It was shown that MBA binds to Cu**L**^{3} *via* π-π interactions between the ligand and the substrate.[5] These interactions are in addition to the H-bonding also shown to exist in this system. However, these results should be treated with caution, as the measurements are taken at low temperatures (10 K), therefore different equilibrium constants are likely to exist than those occurring at room temperature.

6.1.2 Aims of this Research

Polarity is an important issue within this chapter, there are many ways of measuring the polarity of a liquid. In this chapter, relative polarity is inferred from the dielectric constants of the solvents used. This is acceptable, as the values are intended as a qualitative indication of the relative polarity of the solvents only.

The complex (*RR*)-[Zn**L**^{4}](ClO$_4$)$_2$ was prepared and titrated with (*R*) and (*S*)-methylbenzylamine (MBA). Coordination was monitored by ^{1}H NMR spectroscopy. The data was used to determine the difference in association constants of the homochiral and heterochiral adducts. This experiment was repeated for three very different solvents ($CDCl_3$, CD_3CN and CD_3OD) to investigate any possible competition effects that may be present. $CDCl_3$ was chosen as a representative non-

coordinating solvent, due to its low dielectric constant (4.8) the competition between solvent and MBA should be minimal. CD_3CN was chosen due to the relatively high dielectric constant of this solvent (37.5), but its relatively poor H-bonding properties. Conversely, CD_3OD was chosen because of the high H-bonding characteristics, with a dielectric constant of 32.6 it is not the most polar solvent, although it tends to form H-bonds readily. It was anticipated that CD_3CN would provide the highest competition with MBA for Zn binding sites due to the high polarity of the solvent arising from a dielectric constant of 37.5. However, the H-bonding characteristics should also be considered.

6.2 Experimental

^1H NMR Titration Procedure

A procedure representative of that carried out for all titrations within this chapter is shown below.

A 4.6 mM stock solution of *RR*-[Zn**L**^{4}]$(ClO_4)_2$ was prepared in $CDCl_3$ (50 ml). To this was added tetramethylsilane, TMS, (64.8 mg, 735 mM). This solution was split into 0.5 ml aliquots. To these aliquots were added varying amounts of a 5 mM solution of *S*-MBA. ^1H NMR spectra were recorded of each sample (at room temperature) and the integrals measured using the TMS resonance as an internal standard.

Preparation of (RR)-[ZnL^4](ClO$_4$)$_2$

3,5-Di-*tert*-butyl-2-hydroxybenzaldehyde (202 mg, 0.86 mmol) was added to *R, R*-1,2-diaminocyclohexane (50 mg, 0.43 mmol) in ethanol (20 ml). The mixture was stirred for 2 hours and a solution of $Zn(ClO_4)_6$ (270 mg, 0.41 mmol) in ethanol (10 ml) was added. The mixture was stirred at room temperature for a further 30 minutes. The solvent was removed under reduced pressure, and the complex purified by slow diffusion of ether into an ethanolic solution yielding 225 mg (79%) of a colourless crystalline solid. δ_H (400.1 MHz, 25 °C, $CDCl_3$): 1.34 (s, 6H, *t*-Bu), 1.53 (s, 6H, *t*-Bu), 2.02 (m, 2H, NCH*CH*$_2$), 2.54 (m, 2H, NCH*CH*$_2$), 3.92 (m, 2H, NC*H*), 7.55 (s, 2H, Ar), 7.86 (s, 2H, Ar), 8.51 (s, 2H, Ar). δ_C (100.6 MHz, 25 °C, $CDCl_3$) 15.2, 24.0, 27.6, 27.9, 30.2, 65.8, 124.2, 130.4, 133.2, 135.4, 136.6, 170.2. IR (KBr disc, cm^{-1}),

3425(s), 2987(b), 1246(s), 1121(s) and 1002(m). MS(EI), MH^+ exact mass (*calc.*) *m/z* 613.3460 *(obs.)* 613.3445.

6.3 Results and Discussion

6.3.1 Characterisation of (RR)-$[ZnL^4](ClO_4)_2$

The zinc complex, (*RR*)-$[ZnL^4](ClO_4)_2$, was characterized by a range of NMR techniques, the fully assigned ^1H NMR spectrum is shown in fig. 6.1.

In order to determine the nature of the complex in solution, variable temperature (VT) NMR spectra were taken in the solvents which were to be used for the titrations. The VT ^1H NMR spectra of (*RR*)-$[ZnL^4](ClO_4)_2$ in $CDCl_3$ are shown in fig. 6.2. The resonance shown corresponds to the two methine protons of the cyclohexane ring (fig. 6.1, H^a). The resonance clearly decoalesces upon cooling to 223 K, this suggests that the two protons are in different environments. This implies that the complex exists (in $CDCl_3$) as a five coordinate species. When cooled, the observed symmetry is broken, and the two methine protons are no longer equivalent on the NMR timescale. It is probable, in view of the low polarity of the solvent, that the fifth species is a perchlorate counterion, this would give rise to the species shown in fig. 6.3.

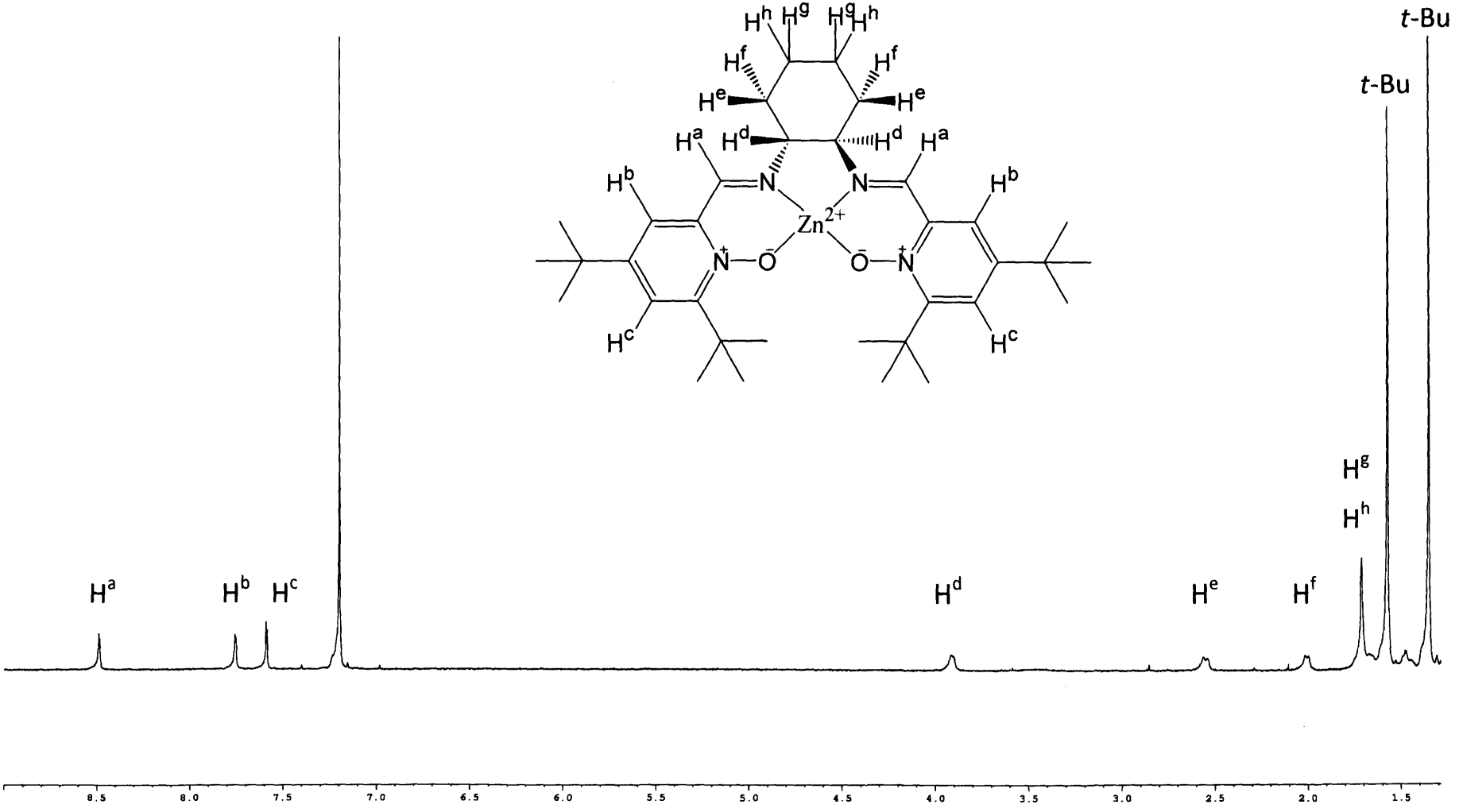

Fig. 6.1: The ^{1}H NMR of (*RR*)-[Zn**L**^{4}](ClO$_4$)$_2$ in CDCl$_3$ at 25°C.

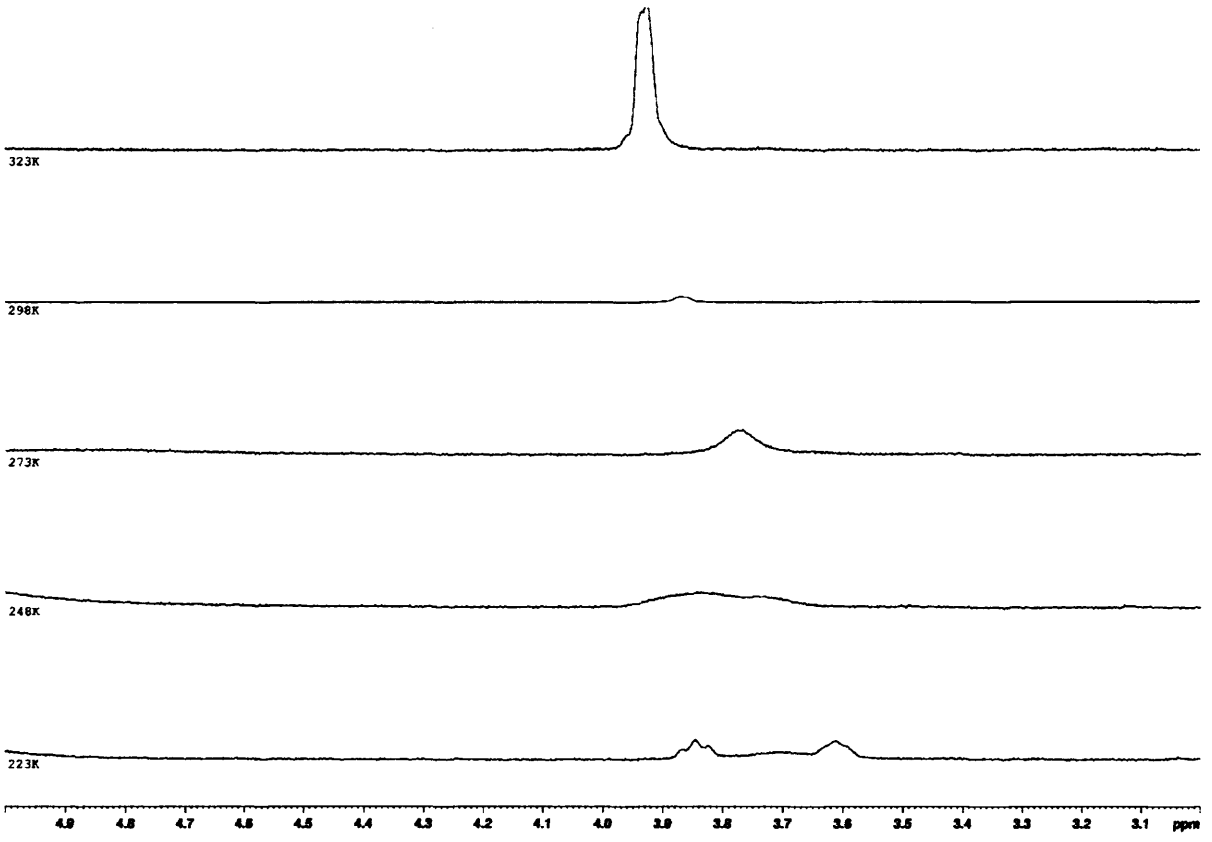

Fig. 6.2: The VT ^{1}H NMR spectra of (*RR*)-[Zn**L**^{4}](ClO$_4$)$_2$ (in CDCl$_3$), revealing a splitting of the resonance corresponding to the methine protons, thus proving that the two protons are inequivalent.

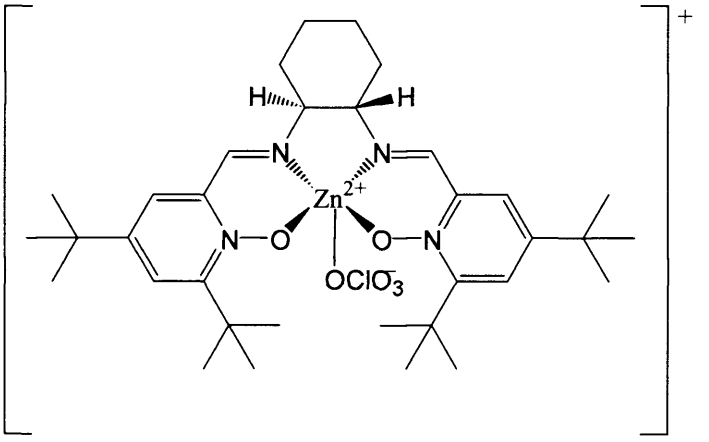

Fig. 6.3: The proposed structure of (*RR*)-[Zn**L**^{4}](ClO$_4$)$_2$ in CDCl$_3$.

The VT ^{1}H NMR study of (*RR*)-[Zn**L**^{4}](ClO$_4$)$_2$ in CD$_3$CN is shown in fig. 6.4. This clearly shows no change to the NMR spectra when cooled to 223 K. This result implies that the complex is symmetrical in a solution of acetonitrile which in turn suggests that the complex adopts either a 4 coordinate square planar conformation with no donor species on the z axis or a 6 coordinate octahedral conformation with two identical donor species on the z axis (fig. 6.5). It is most probable that the latter

is the case with the two donating species being acetonitrile molecules. Perchlorate is a weakly binding counterion while the dielectric constant of acetonitrile (37.5) is high, strongly suggesting solvent coordination. In addition, acetonitrile is a common donor solvent. One other important point to note is the fact that the perchlorate counterion is much larger than that of methanol or acetonitrile, which may also prevent two perchlorates from coordinating. Many examples are present in the literature of acetonitrile coordinating to Zn^{2+} preferentially over perchlorate counterions.[6-9]

It should also be noted that the relative concentrations of perchlorate to acetonitrile are vastly different, this is irrelevant as the relative concentrations are the same for all experiments carried out.

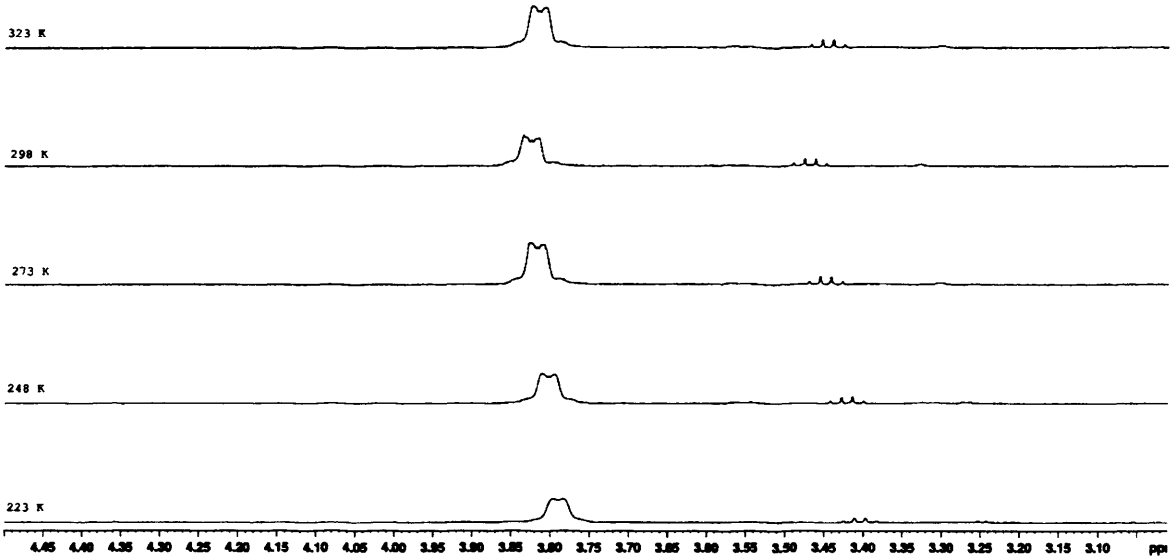

Fig. 6.4: VT ^{1}H NMR spectra of Zn(RR)-[Zn**L**^{4}](ClO4)2 in CD_3CN showing no change to the methine signals upon cooling.

The VT ^{1}H NMR experiment of (*RR*)-[Zn**L**^{4}]$(ClO_4)_2$ in CD_3OD provided similar results to that carried out in CD_3CN in that there appears to be no change upon cooling (fig. 6.6). This experiment involved cooling the sample to near the freezing point of methanol (223 K). In order to check the peak does not in fact split, a separate VT study was carried out in deuterated ethanol, which has a much lower freezing point, but is a very similar solvent to methanol in its polarity and H-bonding character. The results are shown in fig. 6.7. When ethanol is cooled to such temperatures, the viscosity of the solvent increases dramatically, hence rates of

tumbling are decreased for anything dissolved in it. Consequently peak broadening of an NMR spectrum is observed. However, it is possible from this VT experiment to confidently state that the peak at 3.78 ppm is not splitting at temperatures of 223 K. This data combined strongly suggests a 6 coordinate species exists as shown in fig. 6.5 (b).

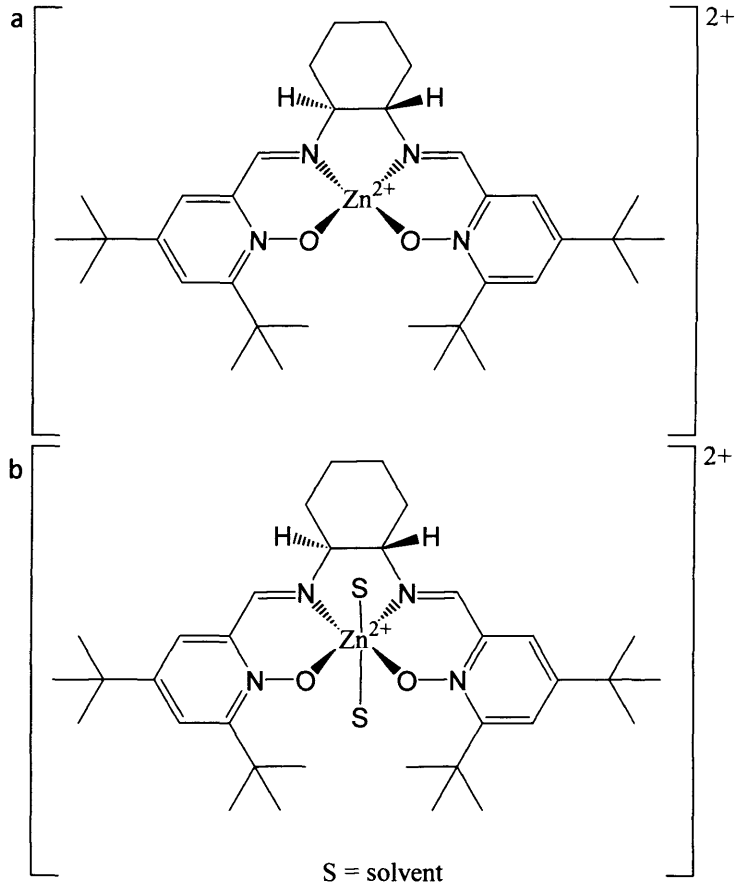

Fig. 6.5: The two possibilities implied for (*RR*)-[Zn**L**^{4}]$(ClO_4)_2$ in acetonitrile solution from the VT NMR experiments are a four coordinate square planar complex (a) and a 6 coordinate octahedral complex (b).

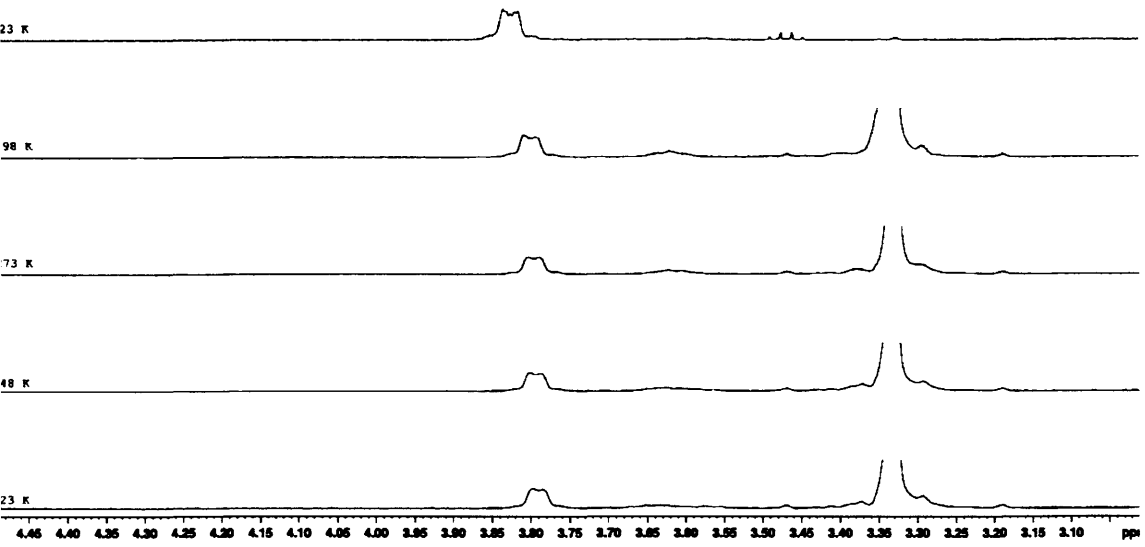

Fig. 6.6: The VT ^{1}H NMR study of (*RR*)-[ZnL^4](ClO$_4$)$_2$ in deuterated methanol implies a six coordinate zinc species similar to that of the same complex dissolved in acetonitrile.

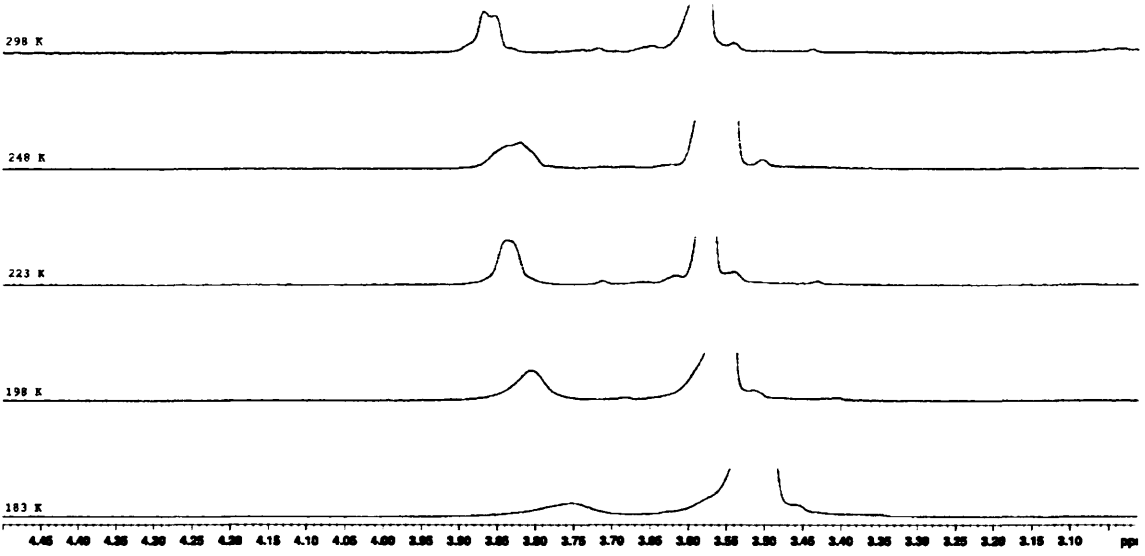

Fig. 6.7: The VT ^{1}H NMR study of (*RR*)-[ZnL^4](ClO$_4$)$_2$ in deuterated ethanol concurs previous results for methanol, implying a six coordinate zinc species.

6.3.2 Determination of binding stoichiometry of (*RR*)-[ZnL^4](ClO$_4$)$_2$ with MBA

Preliminary ^{1}H NMR experiments indicate a 2:1 binding stoichiometry of (*R, R*)-[ZnL^4](ClO$_4$)$_2$ with MBA in all three solvents tested. A representative example of an NMR spectrum of (*RR*)-[ZnL^4](ClO$_4$)$_2$ with excess MBA is shown in fig. 6.8. A relative integration of 1:1 is observed between peaks (a) and (b), this is proof of 2:1 binding. It is perhaps surprising that MBA forms a 2:1, 6 coordinate, complex in a solution of chloroform given that the dielectric constant (4.4 at 20 °C) is lower than that of chloroform (4.8 at 20 °C), which, as discussed earlier, binds in a 1:1, 5 coordinate, manner. However, MBA is a much better H-bonding species than

chloroform. This result, together with the VT studies in the three solvents, would suggest that a species will displace both perchlorate counterions and bind to the complex in a 2:1 manner if it is either a good H-bonding species (such as MBA), it has a high dielectric constant (such as acetonitrile) or both (such as methanol).

A nOe (nuclear overhauser effect) NMR experiment was carried out in order to fully characterise the 1 + 2 adduct of (*RR*)-[Zn**L**^{4}]$(ClO_4)_2$ + MBA (fig. 6.8). The signal corresponding to the imine proton of the ligand was irradiated (9.15 ppm, a), two signal amplifications were detected, one at 4.1 ppm and the other at 4.8 ppm. It is an unfortunate coincidence that the signal of uncoordinated MBA lies directly over that of the methine proton in these spectra, the amplified peak at 4.1 ppm (c) almost certainly corresponds to the signal of the methine proton of the complex. Free MBA is most probably too far away from the imine proton to have such a large effect on the nOe spectra. The amplification observed at 4.8 ppm (b) corresponds to the CH proton of the two coordinated MBA adducts.

6.3.3 ^{1}H NMR Titrations

Titrations were carried out on (*RR*)-[Zn**L**^{4}]$(ClO_4)_2$ by the addition of fixed aliquots of enantiomerically pure MBA, initially these titrations were carried out in $CDCl_3$ to investigate the differences in binding between enantiomers (see 5.2.2). A representative plot of the (*RR*)-[Zn**L**^{4}]$(ClO_4)_2$ + (*R*)-MBA titration is shown in fig. 6.10. Examination of this series of NMR spectra reveals that the zinc complex and MBA are in a slow exchange regime, this is clear by the apparent disappearance and re-emergence of certain peaks relating to the various species present.

Zinc(II) complexes that exhibit slow exchange with ligands (with respect to the NMR timescale) are rare.[6] This fast exchange arises from the filled d shell, which considerably reduces the metal's capability of π-bonding, when compared to other transition metals.[7] A notable example of a Zn(II) complex that gives rise to slow exchange was reported by Kim *et al.*[8] It was reported that the (*RR*) version of complex Zn**L**^{10} binds preferentially, but reversibly, to (*RR*)-1,2-diphenyl ethylenediamine over the (*SS*) diamine (fig. 6.9). The system was found to be in slow exchange within the NMR timescale and consequently distinct signals (rather than

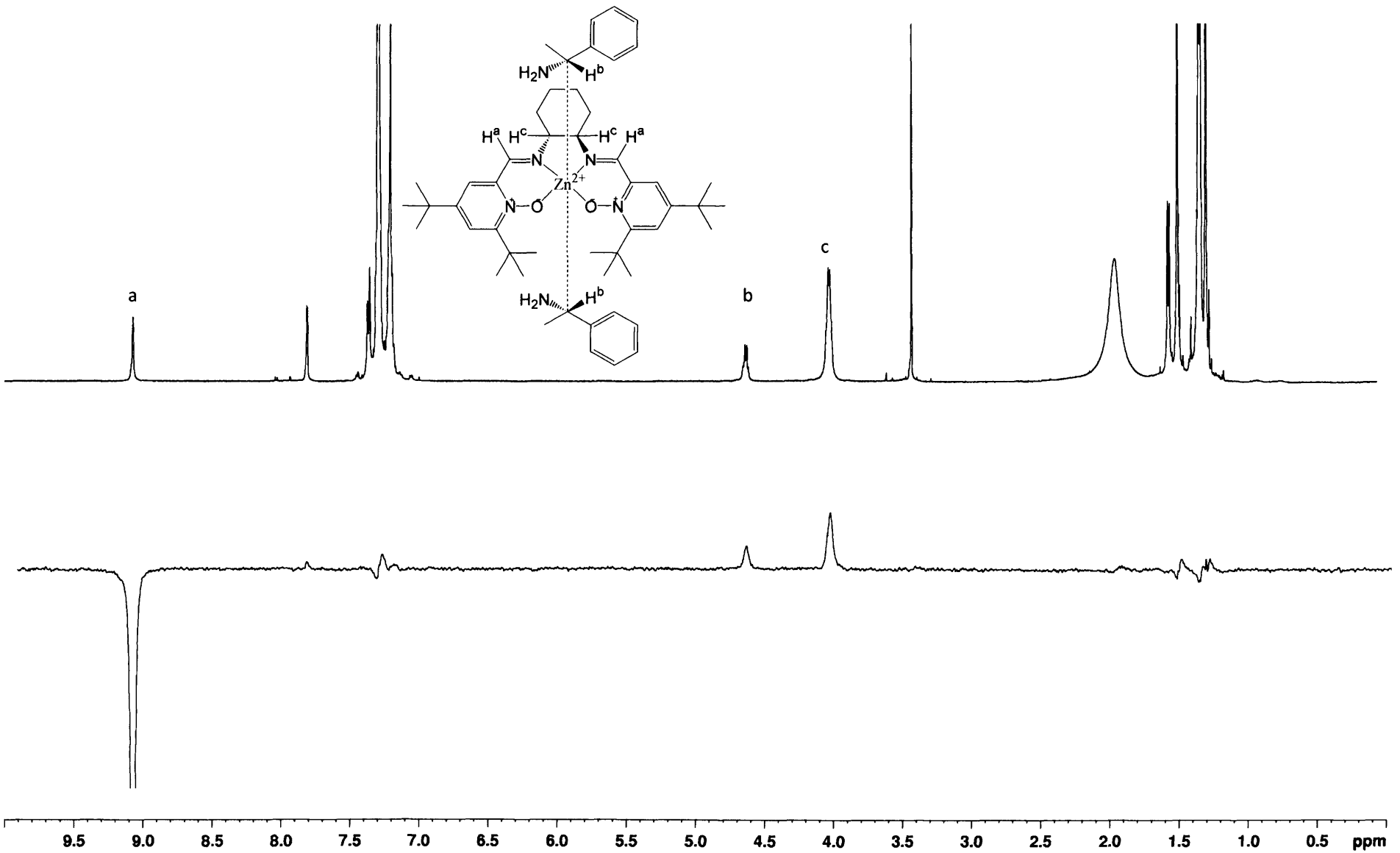

Fig. 6.8: The ^{1}H NMR of (RR)-$[Zn\mathbf{L}^4](ClO_4)_2$ in $CDCl_3$ and an excess MBA at room temperature) clearly shows a 2:1 binding stoichiometry at 25 °C and an nOe irradiated at 9.08 ppm.

averaged signals) for both diastereomers were observed. It was found that the system exists in a 5:1 ratio of homochiral adducts to heterochiral adducts.

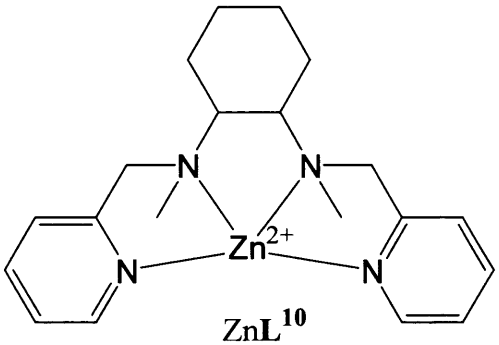

ZnL^{10}

Fig. 6.9: The Zn(II) complex reported by Kim *et al.* exhibits slow exchange with respect to ethylene diamine analogues.

As noted previously, such slow exchange systems are rare, but the presence of π-stacking between complex and substrate, together with hydrogen bonding as observed in similar cases[1, 2, 4, 5] could explain the kinetic inertness of such complexes. As discussed in Chapter four, the metal centres in these complexes have a high degree of Lewis acidity, which further decreases the rate of exchange.

It is clear though, that certain resonances do shift during the titrations, this could be due to the fact that the nature of the solvent is being altered (by the addition of MBA). A change in solvent will be associated with a change in composition of the coordination spheres and hence a varying magnetic environment is observed for the protons. This should not affect the outcome of the titrations as measurements are taken on the integrals of the resonances and not the signal positions.

The experiment was repeated for both enantiomers in three different solvents, $CDCl_3$, CD_3CN and CD_3OD, in order to observe the differences in K_{eq} with differing solvent polarity. Essentially this is a competition experiment for the two coordination sites of the zinc complex between the solvent and MBA. It is anticipated that, as the concentration of MBA within the solvent increases, the species MS (or MS_2 in the case of the more polar solvents) will be converted to ML_2 (where M = (*RR*)-$[ZnL^4](ClO_4)_2$, S = solvent and L = MBA). The non-coordinating nature of the counterion and ease of recrystallisation of the complex were two reasons for choosing the perchlorate counterion.

Speciation graphs for these titrations are shown in figs 5.11, 5.12 and 5.13. When interpreting these graphs, it is important to note that, due to the nature of the titrations, the dashed line representing [M_{tot}] is constantly decreasing. From initial inspection it is clear that titrations carried out in the relatively non-polar solvent, $CDCl_3$, reached an end-point (complete conversion to ML_2) much earlier than those carried out in the relatively polar solvent CD_3OD. The titrations carried out in CD_3CN are qualitatively similar to the CD_3OD experiments but appear to require less MBA to be added to reach an end-point. This is a curious observation as CD_3CN possesses a higher dielectric constant than CD_3OD, this could be attributed to the ability of methanol to coordinate strongly via a hydrogen bond to M, thus increasing the favourability of solvent molecules to bind to the complex over MBA.

From the speciation graphs, a difference between homochiral and heterochiral adducts is observed. When closely examined, the three sets of experiments reach an end point earlier when heterochiral mixtures are used (i.e. *RR*-complex + *S*-MBA) than the homochiral titrations. This indicates a greater affinity for the heterochiral complex, corroborating unpublished results by Fallis *et al.* on the electronically similar complex Cu**L**^{3} with MBA as studied by EPR and ENDOR.[4]

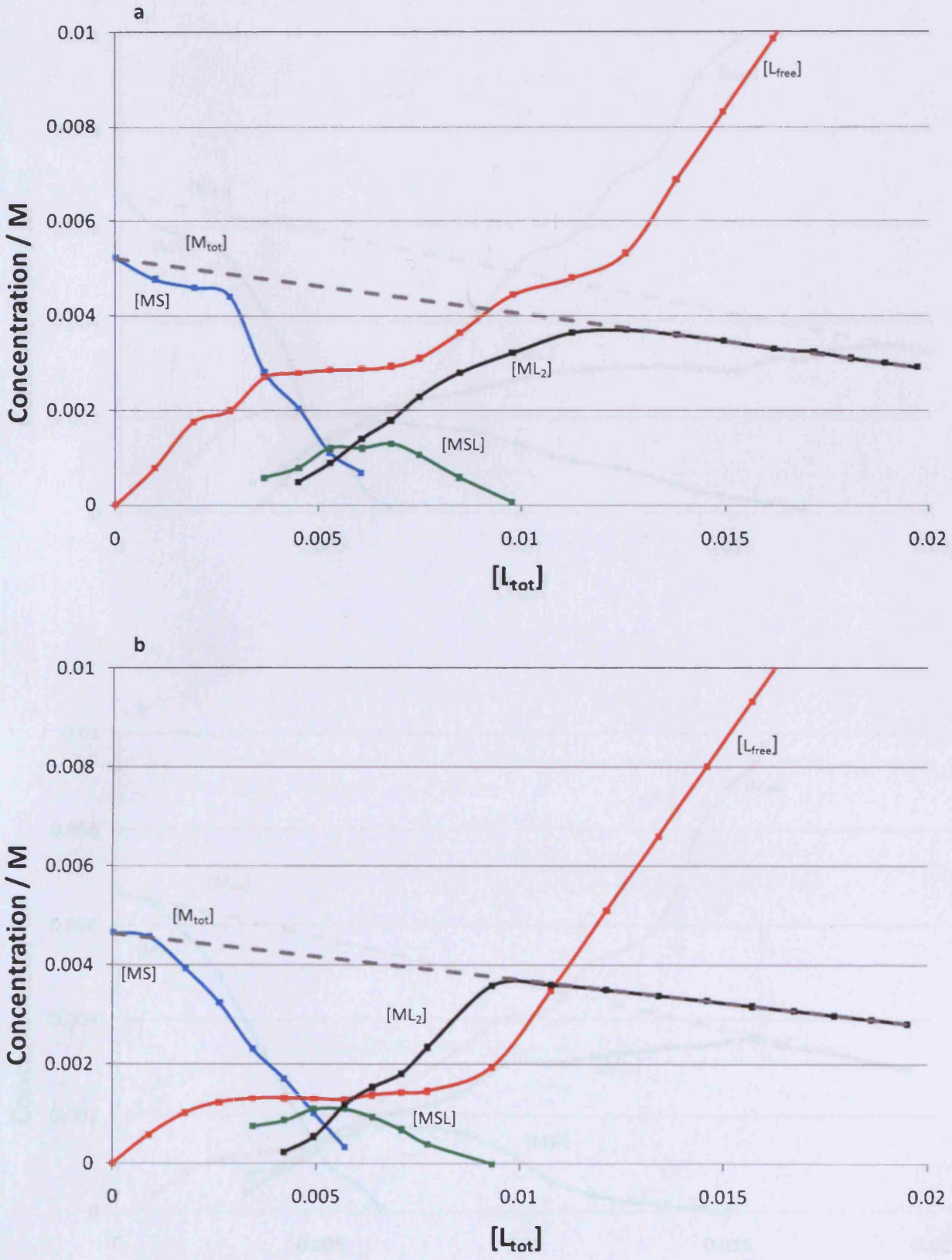

Fig. 6.11: Speciation curves for titrations of (a) (*RR*)-[Zn**L**^{4}]$(ClO_4)_2$ + (*R*)-MBA and (b) (*RR*)-[Zn**L**^{4}]$(ClO_4)_2$ + (*S*)-MBA in $CDCl_3$ at 298K.

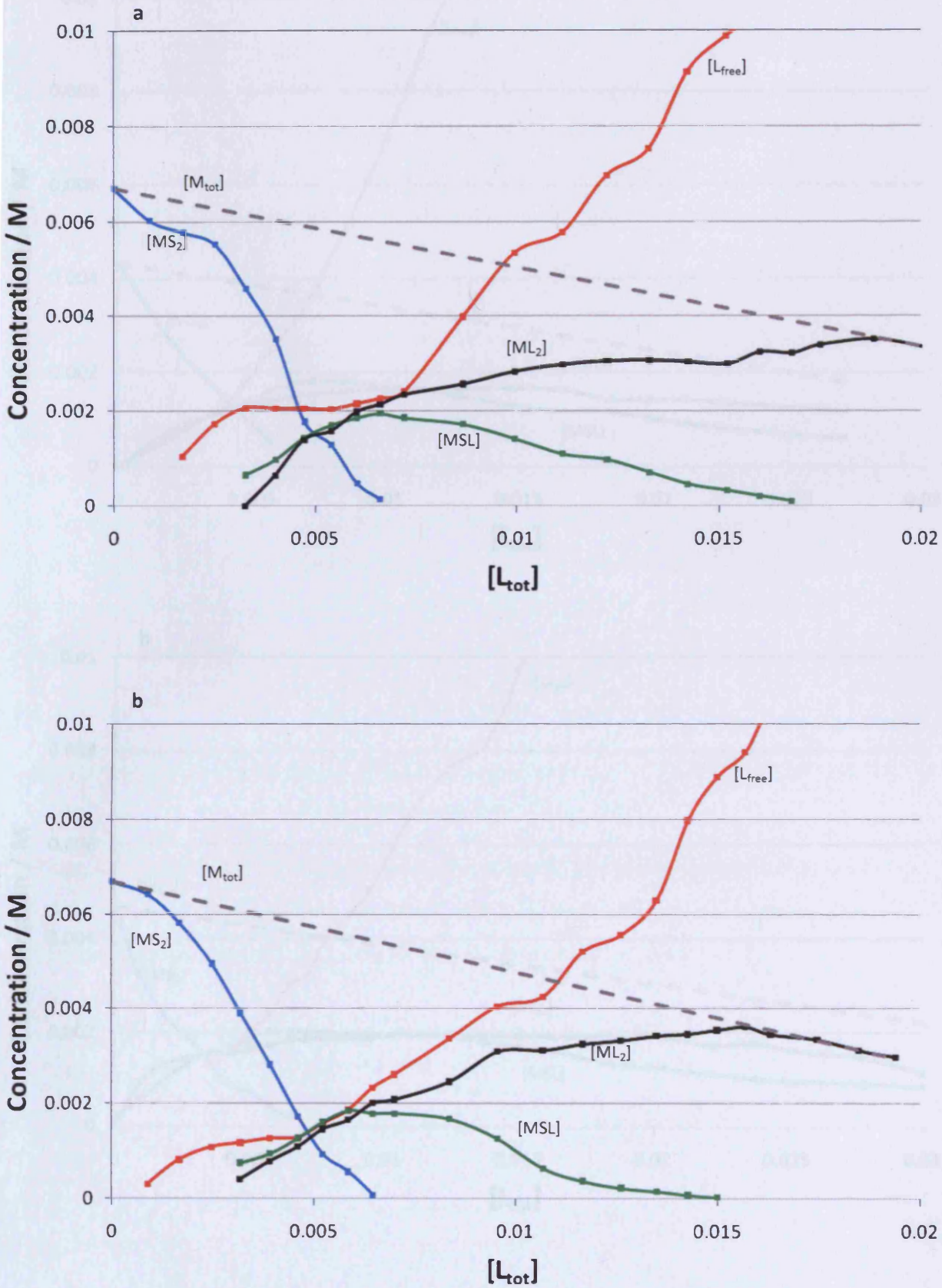

Fig. 6.12: Speciation curves for titrations of (a) (*RR*)-[Zn**L**^{4}]$(ClO_4)_2$ + (*R*)-MBA and (b) (*RR*)-[Zn**L**^{4}]$(ClO_4)_2$ + (*S*)-MBA in CD_3CN at 298K.

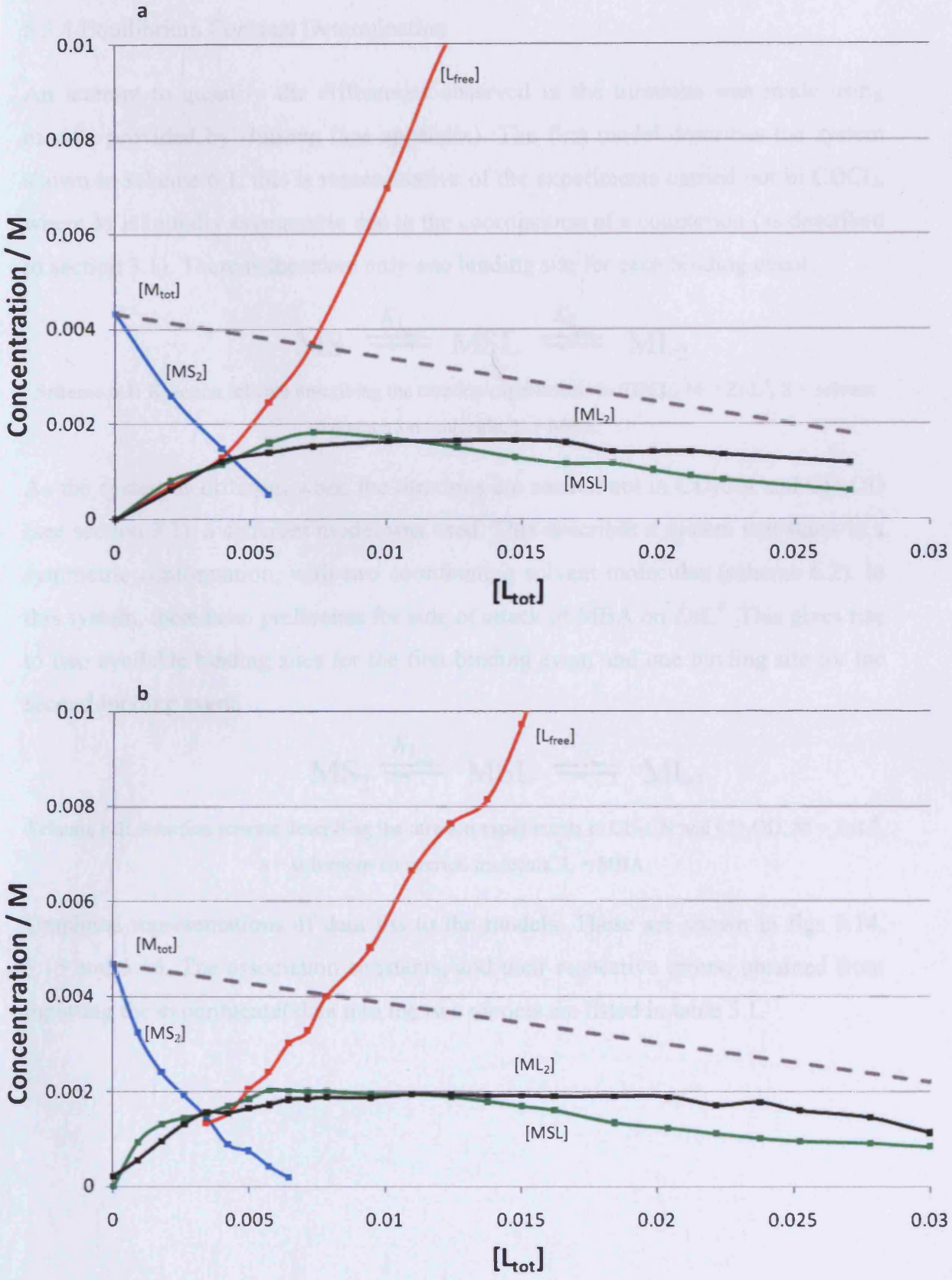

Fig. 6.13: Speciation curves for titrations of (a) (*RR*)-[Zn**L**^{4}](ClO$_4$)$_2$ + (*R*)-MBA and (b) (*RR*)-[Zn**L**^{4}](ClO$_4$)$_2$ + (*S*)-MBA in CD_3OD at 298K.

5.3.4 Equilibrium Constant Determination

An attempt to quantify the differences observed in the titrations was made using models provided by Buurma (see appendix). The first model describes the system shown in scheme 6.1, this is representative of the experiments carried out in $CDCl_3$, where M is initially asymmetric due to the coordination of a counterion (as described in section 3.1). There is therefore only one binding site for each binding event.

$$MS \overset{K_1}{\rightleftharpoons} MSL \overset{K_2}{\rightleftharpoons} ML_2$$

Scheme 6.1: Reaction scheme describing the titration experiments in $CDCl_3$, M = Zn**L**^{4}, S = solvent or counterion molecule, L = MBA.

As the system is different when the titrations are carried out in CD_3CN and CD_3OD (see section 3.1), a different model was used. This describes a system that starts in a symmetric conformation, with two coordinating solvent molecules (scheme 6.2). In this system, there is no preference for side of attack of MBA on Zn**L**^{4}. This gives rise to two available binding sites for the first binding event and one binding site for the second binding event.

$$MS_2 \overset{K_1}{\rightleftharpoons} MSL \overset{K_2}{\rightleftharpoons} ML_2$$

Scheme 6.2: Reaction scheme describing the titration experiments in CD_3CN and CD_3OD, M = Zn**L**^{4}, S = solvent or counterion molecule, L = MBA.

Graphical representations of data fits to the models. These are shown in figs 5.14, 5.15 and 5.16. The association constants, and their respective errors, obtained from inputting the experimental data into the two models are listed in table 5.1.

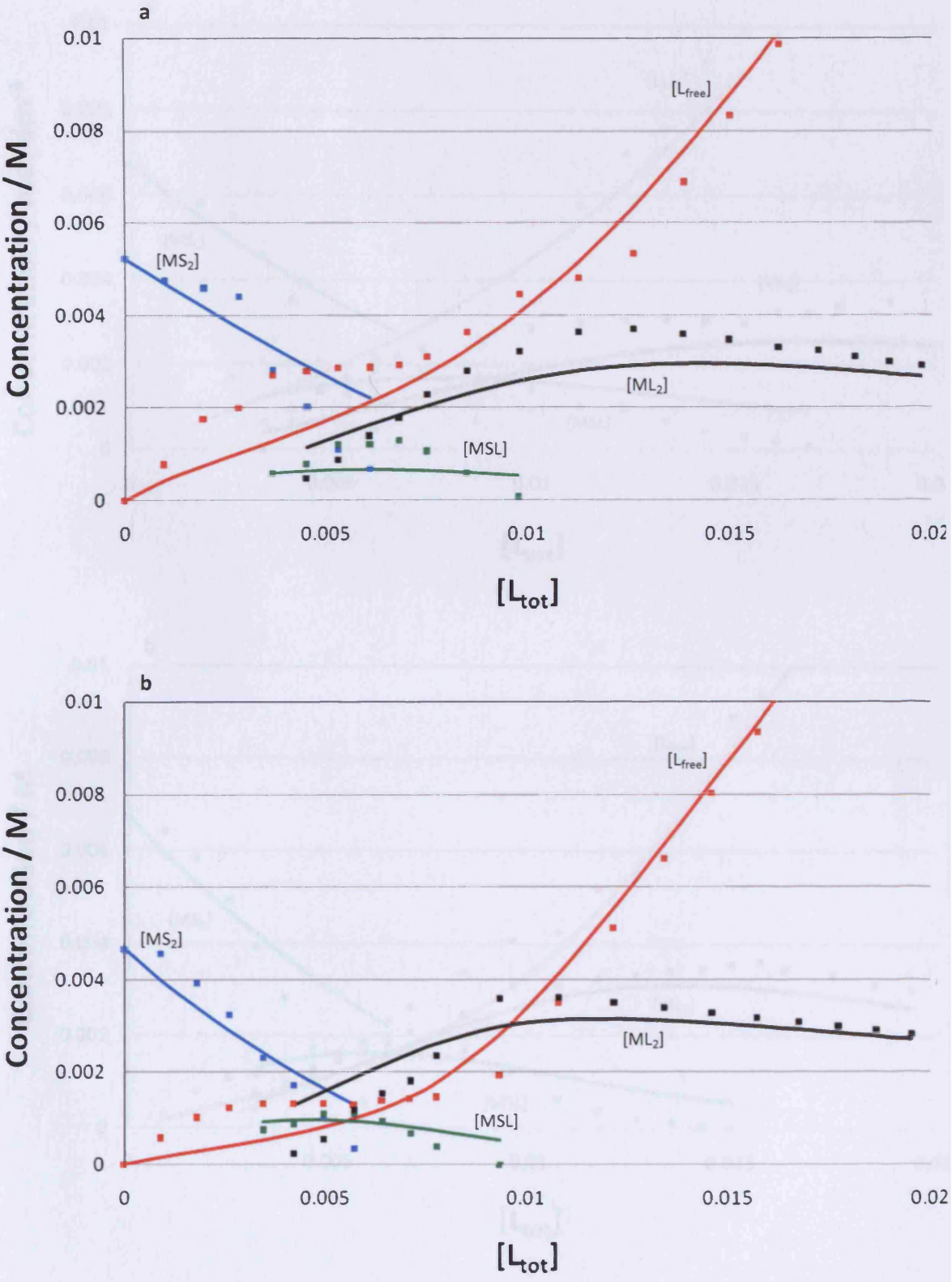

Fig. 6.14: Experimental (dotted lines) and calculated (solid lines) data for titrations of (a) (*RR*)-[Zn**L**^{4}]$(ClO_4)_2$ + (*R*)-MBA and (b) (*RR*)-[Zn**L**^{4}]$(ClO_4)_2$ + (*S*)-MBA in $CDCl_3$.

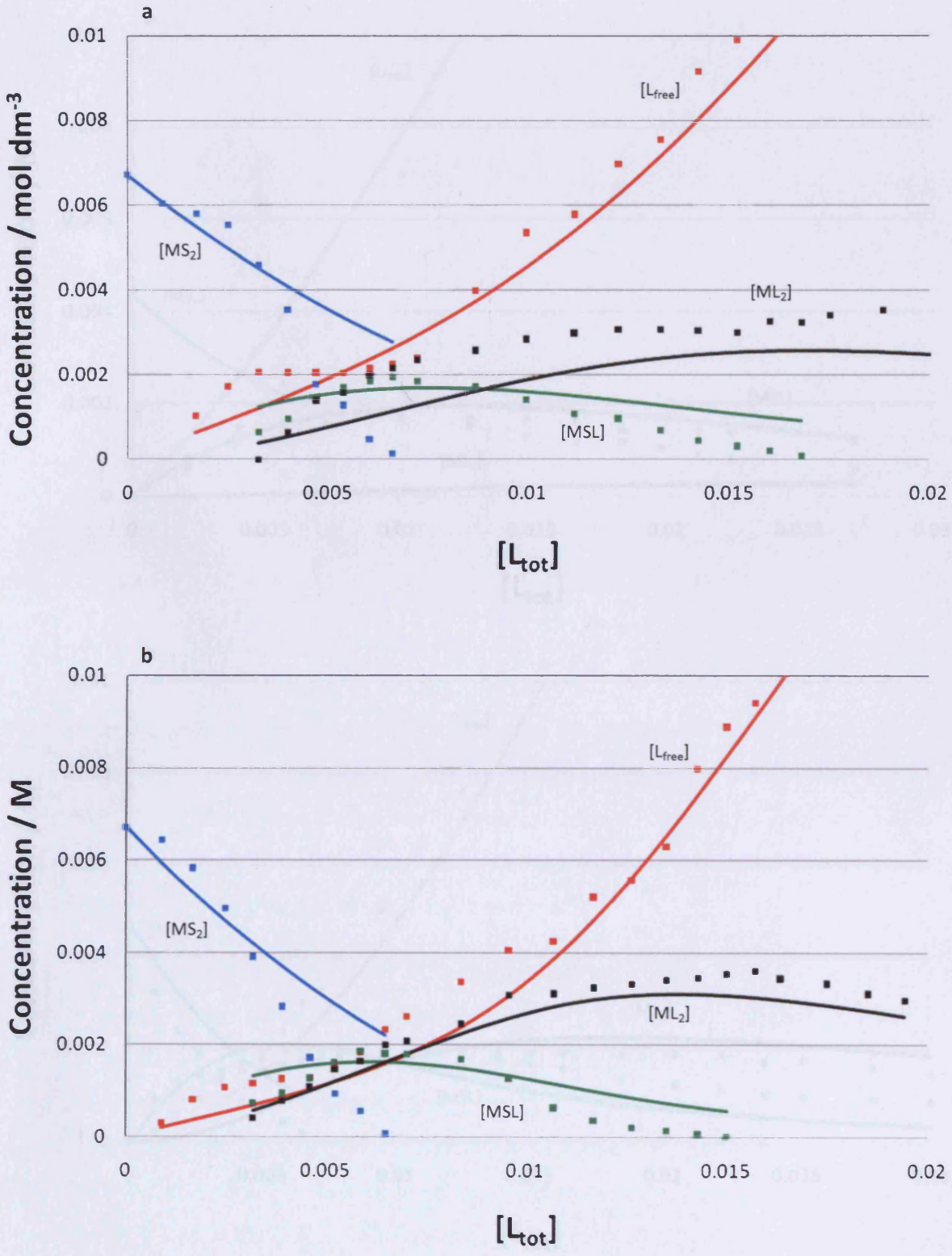

Fig. 6.15: Experimental (dotted lines) and calculated (solid lines) data for titrations of (a) (*RR*)-[Zn**L**^{4}]$(ClO_4)_2$ + (*R*)-MBA and (b) (*RR*)-[Zn**L**^{4}]$(ClO_4)_2$ + (*S*)-MBA in CD_3CN.

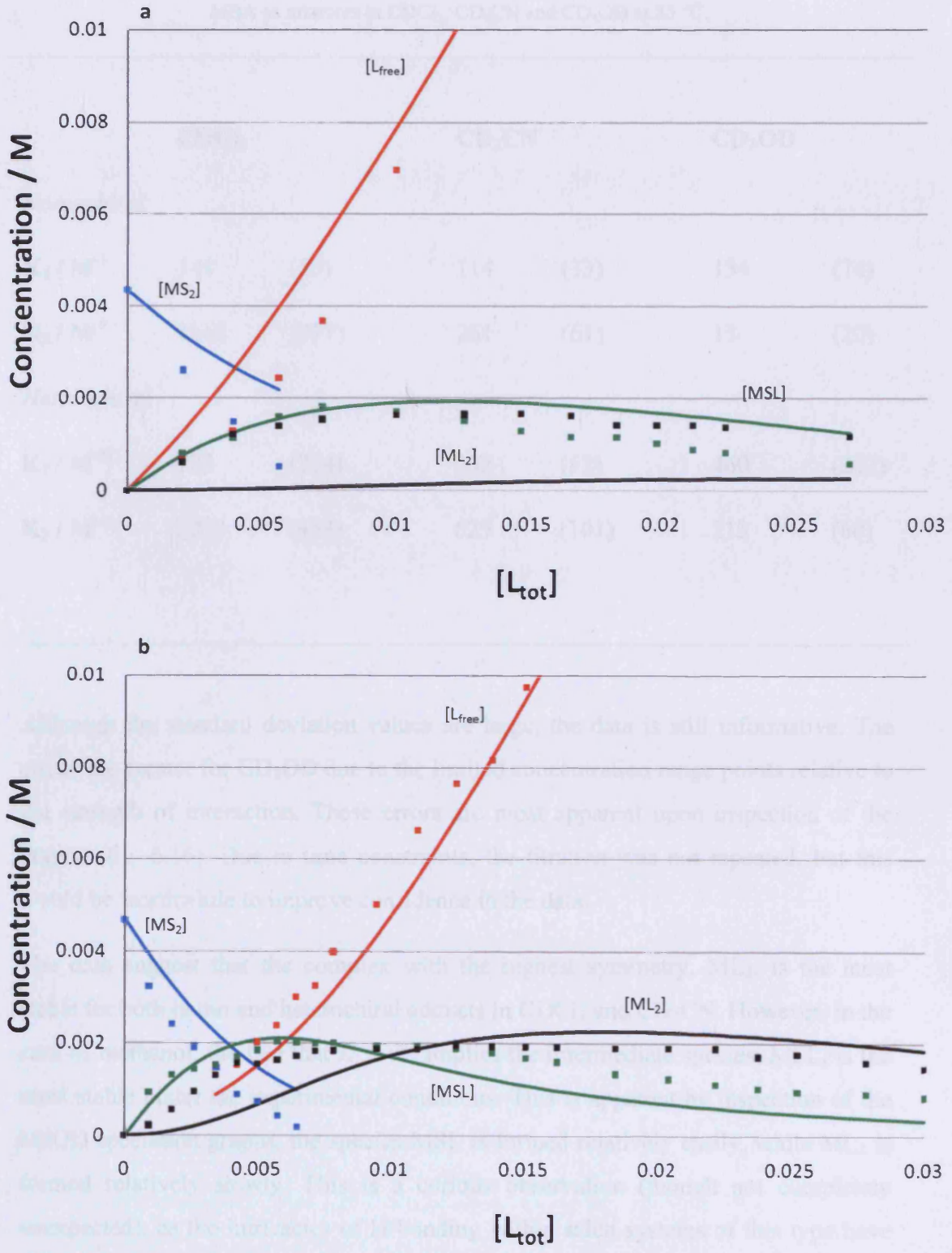

Fig. 6.16: Experimental (dotted lines) and calculated (solid lines) data for titrations of (a) (*RR*)-[Zn**L**^{4}](ClO$_4$)$_2$ + (*R*)-MBA and (b) (*RR*)-[Zn**L**^{4}](ClO$_4$)$_2$ + (*S*)-MBA in CD_3OD.

Table 5.1: Association constants (and errors) for homochiral and heterochiral adducts of ZnL^4 + MBA as mixtures in $CDCl_3$, CD_3CN and CD_3OD at 25 °C.

	$CDCl_3$		CD_3CN		CD_3OD	
Homochiral						
K_1 / M^{-1}	141	(53)	114	(33)	134	(74)
K_2 / M^{-1}	1168	(377)	261	(61)	13	(20)
Heterochiral						
K_1 / M^{-1}	725	(224)	232	(52)	460	(222)
K_2 / M^{-1}	2028	(453)	629	(101)	213	(60)

Although the standard deviation values are large, the data is still informative. The errors are greater for CD_3OD due to the limited concentration range points relative to the strength of interaction. These errors are most apparent upon inspection of the graphs (fig. 6.16). Due to time constraints, the titration was not repeated, but this would be worthwhile to improve confidence in the data.

The data suggest that the complex with the highest symmetry, ML_2, is the most stable for both homo and heterochiral adducts in $CDCl_3$ and CD_3CN. However, in the case of methanol, the fact that $K_1 > K_2$ implies the intermediate species, MSL, is the most stable under the experimental conditions. This is apparent by inspection of the MeOD speciation graphs, the species MSL is formed relatively easily, while ML_2 is formed relatively slowly. This is a curious observation (though not completely unexpected), as the intricacies of H-bonding within salen systems of this type have already been reported by Fallis *et al.*[5] Further investigation into this particular system is required in order for a satisfactory explanation to be achieved. Speculation on the relevance of solvent in this system could lead one to state that dielectric constant (of

the solvent) alone is not the only factor to be considered when comparing potential donors to Zn(salen) systems of this type. The hydrogen bonding capability of both solvent and substrate are also to be considered.

It is clear from the data, that the difference between K_1 and K_2 is much larger for the non-polar $CDCl_3$ than for the polar CD_3CN. This is partly due to the strength of the M-S interactions, which are stronger for the higher polarity solvents than for $CDCl_3$.

The $CDCl_3$ data set displays the greatest selectivity in terms of chirality. Values of K_1 and K_2 are vastly greater in the heterochiral adducts than the homochiral adducts. This implies a strong preference for *RR*-Zn**L**^{4} to bind with *S*-MBA. This is strong evidence that salen complexes have enantioselectivity towards small chiral donors, such as MBA or small epoxides, a detail confirmed by Fallis *et al.*[1, 2] Although, this was not considered in Jacobsen's mechanistic study (see Chapter four).[9]

This chiral selectivity is mirrored in the experiment in CD_3CN, although the differences are much smaller, owing to the much greater affinity of the solvent for the zinc complex. This has the effect of increasing competition for coordination sites, therefore decreasing the association constant of ML_2. Chiral selectivity is also implied for the MeOD data set, again, the heterochiral adducts seemingly possessing the greatest association constants. The errors are large enough that this cannot be stated with a large degree of certainty, this experiment would have to be repeated with a greater number of data points giving rise to a larger concentration range.

6.4 Conclusions and Suggestions for Further Research

It has been shown in this chapter that a simple N-oxide zinc salen complex can chirally discriminate between different enantiomers of simple amine, MBA. The role of the solvent has also been investigated and found to be extremely influential in the coordination to a vacant coordination site.

The results obtained from this study lead to some obvious questions; how comparable are the observations to copper salen systems? Does the symmetry of the ligand have an effect on the coordination of a chiral substrate? How does the choice of solvent affect binding of chiral substrates other than MBA?

The scope for further research into the mechanisms of chiral discrimination is considerable, NMR has proven to be an extremely powerful tool when examining this system. A more detailed study would encompass zinc complexes of the ligands synthesised in Chapter four. This data could then be directly compared to the catalysis data in Chapter five which may reveal more information about the action of coordination during catalytic processes.

6.5 Bibliography

1. Fallis, I. A.; Murphy, D. M.; Willock, D. J.; Tucker, R. J.; Farley, R. D.; Jenkins, R.; Strevens, R. R., Direct Observation of Enantiomer Discrimination of Epoxides by Chiral Salen Complexes Using ENDOR. *J. Am. Chem. Soc.* **2004,** 126, (48), 15660-15661.

2. Murphy Damien, M.; Fallis Ian, A.; Willock David, J.; Landon, J.; Carter, E.; Vinck, E., Discrimination of geometrical epoxide isomers by ENDOR spectroscopy and DFT calculations: the role of hydrogen bonds. *Angew Chem Int Ed Engl* **2008,** 47, (8), 1414-6.

3. Hattori, H.; Otsuka, K., *Science and Technology in Catalysis*. Elsevier: 1998.

4. Fallis Ian, A.; Murphy Damien, M.; Carter, E.; Farley Robert, D.; Caretti, I.; Van Doorslaer, S.; Goebel, M.; Willock, D. J.; Landon, J., *In press*.

5. Van Doorslaer, S.; Murphy, D. M.; Fallis, I. A., Evaluating pi-pi stacking effects in macrocyclic transition metal complexes using EPR techniques. *Res. Chem. Intermed.* **2007,** 33, (8-9), 807-823.

6. Lincoln, S. F.; Hounslow, A. M.; Coates, J. M., Slow Solvent Exchange on Five Coordinate (N,N-Dimethylformamide)2,2',2"-tri(N,N-dimethylamino)-triethylaminozinc(II). *Inorg Chimica Acta* **1983,** 77, 7-9.

7. Cotton, F. A.; Wilkinson, G., *Advanced Inorganic Chemistry, Fifth Ed.* Wiley: 1988.

8. Kim, W.; So, S. M.; Chagal, L.; Lough, A. J.; Kim, B. M.; Chin, J., Stereoselective Recognition of Vicinal Diamines With a Zn(II) Complex. *J. Org. Chem.* **2006,** 71, 8966-8968.

9. Nielsen, L. P. C.; Stevenson, C. P.; Blackmond, D. G.; Jacobsen, E. N., Mechanistic Investigation Leads to a Synthetic Improvement in the Hydrolytic Kinetic Resolution of Terminal Epoxides. *J. Am. Chem. Soc.* **2004,** 126, (5), 1360-1362.

CHAPTER 7

Final Conclusions

7.1 Summary

Although many problems were encountered while conducting the research in chapter two, many new compounds were isolated. Much progress was made in the synthesis of hard ligands capable of coordinating with many transition metals. This work has relevance to other areas of biological chemistry, such as ferredoxins, important in electron transfer. Attempts could be made in the future to rectify the problems encountered with respect to reduction and deprotection of the compounds. Any future work should consider the use of alternative reducing agents. The use of different protecting groups should also be examined.

An interesting result was obtained in chapter three with regards to the partially deprotonated transition metal complexes of $\mathbf{L^1}.H_3$. This could be studied further to give an indication of the relative lability of the coordinating alcohol groups.

The novel salen complexes synthesised in chapters four and five have proved extremely interesting. The differences in electron density of the metal centre between salens and these novel N-oxide salens could be probed to a greater extent. A study of this nature could shed further light on mechanisms of the diverse range of reactions privileged chiral catalysts catalyse. It is entirely possible that one of the complexes synthesised herein is catalytically active in its own right. They should be tested for reactivity in a range of reactions, such as those discussed in chapter four.

The data presented in chapter six provides a considerable insight to the behaviour of transition metal salen complexes with the immediate environment of the metal. A method of studying the interaction of solvents and small chiral amines with Zn^{II} salens has been devised. This work should be continued and repeated for other Zn^{II} complexes and other amines. Again, this may provide insight into the mechanism of attack of small π-donors to Lewis acids.

Appendix A

Unsuccessful reactions

The following reactions were carried out unsuccessfully within the course of this work, the experimental procedures have been included for information to future students.

Reduction of amides 3, 3', 4, 4', 6, 6', 8, 8' and 11

Below are general procedures that were attempted on the above compounds.

Hexa-amide 4,4',4''-(2,2',2''-(1,4,7-triazonane-1,4,7-triyl)tris(2-oxoethane-2,1-diyl))tris(1,4,7-triazonane-1-carbaldehyde) (**11**) (340 mg) was taken up in a suspension of THF in a nitrogen atmosphere. To this was added a solution of BH_3 in THF (9.4 ml, 2 M). The resulting solution was heated under reflux for 3 days. Water (10 ml) was added, the cloudy solution went clear, to this was added hydrochloric acid (10 ml), the solution effervesced. The THF was removed *in vacuo* and the solution taken to Ph 11 with sodium hydroxide solution. The solution was washed with DCM (3 x 20 ml) and the combined organic layers were dried ($MgSO_4$) and filtered. The solvent was removed to leave a brown oil. The ^1H NMR spectrum of the product was uninformative and all attempts at separating *via* chromatographic (HPLC, GC) means were unsuccessful.

N,N',N'',N'''-(1,4,7,10-tetraazacyclododecane-1,4,7,10-tetrayl) tetrakis(2-(4,7-ditoluenesulfonyl-1,4,7-triazonan-1-yl)ethanone) (**8**) (500 mg) was dissolved in THF (15 ml) under an inert atmosphere and cooled in an ice bath. Lithium aluminium hydride (1000 mg) was added in 1 portion and the resulting solution was stirred for 30 minutes at 0°C. The solution was then stirred for a further 16 hours at room temperature. Water (5 ml) was added and the solution effervesced vigorously, sodium hydroxide (200 mg) was added and the solution stirred for 30 minutes. The solution was filtered and the THF removed *in vacuo*. The solution was washed with chloroform (3 x 20 ml) and the combined organic layers were dried ($MgSO_4$) and

filtered. The solvent was removed to leave an off white solid. The ^{1}H NMR spectrum of the product was uninformative and all attempts at separating *via* chromatographic (HPLC, GC) means were unsuccessful.

Addition of a secondary amine to L^1

Below is the experimental procedure for the addition of 1-Methyl homo piperazine to L^1, this procedure was attempted with many other secondary amines.

L^1 (129 mg, 1 mmol) was dissolved in dry ethanol (20 ml), added to this solution was potassium carbonate (2.76g, 20 mmol), the resulting mixture was stirred under an inert atmosphere (N_2) for 3 hours. To this mixture was added a solution of 1-methyl homo piperazine (304 mg, 3 mmol) in ethanol (15 ml). This solution was stirred at room temperature for 72 hours. The solvent was removed *in vacuo* to leave a dark yellow oil. Analysis (by ^{1}H NMR, GC and HPLC) revealed an intractable mixture of compounds that could not be separated.

Deprotection of 6,6',6''-(1,4,7-triazonane-1,4,7-triyl)tris(methylene)tris(1,4-bis(2-nitrophenylsulfonyl)-1,4-diazepan-6-ol). (21')

6,6',6''-(1,4,7-triazonane-1,4,7-triyl)tris(methylene)tris(1,4-bis(2-nitrophenylsulfonyl)-1,4-diazepan-6-ol). (**21'**) (4 g, 2.54 mmol), caesium carbonate (6.64 g, 20.37 mmol) and 4-chlorohiophenol (2.94 g, 20.37 mmol) were dissolved in DMF (20 ml). The mixture was stirred at 80°C for 6 hours. The solution was allowed to cool to room temperature. A high resolution mass spectrum revealed the presence of the fully deprotected compound (513.4115) plus a mixture of partially deprotected relations. Attempts to extract the product were unsuccessful, as were attempts to separate chromatographically.

Appendix B

^{1}H NMR titration data

On the following pages is the raw data used to create the models discussed in Chapter 5. Additional data can be found on the CD supplied.

(RR)-[Zn**L**^{4}](ClO$_4$)$_2$ + *(R)*-MBA in CDCl$_3$

eq [S]	[tBDMS]	Vol/ml	[L]$_{initial}$	[S]$_{initial}$	I$_{[L]}$	[L]$_{obs}$	I$_{[LS2]}$	[LS2]$_{obs}$	[S]$_{calc}$	I$_{[LS]}$	[LS]
0	0.0116	1	0.0052153	0	0.15	0.00522			4.736E-06		
0.2	0.0113503	1.022	0.0052153	0.0009803	0.14	0.0047671			0.0005322		
0.4	0.0111005	1.045	0.0051005	0.0019611	0.146	0.004862			0.0017226		
0.6	0.0108716	1.067	0.0049953	0.0028596	0.135	0.004403			0.0022673		
0.8	0.010652	1.089	0.0048944	0.0037218	0.088	0.0028121			0.0016395	0.017	0.0005433
1	0.0104317	1.112	0.0047932	0.0045868	0.065	0.0020342	0.0158	0.0004945	0.0013333	0.024	0.0007511
1.2	0.0102293	1.134	0.0047002	0.0053813	0.036	0.0011048	0.029	0.0008899	0.0008959	0.03	0.0009206
1.4	0.0100259	1.157	0.0046067	0.0061796	0.023	0.0006918	0.04	0.0012031	0.0010615	0.03	0.0009023
1.6	0.0098388	1.179	0.0045208	0.006914			0.054	0.0015939	0.0007994	0.027	0.0007969
1.8	0.0096586	1.201	0.004438	0.0076216			0.0723	0.002095	0.0010887	0.023	0.0006664
2	0.0094003	1.234	0.0043193	0.0086356			0.0781	0.0022025	0.0021138	0.021	0.0005922
2.5	0.0090625	1.28	0.0041641	0.0099619			0.1	0.0027188	0.0030791	0.003	8.156E-05
3	0.0086826	1.336	0.0039895	0.0114532			0.14	0.0036467	0.0038169		
3.5	0.0083333	1.392	0.003829	0.0128245			0.15	0.00375	0.0052455		
4	0.008011	1.448	0.0036809	0.0140897			0.15	0.003605	0.0068038		
4.5	0.0077128	1.504	0.0035439	0.0152607			0.15	0.0034707	0.0082461		
5	0.0073932	1.569	0.0033971	0.0165151			0.15	0.003327	0.0097911		
5.5	0.0071385	1.625	0.00328	0.0175154			0.15	0.0032123	0.0110231		
6	0.0069007	1.681	0.0031707	0.018449			0.15	0.0031053	0.012173		
6.5	0.0066782	1.737	0.0030685	0.0193224			0.15	0.0030052	0.0132487		
7	0.0064696	1.793	0.0029727	0.0201412			0.15	0.0029113	0.0142572		

(RR)-[Zn**L**^{4}]$(ClO_4)_2$ + *(S)*-MBA in $CDCl_3$

eq [S]	[tBDMS]	Vol/ml	$[L]_{initial}$	$[S]_{initial}$	$I_{[L]}$	$[L]_{obs}$	$I_{[LS2]}$	$[LS2]_{obs}$	$[S]_{calc}$	$I_{[LS]}$	[LS]
0	0.00738	1	0.00465	0	0.21	0.0046494			-6E-07		
0.2	0.0072495	1.018	0.0045678	0.0008813	0.21	0.0045672			0.0008807	0.0093	
0.4	0.0071167	1.037	0.0044841	0.0017783	0.184	0.0039284			0.0012226	0.0145	
0.6	0.0069953	1.055	0.0044076	0.0025983	0.1545	0.0032423			0.001433	0.02496	
0.8	0.0068715	1.074	0.0043296	0.003434	0.112	0.0023088	0.00392		0.0014133	0.0319	0.0006576
1	0.0067582	1.092	0.0042582	0.004199	0.08425	0.0017081	0.01231	0.0002496	0.0013993	0.03802	0.0007708
1.2	0.0066486	1.11	0.0041892	0.0049391	0.05116	0.0010204	0.028	0.0005585	0.0012119	0.04483	0.0008942
1.4	0.0065368	1.129	0.0041187	0.0056947	0.01751	0.0003434	0.0505	0.0009903	0.0009291	0.04729	0.0009274
1.6	0.0064342	1.147	0.0040541	0.0063875			0.0803	0.00155	0.0007835	0.0383	0.0007393
1.8	0.0063293	1.166	0.003988	0.0070956			0.0961	0.0018247	0.0012828	0.0361	0.0006855
2	0.0062331	1.184	0.0039274	0.0077454			0.126	0.0023561	0.0014619	0.0214	0.0004002
2.5	0.006	1.23	0.0037805	0.0093197			0.2	0.0036	0.0019392		0
3	0.0057837	1.276	0.0036442	0.0107804			0.21	0.0036437	0.0034925		
3.5	0.0055825	1.322	0.0035174	0.0121395			0.21	0.0035169	0.0051052		
4	0.0053947	1.368	0.0033991	0.0134073			0.21	0.0033987	0.0066094		
4.5	0.0052192	1.414	0.0032885	0.0145925			0.21	0.0032881	0.0080158		
5	0.0050548	1.46	0.0031849	0.015703			0.21	0.0031845	0.0093336		
5.5	0.0049004	1.506	0.0030876	0.0167457			0.21	0.0030873	0.0105708		
6	0.0047552	1.552	0.0029961	0.0177266			0.21	0.0029957	0.0117347		
6.5	0.0046183	1.598	0.0029099	0.018651			0.21	0.0029095	0.0128316		
7	0.0044891	1.644	0.0028285	0.0195237			0.21	0.0028281	0.0138671		

(RR)-[Zn**L**^{4}]$(ClO_4)_2$ + *(R)*-MBA in CD_3CN

eq [S]	[TMS]	Vol/ml	$[L]_{initial}$	$[S]_{initial}$	$I_{[L]}$	$[L]_{obs}$	$I_{[LS2]}$	$[LS2]_{obs}$	$[S]_{calc}$	$I_{[LS]}$	[LS]
0	0.02938	0.5	0.0067	0	0.038	0.0066986			-1.36E-06	0	
0.2	0.0287476	0.511	0.0065558	0.0008667	0.03498	0.0060335			0.0003444		
0.4	0.0281418	0.522	0.0064176	0.0016968	0.03425	0.0057831			0.0010623		
0.6	0.027561	0.533	0.0062852	0.0024926	0.03341	0.0055249			0.0017323	0.003595	
0.8	0.0270037	0.544	0.0061581	0.0032563	0.02831	0.0045868		0	0.0016851	0.00342	0.0005541
1	0.0264685	0.555	0.006036	0.0039897	0.0222	0.0035256	0.0041	0.0006511	0.0008282	0.00552	0.0008766
1.2	0.0259541	0.566	0.0059187	0.0046946	0.01146	0.0017846	0.00771	0.0012006	-0.00064	0.00924	0.0014389
1.4	0.0254593	0.577	0.0058059	0.0053727	0.00842	0.0012862	0.00908	0.001387	-0.000534	0.01054	0.00161
1.6	0.024983	0.588	0.0056973	0.0060253	0.00321	0.0004812	0.01193	0.0017883	-0.000979	0.01125	0.0016864
1.8	0.0245652	0.598	0.005602	0.0065978	0.001	0.0001474	0.01458	0.002149	-0.001006	0.01121	0.0016523
2	0.0241215	0.609	0.0055008	0.0072058			0.01348	0.0019509	-0.000246	0.01078	0.0015602
2.5	0.0230612	0.637	0.005259	0.0086587			0.01861	0.002575	0.0008247	0.01102	0.0015248
3	0.0221235	0.664	0.0050452	0.0099437			0.02142	0.0028433	0.0020552	0.01011	0.001342
3.5	0.021259	0.691	0.004848	0.0111283			0.02185	0.0027871	0.0034932	0.00761	0.0009707
4	0.0204596	0.718	0.0046657	0.0122238			0.02332	0.0028627	0.0046953	0.00718	0.0008814
4.5	0.0196917	0.746	0.0044906	0.0132761			0.02478	0.0029278	0.0058577	0.00603	0.0007124
5	0.0190039	0.773	0.0043338	0.0142186			0.02584	0.0029464	0.0069385	0.00407	0.0004641
5.5	0.0182939	0.803	0.0041719	0.0151915			0.02736	0.0030031	0.0080165	0.00301	0.0003304
6	0.0176988	0.83	0.0040361	0.016007			0.02943	0.0031253	0.0088456	0.00202	0.0002145
6.5	0.0171212	0.858	0.0039044	0.0167985			0.0305	0.0031332	0.0097609	0.00103	0.0001058
7	0.0165989	0.885	0.0037853	0.0175142			0.03419	0.0034051	0.0103238		
8	0.0156277	0.94	0.0035638	0.0188451			0.03756	0.0035218	0.0117594		
9	0.0147638	0.995	0.0033668	0.0200288			0.03791	0.0033582	0.0133038		
10	0.0139905	1.05	0.0031905	0.0210886			0.038	0.0031898	0.0147083		

(RR)-[Zn**L**^{4}]$(ClO_4)_2$ + *(S)*-MBA in CD_3CN

eq [S]	[TMS]	Vol/ml	$[L]_{initial}$	$[S]_{initial}$	$I_{[L]}$	$[L]_{obs}$	$I_{[LS2]}$	$[LS2]_{obs}$	$[S]_{calc}$	$I_{[LS]}$	[LS]
0	0.02938	0.5	0.0067	0	0.038	0.0066986			-1.36E-06		
0.2	0.0286355	0.513	0.0065302	0.0008824	0.037	0.0063571			0.0007092		
0.4	0.027981	0.525	0.006381	0.0016581	0.0316	0.0053052			0.0005823		
0.6	0.0273048	0.538	0.0062268	0.0024594	0.0281	0.0046036			0.0008362		
0.8	0.0267091	0.55	0.0060909	0.0031655	0.0197	0.003157	0.00263	0.0004215	-0.00019	0.00409	0.0006554
1	0.0260924	0.563	0.0059503	0.0038964	0.01425	0.0022309	0.00509	0.0007969	-0.00062	0.00436	0.0006826
1.2	0.0255035	0.576	0.005816	0.0045943	0.00887	0.0013573	0.0072	0.0011018	-0.000966	0.00707	0.0010819
1.4	0.024983	0.588	0.0056973	0.0052112	0.0053	0.0007945	0.00981	0.0014705	-0.001162	0.00946	0.001418
1.6	0.0244426	0.601	0.005574	0.0058516	0.0021	0.000308	0.01133	0.0016616	-0.001076	0.0113	0.0016572
1.8	0.0239251	0.614	0.005456	0.006465	0.00043	6.173E-05	0.01404	0.0020154	-0.000945	0.01256	0.001803
2	0.0234665	0.626	0.0053514	0.0070085			0.01484	0.0020895	-0.000432	0.01138	0.0016023
2.5	0.0223252	0.658	0.0050912	0.008361			0.0184	0.0024647	0.0008051	0.00959	0.0012846
3	0.0213208	0.689	0.0048621	0.0095515			0.025	0.0031981	0.0014913	0.00912	0.0011667
3.5	0.0203745	0.721	0.0046463	0.010673			0.02055	0.0025122	0.0035145	0.0053	0.0006479
4	0.0195346	0.752	0.0044548	0.0116684			0.02179	0.002554	0.0046597	0.00321	0.0003762
4.5	0.0187372	0.784	0.004273	0.0126134			0.02364	0.0026577	0.0056827	0.00203	0.0002282
5	0.0180025	0.816	0.0041054	0.0134842			0.02495	0.002695	0.0066839	0.00149	0.0001609
5.5	0.0173436	0.847	0.0039551	0.0142651			0.0312	0.0032467	0.0070632	0.00081	8.429E-05
6	0.0167312	0.878	0.0038155	0.0149908			0.03342	0.0033549	0.0078204	0.00032	3.212E-05
6.5	0.0161429	0.91	0.0036813	0.0156881			0.03735	0.0036176	0.0083892		
7	0.0156111	0.941	0.00356	0.0163184			0.03689	0.0034554	0.009303		
8	0.0146315	1.004	0.0033367	0.0174794			0.0381	0.0033448	0.010798		
9	0.0137676	1.067	0.0031396	0.0185032			0.0378	0.0031225	0.0122411		
10	0.013	1.13	0.0029646	0.0194129			0.0382	0.0029796	0.0134687		

(RR)-[Zn$\mathbf{L}^4$]$(ClO_4)_2$ + *(R)*-MBA in CD_3OD

eq [S]	[TMS]	Vol/ml	$[L]_{initial}$	$[S]_{initial}$	$I_{[L]}$	$[L]_{obs}$	$I_{[LS2]}$	$[LS2]_{obs}$	$I_{[LS]}$	[LS]	$I[S]obs$	[S]obs
0	0.041972	0.5	0.0048118	0	0.01146	0.002886	0	0	0	0	0	0
0.5	0.0401262	0.523	0.0046002	0.002271	0.00721	0.0017359	0.00172	0.0004141	0.00224	0.0005393	0.0019	0.0004574
1	0.0384359	0.546	0.0044064	0.0043506	0.00431	0.0009942	0.00382	0.000881	0.0041	0.0009455	0.00372	0.0008579
1.5	0.0368822	0.569	0.0042283	0.0062621	0.00158	0.0003496	0.0046714	0.0010338	0.0048143	0.0010654	0.00738	0.0016331
2	0.0353895	0.593	0.0040572	0.0080987		0	0.0048267	0.0010249	0.0057	0.0012103	0.01157	0.0024567
3	0.0328934	0.638	0.003771	0.0111698		0	0.0055375	0.0010929	0.0057625	0.0011373	0.02354	0.0046459
4	0.0305918	0.686	0.0035071	0.0140015		0	0.0054556	0.0010014	0.0054667	0.0010034	0.03749	0.0068813
5	0.0286694	0.732	0.0032867	0.0163668		0	0.0052313	0.0008999	0.005025	0.0008644	0.04208	0.0072384
6	0.0269743	0.778	0.0030924	0.0184523		0	0.006	0.0009711	0.0053375	0.0008639	0.05553	0.0089873
7	0.0254376	0.825	0.0029162	0.020343			0.0057167	0.0008725	0.0049389	0.0007538	0.0749	0.0114316
8	0.0240941	0.871	0.0027622	0.0219959			0.0058747	0.0008493	0.0049421	0.0007145	0.09542	0.0137944
9	0.0228606	0.918	0.0026208	0.0235136			0.00695	0.0009533	0.00512	0.0007023	0.12019	0.0164857
10	0.0217697	0.964	0.0024957	0.0248558			0.0070071	0.0009153	0.0047786	0.0006242	0.1321	0.0172547
15	0.0175468	1.196	0.0020116	0.0300514			0.0075375	0.0007936	0.0037813	0.0003981	0.16098	0.0169481

(RR)-[Zn**L**^{4}]$(ClO_4)_2$ + *(S)*-MBA in CD_3OD

eq [S]	[TMS]	Vol/ml	$[L]_{initial}$	$[S]_{initial}$	$I_{[L]}$	$[L]_{obs}$	$I_{[LS2]}$	$[LS2]_{obs}$	$[S]_{calc}$	$I_{[LS]}$	[LS]
0	0.02938	0.5	0.0046774	0	0.02086	0.0036775		0	-0.001	0	0
0.2	0.0289173	0.508	0.0046037	0.0008939	0.01527	0.0026494	0.00137	0.0002377	-0.001298	0.00659	0.0011434
0.4	0.028469	0.516	0.0045324	0.00176	0.01415	0.0024178	0.0034722	0.0005931	-0.000948	0.0085514	0.0014607
0.6	0.0280344	0.524	0.0044632	0.0025997	0.01145	0.001926	0.00601	0.0010109	-0.000948	0.00963	0.0016198
0.8	0.0276128	0.532	0.0043961	0.0034141	0.00885	0.0014668	0.0083801	0.0013884	-0.000903	0.0103245	0.0017105
1	0.0272037	0.54	0.0043309	0.0042044	0.00547	0.0008928	0.01014	0.0016551	-0.000889	0.0116	0.0018934
1.2	0.0268066	0.548	0.0042677	0.0049717	0.00468	0.0007526	0.0130193	0.002094	-0.000637	0.0134664	0.0021659
1.4	0.0264209	0.556	0.0042063	0.0057168	0.00272	0.0004312	0.01537	0.0024365	-0.000495	0.0156	0.002473
1.6	0.0260461	0.564	0.0041466	0.0064409	0.00124	0.0001941	0.016775	0.0026215	-0.000133	0.0160653	0.0025106
1.8	0.0256818	0.572	0.0040886	0.0071446			0.0158	0.0024346	0.0006213	0.01565	0.0024115
2	0.0253276	0.58	0.0040322	0.007829			0.0148315	0.0022539	0.0015428	0.0147592	0.0022429
2.5	0.0244833	0.6	0.0038978	0.00946			0.01717	0.0025223	0.0030399	0.01617	0.0023754
3	0.0236935	0.62	0.0037721	0.0109858			0.0177996	0.0025304	0.0046833	0.0159941	0.0022737
3.5	0.0229531	0.64	0.0036542	0.0124163			0.01807	0.0024886	0.0062735	0.0164	0.0022586
4	0.0222576	0.66	0.0035435	0.01376			0.0188495	0.0025173	0.0076993	0.0161089	0.0021513
4.5	0.0216029	0.68	0.0034393	0.0150247			0.01902	0.0024653	0.0091201	0.01652	0.0021413
5	0.0209857	0.7	0.003341	0.0162171			0.0195903	0.0024667	0.0104094	0.0160229	0.0020175
6	0.0198514	0.74	0.0031604	0.0184086			0.0192	0.0022869	0.0129614	0.01438	0.0017128
7	0.0188333	0.78	0.0029983	0.0203754			0.0203026	0.0022942	0.0150829	0.0139882	0.0015807
8	0.0179146	0.82	0.0028521	0.0221502			0.02007	0.0021573	0.0171409	0.01282	0.001378
9	0.0170814	0.86	0.0027194	0.02376			0.0205091	0.0021019	0.0189386	0.0130016	0.0013325
10	0.0163222	0.9	0.0025986	0.0252267			0.01952	0.0019117	0.0207165	0.01095	0.0010724
12	0.0149898	0.98	0.0023864	0.0278008			0.0153114	0.0013771	0.0240373	0.0136058	0.0012237
14	0.0138585	1.06	0.0022063	0.0299864			0.016	0.0013304	0.0264497	0.01249	0.0010386
20	0.0113	1.3	0.001799	0.0349292			0.01775	0.0012035	0.0319268	0.01079	0.0007316